Analytical and Finite Element Modelling of the Dynamic Interaction between Off-Road Tyres and Deformable Terrains

by

Chrysostomos-Alexandros Bekakos

A thesis submitted in partial fulfilment of the requirements for the award of the Degree of Doctor of Philosophy

Department of Aeronautical and Automotive Engineering

Loughborough University

November 2016

Loughborough University, United Kingdom

Keywords: Tyre, Finite element method, tyre-soil interaction, off-road tyre, terramechanics

This thesis is dedicated

to my beloved parents

Michael and Christina

Abstract

Automotive tyres are one of the main components of a vehicle and have an extremely complex structure consisting of several types of steel reinforcing layers embedded in hyperelastic rubber materials. They serve to support, drive – accelerate and decelerate – and steer the vehicle, and to reduce transmitted road vibrations. However, driving is associated with certain types of pollution due to CO_2 emissions, various particles due to tyre wear, as well as noise. The main source of CO_2 emissions is the tyre rolling resistance, which accounts for roughly 30% of the fuel consumed by cars. The phenomenon becomes more pronounced in off-road conditions, where truck vehicles are responsible for about a quarter of the total CO_2 emissions. Appropriate legislation has been introduced, to control all of these pollution aspects. Therefore, tyre simulation (especially in off-road conditions) is essential in order to achieve a feasible design of a vehicle, in terms of economy and safety.

After a concise literature review and critical evaluation of the state-of-the-art models related to simulation and analysis of off-road tyres, the various limitations of the existing tyre models in terms of representing the rolling response and driving behaviour of actual tyres have been identified (e.g. utilization of non-invariant soil parameters). Finite element models for the terrain have been developed in which invariant soil parameters have been designated which are used for the description of the tyre – terrain interaction. Similar to the development of the soil models, a realistic tyre model was established via a novel coupled MATLAB – ABAQUS optimisation algorithm. The agreement of the tyre structure with reality was achieved through matching of its eigenproperties with analogous data from actual tyres. Subsequently, the interaction between a 235/75R17 tyre and a road – which is considered to be either rigid or deformable – was modelled with the finite element method and the rolling response of towed and driven wheels under various driving conditions was investigated. Regarding the limitations of the models used, it should be noted that the soil material is described by the linear Drucker-Prager constitutive model and the tyre parameters have been obtained via an optimisation procedure. More accurate soil constitutive models and calibration of their corresponding parameters, as well as

realistic tyre properties can be used for further development of the various models involved in the thesis, the results of which can be validated with experimental data.

Additionally, a novel semi-analytical solution for the estimation of the response of a pneumatic tyre rolling on deformable terrain has been introduced, which involves substantial improvements compared to other existing semi-analytical solutions. Among others, lateral forces as well as the effects of treaded pattern and multi-pass have been taken into account. Although the developed analytical model is based on invariant soil parameters, it remains a semi analytical approach, as it involves empirical parameters such as the shear deformation modulus and empirical parameters related to distribution of the pressures between the tyre and the soil. Furthermore, it is assumed that the pressures at the tyre-soil interface are uniform along the width of the tyre which can lead to significant deviation of the results, especially for low inflated tyres (<15kPa) with large contact area.

Acknowledgements

It is my pleasure to thank all of those who made this thesis possible. First and foremost I would like to thank my supervisors, Dr. Dan O'Boy and Dr. George Mavros for giving me the opportunity to undertake this research and also for their valuable help and guidance throughout the research period. Their friendship and advice both in technical and personal related issues are highly appreciated.

Secondly, I would like to thank Jaguar Land Rover and the UK-EPSRC grant EP/K014102/1 where as part of the jointly funded Programme for Simulation Innovation, I was able to investigate the very interesting topic of Terramechanics. Furthermore, I would like to thank my industrial partner, Jan Prins, who despite his heavy work load was always there for me and with his advice and help I was able to overcome many difficulties.

I would like to thank all of friends and colleagues at the Department of Aeronautical and Automotive Engineering, Loughborough University, for their support, help and resources required for the successful completion of this research. Special thanks go to Giancarlo Pavia, Agis Skarlas and Karol Bogdanski.

I would like to thank all of my friends and especially, Manolis Petrovitsos, Charis Akpinar, Kon/nos Thomopoulos, Christos Katrakazas and Leonidas Paouris for their help and support all of these years. Special thanks along with my sincere gratitude and highest appreciation goes to George Papazafeiropoulos, who apart from being an excellent colleague with remarkable research and critical skills was always there to support me and guide me throughout any difficulties I faced with personal and/or professional issues, thank you George.

Finally, and most of all, I would like to thank my family who has been always there to support me and encourage me to overcome any difficulty and made me believe that I can complete this academic route. I wouldn't have done anything without them. From the bottom of my heart, thank you mom and dad.

Nomenclature

a, a_0, a_1	Empirical constant	[-]
a	Half width defining the loading area, used in Eq. 2.16	[m]
a_1	Angle of approach	[^{o}]
a_r	Cord orientation angle	[^{o}]
A_0	Ageikin coefficient	[-]
A_R	Cord area	[m]
B, b	Width of the plate or the wheel	[m]
B_H	Ageikin parameter based on Bi	[Pa]
B_i	Soil bearing capacity	[Pa]
B_n	Mobility number as defined by Brixus(1987)	[-]
CI	Cone Index	[-]
c	Cohesion	[Pa]
c_1,c_2	Empirical coefficients required for the determination of the relative position of θ_M	[-]
C_b	Number of penetrometer blows	[-]
C_n	Wheel numeric (dimensions must be selected such that the wheel numeric is dimensionless)	[-]
C_{10},D_1	Temperature dependent material parameters	[-]
$C_{1L},C_{2L},$ C_{3L}, C_{4L}:	Pokrovsky's theoretical values	[-]
C_z	Tyre Vertical Stiffness	[N/m]
d_{DP}	Cohesion for Drucker-Prager	[Pa]
D^*	Elastic tyre with bigger diameter	[m]
D,d	Diameter of the wheel	[m]
D_h	Hydraulic diameter of the contact area	[m]
D_1,D_2,ξ,ω	Parameters in Eq. (2.25) used as found on p.16-17 of Lyasko (2010)	[-]
D_t	Tyre damping coefficient	[Ns/m]
e	Tread height	[m]
E	Soil modulus of elasticity	[Pa]
g	Gravity constant	[m/s^2]
G	Shear modulus	[Pa]

f_o	Deflection of the elastic tyre	[m]
f_m, f_k	Dimensionless Kacigin's friction coefficients of motion and rest respectively	[-]
F_{MC}	Failure surface of MC model	[Pa]
F_{DP}	Failure surface of DP model	[Pa]
F_x	Longitudinal Force	[N]
F_z	Vertical Force	[N]
g	Gravity constant	[m/s^2]
h_L	Height of the lug	[m]
H_0	Hardpan depth	[m]
H_1	New hardpan depth, Multi-pass model	[m]
i,s	Wheel slip/skid	[-]
I_1	First deviatoric strain	[-]
J	Ageikin coefficient	[-]
j	Shear displacement	[m]
j_x	Longitudinal shear displacement	[m]
j_y	Lateral shear displacement	[m]
J^{el}	Elastic volume ratio	[-]
k	Modulus of soil deformation, Bernstein-Goriatchkin	[$m/N^{1/2}$]
k_c	Soil deformation modulus due to cohesive behavior	[N/m^{n+1}]
k_φ	Soil deformation modulus due to frictional behavior	[N/m^{n+2}]
k_c',k_φ'	Dimensionless modulus of sinkage	[-]
K_1, K_2	Parameters characterizing the shear stress-shear displacement relationship	[-]
K_r	Tyre sinkage ratio	[-]
K_s	Stiffness modulus of the terrain	[Pa/m]
k_G	Equivalent static stiffness	[N/m^3]
k_p	Stiffness parameter for the soft substrate	[N/m^3]
k_z	Kacigin and Guskov's coefficient of soil deformation	[-]
k_x	Longitudinal shear deformation modulus	[m]
k_y	Lateral shear deformation modulus	[m]
K_c, K_γ,t	Parameters in Eq. (2.10) used as on p.78 of Bekker(1960)	[-]
K, K_0	Shear deformation modulus	[m]

K_r	Ratio of residual shear stress τ_r to the maximum shear stress τ_{max}	[-]
K_w	Shear displacement where the τ_{max} occurs	[m]
L, l	Length of the rectangular plate or the contact patch of the wheel	[m]
m	Diameter exponent	[-]
m_m	Strength parameter for the surface mat	[N/m^3]
MP	Soil parameter that depends on moisture content	[-]
n	Exponent of deformation	[-]
n_0, n_1	Sinkage exponent coefficients as used by Ding et al.(2014)	[-]
N_γ,N_c, N_q	Terzaghi's parameters	[-]
N_φ	Flow value	[-]
p_{gr}	Average ground pressure	[Pa]
P	Pressure	[Pa]
q	Bearing capacity of clay	[Pa]
$q_{f:}$	Ultimate bearing stress	[Pa]
q_{max}	Ultimate bearing capacity	[Pa]
q_o	Surcharge of the soil	[Pa]
Q_1	Ageikin parameter	[-]
Q_v	Vertical load on wheel centre	[N]
R,r	Wheel radius	[m]
R_b	Resistance due to soil mass gathered in front of the wheel	[N]
R_c	Resistance due to compaction of the soil	[N]
R_t	Resistance due to tyre deformation	[N]
R_{tot}	Total Rolling resistance	[N]
S	Cord spacing	[m]
t	Width of tread contact area	[m]
U	Strain energy per unit of reference volume	[-]
V_t	Tyre deformation velocity in the vertical direction	[m/s^2]
V_x	Longitudinal velocity	[m/sec]
W	Vertical load	[N]
z, s	Tyre sinkage	[m]
z_{el}	Elastic deformation of the soil	[m]

z_L	Sinkage at the tip of the lug	[m]
z_r	Rebound sinkage	[m]
z_T	Depth of the track	[m]
α,ε	Parameters used as on Wong(2001), p.191	[-]
β	Slip angle	[^{o}]
γ	Soil unit weight	[kg/m^3]
γ_1	New soil unit weight for multi-pass	[kg/m^3]
δ_t	Tyre deflection	[m]
θ	Arbitrary angle along the wheel soil contact arc	[rad]
θ_s, θ_1, θ_0	Entry angle of the wheel	[rad]
θ_2, θ_r:	Exit angle of the wheel	[rad]
θ_4:	Angle of transition for towed wheels	[rad]
θ_M	Angle where the maximum radial stress occurs	[rad]
θ_e	Entry angle for Gee-Clough model(90-θ_1)	[rad]
ρ	Soil density	[kg/m^3]
$\sigma_1,\sigma_2,\sigma_3$	Principal stresses	[Pa]
τ, τ_j	Shear stress	[Pa]
φ	Friction angle	[^{o}]
ψ	Soil dilation angle	[^{o}]
ω	Angular velocity	[rad/sec^2]

Contents

List of Figures

Chapter 1

Introduction

1.1. Introduction

There are many instances in which an off-road vehicle is required to travel on deformable terrain, such as space missions, agriculture, construction, etc, in which cases realistic off-road tyre models are needed for the prediction of the interaction of the vehicle with the supporting terrain. However, little research has been done in this area, since the majority of research in tyre development has concentrated on on-road vehicles. In this chapter the context of the research is presented followed by the aim and the desired objectives. Next, the novelties and contributions of this study are briefly presented along with a short summary of the subsequent chapters.

Since the computational power of modern computers is continuously growing, simulations are becoming essential tools for mechanical engineers. In this aspect, vehicle manufacturers are funding projects where full vehicle models, capable of assessing a vehicle design prior to its production, are developed. Tyre as one of the most important components of an automobile constitutes the main link between the vehicle and the ground and is mainly responsible for the driving response of the vehicle under accelerating/braking and steering conditions; therefore, accurate and realistic tyre models – which can then be integrated into full vehicle models – are necessary.

1.2. Project Context

This work was supported by Jaguar Land Rover and the UK-EPSRC grant EP/K014102/1 as part of the jointly funded Programme for Simulation Innovation. The help and guidance provided by Jaguar Land Rover are highly appreciated and were crucial for the completion of this project.

In many cases there is the necessity for construction of vehicles which are capable of traveling on off-road terrains. Therefore, efficient simulation of the dynamic interaction between off-road tyres and deformable terrains is of high importance. Among the various applications of off-road vehicles, the latter are used in agriculture operations, where economy during excavations for tillage is desired, and potential immobilization of the vehicles has to be avoided. In addition, military tracked and wheeled vehicles are necessary in the national defence of each country, and to maximize their potential, they have to be designed for optimum performance during travelling on soft terrain and/or snow. Furthermore, off-road vehicles are needed in various construction sites, where pavements and/or rigid foundations are not present. In this case, the vehicles need to be appropriately immobilized to ensure safety and to ensure that the construction works are carried out properly. Commercial off-road vehicles are also needed for cross-country transportation and racing (e.g. rally or desert racing), where it is obvious that they have to perform optimally on non-homogeneous terrain, such as rocky and granular soils.

On-road tyres have attracted significant more attention compared to off-road tyres in the past years and for that reason the majority of the existing off-road tyre models are usually utilizing simplistic empirical and/or semi-analytical equations with inherent limitations and a number of restrictive assumptions. For instance, use of non-invariant soil parameters into tyre models (e.g. Bekker, 1956), necessitates continuous soil experimental measurements which in return increase the overall cost. Furthermore, such models can be applied only for a limited range of tyre geometries, where the width of the tyre has to be sufficiently large in order to avoid significant deviations from experimental measurements (Meirion-Griffith & Spenko, 2010); therefore the utilization of such models in lunar rovers, where narrow wheels are predominantly used, would yield inadequate results. Another major assumption commonly used in the off-road tyre mechanics is that of a constant pressure distribution along the width of the wheel, which often tends to underestimate or overestimate the traction response of the tyre. Finally, in the majority of empirical tyre models, the dynamic sinkage caused by the slip/skid rolling conditions of the tyre is either not reflected, or taken into account in a very simplistic way (Lyasko, 2010b).

It is expected that the results of this thesis will be used for the establishment of guidelines and relevant methodologies for off-road tyres rolling on soft terrains intended to minimize their production cost and maximize their rolling performance.

1.3. Aim

The purposes of this thesis are the following:

- Understanding the current status of off-road tyre model development and identification of the limitations present in such models. Based on these, it is easier to decide where additional knowledge is necessary in terms of improving the existing models.
- Determination of the most important tyre design parameters with regards to off-road tyre locomotion, such as tyre width, inflation pressure, tread pattern/void ratio and detailed geometric characteristics of the tyre structure. The latter, apart from providing a conceptual description of this phenomenon, will also help other researchers in their future studies to focus on specific parameters which have the largest impact on the tyre response and reduce unnecessary complexity.
- Improvement of existing models (analytical and numerical) so that they provide a better description of the phenomena of static and dynamic off-road tyre – terrain interaction. Attempts will be made towards the exclusion of non-invariant soil parameters from the analytical off-road tyre modelling techniques and the inclusion of tyre structure details in the numerical models, such as cord orientation and reinforcing layers' thicknesses.
- To develop efficient optimization techniques for the parameterization of both the soil and the tyre.

1.4. Objectives

This research is mainly focused on the development of novel tyre-terrain models, both numerically and analytically, in order to accurately calculate the dynamic response of an off-road tyre by attempting to eliminate a number of limitations associated with the current status of off-road tyre modelling. Reliable numerical modelling of off-road tyres is vital for obtaining realistic results which are used for the design.

- Development of numerical tyre-terrain models using the commercial finite element code Abaqus v.6.13. Both rigid and pneumatic tyres, either driven or towed, interacting with various types of deformable soils will be modeled in order to improve existing models and provide a better understanding of the static and dynamic off-road tyre – terrain interaction.
- Development of a semi-analytical tyre-terrain model using the programming language MATLAB in order to identify how the compliance of the tyre, its geometrical characteristics and dynamic loading effects (such as rolling velocity and vertical load) affect the rolling response of the tyre on terrains with various bearing capacities.
- Both numerical and analytical models will be used to carry out parametric studies in order to determine the effect of various design, operational and environmental (soil) parameters in tyre behavior.
- Finally, one of the main objectives with principal interest for this thesis is the identification of the most important invariant soil parameters which determine the tyre behaviour, which is governed to a large extent by the alteration of the soil properties due to vehicle loads. It is apparent that soil compaction caused by a rolling wheel affects its structure, decreases its porosity and water and air infiltration, (e.g. reduces crop yield which is caused by hindering of root penetration). Following that, the energy efficiency of an off-road tyre in terms of rolling resistance and inflation pressure will be addressed.

1.5. Research Contribution

A robust methodology regarding the development of a valid FE tyre – terrain model has been presented, which involves two different FE models: (a) the soil model and (b) the tyre model. With regards to the soil model, a rigid wheel – deformable terrain coupled model has been developed in order to assess the accuracy and robustness of the models involved. A novel equation for conversion of the Mohr-Coulomb to Drucker-Prager soil model and vice-versa has been developed for triaxial tension or compression.

Following that, a pneumatic tyre model has been developed and the natural frequencies of the tyre structure have been extracted. A novel coupling MATLAB – ABAQUS optimisation technique for tyre development has been proposed where the

geometrical characteristics with high impact on the behaviour of the tyre, such as the thickness of the belt and/or the orientation of the cords, are the design variables, and the objective function describes how well the natural frequencies of the numerical tyre model and those obtained from experimental testing found in the literature are matched.

With regards to the semi-analytical formulations, the majority of the existing semi-analytical off-road tyre models are based on empirical material laws (Bekker, 1956 & Reece, 1965) which use non-invariant soil parameters such as k_c and k_φ. In the current study Lyasko's (2010a) analytical mathematical model for describing the rigid plate – soil indentation is utilised and modified accordingly in order to incorporate the geometry of rolling wheel being either rigid or pneumatic. Thereafter, a novel semi-analytical tyre model has been developed with the use of four invariant soil parameters, namely as the cohesion, the friction angle, the soil unit weight and the Young modulus. These soil parameters can be easily measured in-situ with hand held instruments like a bevameter or a cone penetrometer. Furthermore, the slip sinkage effect has been incorporated in the model where with every increase on the slip conditions of the wheel, there is an increase in the vertical displacement of the wheel into the soil, capturing the digging effect.

Due to the existing lack in the literature of studies containing models that use realistic invariant soil parameters and tyre physical properties, in this thesis the models developed were verified in terms of their qualitative response; therefore further validation studies are necessary in order to establish the level of quantitative agreement with measurements.

1.6. Outline

Chapter 2 presents a thorough literature review and critical assessment on the state-of-the-art techniques with regards to the existing empirical, analytical and numerical methods for the assessment of the off road vehicle performance. In addition to that, techniques of off-road tyre modelling which incorporate the aforementioned methods have been reported. Literature finding are critically evaluated and the aims/objectives of the work are revisited.

Chapter 3 introduces the FE modelling technique based on which the soil properties used for the various models in this study have been established. Dimensionless graphs have been produced and the validity of the soil model has been confirmed with comparison of experimental results found in the literature.

Chapter 4 focuses on the development of a realistic numerical tyre model via a novel coupled MATLAB – ABAQUS optimisation algorithm. The eigenfrequencies and eigenvalues of the tyre structure have been extracted and their variation with increasing inflation pressure has been illustrated.

Chapter 5 incorporates the two aforementioned FE models into a single FE model capable of predicting the off road performance of a realistic 235/75R17 tyre. The response of the pneumatic tyre in contact with a rigid surface, for a number of inflation pressures and vertical loads has initially been examined, and results of the contact area and the vertical deflection, measured from the centre of the wheel, have been presented. Following that, the response of the rim for a pneumatic tyre rolling over a speed bump has been illustrated. Furthermore, towed and driven wheels interacting with cohesive and frictional deformable terrains have been modelled and the effect of various parameters such as the inflation pressure, on the overall driving response has been presented.

Chapter 6 introduces a novel semi-analytical tyre model capable of quantitatively capturing the realistic response of a pneumatic tyre rolling on a deformable terrain. The proposed equation utilizes invariant soil parameters and is derived from soil mechanics theory. Initially, a rigid plate is forced into the soil and the pressure-sinkage response is presented according to Lyasko's (2010a) equations for a number of different soils. Following that, a rigid wheel has been modelled and the effects of the vertical load, the width of the tyre and the tread pattern on the overall driving response have been illustrated. In addition, a pneumatic tyre has been modelled under the same concept with the one initially proposed by Bekker (1956) and further implemented by Harnisch et al. (2005). Finally, the multi-pass effect has been modelled in a similar manner with the one presented by Harnisch et al. (2005) under the assumption that the rear wheel rolls over the exact same rut path created by the front wheel.

Finally, Chapter 7 summarizes the results drawn from the current study and focuses on recommended future work for further implementation and validation of the developed models. An outline of the research is presented in Fig. 1.1.

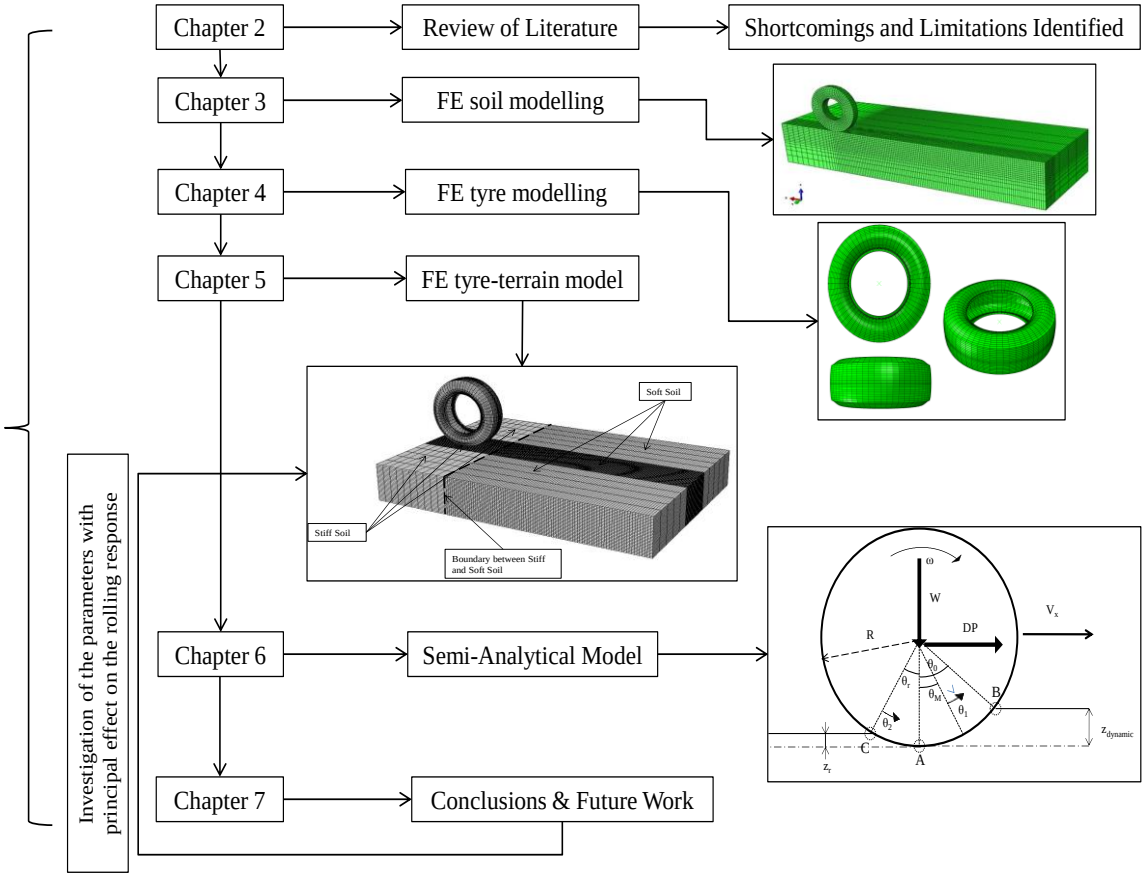

Figure 1.1.*Flowchart of the research*

Chapter 2

Review of Literature

2.1. Introduction

This chapter presents the available methods and techniques regarding the assessment of a vehicle performance on off road conditions. Initially, the empirical methods related to the characterization of the strength of the soil, the pressure sinkage and/or the shear stress-shear displacement responses are presented, followed by the equivalent analytical and numerical formulations.

Terramechanics is the field of science that deals with the interaction of a vehicle with the underlying deformable soil. Understanding the underpinning principles by which tyre forces, such as rolling resistance and drawbar pull, are developed will encourage the manufacturing of optimal off road tyres. In addition, this understanding will assist on the prediction of vehicle performance on soft soils. Whilst, the interaction between on road tyres and urban pavements has received much attention and has been subjected to significant research in the past, the same type of interaction in off road conditions has not been adequately represented to a similar extent in terms of analytical and/or numerical methods. This lack is mainly based on the multivariable and complex nature of the physical interaction of an off road tyre with the underlying soft soil. For instance, a simplified dynamic off road tyre-soil interaction will be represented by the summation of the movement of the particles of the soil and the deformation of the tyre as the total deformation; while for the on road tyre community and for a simplified on road tyre model, since the pavement is regarded as a rigid surface, the total deformation is concentrated only on the tyre interface.

Given the complexity of tyre-soil interaction several assumptions have to be made in terms of creating accurate and yet computationally efficient methods. These assumptions may range from a simplified linear soil material response, such as a purely cohesive and/or a purely frictional soil, up to a rigid wheel tyre response where

a highly inflated tyre (inflation pressure larger than 250kPa) is assumed to roll over a relatively soft soil. To this regard, various methods have been developed, where the ability of tracked and/or wheeled vehicles to roll over a deformable terrain can be feasibly characterized.

2.2. Empirical Methods

2.2.1 Soil assessment

Identifying the principal characteristics regarding the response of the terrain, such as cohesion and friction angles, under normal loading and shear stress is the primary focus in the field of Terramechanics. The most pronounced methods with regards to the terrain classification, involve hand held instruments and techniques like: i) the cone penetrometer, ii) the bevameter and iii) traditional soil mechanic techniques used in the field of civil engineering (Wong, 2001). Following that, system metrics such as, the Vehicle Cone Index (VCI), the Mobility Index (MI) and the Mean Maximum Pressure (MMP) have been developed (Priddy & Willoughby, 2006), which permit a long term characterization of the ability of the vehicle to roll over specific types of terrains.

VCI is defined as the minimum soil strength, necessary for a self-propelled vehicle, to traverse a certain type of soil for a prescribed number of times without getting immobilized (VCI_1 and VCI_{50}). Numerous empirical equations have been developed through which VCI can be measured with the use of easily captured parameters, like the weight of the vehicle. With regards to correlating vehicle characteristics with the VCI's value, the principal parameter MI was developed. Based on that value the locomotion of the vehicle can be assessed. At the same time, the United Kingdom's Ministry of Defence used a different index (MMP) to characterize the traversability of a vehicle. Herein, a common misconception should be clarified since the MMP should not be compared with the VCI, but instead with the MI. This is due to the fact that the former is a performance metric and not a set of predictive equations (Priddy & Willoughby, 2006).

Furthermore, the cone penetrometer was developed by the Waterways Experiment Station (WES) of the US Army Corps of Engineers as a hand held device, consisting of a 30 degree circular cone with a base area of 3.23 cm^2, Fig. 2.1. By utilizing this device, the parameter so called, cone index, which represents a combination of the shear and compressive characteristics of the soil may be obtained. This technique was developed as "go/no go" device during the Second World War, with regards to the assessment of a vehicle's capacity to roll over a certain terrain without being immobilized. However, ambiguous opinions exist to whether this device can adequately assess the aforementioned potential for immobilization such as work conducted by Reece & Peca (2006). They state that, the latter device can successfully capture the response of frictionless clay but remains still inadequate to characterize the properties of sand. Therefore, the necessity for of a handheld device and/or a set of equations capable of predicting the behavior of both cohesive and frictional terrains is apparent.

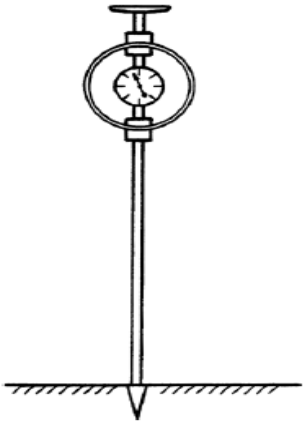

Figure 2.1*.Cone Penetrometer (Wong, 2001).*

Based on the resulting measurement of the cone penetrometer (Cone Index, CI), several techniques and/or methods have been developed for vehicle performance assessment. Wismer & Ruth (1973) proposed Eq. 2.1 as a function of CI where the first term is the gross traction and the second term is the resistance. However, the slip sinkage effect was not included in the above-stated model and, for this reason, Brixius (1987) further developed Eq. 2.1 into Eq. 2.2. Brixius' empirical model is extensively used on off-road vehicle simulations. Following Eq. 2.1 and 2.2, similar empirical models have been developed (see Grisso et al., 2006) in an attempt to correlate vehicle performance with CI. However, currently, empirical models which only depend on CI values are considered to be deficient in vehicle performance

measurements since it is well established that soil characteristics, like compactness and hardness, cannot be correlated with CI measurements.

$$\frac{P}{W} = 0.75 \cdot \left(1 - e^{-0.3 \cdot C_n \cdot S}\right) \cdot \left(\frac{1.2}{C_n} + 0.04\right) \tag{2.1}$$

$$\frac{Q}{r \cdot W} = 0.88 \cdot \left(1 - e^{-0.1 \cdot B_n}\right) \cdot \left(1 - e^{-7.5 \cdot i}\right) + 0.04 \tag{2.2}$$

The bevameter technique developed by Bekker (1957) is based on the hypothesis that terrain characteristics relevant to off road locomotion are best measured under the same loading conditions as those exerted by an off-road vehicle. In this respect, two separate tests have been developed. The first test refers to the evaluation of the pressure-vertical displacement equation, when a certain pressure, similar to that exerted by vehicles, is acting on a simulation plate with a size similar to that of the contact patch of a vehicle's running gear. In the second test, the shear stress - shear displacement equation, presented in the following sections, is considered under multiple normal loads, thus measuring parameters like the tractive effort or the slip characteristics of a vehicle. Henceforth, the vertical displacement caused by the running gear (rigid wheel, pneumatic tyre) into the soil will be referred to as sinkage which is the main term used in the field of Terramechanics.

Additionally, classic soil characterization methods have been developed by civil engineers, whereby soil samples are taken from the field and tested in the laboratory with the use of devices such as a triaxial apparatus and/or a direct shear box. Gan et al. (1988) preferred the shear box technique over the triaxial apparatus (since less time is required to fail the specimen) and several tests have been performed on unsaturated soil. However, it can be argued that the use of the cone penetrometer and the bevameter constitutes a more realistic approach since the soil is at its natural state, while a civil engineering method would necessitate the disturbance of the terrain for the sampling process.

2.2.2 Pressure – Sinkage Equation

To the best of the author's knowledge, regardless of the assumptions involved, in most of the models published in the literature the off-road tyre-soil interaction is studied in terms of two main effects. The first is responsible for the relationship

between the vertical load exerted by the vehicle and the respective sinkage of the wheel into the soil; the second, deals with the shear stress-shear displacement developed at the tyre-soil interface due to tyre movement. In the following section, the most important empirical equations existing within the literature will be presented along with a critical evaluation of their respective advantages and disadvantages. In a pioneering paper, representative of the first effect, Bernstein (1913), having observed that the main resistance in a tyre's movement is due to the effort of creating a rut to cross over, proposed Eq. 2.3, which was later extended by Goriatchkin (1936) to its more generalized version, that of Eq. 2.4.

$$p = k \cdot z^{0.5} \tag{2.3}$$

$$p = k \cdot z^{n} \tag{2.4}$$

The aforementioned equations were developed based on the assumptions that the soil is homogeneous and that *k,n* are constants in a given soil within a varied plate geometry, size, and dimension range. However, the latter assumption was found not to be valid since parameter *k* is highly affected by the dimensions of the plate and the soil conditions. With regards to the dimensions of the plate, it is evident that the pressure calculated using Eq. 2.3 and Eq. 2.4 is independent of the width and/or the length of the plate. Furthermore, regarding the soil conditions, the parameter *k* is also independent of important soil parameters such as soil moisture. Thus, use of the aforementioned equations will necessitate repetitive tests and measurements for the extraction and calculation of parameter *k*.

Evans (1964) experimentally studied tracked vehicles operating on clay soils and, based on his results, he proposed Eq. 2.5. Evans was the first who considered that the modulus of soil deformation *k*, proposed in Eq. 2.3, 2.4, consists of two different components, the first being responsible for the cohesion of the soil and the second being related to a deformation constant. In addition, Evans was the first who took into consideration the width of the wheel which had until then been omitted by every previous researcher.

$$q = q_{max} \cdot \left(1 - e^{-az/2b}\right) \tag{2.5}$$

M. G. Bekker, a pioneer and leading specialist in the field of Terramechanics, studied Eq. 2.4 and analyzed results with experimental data. Bekker (1957) introduced two

different moduli for the soil; k_c for the cohesive part of the soil and k_φ for the respective frictional behaviour. He developed and proposed Eq. 2.6 where the width of the rectangular plate was also included. Two basic assumptions used in the development of the current model are that: i) the soil is considered to be homogeneous and ii) a linear relationship exists between k and $1/B$ as $k=k_c/b+k_\varphi$.

$$p = \left(\frac{k_c}{b} + k_\varphi \right) \cdot z^n \tag{2.6}$$

Subsequently, Bekker introduced Eq. 2.7 which describes the compaction resistance for a rectangular uniformly loaded plate area.

$$R_c = \frac{1}{(n+1)\left(k_c + b \cdot k_\varphi\right)^{1/n}} \cdot \left(\frac{W}{l} \right)^{(n+1)/n} \tag{2.7}$$

By assessing Eq. 2.6, it is noted that in the case of cohesive clay, an increase in width b would yield a reduction in pressure, while in the case of frictional sand, a variation in width would have no effect on the respective results. Furthermore, Bekker's equation does not take into consideration significant soil parameters like soil unit weight and moisture. Onafenko & Reece (1967) claimed that Eq. 2.6 did not take into consideration the slip and skid conditions, something which would yield significant errors and drawbacks in tyre modelling aspects. Another fundamental limitation of the aforementioned equation lies in the assumption of a constant pressure distribution across the width of the wheel, an assumption leading to significant errors for small rigid wheels (Meirrion-Griffith & Spenko, 2010). Furthermore, parameters k_c and k_φ are non-invariant parameters which are highly dependent on the dimensions of the plate which has been used for the characterization of the terrain. Thus, the argument made by Bekker for global k_c and k_φ factors for a given soil condition is not valid. An evaluation of Eq. 2.7 revealed that, in order to reduce the resistance due to compaction, it was more effective to increase the length of the rectangular plate rather than the width, as the latter appears in Eq. 2.7 in a higher power than the former. Finally, similarly to equations proposed by Bernstein and Goriatchkin, Eq. 2.6 adopts parameters independent of important physical soil parameters such as soil moisture, leading us to the conclusion that it can be used only for homogeneous soils.

Later on, Bekker (1960) developed models which yielded a more accurate and representative result with regards to rigid wheels rolling response. Figure 2.2 displays a schematic representation of a rigid wheel rolling on soft terrain where the pressure acting on the circumference of the wheel is set to act radially. Bekker then proposed Eq. 2.8 in order to describe the resistance due to compaction for a towed rigid wheel, by taking into account the curvature of the wheel while at the same time omitting the contribution of tangential stresses to the lift and drag forces. Equation 2.8 was developed considering the equilibrium of forces acting on the wheel in the vertical and horizontal direction. In addition, only the front region of the contact patch of the tyre-soil interaction was set to contribute to the overall rolling resistance (from point A to point B), which – as the following sections will show – lead to significant errors and limitations in tyre traction predictions. Furthermore, Bekker proposed Eq. 2.9 for the characterization of the maximum allowed sinkage of a towed wheel.

$$R_c = \frac{1}{(3-n)^{(2n+2)/(2n+1)}(n+1)(k_c + bk_\varphi)^{1/(2n+1)}}\left(\frac{3W}{\sqrt{d}}\right)^{(2n+2)/(2n+1)} \tag{2.8}$$

$$z = \left[\frac{3W}{(3-n)(k_c + bk_\varphi)\sqrt{d}}\right]^{2/(2n+1)} \tag{2.9}$$

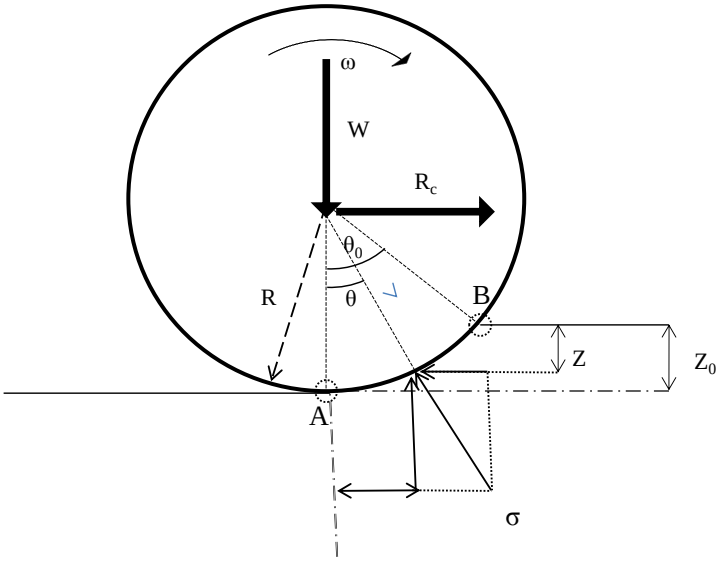

Figure 2.2.*Dynamic behaviour of a rolling rigid wheel.*

However, the rolling resistance due to compaction Rc is only one of the components of the total rolling resistance of the wheel. In particular, for a towed wheel, resistance due to bulldozing conditions must also be accounted for since the terrain is

accumulated in front of the tyre thus adding to the existing resistance. Bekker (1960) proposed Eq. 2.10 in order to estimate the bulldozing resistance Rb of a wheel rolling on a soil with a soft upper layer. Furthermore, an additional Rt resistance must be accounted for, which represents the resistance caused by the tyre deformation. Although Rt is omitted in most of the cases by the majority of the researchers, since the level of soil deformation is incomparably larger than that of the tyre deformation, Bekker & Semonin (1975) proposed Eq. 2.11for the calculation of Rt. Thus, the total rolling resistance is given in Eq. 2.12.

$$R_b = \frac{b\sin(a+\varphi)}{2\sin\alpha\cos\varphi}\left[2zcK_c + \gamma z^2 K_\gamma\right] + \frac{\pi t^3\gamma(90-\varphi)}{540} + \frac{c\pi t^2}{180} + ct^2\tan\left(45+\varphi/2\right) \quad (2.10)$$

$$R_t = \left[3.581bD^2 p_{gr}\varepsilon(0.0349\alpha - \sin 2\alpha)\right] / \alpha(D - 2\delta_t) \quad (2.11)$$

$$R_{tot} = R_c + R_b + R_t \quad (2.12)$$

In addition, Bekker (1960) considered the response of a pneumatic tyre interacting with a soft soil in which case a flat contact patch approximation was used and tyre deflection was set to affect the rolling resistance due to compaction; following that, Eq. 2.13 was proposed.

$$R_c = \left(b \cdot p_{gr}^{\frac{n+1}{n}}\right) \Bigg/ \left[(n+1)\cdot\left(\frac{k_c}{b} + k_\varphi\right)^{\frac{1}{n}}\right] \quad (2.13)$$

Bekker introduced numerous vehicle performance metrics, such as Thrust (H) and Drawbar Pull (DP), based on which the locomotion of a wheel can be assessed. Reece observed that kc and kφ of Bekker's model have variable dimensions and their value is dependent on the exponent n; thus, the improved Reece " model I " was proposed (Reece, 1965; Onafenko & Reece, 1967). This model, as illustrated in Eq. 2.14, utilizes two parameters with constant dimensions of Pa and Pa/m respectively.

$$p = (k_1 + k_2 \cdot b)\cdot\left(\frac{z}{b}\right)^n \quad (2.14)$$

Following that, Reece (1965) based on, Terzaghi's (1944) and Meyerhofs's (1951) bearing capacity theories for plasticity, used soil mechanics to examine the soil failure underneath a strip. Reece proposed Eq. 2.15, which has the advantage of a sound

theoretical basis and two dimensionless moduli, k_c' and k_φ' (Reece model II). Furthermore, Reece noted that k_c' and k_φ' are invariant parameters for given soil conditions and do not depend on the dimensions of the plate. However, as it was highlighted by Upadhyaya et al. (1993), Reece's proposed equation provided improved predictions in terms of pressure-sinkage compared to Eq. 2.6, but k_c' and k_φ' remained parameters dependent on the dimensions of the plate. Furthermore, Wills (1963) and Lyasko (2010a) proved that there is no linear relation between *k* and *b*, since the influence of plate dimensions on k_c' *and* k_φ' was significant.

$$p = \left(ck_c' + \gamma b k_\varphi'\right)\left(z/b\right)^n \tag{2.15}$$

It is evident that for frictional sand, with significantly no cohesion, the first term in Eq. 2.15 will be omitted while for cohesive clay the second term will exhibit negligible levels. Reece's relationship is regarded to be a significant improvement in the field of Terramechanics and a major contribution to the overall tyre-soil interaction. Extensive experimental work conducted by Wills (1963) confirmed the value of Reece's Eq. 2.15 despite the fact that his model varied from Eq. 2.4 only in its response regarding the width *b*. By assessing Eq. 2.15 and by increasing plate width *b* loaded on cohesive clay, a linear increase in pressure is caused. On the contrary, in the case of frictional sand a variation in width *b* would yield a pressure proportional to b/b^n. Finally, it is apparent that significant soil parameters, such as soil moisture and hardpan depth (the thickness of the upper layer of the soil which can be deformed under loading) are not taken into consideration.

Yousesef & Ali (1982) proposed Eq. 2.16 where K_1 and K_2 are soil shear values and *a* and β are dimensionless geometrical constants. Equation 2.16 was validated with many penetration tests and following that, a direct comparison with Bekker's coefficients was found. It should be mentioned once more that the parameters used in Eq. 2.16 are non-invariant parameters, since direct correlation with Bekker's parameters exists, a fact which necessitates continuous measurements and in situ tests regarding the calculation of their values. It is also worth repeating that the above-stated pressure sinkage equations can represent mostly homogeneous terrains (no hardpan depth). For non-homogeneous terrains, different approaches are available to account for the inherent behavior of the different layers of the soils. An example of

such an expression is proposed by Wong (2001) with Eq. 2. 17; suitable for representing organic terrains (muskeg).

$$p = \left(K_1 + a \cdot B \cdot K_2\right) \cdot \beta^n \cdot \left(\frac{z}{B}\right)^n \tag{2.16}$$

$$p = k_p z + \frac{4 m_m z^2}{D_h} \tag{2.17}$$

All the equations mentioned in the current section contain non-invariant parameters, highly dependable on the physical characteristics of soils and applicable only to homogeneous terrains where a monotonic sinkage decrease with a ground pressure increase can be considered. Therefore, the values for these parameters (involved in all the above mathematical models) cannot be used beyond the soil conditions for which they have been measured without additional experimental testing.

2.2.3 Shear Stress-Shear Displacement

The second target relationship deals with the relationship between shear stress andshear displacement. Shear stress is applied on the terrain surface via a vehicle's running gear, causing in this way the development of thrust and its associated slip characteristics. The limits of soil strength prior to terrain failure are crucial for the development of such models. The following section reviews the most prevalent equations in the field of Terramechanics, used for capturing accurately the off road tyre-soil interaction. In this section the soil shear stress response is divided into three main categories. The word "hump" (peak) will be utilised with the same meaning as by Wong (2010).

The first category tends to capture the behavior of soils similar to sands, saturated clay and fresh snow. These soils do not exhibit a "hump" of maximum shear stress, Fig.2.3(a), thus by increasing the shear displacement *j*, the shear stress reaches a maximum value and remains constant with further increase in *j* . Janosi & Hanamoto (1961) proposed Eq. 2.18 in their effort to capture the response of the above stated category and remains until now one of the most widely used and adopted equations. In Eq. 2.18 the term in the first brackets represents the maximum shear stress; this mathematical relationship expresses the maximum shear strength of a soil specimen and was initially proposed by a French physicist, Charles Augustin de Coulomb, and further developed by a civil engineer, Christian Otto Mohr, leading to the well-

established final Mohr-Coulomb failure criterion. This postulates that the material will fail at a point where the shear stress reaches a maximum value. Furthermore, it should be noted that an incorrect value for the shear deformation modulus (K_x) may lead to incorrect shear stress values which in return will create an unrealistic and unreliable tyre-soil interaction model. Available experimental data in the literature (e.g. Wong, 2001) suggest that K_x is highly dependent on ground pressure; however, an accurate empirical and/or analytical relationship is yet to be determined. Nevertheless, Lyasko (2010c) having conducted numerous tests for tracked vehicles in various soil conditions stated that $K_x$is a function of the internal friction angle and for $15^0 \leq \varphi_0 \leq 40^0$ he proposed Eq. 2.19.

$$\tau(\theta) = \left(c + p(\theta) \cdot \tan\varphi\right)\left(1 - e^{-j_x / K_x}\right) \tag{2.18}$$

$$K_0 = 0.0039 \cdot \varphi_0 - 0.055 \tag{2.19}$$

Wong (1979) and Wong & Preston-Thomas (1983) proposed Eq. 2.20 for soils which exhibit a "hump" of maximum shear stress and then by further increasing the shear displacement the shear stress continuously decrease Fig.2.3 (b). Equation 2.20 was validated and close agreement with experimental results was observed.

$$\tau = (c + p\tan\varphi)(j / K_w)e^{(1-j/K_w)} \tag{2.20}$$

With regards to the third category of shear stress response, the shear stress exhibits a "hump" which then with further increase in the shear displacement, decreases to a constant value. This trend is illustrated in Fig.2.3(c). Oida (1979) based on work of Pokrovski's and of Kacigin and Guskov (1968), proposed a mathematical expression representative of this category, which was further modified and established in its final form by Wong (1983) as in Eq. 2.21. However, as Lyasko (2010d) states, K_r and K_w used in Eq. 2.20 and 2.21 are non-invariant soil plate parameters and can be determined only experimentally.

$$\tau = \left(c + p \cdot \tan\varphi\right) K_r \left\{1 + \left[1 / \left(K_r\left(1 - 1/e\right)\right) - 1\right] e^{(j/K_w)}\right\}\left(1 - e^{(1-j/K_w)}\right) \tag{2.21}$$

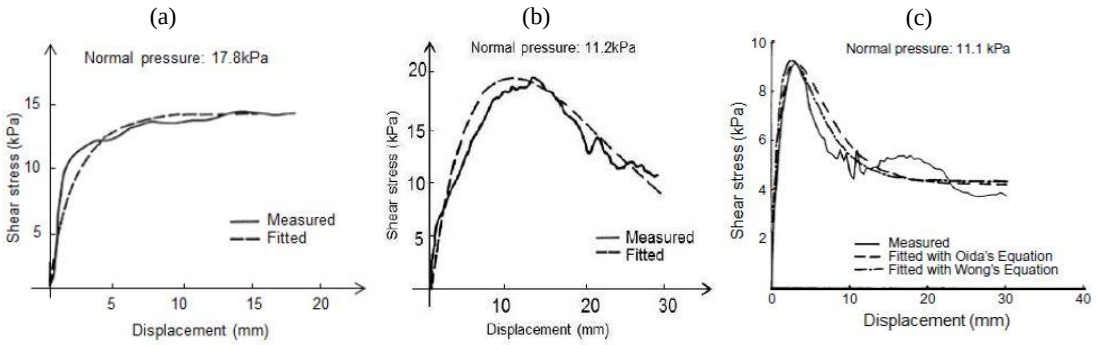

Figure 2.3. *Soils' Shear Stress response for three different types of soil, Wong(2001).*

It should be highlighted that changes in soil conditions (e.g. moisture content variation) influence tyre and consequently vehicle performance to a greater extent, compared to changes in tyre inflation/loading conditions and/or its size and dimensions (Upadhyaya et al., 1989). In addition, it can be argued that it is impossible to carry out identical tests under the same conditions (e.g. identical moisture content) due to a variety of soil parameters such as the fluctuation of the weather. Following that, an increase in the number of runs would be a prerequisite in terms of reducing the overall experimental error. Therefore, it should be noted that soil characteristics (e.g. shear strength) must be defined in an analytical manner, and not via empirical equations, with the use of invariant soil parameters such as, cohesion and internal friction angle.

Occasionally, use of the above empirical equations may lead to incorrect results and ambiguous answers regarding a vehicle's tranversability. For instance, having studied a rubber belted tractor on three different soils for three different belt widths, Zoz (1997) suggests that with the use of wider belts there is an increase in the traction performance of the tractor. This is contrary to the findings of a similar study, conducted by Bashford & Kocher (1999) which argues that the tyres with narrower belts provide the optimum traction performance. Yet, Upadhyaya et al. (2001), suggest that the belt width does not significantly affect the tractive performance of a vehicle. It is evident, that in the above-mentioned studies, use of an empirical relationship led to three different conclusions associated with the width of the belt, regarding the overall tractive performance of a vehicle on deformable soils; a fact which highlights the assertion that empirical equations may lead to erroneous or ambiguous findings.

2.3. Analytical Methods

The equations presented in the previous section are empirical relationships, containing non-invariant parameters. The latter must either be measured in situ or soil specimens must be removed and studied in the laboratory to ascertain their natural state and complete the calculations. These parameters, are case-depended (e.g. a small deviation in the soil's moisture content may cause a significant change on the non-invariant coefficients) and can only be determined experimentally using a load-sinkage curve fitting procedure. On the contrary, analytical methods have been developed; depending only on basic invariant parameters (soil principal characteristics) such as, the cohesion and the internal friction angle of the soil. However, a large percentage of the Terramechanics community (Wong, 2001) argue that the majority of analytical models developed so far are incapable of describing the tyre-soil interaction accurately, since both the tyre and the soil have inconsistent physical properties in the majority of the cases.

2.3.1 Pressure – Sinkage Equation

Kacigin & Guskov (1968) proposed one of the first analytical relationships, Eq. 2.22, using a hyperbolic function which correlates the vertical displacement with the normal pressure for plates loaded on deformable soils of an infinite hardpan depth. According to the authors k_z and B_i are independent of the dimensions of the plate and depend only on the type of the soil and its moisture content. However, the values for these parameters were given for certain types of soils, based on which Kacigin & Guskov (1968) performed the validation. Hence, for a different type of soil a test fitting procedure should be performed in order to determine k_z and B_i.

$$z = \frac{B_i}{k_z} \operatorname{arctanh}\left(\frac{p}{B_i}\right) \tag{2.22}$$

Furthermore, based on an analytical mathematical expression (Eq. 2.23) which relates the stress distribution under a plate contact area with the average ground pressure, Ageikin (1987) proposed Eq. 2.24. The latter mathematical relationship was the first to include directly invariant soil parameters which can be measured for any soil with the use of routine test methods of classical soil mechanics. However, a certain

limitation, presented and analytically explained by Lyasko (2010a), exists with this model, as the stresses under a plate, depend on the maximum pressure and not on the average ground pressure as was suggested by Eq. 2.23.

$$\sigma_z = \frac{J \cdot p}{1 + \left(\frac{z}{A_0 \cdot B} \right)^2} \tag{2.23}$$

$$p = \frac{2 \cdot E \cdot B_H \cdot z}{2 \cdot E \cdot z + \pi \cdot B_H \cdot A_o \cdot B \cdot J \cdot Q_1} \tag{2.24}$$

Hambleton & Drescher (2008, 2009) studied the indentation and rolling process of rigid wheels on cohesive and frictional soils. Hambleton et al., among other hypotheses, assumed that the soil can be represented with an elastic perfectly plastic material response described by the Mohr-Coulomb law and proposed the so-called inclinated force method and the inclined footing method. Limitations also exist within these methods since the assumption that the contact area can be considered equivalent to a flat rectangular surface with area determined purely by the vertical displacement of the soil may give rise to significant errors and deviations when it comes to modelling pneumatic tyres interacting with deformable terrains.

Lyasko in a series of papers (2010a, 2010b, 2010c, 2010d) based on Eq. 2.24, developed his own Load Sinkage Analytical (LSA) model, Eq. 2.25. The LSA model depends on four invariant soil physical parameters such as, cohesion, friction angle, soil unit weight and modulus of elasticity. The main advantage of Lyasko's proposed Eq. 2.25 lies with the fact that its parameters do not depend on plate shape, size or plate soil boundary conditions. In addition, Lyasko's Eq. 2.25 is developed and proposed based on experimental data (Lyasko & Kurdenkov, 1989)and on the consideration that the stresses developed under a plate are a function of the maximum ground pressure and not of the average ground pressure as considered by Ageikin, a fact which constitutes a significant improvement to the overall response of the model.

Lyasko's results were found to have a good correlation with experimental results (Lyasko, 2010a) and Eq. 2.25 is considered to be a significant improvement on the field of Terramechanics.

$$p = \frac{1}{\frac{D_1}{B_i} + \frac{D_2}{E \cdot z} \cdot \omega \cdot B \cdot \xi} \tag{2.25}$$

All the parameters involved in the expression of Eq. 2.25 are presented and explained to a great extent by Lyasko (2010a) and will be also presented in the following chapters. However, it should be noted that this model is extremely complex in terms of numerical calculations and requires a deep theoretical understanding and background in soil mechanics, so that it can be successfully implemented in tyre models. Certain difficulties and unknown areas also exist herein such as, the inability of current methods to accurately measure soil characteristics like the hardpan depth and/or the utilization of the dimensionless coefficient Y_0(defined in Lyasko, 2010a, as $Y_0=0.114+0.00317C_0$).

With regards to tyre modelling, the aforementioned pressure-sinkage equations (Eq. 2.3-2.25) are used in accordance with two basic assumptions. The first assumption has its foundation on the radial stress distribution along the circumference of the tyre (in order to analyze the radial stress into vertical and horizontal components) and the second assumption is based on that the latter stress is equal to the normal pressure beneath a rigid plate located at the same sinkage (described by Eq. 2.3-2.25).

2.3.2 Shear Stress – Shear Displacement

The dependency of empirical models on invariant soil parameters such as, the shear deformation modulus, can lead to an increased experimental monetary cost since there is the necessity for continuous experimental measurements. Furthermore, possible miscalculation of these parameters can inject inaccuraciesin the tyre-soil interaction model. In an attempt to overcome these inherent limitations, Guskov (1966) used Kacigin's & Guskov's (1968) Eq. 2.26. However, as it is stated by Ageikin (1987), although Eq. 2.26 provides numerical results in agreement with experimental measurements, parameters f_m, f_k *and* $k_\tau$depend on non-invariant parameters; therefore it can only be determined and used for a given soil condition.

$$\tau_j = f_m \cdot p \cdot \left[1 + \frac{f_k}{\cosh\left(\frac{j}{k_\tau} \right)} \right] \cdot \tanh\left(\frac{j}{k_\tau} \right) \tag{2.26}$$

Vasil'ev et al. (1969) proposed Eq. 2.27, originally developed by Pokrovsky (1937), in order to characterize the shearing behaviour of most soil types. In Eq. 2.27 by substituting $C_{1L}=0$, $C_{2L}=\tau_{max}$, $C_{3L}=0$, *and* $C_{4L}=1/K_0$ the shear stress response of soils which do not exhibit a "hump" of maximum shear stress, such as those illustrated in Fig.3a, can be successfully captured. With the aforementioned substitutions it can be easily noticed that Eq. 2.27 transforms into Eq. 2.18. Respective values for Pokrovsky's parameters C_{1L}, C_{2L}, C_{3L} and C_{4L} have been proposed for soils which exhibit a "hump" and can be found in Vasil'ev's et al. (1969) study.

$$\tau_j = \left[C_{1L} \cdot e^{(-C_{3L} \cdot j)} + C_{2L} \right] \cdot \left[1 - e^{(-C_{4L} \cdot j)} \right] \tag{2.27}$$

Regarding soils which do not exhibit a hump (Fig.3c) Vasil'ev et al. (1969) proposed $C_{1L}=b*\tau_p$, $C_{2L}=\tau_{max}$, $C_{3L}=a/K_1$and $C_{4L}=1/K_1$, where $K_1=K_0/0.266$. However, from the definition of the above-stated parameters used in Eq. 2.27, it is evident that C_1, $C_3$and K_1 are empirical parameters which must be acquired from experimental measurements and can be used only for the soil conditions existing during the experiment. Following that, Lyasko (2010d) further developed Eq. 2.27, by proposing analytical mathematical formulation for C_1, $C_3$and K_1 based on invariant soil parameters. The principal benefit of the latter work was the dependency of the proposed model (Lyasko, 2010d) on soil invariant parameters, such as bulk density, moisture content, hardpan location and number of dynamic penetrometer blows.

2.3.3 Tyre – Terrain Interaction Modelling

The necessity for efficient predictions of vehicle traction and fuel consumption has as a prerequisite, that of the development of accurate and realistic tyre models. These models will implement a suitable combination of the above-stated empirical and/or analytical relationships, responsible for the pressure-sinkage and shear stress-shear displacement relationships, so that the developed stress at the tyre – soil interface can be accurately calculated.

Wong& Reece (1966) experimentally observed that underneath a rigid rolling wheel interacting with soft terrain, two failure zones exist which join at the point where the maximum radial stress occurs (point at angle θ_M). Angle $\theta_M$represent the point where the two failure zones join each other and it is the point where the maximum radial stress occurs. The first failure zones (front region) is from the point where the wheel comes into contact with the soil up to angle θ_M, and the second zone (rear region) is from the point of θ_M up to the point where the wheel loses its contact with the ground. Following that, Wong & Reece (1967a) again considered rigid driven wheels interacting with soft sand, where driven wheel is defined as a wheel with non-zero torque acting at the axle. Based on their observations, they proposed Eq. 2.28 for the radial pressure acting on the tyre-soil interface, for the front and rear region respectively. Due to the difficulty of accurately determining angle θ_M, empirical Eq. 2.29 was proposed for the determination of the point with the maximum radial stress. Equation 2.28 lies on Reece's proposed relationship (Eq. 2.15) for the determination of the pressure distribution underneath a rigid plate, with the extra asset of substituting the sinkage [z] with the curvature of the wheel[$r(cos\theta - cos\theta_1)$] for the two distinct failure zones. In order to establish their complete tyre model, Janosi-Hanamoto's empirical Eq.2.18 was used for the shear stress-shear displacement response, where the shear displacement was defined as in Eq. 2.30.

$$\sigma(\theta)=\begin{cases}\left(c k_c^{'}+\gamma b k_\varphi^{'}\right)\left(\dfrac{r}{b}\right)^n\left(\cos\theta-\cos\theta_0\right)^n, \theta_M \le \theta < \theta_0 \\ \left(c k_c^{'}+\gamma b k_\varphi^{'}\right)\left(\dfrac{r}{b}\right)^n\left\{\cos\left[\theta_0-\left(\dfrac{\theta-\theta_r}{\theta_M-\theta_r}\right)\left(\theta_0-\theta_M\right)\right]-\cos\theta_0\right\}^n, \theta_r \le \theta < \theta_M\end{cases} \tag{2.28}$$

$$\frac{\theta_M}{\theta_1}=C_1+C_2 i \tag{2.29}$$

$$j(\theta)=R\cdot\left[\left(\theta_0-\theta\right)-(1-i)\cdot\left(\sin\theta_0-\sin\theta\right)\right] \tag{2.30}$$

Based on the current methodology, a great number of researchers established their own models for driven wheels, i.e. Ishigami (2008) and Ding et al. (2009). Although Eq.2.28 is regarded as a major contribution on the pressure sinkage behavior of a rolling wheel, the necessity of experimentally determining angle θ_M is still present. Furthermore, Wong & Reece (1967a) concluded that for rigid wheels rolling on sand

under the effect of an increasing slip, the maximum radial pressure shifts forward. In this aspect, rolling resistance and sinkage are considered to be functions of slip. Following that, Wong & Reece (1967b) conducted research on towed rigid wheels, where a towed wheel is defined as a wheel with zero torque acting on the axle. Similarly to the driven wheels, Eq. 2.28 was used for the definition of the radial pressure acting on the towed wheels interface. However, alternative approaches were used for the determination of the shear displacement – for the front and rear region – and the angle θ_M were Eq. 2.31 and Eq. 2.32 were used respectively. Experimental results published by Onafenko & Reece (1967) confirmed the validity of the above stated equations.

$$\tan\left(45-\frac{\varphi}{2}\right)=\frac{\cos\theta_M-\frac{1}{1+i}}{\sin\theta_M} \tag{2.31}$$

$$j(\theta)=\begin{cases} r\cdot\left\{(\theta_0-\theta)\cdot\left[1+K_U\cdot(1+i)\right]-(1+i)\cdot(\sin\theta_0-\sin\theta)\right\}, \theta_M\le\theta<\theta_1 \\ r\cdot\left[(\theta_M-\theta)-(1+i)\cdot(\sin\theta_M-\sin\theta)\right], \theta_r\le\theta<\theta_M \end{cases} \tag{2.32}$$

whereK_U is given by Eq. 2.33:

$$K_U=\frac{1}{(1+i)}\cdot\left[\frac{(1+i)\cdot(\sin\theta_0-\sin\theta_M)}{(\theta_0-\theta_M)}-1\right] \tag{2.33}$$

Gee-Clough (1976) conducted research on Eq.2.8 and its inherent weaknesses, such as neglecting skid sinkage, and proposed Eq. 2.34 for the determination of the rolling resistance due to compaction for a towed wheel. For purely cohesive soils the wheel skid – negative slip – can be determined by Eq. 2.35 and for purely frictional soils by Eq. 2.36.

On frictional soils – sand – good correlation has been achieved for both rolling resistance and sinkage compared to experimental results published by Wills et. al. (1965), while on cohesive soil – clay – the correlation was not as good due to the overestimation of the wheel skid.

$$R_c=\left[\frac{1}{(3-n)^{(2n+2)/(2n+1)}(n+1)\left(k_c+bk_\varphi\right)^{1/(2n+1)}}\left(\frac{3W}{\sqrt{d}}\right)^{(2n+2)/(2n+1)}\right]\cdot\frac{1}{(1+i)^{n/(2n+1)}} \tag{2.34}$$

$$i = \frac{\frac{\pi^2}{8} - \left(\frac{\theta_e}{2}\right)(\pi - \theta_e)}{\left(\frac{\pi}{2} - \theta_e\right)\cos\theta_e - (1 - \sin\theta_e)} - 1 \tag{2.35}$$

$$i = \frac{\sin\theta_e\left[\frac{\pi^2}{8} + 1 - \left(\frac{\theta_e}{2}\right)(\pi - \theta_e)\right] - 1}{\sin\theta_e\left[\left(\frac{\pi}{2} - \theta_e\right)\cos\theta_e + \frac{3}{2}\sin\theta_e - 1\right] - \frac{1}{2}} - 1 \tag{2.36}$$

Later, Hetherington & Littleton (1978) presented Eq. 2.37 for the rolling resistance of a towed rigid wheel rolling on a granular soil. With the use of the intersecting chord theorem of the circle, used for the derivation and discretization of the contact patch, and the assumption that the ultimate bearing stress of a cohesionless soil is given by$q_f = q_0 N_q$, Hetherington & Littleton (1978) established a novel approach for the measurement of the rolling resistance of a towed wheel. The primary advantage of the aforementioned relationship was the ability to predict the rolling resistance of any towed wheel as a function of the vertical load, the tyre geometry and two invariant soil parameters. However, certain limitations lay on Eq. 2.37 mainly due to the assumption that the ultimate bearing stress for a frictional soil is given by $q_f = q_0 N_q$; neglecting in such way the remainingTerzaghi's factors.

$$R_c = \left(2W^4 / bd^2 \gamma N_q\right)^{1/3} \tag{2.37}$$

El-Gawwad et. al. (1999a, 1999b) conducted research on the effect of straight lugs (1999a) and camber angle (1999b) on the rolling response of the tyres. Using Bekker's equation for the normal pressure and Janosi-Hanamoto's one for the shear stress, a novel multi-spoke tyre model was developed. Equation 2.38 was proposed for a treaded wheel and it was found that by adding lugs on the tyre circumference, an increase on the tractive and lateral forces is achieved compared to what occurs when a smooth tyre is used. Furthermore, it was noticed that by increasing the lug height there is a reduction on the tyre forces and moments.

$$p = \begin{cases} \left[\left(k_c / b\right) + k_\varphi\right] z_L^{\,n} \\ \left[\left(k_c / b\right) + k_\varphi\right] \cdot (z - h_L)^n \end{cases} \tag{2.38}$$

In addition, El-Gawwad et. al. (1999b) concluded that the effect of the camber angle can be significant on off road tyres performance and an increase in soil hardness can

lead to a reduction on the resulting tyre forces and moments. The outcomes and conclusions drawn from El-Gawwad's research are in agreement with indoor and outdoor experimental work carried out by Bhoopalam et. al. (2015a, 2015b). The latter, studied the effect of the vertical load, the inflation pressure, the toe angle, the camber angle and the temperature variation on a pneumatic tyre interacting with ice. Regarding Bhoopalam et al.'s (2015a) indoor testing, it was found that an increase in normal load was causing a reduction in the drawbar pull, while an increase in the drawbar pull was observed with a reduction in the inflation pressure. Furthermore, the important role of the tread pattern (lug effect) on increasing the friction forces was outlined for all conditions of vertical load and inflation pressure. However, on the outdoor testing (Bhoopalam et. al., 2015b) the variation of friction levels, as a function of normal load, was seen with an antithetical tendency for low slip conditions; while for high slip conditions the variation of the normal load had an insignificant impact on the tyre performance. Furthermore in the latter study, variation of the inflation pressure had an infinitesimal effect on the drawbar pull, whereas the significance of the tread pattern was highlighted in a similar manner with the indoor testing.

Nakajima (2003) based on the original work and the corresponding experimental measurements of Muro & Raymond (1980a, 1980b) developed an analytical model for longitudinal tyre traction estimations in snow. The main idea of the aforementioned model was the analysis of the total traction force, into four main components such as: i) braking force, ii) shear force resulting from the tread void pattern, iii) frictional force on the tyre snow interface and iv) digging effect of the tyre into the snow. Predictions from the analytical model were found in close agreement with experimental data from the literature. Liang et al. (2004), proposed a tyre model for the calculations of the longitudinal and lateral tyre forces, which was based on Bekker's model for the pressure sinkage correlation. For the lateral force generation, they considered two factors: i) lateral force generation due to soil shear strength and ii) extra contribution due to bulldozing force. Once more the forces proposed by the latter model are validated by experimental results published through the literature and good agreement was found. Most of the aforementioned models so far, are accurate for large diameter wheels, where the sinkage/diameter ratio is considered to be relatively small. However, for small wheels, the wheel diameter decreases, hence the

sinkage/diameter ratio increases and the overwhelming majority of the aforementioned models are no longer reliable.

Among the solutions targeted at flexible tyres, a first direction was given by Bekker (1960), who expressed the basic idea of the replacement of a deformable wheel by a larger substitute circle, as seen in Fig.2.4. Following that Harnisch et al. (2005) implemented the aforementioned idea and satisfactory results were obtained which were close to experimental data. The proposed model, named as AS^{2}TM (2005), constitutes one of the most complete and up-to-date tyre-soil interaction models, suitable for implementation in full vehicle dynamics. Attributes like the tread pattern, the inclusion of cornering forces, and the multi-pass effect, where a rear wheel rolls over an already deformed region created by the front wheel, can be fully captured and the numerical results can be further validated with experiments. The AS^{2}TM model utilizes Bekker's pressure sinkage equation and Janosi-Hanamoto's shear stress-shear displacement relationship.

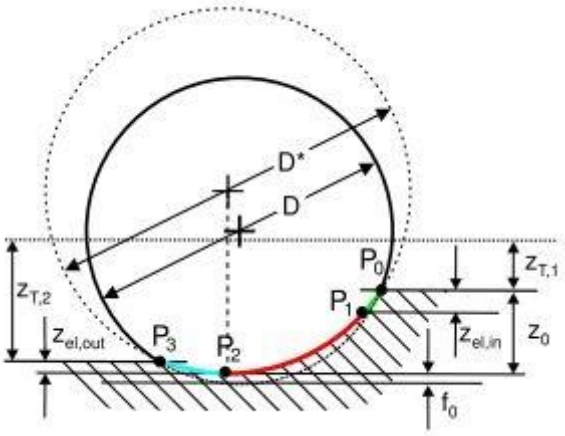

Figure 2.4.*Pneumatic Tyre on soft soil (Harnisch et al., 2005).*

Hambleton & Drescher (2008, 2009) conducted research on the interaction of a rigid wheel with a soft soil. They separated the latter interaction into indentation and rolling processes and, based on Meyerhof's (1951) formula for ultimate bearing stress, they proposed an analytical method which correlates the vertical load with the penetration of the wheel into the soil, given that the geometrical characteristics of the wheel and the soil material specifications are known parameters. The soil specimens were categorized on purely cohesive and purely frictional soils and the associated values for cohesion and friction angle where directly correlated with the width and the radius

of the wheel. Hence, the methodology proposed includes dimensionless soil parameters and corresponding experimental validation, which is an important asset for the current work as it will be shown in the process.

Ding et al. (2009) conducted rigorous research on some of the deficiencies of Bekker's and Wong-Reece's model for the calculation of the normal pressure underneath a rolling wheel. Following that, Ding et al. proposed Eq. 2.39 as an improved Bekker's soil sinkage exponent, where n_0 and $n_1$are experimentally identified soil parameters. The proposed model has been validated through a great number of experimental results for different wheel widths in a series of papers such as: i) Ding et al. (2010), ii) Ding et al. (2014) and iii) Ding et al. (2015) and remains to this date one of the most capable and accurate wheel-soil interacting models. In the latter study, Janosi-Hanamoto's equation is used for the tangential stress developed on the wheel-soil interface. The main attribute of this model is the ability to capture the dynamic sinkage of a wheel, overcoming in this way the great deficiencies and major drawbacks of the conventional Terramechanics models (e.g. Bekker, 1957), where, regardless of the increase in slip ratio, no digging effect of the wheel into the soil is observed. In particular, Ding et al. (2014) introduced a novel concept for characterizing the pressure-sinkage response, where by using a constant K_s and a variable exponent N high fidelity results were obtained. In the aforementioned research, five groups of soils were created according to the values of the sinkage exponent n such as: i) for $n \leq 1.1$ – the soil is referred as hardening terrain – ii) and iii) for $0.5 \leq n \leq 1.1$ – the soil is referred as elastic terrain – iv) for $0.3 \leq n \leq 0.5$ – as elastoplastic terrain – and v) for $n \leq 0.3$ – the terrain exhibited purely plastic behaviour. Following that, small rigid wheels were tested and slip and skid sinkages were reflected well and in accordance with experimental results.

$$\text{where,} \quad \begin{aligned} p &= K_s z^N \\ N &= n_0 + n_1 i \end{aligned} \tag{2.39}$$

The empirical or semi-empirical equations mentioned so far can accurately capture the dynamic response of large wheels. However, use of such an equation can lead to increased uncontrollable errors when small wheels are to be considered: Meirion-Griffith & Spenko (2010, 2011a) conducted experimental research on small rigid

wheels rolling on dry sand, calcium silicate and moist earth (i.e. soil with increased percentage of moisture). Following the analysis of the results, Eq. 2.40 was proposed and close agreement with experimental results was observed. Meirion-Griffith & Spenko (2011b) further developed the aforementioned model by taking into account the semi-elliptical distribution of normal pressure underneath a wheel and discretizing the total sinkage into static sinkage and dynamic sinkage where $z_{dynamic}$ was calculated with the use of Lyasko's (2010b) equation. Regarding their model, an approach similar to that proposed by Wong & Reece (1967a) was taken and Eq. 2.41 was developed. Numerical results were validated with experimental results obtained with the use of an unmanned ground vehicle, named IIT Robotics Laboratory's Variable Inertia Vehicle (VIV).

$$p = \hat{k} \cdot z^{\hat{n}} \cdot D^{\hat{m}} \tag{2.40}$$

$$p(\theta) = \begin{cases} \hat{k} \cdot r^{\hat{n}} \cdot D^{\hat{m}} \cdot \left(\cos\theta - \cos\theta_0\right)^{\hat{n}}, \theta_M \le \theta < \theta_0 \\ \hat{k} \cdot r^{\hat{n}} \cdot D^{\hat{m}} \cdot \left\{\cos\left[\theta_0 - \left(\frac{\theta - \theta_r}{\theta_M - \theta_r}\right)\left(\theta_0 - \theta_M\right)\right] - \cos\theta_0\right\}^{\hat{n}}, \theta_r \le \theta < \theta_M \end{cases} \tag{2.41}$$

In the majority of the tyre models presented so far, the width of the wheel is omitted from the equations, since a constant pressure distribution along the width is assumed. Meirion-Griffith & Spenko (2012, 2013) conducted thorough research, on various soils, on the pressure-sinkage dependency on the width of the wheel. It was shown (Meirion-Griffith & Spenko, 2012) that the width of the wheel had a significant effect on large wheels interacting with dilative soils – soils which face an increase in void ratio with an increase in pressure, e.g sand while for small wheels, this effect was insignificant. On the contrary, implementation of the same proposed semi-empirical equation on compactive soils revealed an increase in sinkage as the wheel width increases (Meirion-Griffith & Spenko, 2013). In an attempt to overcome the assumption of a constant pressure distribution along the width of the wheel, Merion-Griffith & Spenko (2014), proposed a width dependent model as in Eq. 2.42. The latter equation has been extensively validated with the use of a VIV (Variable Inertia Vehicle) for dilative soils, but its reliability on compactive soils is yet to be confirmed.

$$p = \hat{k} \cdot r^{\hat{n}} \cdot \left(\cos\theta - \cos\theta_0\right)^{\hat{n}} \cdot D^{\hat{m}} \cdot a^{Q\frac{D}{b}} \tag{2.42}$$

Iagnemma et al. (2011) developed the ARTEMIS model using MSC-Adams multi-body dynamics simulation software. The model includes Bekker's empirical pressure sinkage relationship along with Wong & Reece's proposed method for two regions of contact patch. Following that, Wong's shear displacement expression is used and the bulldozing force and grouser effect is modelled after Terzaghi's bearing capacity relationship, as in Eq. 2.43 and Eq. 2.44 respectively, where Eq. 2.44 is integrated along the tyre sidewall. Similar multi-body (MBS) dynamic models for rigid wheels exist within the literature, for instance, the wheel terrain interaction model (WTIM) integrated in Simulink proposed by Jia et al. (2012) and/or an analytical model integrated in Adams by Li & Schindler (2014). However, an extensive report of them will not be made, since the majority of them are based on the same procedure, with small variations on the use of alternative empirical equations.

$$F_b = \int_{-r\sin\theta_f}^{r\sin\theta_f} \left[\gamma N_\gamma f(x) + cN_c + qN_q\right] f(x)\,dx \tag{2.43}$$

$$F_g = b \cdot \left[\frac{1}{2}\gamma h_g^2 N_\varphi + 2ch_g\sqrt{N_\varphi}\right]\cos\alpha \tag{2.44}$$

Chan & Sandu (2008) proposed a tyre model based on the Mohr-Coulomb failure criterion and the theory of plastic equilibrium. Although the aforementioned model possesses a sound theoretical basis compared to other empirical equations, it does not always lead to accurate sinkage predictions. Following that, Senatore & Sandu (2011) established an enhanced off-road tyre model capable of accurately predicting the traction, the slip sinkage and the multi-pass effect. In this attempt of accurately estimating the slip sinkage dynamic interaction, the fundamental assumption proposed in Eq. 2.39 by Liang et al. (2009) is implemented in the model. A significant attribute of the models proposed by Prof. Sandu and her colleagues is the direct correlation of tyre properties, such as the inflation pressure and the carcass stiffness, with the vertical deformation of the tyre.

Gipser (2003) presented the FTire family, constituting of three models namely: i) the Flexible Ring model (FTire), ii) the Rigid Ring Model (RTire), and iii) the Finite element tyre model (FETire). FTire is one of the most widely used commercial tyre models suitable for integration in MBS like Adams. Modules capable of representing a detailed tread pattern and its degradation, along with tyre's thermal distribution have

been incorporated into the model, making it one of the most complete and up-to-date tyre models. RTire is a simplified tyre model sufficient for test rig and real time simulations. Moreover, the FETire forms a detailed complex finite element tyre model. With regards to off-road tyre-soil interaction, traditional regular roads have been enhanced with a pressure sinkage dependency, making this way the off-road tyre interaction with deformable terrains feasible (Taheri et al., 2015). In particular, for granular and brittle materials, Cosin/prm has been developed as an additional tool implemented in FTire. Cosin/prm is based on a discrete element method (DEM), where soil particles are represented as an assemblage of discrete elements – the following section will provide a more detailed description with regards to DEM.

Correlating detailed models with sound theoretical background and analytical approaches with MBS is not pertinent at the moment, since most of these models, necessitate increased computational cost. In this aspect, empirical or semi-empirical models are more suitable candidates for use in full vehicle dynamics. Following that, Terramechanics' community continues to spend sources and time on the development of high fidelity empirical model which would permit, low computational cost and small number of variables.

2.4. Numerical Methods

Tyres play a major role on the overall dynamic interaction between a vehicle and the ground surface, whether a stiff pavement or soft soil. There is an increasing demand to determine the bearing capacity of the various types of rolling surfaces, and thus to select the most suitable tyre in terms of a vehicle's energy efficiency and tread wear retardation, a fact which will enable a vehicle to have the optimum traction performance. To achieve this match early in the vehicle design phase, it is necessary that accurate numerical models should be developed, firstly of the tyre and of the road – either stiff or deformable – as well as of the static or dynamic interaction between them. This allows the investigation of the way in which the constitutive properties of the road affect the tyre performance. The degree in which the numerical simulations capture the real conditions is closely related to the technically correct and economical tyre design. Moreover, the complex nature of the phenomena involved in the tyre-road interaction usually cannot be sufficiently described by simpler analytical and/or

empirical solutions, and in many cases resorting to numerical simulations is the only effective alternative. As a result of the above, the open issue of interaction between tyres and roads has drawn much attention from various researchers, aiming at providing a thorough explanation of this complicated phenomenon.

Validating the dynamic properties of a tyre model prior to its implementation into a transient dynamic model is essential in terms of ensuring that the tyre model represents a realistic tyre and can be implemented on a range of conditions. These dynamic properties of a tyre can be evaluated by considering its natural frequencies, mode shapes and modal loss factors. Furthermore, the dynamic excitation of a rolling tyre comes primarily from three main sources: (a) road surface irregularities, potholes, bumps, (b) dynamic loads originating from various non-uniformities of the tyre, such as slight imbalances or asymmetric tread pattern designs, and (c) vehicle control inputs such as steering and braking. Consequently, the dynamic response of a tyre, is of high importance.

The majority of the analytical and semi-analytical off road tyre models found in the literature incorporate simplified tyre models (e.g. spring models) interacting with homogeneous deformable terrains. With the increase in computing power, the majority of the researchers have focused on developing three dimensional models that can deal with complicated wheel-soil systems. Different numerical methods have been developed, among others the finite element method (FEM), the discrete element method (DEM) and the smooth particle hydrodynamics method (SPH). Within the first two methods, parts are described as an assemblage of elements, either interconnected at certain nodes (FEM) or as discrete elements (DEM) whereas for the SPH method there is a centroid element which is affected by the surrounding elements within a certain radius. Combining these methods is the optimum way to ensure that their various assumptions and shortcomings are excluded, particularly those related to increased computational effort.

Despite the fact that most of the numerical methods developed so far are hampered by the same disadvantage, that of increased computational cost compared to real-time models, they still remain very promising methods capable of creating accurate and detailed tyre structures. Therefore, detailed numerical tyre models can be used for

parametric studies, where the sensitivity of various parameters such as the belt thickness, the cord orientation and the material properties can be further investigated. Regarding the modelling of the soil, numerical methods are also capable of integrating heterogeneous soil models such as granular and rocky terrains. For the above reasons, the off road tyre research community turned its interest towards the development of accurate and detailed numerical models which would permit an easier assessment of the tyre rolling response and consequently the vehicle behavior under various driving conditions.

2.4.1 Finite Element Method

Pioneers in the off road tyre FEM, Yong & Fattaah (1976) modelled the interaction of a two dimensional rigid wheel with a deformable terrain. In that study, the wheel was defined with prescribed displacements and the terrain was set to behave as a non-linear material and results indicated the ability of FEM to predict the soil deformation and traction response of the rolling wheel. Following that, Yong et al. (1978) incorporated a flexible tyre and replaced the prescribed displacements with a stepwise forward moving stress distribution, both in the normal and the shear directions. From another point of view and with regards to soil deformation, Pi (1988) investigated the high speed landing of an aircraft on a deformable terrain, where the latter was modelled as a viscoelastic material.

Work done by Aubel (1993) on rolling wheels interacting with deformable terrains, utilised the linear Drucker-Prager (DP) failure criterion in conjunction with the general contact algorithm available in the finite element program ABAQUS. An important limitation of that model was that DP was not able to represent soil compaction under hydrostatic pressure. Liu & Wong (1996), using another finite element program (MARC), developed a 2D (two dimensional) FEM rigid wheel-soil model and confirmed the validity of their findings with experimental results from various types of soils. Following that, Liu et al. (2000) investigated the rolling response of two 2D rigid wheels with different dimensions rolling on two different types of sand – Ottawa sand and loose sand – revealing a close agreement with experimental results. In their model, a modified critical state soil model was proposed along with a new nonlinear elastic law. However, it should be noted that 2D models

cannot capture the effects of slip angle and lateral compaction resistance of a steering wheel. Furthermore, Kölsch (2000) studied the dynamic behaviour of a vehicle rolling on soft soil, modelled as linear Drucker-Prager material, and found that the soil deformed by the front wheels can excite the rear wheels, triggering thus undesirable oscillations of the vehicle.

Shoop (2001) created a 3D model for tyre-terrain interaction, in which two material models were taken into account, namely a modified Drucker–Prager cap plasticity model and a critical-state, crushable foam model. Both models were considered adequate for the simulation of fresh snow, whereas only the cap model was used for modelling the sandy soil. Both rigid and deformable tyres were considered; however, it is worth mentioning again that a deformable tyre with a relatively high inflation pressure rolling on a relatively soft terrain can be assumed to behave as rigid. On their part, Seta et al. (2003) presented a combined tyre-soil model where the former was modelled with FEM and the latter with the Finite Volume Method (FVM). The simplification of an elasto-plastic deformable terrain was adopted in that study and three different failure criteria were utilised for the soil – (i) Mohr-Coulomb, (ii) Drucker-Prager Cap Plasticity and (iii) Cam-Clay – while the interaction between the tyre - Lagrangian part – and the soil – Eulerian part – was solved using coupling elements. It was shown that the later model can sufficiently capture the tire traction performance of a rolling wheel on snow. Nakashima and Oida (2004) proposed an alternative coupling method where the tyre was modelled with FEM and the soil with DEM. With regards to the indentation process of the wheel into the soil, good correlation with experimental results was accomplished.

Further research on pneumatic tyres rolling over deformable terrains was conducted by Fervers (2004) for two types of soils described by the Drucker–Prager cap plasticity model. The first soil type was set to have high cohesion and zero friction angle (cohesive), representative of wet loose loam while the second soil type was set to have low cohesion and high value of friction angle (frictional), representative of dry sand. It was shown that by reducing the inflation pressure the soil compaction on cohesive soils was also reduced while for the frictional terrains and for the deeper layers the soil compaction was approximately the same with a change in the inflation pressure. However, by reducing the inflation pressure and for a wheel rolling on

frictional terrains, the upper layers of the soil exhibited an increase in the soil compaction leading to completely different soil response compared to the cohesive soils. Chiroux et al. (2005) modelled the interaction of a rigid wheel with a deformable terrain using again the above mentioned soil constitutive model and observed that the soil tends to rebound after the passage of the wheel. Despite the rebound, the numerical results were found in close agreement with experimental data. The latter was also noticed by the author in the numerical results presented in the following sections. Hambleton & Drescher (2008, 2009) studied the response of a rigid wheel while being indented and rolling on deformable soil respectively. In that study, the soil was modelled as an elastic-perfectly plastic material and the effects of varying wheel aspect ratio on the sinkage and required horizontal force are demonstrated.

Lee (2009) studied the quasi-static indentation of a rectangular rigid plate and a pneumatic tyre on snow. It was found that the plate and the tyre yield a similar pressure-sinkage response on the soil, with the latter being discretized into three deformation zones; a small linear elastic zone, a propagating hardening plastic zone and a zone with a finite depth. Following that, Lee (2011) used the Drucker-Prager Cap plasticity constitutive model to represent snow and studied the tyre forces which are developed under various rolling conditions. It was observed that the sinkage – vertical displacement – of the tyre into the soil depends highly on the longitudinal and lateral slip. Furthermore, the deflection of the tyre was negligible compared to the deformation of the snow, a fact which justifies the use of a rigid wheel model. Xia (2011) in his proposed tyre-soil model neglected the tread pattern effect and defined the material behaviour of the tyre via a user subroutine. The soil was described by the failure criterion stated above and a parametric study on the effects of the inflation pressure, the angular velocity and the friction coefficient at the tyre soil interface was conducted. Choi et al. (2012) discussed a coupled Eulerian-Lagrangian model where the tyre was modelled as a moving Lagrangian part and the soil as a stationary Eulerian mesh through which the material flows. The effect of snow hardness, lug height and tread pattern on tyre's traction performance were evaluated. However, the validity of the proposed model has been justified only in a qualitative manner.

Li & Schindler (2012,2013,2014) developed a detailed agriculture FE model, considering the carcass, the belts, the bead and the rim. In that instance, the Neo-Hookean hyperelastic model was used for the material definition of the tyre and the Drucker-Prager Cap plasticity model for the soil. The effects of axle load and inflation pressure on soil compaction were studied and close agreement with experimental results was found.

The primary method employed for the numerical models presented in the following sections is the FE modelling technique. For this reason only a brief description has been provided on the other two methods (DEM and SPH). However, the ability of DEM and SPH methods to successfully capture physical phenomena which FEM are incapable of, should be clearly noted (e.g. granular and rocky terrains). Despite this, FEM was utilized in this thesis, since it is faster than the other two numerical methods in terms of computational effort required.

2.4.2 Discrete Element Method

The Finite Element Method has been developed in the scheme of homogeneous soils and continuum mediums. Hence, FEM would yield significant difficulties and errors in describing granular soils. Therefore, another method called Discrete (Distinct) Element Method (DEM) has been developed. More particularly, in DEM, soils are presented as an assemblage of a number of discrete elements. In its basic form, it assumes that each element has stiffness which is characterized by a spring constant k and possesses damping, characterized by a viscous damping coefficient η. It is also assumed that friction arises in the tangential direction and it is characterized by a friction coefficient μ. A more thorough mathematical formulation has been provided by Wong (2010). However, certain disadvantages within DEM have narrowed its wide applicability on terramechanics. For instance, the discretization of the elements is considered to be at least one magnitude bigger than the realistic size of the particles, in terms of maintaining the computational cost to the lowest possible level. Furthermore, there is a lack of generally accepted methods for determining the values of the model parameters which represent the behavior of the particles within the soil.

Given the disadvantages from each method, the terramechanics scientific community directed their interest towards a combined FEM-DEM method. This coupled method

would overcome most of the existing difficulties and would yield more accurate results. In this perspective, Nakashima & Oida (2004) developed a simple algorithm of a FE-DE coupled method. Following this, Nakashima et al. (2010) developed a 2D discrete element model of a lugged wheel for a lunar micro rover rolling on a sloped terrain. Among others, the study focused on the effect of the diameter of the wheel, the vertical load, the width and the lug height on the rolling response of the wheel. The validity of the proposed model was confirmed with experimental results conducted on lunar regolith simulant.

2.4.3 Smooth Particle Hydrodynamics

The majority of the models mentioned so far consider the soil as homogeneous. In reality, soils are composed of non-homogeneous particles with anisotropic properties. The optimum way to represent soils is through a large number of non-homogeneous free particles, capable of moving independently to each other, and also capable of interacting with particles in their vicinity. A fundamental limitation which led the scientific community towards the development of SPH as an alternative approach is the inherent sponge effect, in other words, the movement of a particular element which corresponds to the movement of all of the surrounding elements since they share common nodes in FEM soils. In the SPH method, an element movement is related to the movement of the elements in their vicinity without the need for common nodes (FEM method). Following that and contrary to FEM, no penetration issues, or solver errors can exist herein.

Dhillon et al. (2013) investigated soil models both through FEM and SPH methods. SPH is applied to many different soil models such as dry sand, clayey soil, heavy clay and lete sand. Following that, the numerical predictions from the latter method were compared with results obtained from FEA models and soil experimental measurements found in Wong (2001). In addition, Bekker's empirical pressure-sinkage model was utilised for the comparison between the experimental and the numerical results. Furthermore, a truck tyre model was created based on a standard heavy vehicle and the rolling response on various soils was investigated. It was found that FEA soils exhibit lower rolling resistance compared to the one obtained from the SPH modelling technique However, as the authors mention, it is possible that the material type chosen for the SPH soil, that is, an isotropic, elastic-plastic

hydrodynamic material, was not ideal for the illustration of the shear behavior of all soils and further investigation should be performed.

2.5. Discussion

It is evident that the majority of the empirical and semi-analytical models used in the literature in order to assess the performance of a vehicle interacting with an off-road terrain, incorporate inherent limitations, such as the utilization of non-invariant soil parameters. Inclusion of those parameters into semi-analytical mathematical models with regards to pressure-sinkage estimations would require a large number of experimental tests in order for those parameters to be determined, and therefore that would lead to an increased economic cost. In terms of numerical techniques, FE method was found to be the prevailing approach in tyre modelling compared to DEM and SPH. Based on the ability of creating detailed tyre structures, where the effect of various components – such as the cord orientation and the belt thickness – on the overall rolling response of the wheel would be assessed, this technique was established as the dominant tyre modelling method when real time simulations were not necessary.

One of the main objectives of this research was appointed towards the development of a novel analytical tyre model which would incorporate soil invariant parameters with principal effect on the behaviour of the soil, like the cohesion and the friction angle. In addition, the complexity of the numerical approach with regards to tyre-soil interaction necessitated the development of a robust modelling technique which would limit potential errors. Therefore, the aim on this area of research was the development of a solely numerical soil model and a solely numerical tyre model – along with their validation – prior to the development of the final tyre-terrain configuration.

Chapter 3

Finite Element Modelling of Soil

3.1. Introduction

In this chapter the importance of an accurate soil model prior to the final tyre – terrain model is addressed. In this aspect, a novel equation which correlates two different failure criteria, namely the MC and DP, has been developed and its response has been validated with experimental results from the literature. Subsequently, the indentation and the rolling interaction of a rigid wheel with a deformable terrain, being either cohesive or frictional, have been studied. The effects of the vertical load, the tread pattern, the width of the tyre and the dilation angle of the soil on the rolling behaviour of the wheel have been investigated.

Numerical modelling techniques such as FEM, DEM and SPH are frequently used to predict the behavior of vehicle moving on a deformable terrain. In this aspect, detailed tyre models have been developed, with and without tread pattern, and homogeneous and heterogeneous terrains have been considered. In the current study, purely cohesive and purely frictional terrains interacting with rigid and deformable tyres will be presented. In the first soil category, that of cohesive soils, the cohesion is set to a relatively large value and the friction angle to zero. However, for the second category, that of frictional soils, the cohesive value is set to a very small value, but not zero in order to avoid possible numerical inconsistencies, and the friction angle is set to a relatively large value. Various soil parameters, for instance, the dilation angle, will be included in the model and their effect on the overall driving response will be presented.

A complete FE tyre-soil interactive model constitutes a complex 3D – three dimensional – problem prone to errors and numerical instabilities. The necessity for a robust approach and methodology is apparent and will be extensively presented in the

following sections. Therefore, in the current thesis, two different FE models (i,ii) have been developed prior to the development of the complete FE tyre-soil model, in order to validate the separate components. The first (i) FE model – presented herein – deals with the modelling technique of the soil and the validity of its behaviour whereas the second model (ii) – presented in Chapter 4 – consists of the FE tyre model and its realistic response in terms of physical behavior. Once the reliability of the aforementioned models is confirmed, the final tyre-soil interactive FE model will be presented. The FE models presented in the following sections utilize the ABAQUS commercial software, v.6.13. It has to be highlighted that the use of Abaqus was requested by JLR and that since adaptive meshing techniques are used in the models, the analyses could not be run with use of parallel processing (e.g. a high performance HPC cluster).

Soil Modelling – Model (i)

In the literature, the Mohr-Coulomb and Drucker-Prager failure criteria were found to prevail for capturing the most important soil attributes, such as compaction, internal friction, cohesion etc (e.g. Shoop, 2001 & Xia, 2011). These two criteria are chosen for the representation of the soil and a novel mathematical formulation which correlates the response between these two, on triaxial compression and triaxial tension modes, is proposed. With regards to the Drucker & Prager (1952) constitutive failure criterion, both the linear and the non-linear (Cap plasticity) models have been considered.

3.2. Rigid Plate – Deformable Terrain

As a preliminary interactive model, the response of a rigid plate subjected to various normal and shear loading conditions was studied. The soil was defined via the non-linear Drucker Prager (Cap Plasticity) constitutive law and the respective material parameters were obtained from Li & Schindler (2013) as in Table 3.1 and Table 3.2. The soil was considered to be a Lagrangian part, defined as a homogeneous deformable terrain and the plate was modelled as rigid rectangular plate with the use of a rigid body constraint. An implicit integration was considered with the use of Abaqus/Standard and an explicit integration with the use of Abaqus/Explicit, v.6.13.

For the dynamic behavior of the soil two different steps were used; in the first step a normal load was applied on the plate until the steady state sinkage was reached, and in the second step a predefined longitudinal displacement was defined at the same reference point.

Young Modulus [MPa]	Poisson ratio	Cap eccentricity R_s	Initial Yield surface position
50.5	0.25	0.1	0.001
Soil cohesion [MPa]	Friction angle $\beta[^0]$	Transition surface radius α	Flow stress ratio K_r
0.113	14.56	0.03	1

***Table 3.1**. Soil material parameters for Drucker-Prager Cap Plasticity, (Li & Schindler, 2013)*

Yield Stress [MPa]	0.02	0.025	0.063	0.13	0.24	0.42	0.61	0.93	2.52
Volumetric Inelastic Strain	0	0.005	0.01	0.02	0.03	0.04	0.05	0.06	0.1

***Table 3.2**. Parameters for Soil Hardening Effect, (Li & Schindler, 2013)*

The model was comprised of a 3D Lagrangian deformable soil with dimensions of *0.5x0.5x0.25 (m)* and a 3D deformable rectangular plate with dimensions of *0.16x0.08x0.05 (m)*; both parts were modelled using continuum elements. The rigidity of the plate was achieved with the use of a rigid body constraint. The latter was enabled with the use of a reference point which was located on the top surface of the plate. Following that a coupling constraint was inserted where the nodes of the rectangular plate were coupled with the reference point. Hence, every dynamic condition applied on the reference point would be transmitted on the rectangular plate.

The capabilities of the Standard and the Explicit solver were studied and close agreement between their results was found. Since the deviation on the results – on average Von Mises stress - between the two solvers was less than 7% ($7.95 \cdot 10^{-4}$m and $7.14 \cdot 10^{-4}$m of vertical displacement for the Implicit and Explicit solvers respectively), the Explicit solver was chosen as the default solver in order to maintain the computational cost at the lowest possible level. In this regard reduced integration elements were used and a mesh sensitivity study was conducted; the final mesh size

was chosen so that the reduction of the element size in successive refinements of the mesh resulted in an increase or reduction in stress of lower than 5%.

The soil was partitioned appropriately, so that in the areas of interest (plate – soil interface) the mesh was finer but coarser towards the edges where there was no contact; the final mesh configuration of the road consisted of 32,000 elements with a bias configuration towards the edges, Fig.3.1. Contact between the plate and the soil for the tangential direction was governed by the Coulomb friction rule with friction coefficient equal to 1.0 and for the normal direction hard contact was specified. The base and the outer sidewalls of the soil were fully constrained in all three translational degrees of freedom and all the top surface of the soil was allowed to deform. Following SAE (2008) conventions the vertical movement of the plate was defined along the *y* axis, and the longitudinal movement along the *x* axis respectively, Fig.3.1.

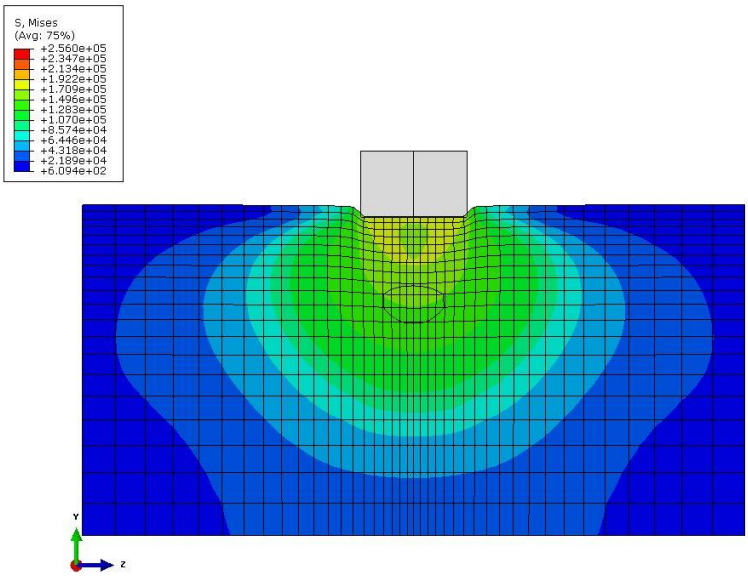

Figure 3.1. *Average Von Mises stress for a Treadless Rigid plate interacting with a deformable soil under 4kN of vertical load.*

The numerical results obtained from the FE model were validated with the analytical equation proposed by Gazetas (1983), Eq. 3.1. This mathematical relationship describes the equivalent static stiffness for a rectangular rigid foundation. The error between the aforementioned analytical solution and the FE model using the Explicit solver was less than 7% - $7.279 \cdot 10^{-4}$N/m and $6.78 \cdot 10^{-4}$N/m respectively. The FE soil model and the respective numerical results were therefore considered accurate.

$$k_G = \frac{4 \cdot G \cdot R_0}{1-\nu} \cdot J_v \ , \qquad \text{where } R_0 = \sqrt{\frac{2B \cdot 2L}{\pi}} \tag{3.1}$$

In Fig.3.2 and Fig.3.3, results from the dynamic interaction of the rectangular plate with the deformable terrain are presented. Fig.3.2 illustrates the response of the plate under the effect of an increasing normal pressure. It should be mentioned that all the empirical and semi-analytical equations presented in the previous section, such as Bekkers' pressure sinkage equation attempt to capture the pressure sinkage response of the soil in a similar manner with Fig.3.2. It is evident that by increasing the normal load on the plate the vertical displacement has a non-linear increase related to the bearing capacity of the soil. In Fig.3.3 the results of the shear stress developed on the plate – soil interface under a longitudinal displacement from 0-10mm and for various normal pressures are presented. It is noted that the deformable terrain exhibits a similar trend with the behaviour described by the Janosi-Hanamoto (1961) semi-empirical relationship for homogeneous soils which do not exhibit a peak on their shear stress response. Thereafter, it is evident that for an increase in the normal pressure there is an increase in the respective developed shear stress up to a certain maximum defined by the maximum strength of the soil. Finally, it is observed from the curve for vertical pressure 390 kPa that in this case the shear stress for small shear displacements is the lowest among the other cases which correspond to lower vertical pressures. This happens due to the fact that a relatively large vertical stress is applied through the plate to the soil. The latter, due to the increased distress, cannot develop large shear stresses until failure occurs. It is noted in Fig.3.3 that a plate subject to normal pressures of 312kPa and 390kPa exhibits a similar shear stress response which is limited by the shear strength of the soil.

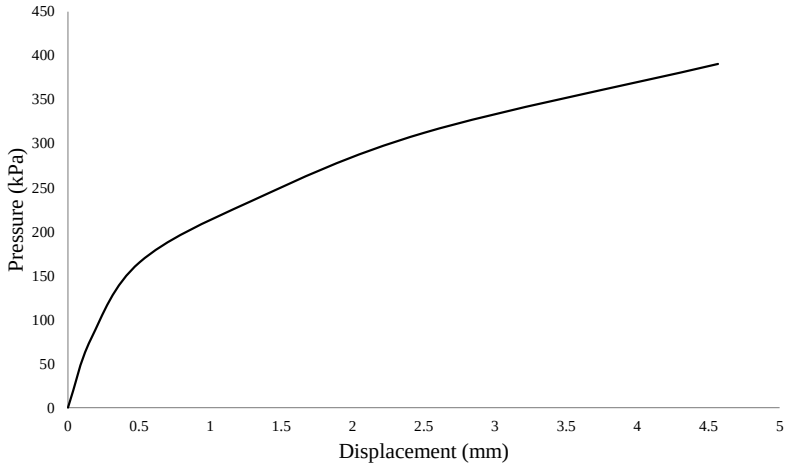

Figure 3.2. *Pressure Sinkage response of the soil for various normal pressures acting on the plate*

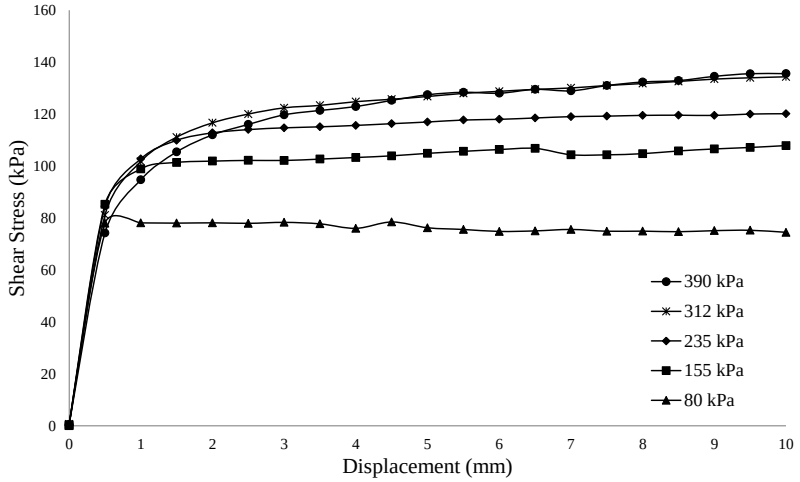

Figure 3.3. *Shear Stress developed on the plate – soil interface for various normal pressures acting on the plate.*

3.3. Constitutive material model

Due to the additional material properties which are required for the representation of the non-linear Drucker-Prager model – Cap Plasticity – like the softening-hardening behavior of the soil, the latter was assumed to behave as an elastic-perfectly plastic medium with linear response.Therefore, the linear Mohr-Coulomb (MC) and the linear Drucker-Prager (DP) failure criteria were chosen to represent the plastic deformation of the soil. Equations that correlate the friction angle and the cohesion between these two failure criteria already exist only for specific cases, for instance, triaxial compression or tension and plane stress/strain conditions. However, in the rolling motion of a wheel, the problem becomes essentially three dimensional, in which case the various principal stresses are diverse and consequently, there is not a unique way to match one model to another.

A novel relationship has been developed which can be used to approximately match the two constitutive models approximately. The yield surface for DP (Drucker & Prager, 1952) is given as:

$$F_{DP} = q - p\tan\beta - d \tag{3.2}$$

where,
$$q = \sqrt{(\sigma_1 - \sigma_2)^2 + (\sigma_2 - \sigma_3)^2 + (\sigma_3 - \sigma_1)^2} \tag{3.3}$$

$$p = -\frac{1}{3}(\sigma_1 + \sigma_2 + \sigma_3) \tag{3.4}$$

Finally the yield surface for DP can be written as in Eq. 3.4 and the respective relationship for MC can be presented as in Eq.3.5.

$$F_{DP} = \sqrt{(\sigma_1 - \sigma_2)^2 + (\sigma_2 - \sigma_3)^2 + (\sigma_3 - \sigma_1)^2} + \frac{1}{3}(\sigma_1 + \sigma_2 + \sigma_3)\tan\beta - d_{DP} \tag{3.5}$$

$$F_{MC} = (1 + \sin\varphi)\sigma_1 - (1 - \sin\varphi)\sigma_3 - 2c\cos\varphi \tag{3.6}$$

The vertical vectors on the DP and MC yield surfaces are presented in Eq.3.6 and Eq.3.7 respectively. By equating the components of each of these terms at an arbitrary principal stress state, Eq.3.8 – Eq. 3.10 are developed.

$$V_{DP} = \left(\frac{\partial F_{DP}}{\partial \sigma_1}, \frac{\partial F_{DP}}{\partial \sigma_2}, \frac{\partial F_{DP}}{\partial \sigma_3}\right) \Rightarrow$$

$$V_{DP} = \left(\frac{2\sigma_1 - \sigma_2 - \sigma_3}{q} + \frac{1}{3}\tan\beta, \frac{2\sigma_2 - \sigma_1 - \sigma_3}{q} + \frac{1}{3}\tan\beta, \frac{2\sigma_3 - \sigma_1 - \sigma_2}{q} + \frac{1}{3}\tan\beta\right) \tag{3.7}$$

$$V_{MC} = (1 + \sin\varphi, 0, -1 + \sin\varphi) \tag{3.8}$$

$$\frac{2\sigma_1 - \sigma_2 - \sigma_3}{q} + \frac{1}{3}\tan\beta = 1 + \sin\varphi \tag{3.9}$$

$$\frac{2\sigma_2 - \sigma_1 - \sigma_3}{q} + \frac{1}{3}\tan\beta = 0 \tag{3.10}$$

$$\frac{2\sigma_3 - \sigma_1 - \sigma_2}{q} + \frac{1}{3}\tan\beta = -1 + \sin\varphi \tag{3.11}$$

Following that, equating the two normal vectors of the DP and MC yield surfaces at an arbitrary principal stress state, the following relations result:

$$\beta = \arctan\left(2\sin\varphi\right) \tag{3.12}$$

In addition, by assuming that the hydrostatic pressure – a condition where $\sigma_1=\sigma_2=\sigma_3=p$ – is equal to zero and by equating relations 3.5 and 3.6 results in:

$$d_{DP} = 2c\cos\varphi \tag{3.13}$$

The two last equations are used to convert the MC parameters to DP parameters in ABAQUS and vice versa. The flow stress ratio in the DP model was set to unity which means that the yield stress in triaxial tension is equal to the yield stress in triaxial compression.

3.4. Rigid Wheel – Deformable Terrain

Following the preliminary soil models and their response under various loading effects in contact with a rectangular plate, a more complex and detailed deformable road model in contact with a rigid wheel was developed.

The indentation and the rolling response of a rigid wheel interacting with a deformable terrain are modelled numerically using the finite element code Abaqus 6.13. An explicit integration procedure was implemented by using Abaqus/Explicit, since it allows for a solution which is less computationally expensive and less susceptible to errors, for instance, due to excessive element distortion, especially when adaptive meshing rules are used. Symmetric geometrical conditions were assumed about a plane normal to the road; thus only one half of the model was created, for the purposes of reducing the computational requirements. For the indentation model, illustrated in Fig.3.4 a simplified rectangular block of soil was modelled and two steps were used; in the first step the gravity was applied on the soil, and in the second step a predefined sufficiently small velocity was applied on the wheel for a given time duration. Regarding the rolling wheel model, shown in Fig. 3.5, a more complex road geometry was utilised and again two steps were used, where in the first step the gravity was applied, whereas in the second step a vertical force and a horizontal velocity were imposed at the centre of the wheel at appropriate time instants, so that the wheel rotates with constant velocity under a constant vertical load over a given time period.

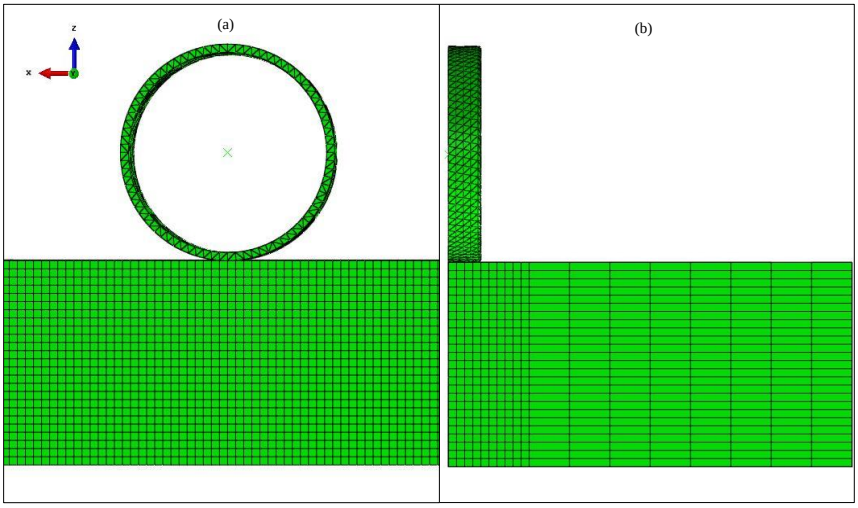

Figure 3.4. *Reference configuration used for the indentation process of a rigid wheel, (a) Front view and (b) Rightview.*

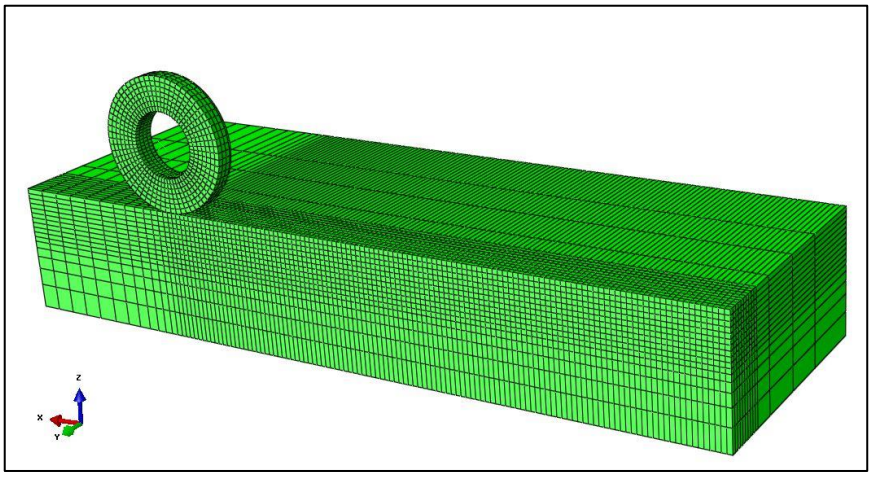

Figure 3.5. *Reference configuration of the rolling rigid wheel model*

For the indentation process, purely cohesive and purely frictional soils were studied, while for the rolling procedure and, specifically for the frictional soils, the cohesion was set sufficiently larger than zero to avoid numerical instabilities in the analysis. For the indentation, the cohesive soils were defined with $\varphi=0^{o}$ and dimensionless cohesion $c/\gamma gd=1.25$ whereas the frictional soil was defined with a friction angle of $\varphi=45^{o}$ and dimensionless cohesion $c/\gamma gd=1.25 \times 10^{-2}$. For the rolling process and for the cohesive soils, the soil parameters were identical to the indentation process while for the frictional/cohesive soils, the friction angle was $\varphi=45^{o}$ and the dimensionless cohesion was set to $c/\gamma gd=0.25$. For the indentation process, the wheel was predefined with a velocity boundary condition to move vertically until it reaches the maximum

dimensionless sinkage s/d=0.1. For the rolling process, a constant vertical force was applied on the wheel equal to $Q_v=1.9\gamma gbd^2$. The soil unit weight and the vertical force Q_v were applied with a ramp amplitude over a period of $60d(\rho/E)1/2$ and $180d(\rho/E)1/2$ respectively, and the total duration of the second step was equal to $1180d(\rho/E)1/2$. Concentrated mass equal to Q_v/g, as well as rotary inertia were added to the wheel centre. The rotary inertia was set to a nonzero number to avoid firstly numerical problems emerging from zero pivots. At the same time, the last was selected to be sufficiently small to avoid interference of the inertial behavior of the wheel with the steady state results.

The soil was considered to be homogeneous and the wheel was considered as rigid body through a rigid body constraint. The velocity of the wheel was kept steady during the rolling process and it was set to act instantaneously. The value of the velocity was chosen so that the wheel travels most of the soil region, which for the current configuration and for the applied time step was 0.137m/s. Contact between the wheel and the road for the tangential direction was governed by the Coulomb friction rule with friction coefficient equal to 0.5 and for the normal direction hard contact was specified. The base and the outer sidewalls of the soil were fully constrained in all three translational degrees of freedom. Symmetric boundary conditions were applied on the inner side of the road so that the symmetry of the half model can be utilised. The rigid wheel was coupled with a reference point (RP) located at its centre through a coupling constraint. The RP is set to have no lateral displacement, so that it can only move in the vertical and longitudinal directions.

During the modelling process of the indentation and the rolling procedure of the rigid wheel, high element distortion was observed on the soil, causing numerical errors and convergence instabilities. To avoid these issues the adaptive meshing (ALE) option offered in Abaqus/Explicit was utilised in the simulation. One remeshing sweep every 10 increments was performed, where the calculation of the new mesh is based on the priority of improving the aspect ratio of the elements. The ALE was set only on the region of the model where the fine mesh was located. Given that ALE cannot be implemented in a parallel processing mode, the size of the mesh was minimized, since otherwise high computational cost may occur. A mesh sensitivity study has been

performed and the final mesh size was chosen such so that the average Von Mises stress was not exhibiting a difference of 5% between two successive refinements.

Indentation Model

In the current section the wheel indentation process is being modelled as a quasi-static procedure and the results are validated with numerical and experimental results from the literature (Hambleton et al., 2008,2009). Results are being presented for two distinct soil categories; for cohesive soils as presented in Fig.3.6 and for frictional soils as illustrated in Fig.3.7. Both the MC and DP failure criteria are being used and a comparison of their behaviour is presented.

The soil constitutive model which gives the results presented in Figure 3.6. contains the shear type linear Drucker-Prager failure criterion with cohesion and shear stress limit equal to 26kPa. Moreover, the soil is cohesive with negligible friction angle, and this suggests that the von Mises stress that develops in the regions of the model that have yielded is equal to the cohesion of the DP model. Given that the friction angle of the DP constitutive model is zero, the yield criterion (according to section 23.3.1 in Abaqus Analysis User's Manual) is given by the relation:

$$F = t - d = 0 \tag{3.14}$$

where t is given by the relation:

$$t = \frac{1}{2} q \left[1 + \frac{1}{K} - \left(1 - \frac{1}{K} \right) \left(\frac{r}{q} \right)^3 \right] \tag{3.15}$$

In equation (3.15) q is the equivalent Mises stress, K is the ratio of the yield stress in triaxial tension to the yield stress in triaxial compression, which for the research conducted in the PhD thesis is set equal to unity, and r is the third invariant of deviatoric stress. For K=1, equation (3.15) gives:

$$t = q \tag{3.16}$$

Therefore, equation (3.14) becomes:

$$F = q - d = 0 \tag{3.17}$$

And from (3.17) it is concluded that the equivalent Mises stress will be equal to the Drucker-Prager cohesion of the material, in the regions of the model that have yielded. As a result of the aforementioned points, in the regions of the model where the von Mises stress has reached its maximum (nearly 26kPa) the soil has marginally

failed. In the other areas far from the wheel with stresses lower than the maximum, the failure state has not yet been reached. This situation is an idealized case of a cohesive soil since it is based on the assumption of categorizing the soil into two distinct groups – purely cohesive and purely frictional – and is merely intended to show the effect of the soil material properties.

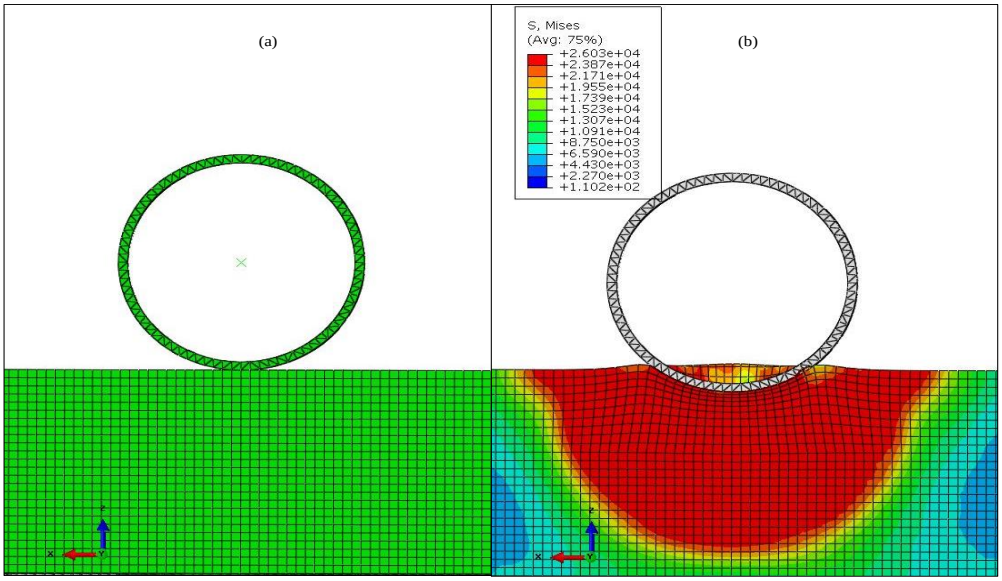

Figure 3.6. *Indentation model on cohesive soils: (a) Undeformed shape and (b) deformed shape*

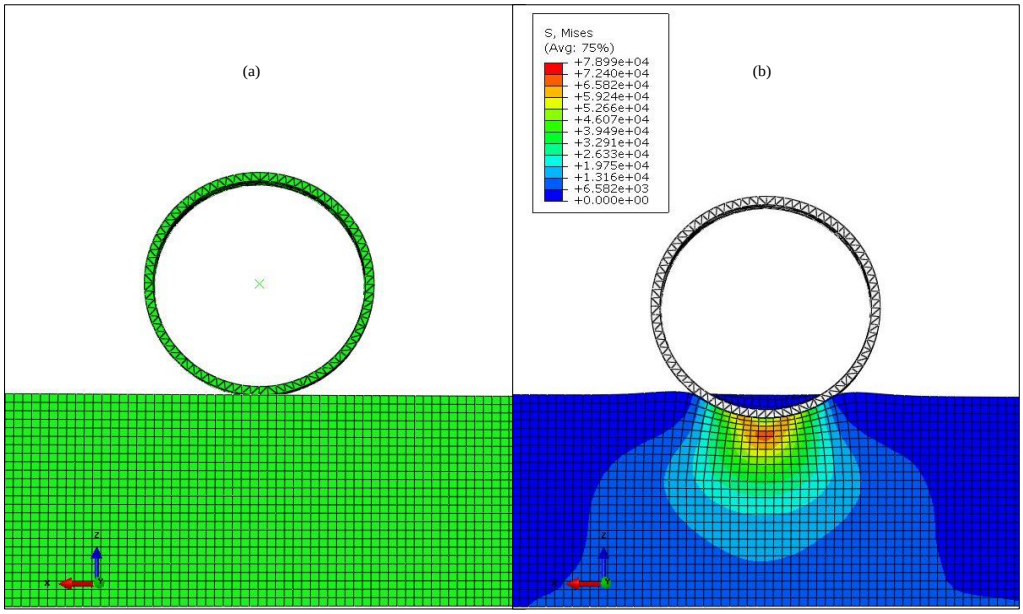

Figure 3.7. *Indentation model on frictional soils: (a) Undeformed shape and (b) deformed shape*

Figure 3.8 illustrates a comparison between the MC and DP failure criteria for the indentation of a rigid wheel with aspect ratio b/d=0.3 on a cohesive soil. It is obvious

that the numerical results associated to the DP criterion match closely to the corresponding results associated to the MC criterion as well as the numerical results found in Hambleton & Drescher (2008). The dimensionless vertical force that is required for a specific sinkage of the wheel increases monotonically for s/d<0.1; however, the rate of increase gradually decreases as sinkage increases. This fact can be attributed to local soil failure occurring as the wheel displaces downwards.

In Fig. 3.9 the corresponding results for a frictional soil are presented. In contrast to the cohesive soil, here the MC failure criterion seems to overestimate the expected results. However, the DP criterion bears a close match with the results from Hambleton & Drescher (2008). Additionally, in both Fig. 3.8 and Fig. 3.9 it was observed that for small values of vertical displacements there is good agreement between the results of the two types of soils, while with further increase in the sinkage the DP criterion seems to be more reliable. For the frictional soil a non-associated flow was used ($\varphi \neq \psi$), since frictional models with associated flow have proved to be unstable. The vertical force varies in a quasi-linear way with sinkage in the case of frictional soil.

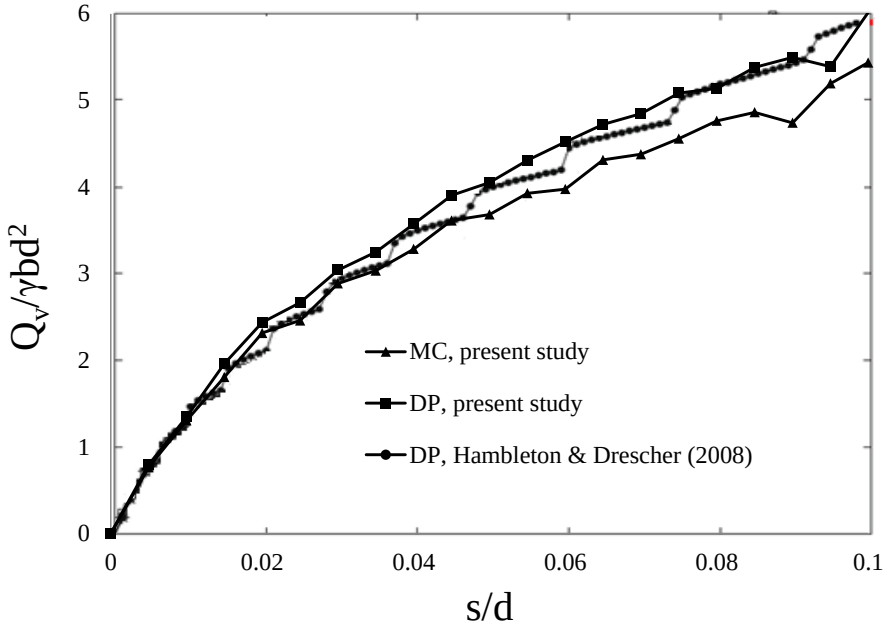

Figure 3.8. *Dimensionless vertical load versus dimensionless sinkage for wheel with b/d=0.3 on cohesive soil ($\varphi=0^o$, $\psi=0^o$ and $c/\gamma gd=1.25$).*

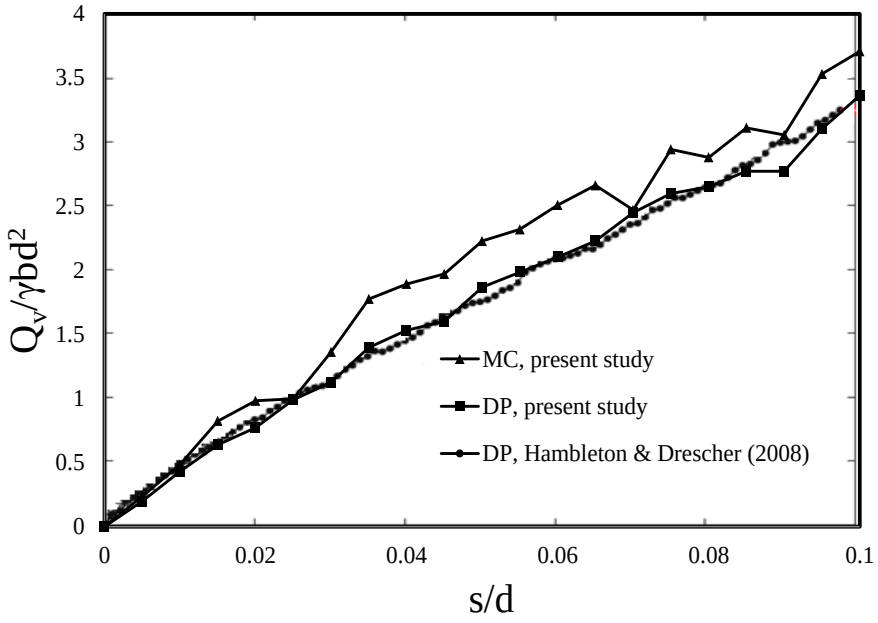

Figure 3.9. *Dimensionless vertical load versus dimensionless sinkage for wheel with b/d=0.3 on frictional soil ($\varphi=45^o$, $\psi=0^o$ and $c/\gamma gd=1.25 \times 10^{-2}$).*

Rolling Model

The model, presented in Fig.3.5 is comprised of a 3D rigid wheel with diameter *d* and width *b* and a deformable road. The road was 3.0 m in length, 0.5 m in height and 1.0 m in width. Different aspect ratios, that is, wheel width to wheel diameter ratio, were set in the model. As a starting case, a wheel with aspect ratio b/d=0.3 was created where b=0.16m and d=0.53m. Several different combinations of b and d which result in b/d=0.3 have been tested and the results presented the exact same response. The road was partitioned appropriately, so that in the areas closer to the surface and to the rolling region the mesh was finer; the mesh was coarser in regions far from the wheel. The wheel was located 0.74 m in front of the starting point of the soil so that sufficient space was left from the wheel contact patch for the development of stress and deformation. The inclusion of a fillet around the edges of the wheel was mandatory in order to avoid numerical instabilities caused by sharp edges on the circumference of the wheel. Rigid wheels with only lateral and only longitudinal tread patterns were considered. In the former case the lateral tread was added as an extra rigid part and by using a tie constraint, the elements of the tread were tied with the

elements of the wheel. In the latter case the longitudinal treads were created by "cutting" a region out of the initial rigid wheel.

Initially a treadless wheel was developed and different aspect ratios (b/d) were examined. Typical aspect ratios for wheel are within the limits of $0.1 \leq b/d \leq 0.5$; however, in this study, aiming to highlight the various trends in the results, wheels with a maximum of b/d=1.0 have been considered. Similar to the indentation results, the results of the rolling motion were validated with numerical and experimental results from the literature review (Hambleton & Drescher, 2009). Once the treadless rolling rigid wheel model was validated the lateral and longitudinal treads were added.

Figures 3.10 and 3.11 illustrate the sinkage of a wheel with aspect ratio of b/d=0.3 rolling on a cohesive soil and carrying various vertical loads. It is observed that the sinkage after the imposition of the vertical force increases until it reaches a peak value, a fact which occurs after the imposed vertical force has reached its maximum value. After this peak value, the sinkage decreases and eventually it stabilizes at a constant value, known as the steady-state sinkage. Steady-state response is presented for a simulation time of roughly 10 sec. It is apparent that 20% reduction in the vertical load – $Q_v/\gamma bd^2=2.4$ *to* $Q_v/\gamma bd^2=1.9$ – results in approximately 30% reduction of the dimensionless steady state sinkage, whereas for the low values of vertical load, a reduction of 50% – $Q_v/\gamma bd^2=1.25$ *to* $Q_v/\gamma bd^2=0.6$ – leads to a reduction of more than 70% in the dimensionless steady state sinkage of the wheel into the soil. In addition, it has to be noted that the time period required for the wheel to attain its steady-state response is a function of its size (aspect ratio) and the soil properties (density and elasticity modulus). Figure 3.11 shows the steady-state sinkage versus the applied vertical load at the wheel centre. Several simulations with different vertical loads were required in order to obtain the curve shown in Fig. 3.11. Good agreement is observed when the produced results are compared to numerical and experimental results from the literature (Hambleton & Drescher, 2009).

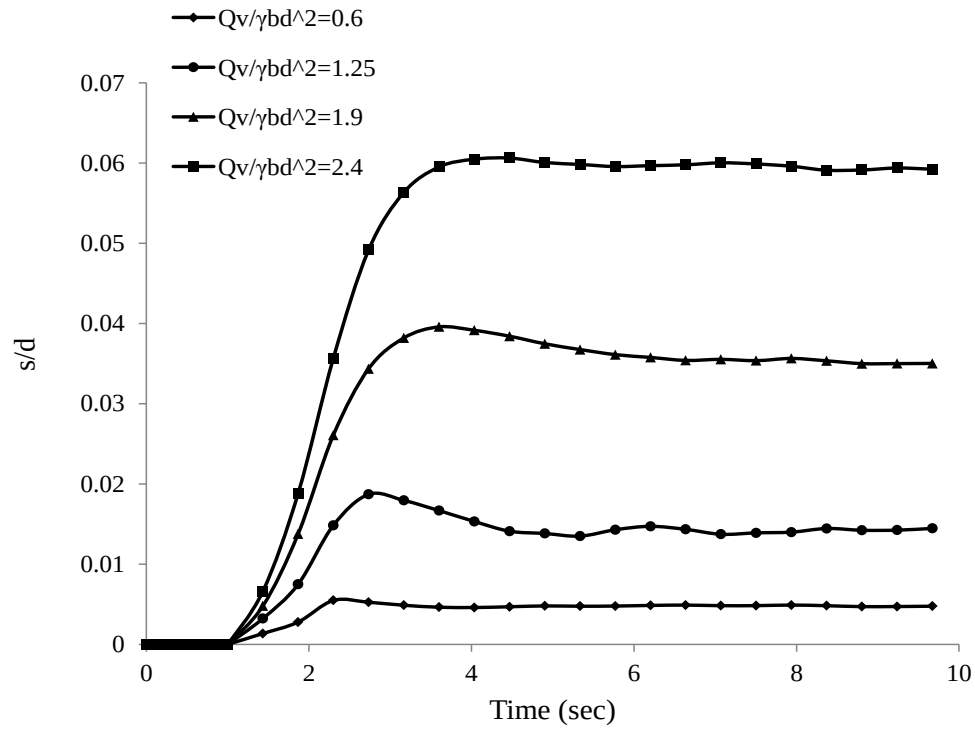

Figure 3.10.*Dimensionless sinkage versus time for wheel with b/d=0.3 (φ=0°, ψ=0°, c/γgd=1.25) and various values of dimensionless vertical load ($Q_v/\gamma bd^2$).*

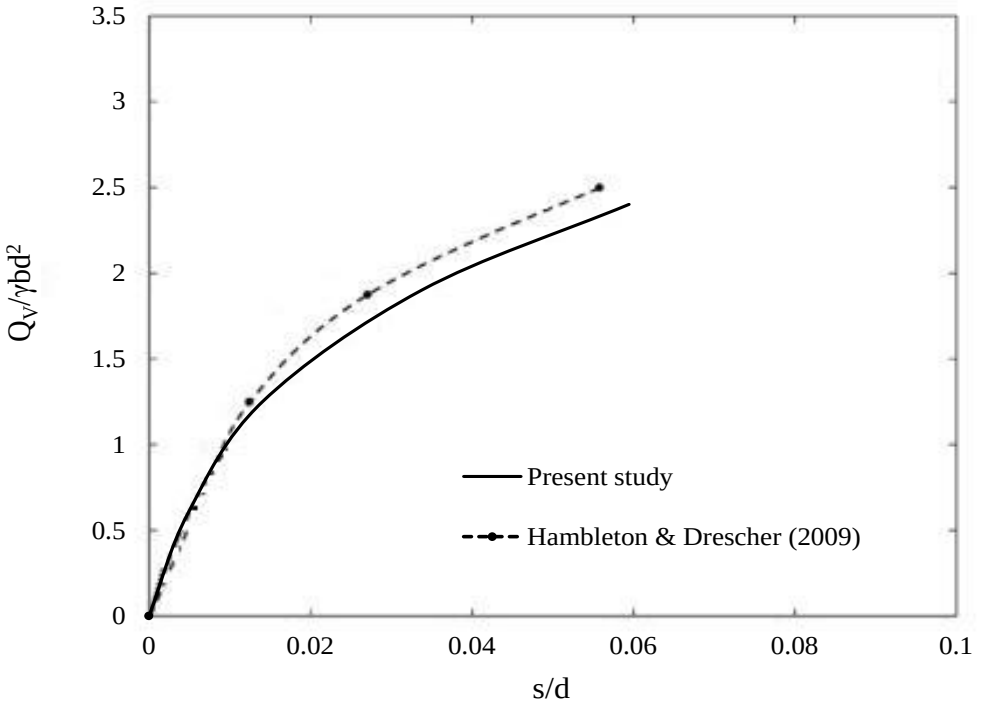

Figure 3.11.*Dimensionless steady-state sinkage for a wheel with aspect ratio b/d=0.3 (φ=0°, ψ=0° and c/γgd=1.25).*

Different aspect ratios of a treadless wheel have been considered for both cohesive and frictional soils and the results for sinkage (until a steady state response is obtained) are presented in Fig.3.12 and Fig.3.13 respectively. It is clearly shown that by increasing the aspect ratio of the wheel and for the same amount of vertical load the transient as well as the steady state vertical displacement are decreasing. Initially, an increase of 60% in the aspect ratio of the wheel – b/d=0.3 to b/d=0.5 – results in a decrease of more than 70% on the dimensionless steady state sinkage, whereas a further increase on the aspect ratio leads to a significantly lower rate of reduction of the steady state sinkage. Similar trends have been observed both for cohesive and frictional terrains.However, by increasing the aspect ratio the accumulation of soil in front of the wheel increases, thus causing an increase in the bulldozing rolling resistance. This bulldozing effect has been noticed in almost all rolling models considered in the current study, a typical case of which is shown in Fig.3.14, where the deformed geometry of the soil after its interaction with the wheel is shown. In addition, in the cases involving the rolling wheel on frictional soils the cohesion was set to a larger value than that in the cases where wheel indentation was modelled, in order to avoid any numerical instabilities during the solution. Although both the MC and the DP failure criteria have been used for modelling the rolling wheel response, only the results corresponding to the DP failure criterion are presented herein – the results related to the MC failure criterion are presented in the Appendix – since similar trends were observed in terms of dimensionless sinkage and rolling response.

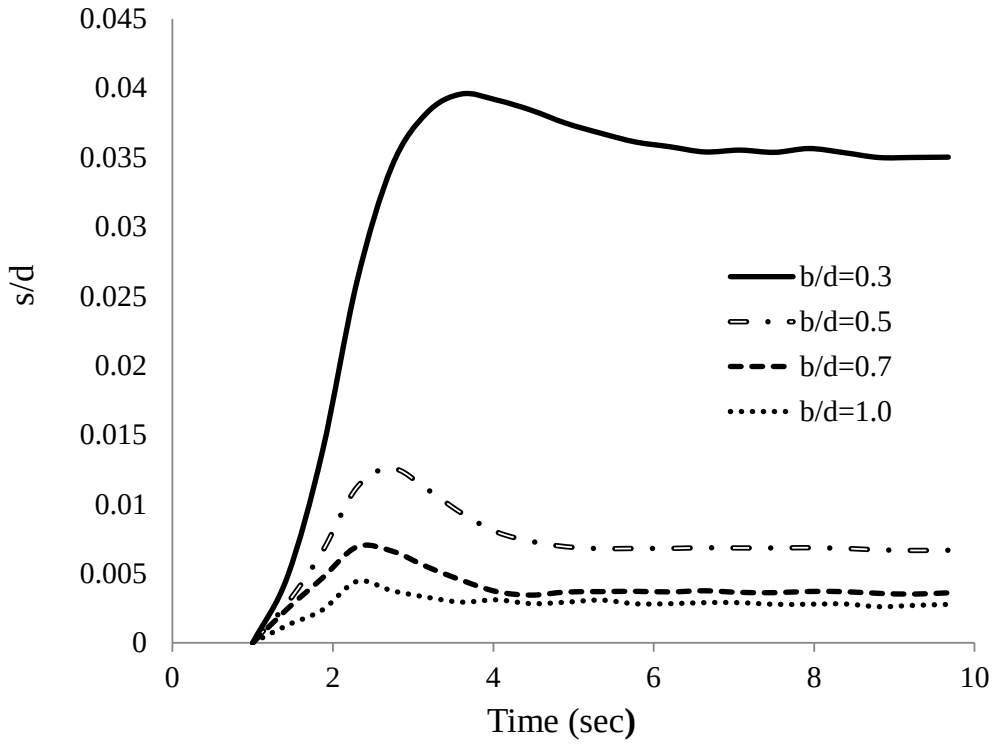

Figure 3.12.*Dimensionless sinkage versus time for various aspect ratios of the wheel rolling on soil with* $\varphi=0^o$, $\psi=0^o$ *and* $c/\gamma gd=1.25$ *and* $Q\sqrt{\gamma bd^2}=1.9$.

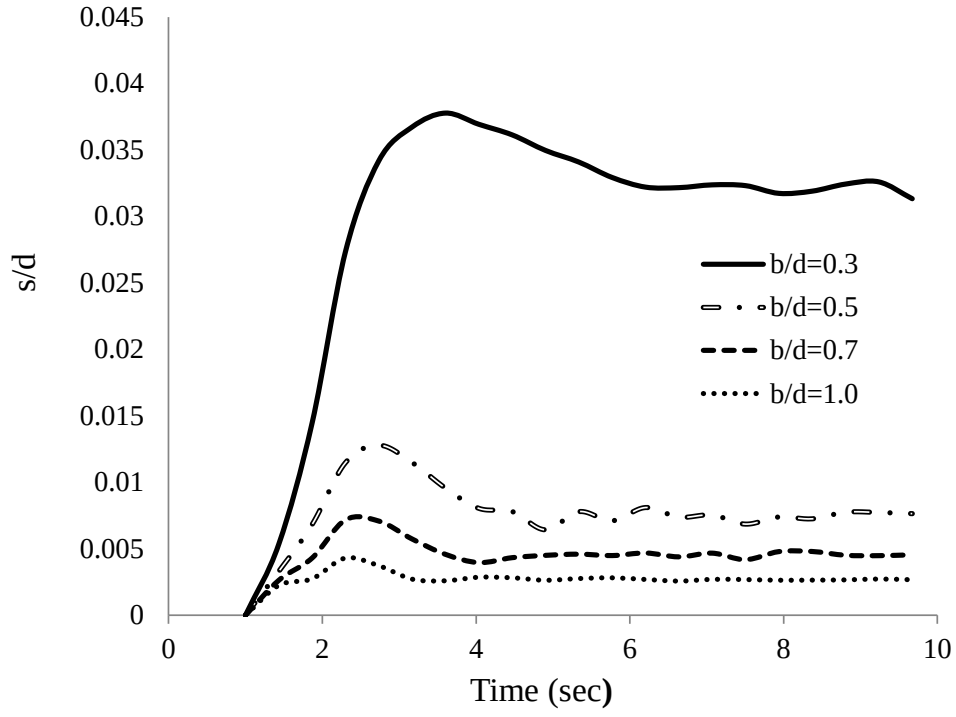

Figure 3.13.*Dimensionless sinkage versus time for various aspect ratios of the wheel rolling on soil with* $\varphi=45^o$, $\psi=0^o$ *and* $c/\gamma gd=0.25$ *and* $Q\sqrt{\gamma bd^2}=1.9$.

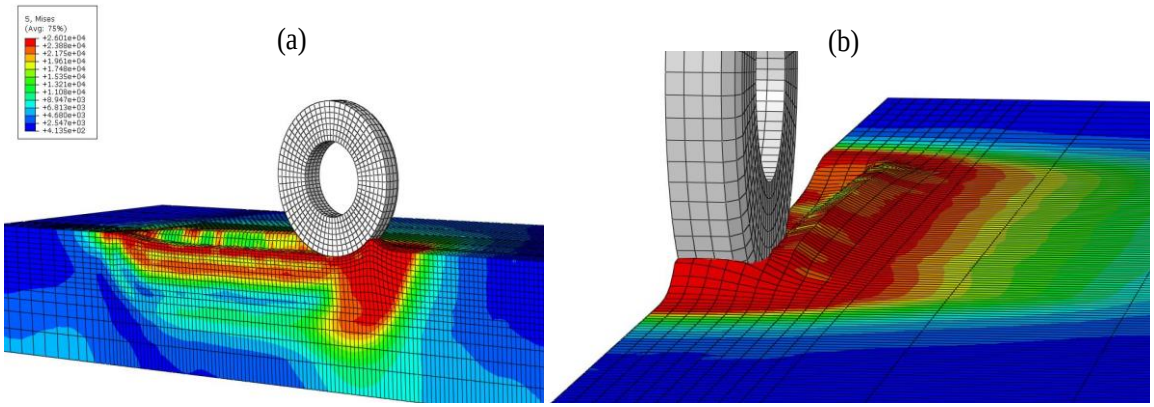

Figure 3.14.*Wheel with b/d=0.3 (φ=0°, ψ=0°, c/γgd=1.25, $Q_v/\gamma bd^2$=2.4): (a) Direction of travel from left to the right and (b) front view of the wheel.*

The effect of the dilation angle on the rolling response of the treadless wheel is demonstrated by examining various dilation angles for soil with non-associated flow for a frictional soil and the steady-state results are presented in Fig. 3.15. Similar analyses have been performed for purely cohesive soils, but due to numerical instabilities associated with the failure models involved, the dilation angle cannot be much larger than the friction angle, so their results are not presented here. It is apparent in Fig. 3.15 that under constant vertical load and with increasing dilation angle the bearing capacity of the soil increases, a fact which leads to lower sinkage of the wheel into the soil. More specifically, an increase of 10^oin the dilation angle leads to approximately 60% decrease in the dimensionless sinkage. This fact has been already noted in the literature; for example Borst & Vermeer (1984) carried out finite element analyses for strip and circular footings on a material with $\varphi=40^o$ and dilation angle $\psi=20^o$ and $\psi=40^o$, where it was found that the analysis with higher angle of dilation showed a peak bearing capacity about 13% higher than that with the lower dilation angle.

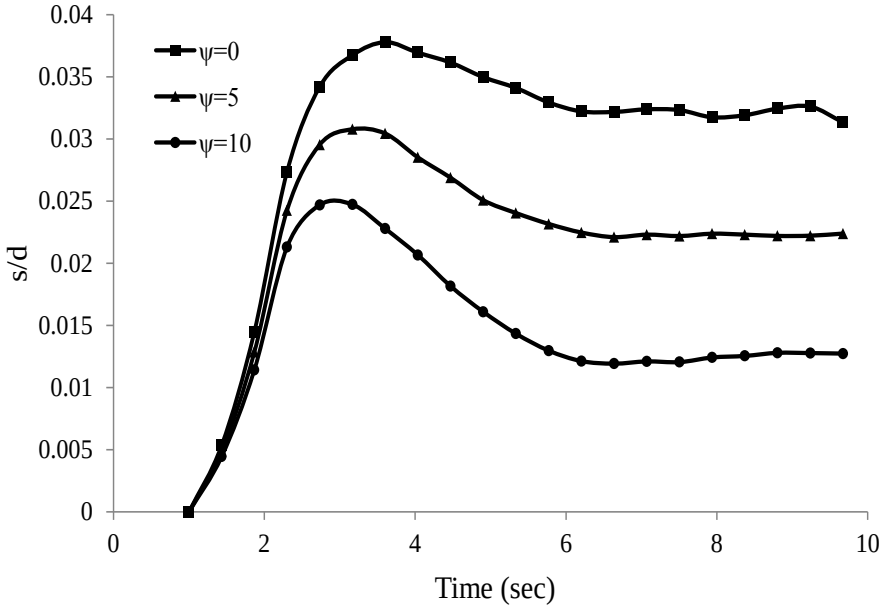

Figure 3.15. *Dimensionless sinkage versus time for a rolling wheel with b/d=0.3, φ=45°, c/γgd=0.25, $Q_v/\gamma bd^2$=1.9 for various values of the soil dilation angle (degrees).*

Except for the treadless wheel, longitudinally and laterally treaded wheels, illustrated in Fig.3.16 (a) and (b) respectively, were also considered in this study. An aspect ratio of b/d=0.5 was chosen for the treaded wheel, with b=0.27m and d=0.54m. Initially, longitudinal tread patterns were created on the wheel and the rolling behaviour on frictional and cohesive soils was examined. The longitudinal tread patterns are characterized by two quantities which have dimensions of length: (a) the depth of the tread, denoted by "*e*", and (b) the width of the tread contact area, denoted by "*t*". Therefore, a dimensionless longitudinal tread parameter can be defined by the ratio of the two aforementioned lengths, *e/t*. Fig. 3.17 presents the values of dimensionless horizontal displacement – along the axis of wheel motion – and dimensionless horizontal force developed on the wheel for a frictional soil and two different tread depths. For the given vertical load of $Q_v/\gamma bd^2$=1.9 the wheel with smaller ratio e/t requires higher horizontal force than the wheel with higher ratio e/t. This is caused mainly due to the fact that the longitudinal treads with higher e/t ratio are not totally filled with soil, thus producing a resultant traction force which is mainly caused by the tread area which comes in contact with the underlying soil. On the other hand the longitudinal treads with smaller *e/t* ratio are filled with soil to a higher degree than in the former case, a fact which results in higher traction at the wheel – soil contact area, since most of the contact patch interacts with the soil. By further increasing the vertical load the wheel with the larger *e/t* ratio requires even greater horizontal force

to move. Hence, the optimum *e/t* ratio for a tyre depends mainly on the soil properties and the respective bearing capacity factors. It is clear that for different vertical loads the steady state response of the wheel varies accordingly.

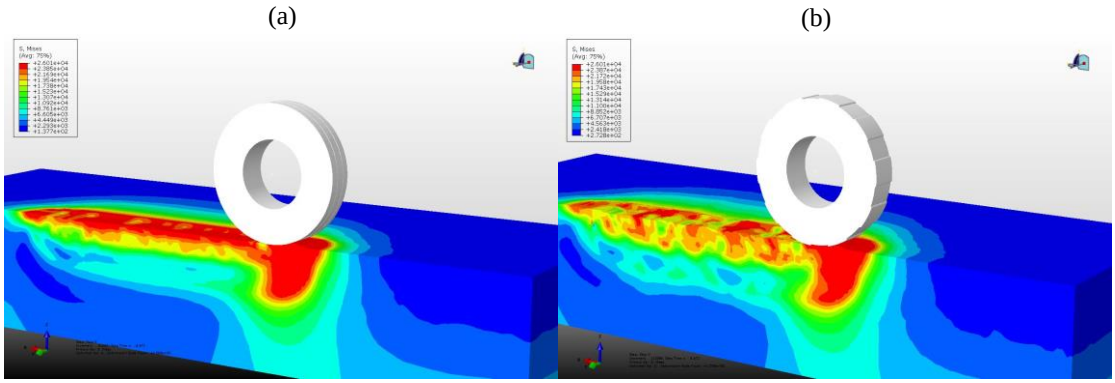

Figure 3.16. *Treaded wheel with b/d=0.3rolling on cohesive soil ($\varphi=0^o$, $\psi=0^o$, $c/\gamma gd=1.25$): (a) Purely longitudinal tread pattern and (b) purely lateral tread pattern.*

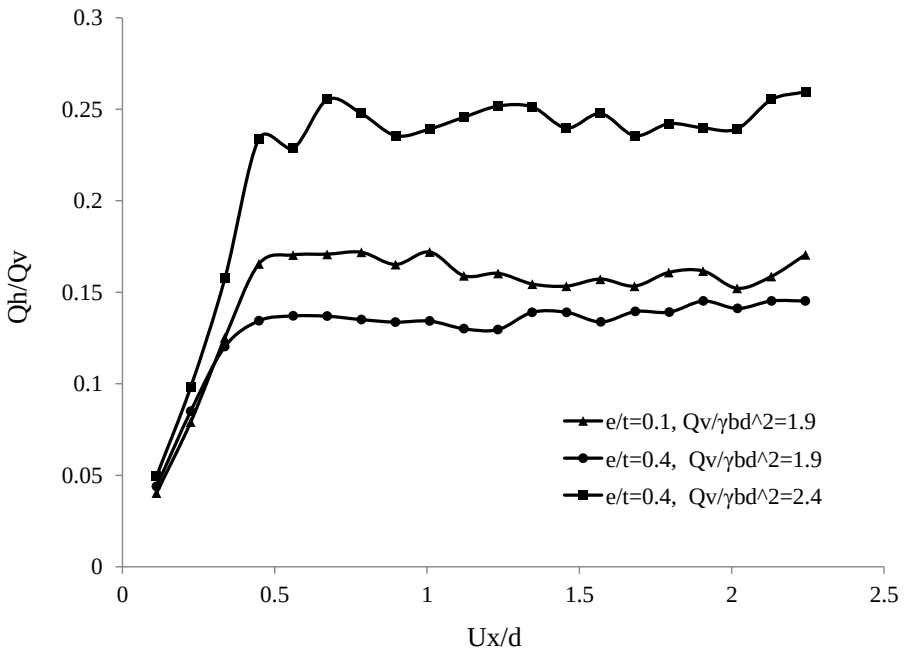

Figure 3.17. *Ratio of required horizontal force to vertical load of rolling wheel with b/d=0.5 ($\varphi=45^o$, $c/\gamma gd=0.25$) for various combinations of longitudinal tread ratio e/t and dimensionless vertical load $Q_v/\gamma bd^2$.*

Finally, a laterally treaded rolling wheel was considered with aspect ratio b/d=0.5. The lateral treads were described in an analogous manner with the longitudinal treads, by two parameters: (a) the ratio of the tread height – width of lug tip – to the wheel diameter (*e/d*) and (b) the ratio of the tread contact area to the wheel diameter (t/d). The lateral treads were created on the wheel perimeter based on their epicentral angle,

φ_d, which is the angle with vertex at the wheel centre and corresponding to the circular arc of the tread. Figure 3.18 illustrates the results from a rigid rolling laterally treaded wheel. Several analyses have been conducted and the slip ratio was measured for each model. The slip ratio has already been defined in the previous sections, and relates the translational motion of the wheel to its respective rotational motion. In an ideal case in which no slip occurs between the wheel and the soil, the slip ratio is zero by definition. Each curve in Fig. 3.18 corresponds to a constant t/d ratio, and describes the variation of the mean value of the slip ratio with the e/d ratio. It is observed that for constant *t/d* ratio of the wheel, as the *e/d* ratio increases, the mean slip ratio decreases, which is expected since for increasing *e/d* the lateral treads at the perimeter of the wheel control the overall rolling response to a higher degree. However, there is not any clear trend regarding the variation of *t/d*, for constant *e/d*, as it is observed that for the largest *t/d* ratio, the mean slip ratio remains in an intermediate range with respect to lower values of *t/d*.

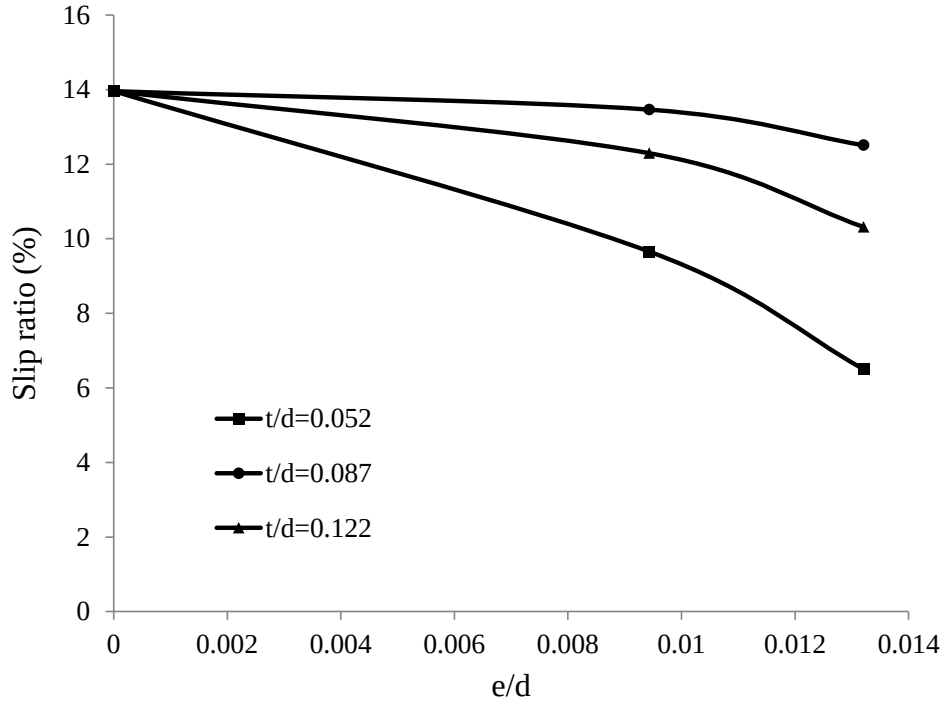

Figure 3.18. *Slip ratio of rolling laterally treaded wheel with b/d=0.5 (φ=45^o, ψ=0^o, c/γgd=0.25) versus the lateral tread ratio e/d for various lateral tread ratios t/d.*

3.5. Discussion

In this chapter, a novel relationship has been developed which correlates the MC and DP in both triaxial tensions and triaxial compressions and close agreement with experimental results from the literature has been observed. Furthermore, the indentation and the rolling response of a rigid wheel in cohesive and frictional soils have been presented and the effect of the aspect ratio on the quasi-static steady state response of the rolling wheel has been investigated. The majority of the figures are plotted in a dimensionless way so that future researchers can validate their soil models with the results presented herein.

It was found that the wheel sinkage decreases as its width increases with the same being observed for increasing dilation angle of the underlying soil. Additionally, the bulldozing effect has been successfully reproduced during the analyses – via the ALE method – and the effects of the longitudinal and lateral tread patterns on the wheel slip ratio have been investigated in a similar dimensionless manner. As the wheel actively interacts with the soil, at the wheel-soil interface the von Mises stress is equal to the limiting stress at failure, which decreases with depth as seen just under the wheel. However, in areas along which the wheel has already passed, under the region with the limiting stress, a region with lower stress appears and in the adjacent deeper area the stress increases again. This is due to remaining plastic deformation within the soil, which, interacting with elastic deformation, produces a residual stress redistribution. This effect can be understood by consideration of a beam subjected to a moment that results in stresses beyond its elastic limit. When withdrawing the moment it is possible to have a high stress in the surface which initially reduces in the inward to the beam direction but then increases again, creating an alternating effect (see. Fig 15.5, p 432 in Mechanics of Engineering Materials by Benham, PP., Crawford, RJ & Armstrong, CG, 1996, second edition, Addison Wesley Longman Limited).

In highly plastic soils the same mechanism of interaction between elastic and plastic deformation is related to the rebouncing effect, i.e. the decrease of the soil sinkage after the passage of the wheel, as elastic deformations attempt to reduce. In this attempt they interact with areas of permanent plastic deformation, resulting in a stress redistribution involving successive areas of high and low stress. This is something

that has also been observed in similar models in the literature (i.e. Chiroux et al., 2005).

Following the above-mentioned results, it can now be stated that a robust methodology has been created for the development of a realistic and reliable soil model with the use of dimensionless parameters. The results from the rigid wheel – soil interaction indicate the realistic physical response of the soil model and further confidence on the soil modelling technique arises from the validation of the outputs with the experimental and/or the numerical results from the literature. Thereafter, the next step, prior to the creation of the final tyre – soil configuration, would incorporate the development of a realistic and accurate pneumatic tyre model.

Chapter 4
Finite Element Modelling of Tyre

4.1. Introduction

A tyre constitutes the main link between the vehicle and the ground and is highly responsible for the driving behavior of the vehicle. The complex structure of the tyre illustrated in Fig.4.1, in conjunction with the multi-physical nature of its material, establishes it as one of the most complex components of the vehicle. It is evident that accurate and realistic tyre models must be developed prior to any tyre – terrain interaction. In the current chapter a FE tyre modelling methodology and respective validation techniques will be presented.

Numerical methods with the ability to create realistic and detailed tyre structures have been established as the dominant tool for tyre development within the tyre industry. The tyre modelling process commences with the acquisition of a 2D axisymmetric cross section, either experimentally or from the literature. In the current study, a P235/75R17 axisymmetric cross section was modelled in accordance with the FE tyre model presented by Wheeler et al. (2005). Then, the realistic response and the physical behaviour of the tyre were compared via two different methods. The first method consists of a Modal Analysis technique where the natural frequencies of the tyre are obtained numerically and validated with results from the literature; while in the second method the pneumatic tyre interacts with a rigid surface and a footprint analysis is carried out. This is performed in conjunction with a steady state transport investigation for a variety of inflation pressures.

Tyre Modelling – Model (ii)

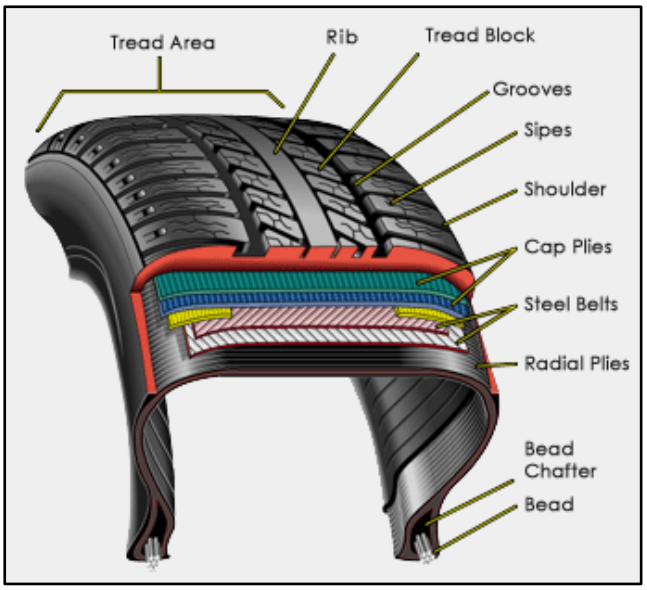

Figure 4.1. *Tyre Structure (http://www.avtogumi.com/en/polezno/struktura.php).*

With regards to the first method, Wheeler et al. (2005) performed FEM analyses to extract the various eigenmodes of a P235/75R17 tyre, which were further categorized in a way that describes best the meaning and value of the individual mode. The vibration modes of radial tyres on a fixed spindle are presented and the effect of the tyre components and their contribution to the mode shapes is investigated. Given the fact that in many cases the material properties and/or the geometry of a tyre are not explicitly known, an optimisation analysis was created and conducted in order to obtain a number of these properties, such as belt thickness, with the constraint that the eigenfrequencies are equal to the corresponding eigenfrequencies given by Wheeler et al. (2005). Modal analysis has been applied for tyres in many ways; for example Bolarinwa & Olatunbosun (2015) obtained the footprint of a tyre under purely vertical load, and performed a frequency analysis maintaining the contact conditions by applying an equivalent distributed vertical load, while the centre of the wheel was set free in all degrees of freedom. It was found that the boundary conditions on the tyre model can have large impact on its eigenmode response.

Regarding the second validation method, it is widely acknowledged that the contact conditions between the tyre and the road or terrain have a significant impact on the dynamic response of the former. One of the major factors which control the contact

conditions is the friction at the tyre-terrain interface. In many cases, it is ideal that the effects of friction be eliminated, in order to focus on the effect of the remaining parameters affecting the tyre-terrain interaction. The state at which there is no torque applied at the wheel centre – free rolling condition – is necessary to be obtained and is usually calculated by conducting a steady state transport analysis. Those types of analysis have been presented by Ghoreishy (2006) for a 175/70R14 steel-belted radial tyre under footprint load and close agreement with experimental data had been observed.

It is noted that the steady state transport analysis cannot incorporate any transient effects, such as tyres rolling over bumps, or other irregularities. After calculating the free rolling conditions for the pneumatic tyre of interest, the transient response can be modelled, where the tyre-terrain interaction mechanism can be explicitly observed. More specifically, Kamoulakos & Kao (1998) studied the transient dynamic response of a rolling tyre impacting a road imperfection (bump) represented by a cleat on a rotating drum using PAM-SHOCK and good correlation between the results and experimental data was found. In addition, Cho et al. (2005) studied the transient dynamic analysis of a 3D treaded tyre subject to impact loading originating from a rigid cleat. The numerical results were verified by experimental data, and a parametric analysis was conducted. It was shown that the horizontal and vertical forces at the tire axis were highly affected by the rolling speed, while the inflation pressure had a less important effect. Finally, Wei & Olatunbosun (2014) modelled the transient dynamic response of a pneumatic tyre rolling over obstacles of different heights and studied the effects of traveling velocity and height of the rectangular cleat. They concluded that the resonant amplitude of the reaction forces was influenced to a great extent by both speed and height of the obstacle.

In this study the transient dynamic response of a pneumatic tyre rolling over rigid and deformable terrains is examined. In the case of rigid terrains, steady state transport analyses are conducted in order to calculate the free rolling conditions of the tyre. Following that, the combinations of linear and angular velocities corresponding to the free rolling condition are used to study the dynamic behaviour of the tyre rolling over rigid surfaces with bumps. In addition to these, a parametric study of the dynamic interaction between a deformable tyre and soft cohesive soil, described by the linear DP constitutive model is examined for the cases of a towed and driven wheel.

4.2. Tyre Structure

The cross section of the tyre, P235/75R17, is shown in Fig. 4.2. The three main components of the tyre are the belt, the tread and the side wall. The belt region contains the reinforcement of the two belt layers (illustrated as Belt layer 1 & 2 in the Figure), and the reinforcement of the carcass. The latter extends over the belt region, covers the side walls and surrounds the bead. Both belt layers and the carcass are discretized with surface elements with twist (SMFGAX1). The rim is discretized with 2-node, linear links for axisymmetric planar geometries (RAX2) and the belt, bead, sidewall and tread regions are discretized with 4-node bi-linear, reduced integration elements with hourglass control (CGAX4R). The nodes of the surface elements of the carcass share the same nodes with those of the belt region elements, in order to avoid numerical instabilities which may arise during the analysis. It has to be noted that the rebar cross section areas of the belt and the carcass have been determined in a way that the dynamic properties of the tyre (in terms of its eigenmodes and eigenfrequencies) fit best with analogous results in the literature (Wheeler et al., 2005) a process which will be explained in greater detail in the following sections. Their values – $3.6482 \cdot 10^{-7}$ m^2 and $8.0113 \cdot 10^{-8}$ m^2 for the belts and the carcass respectively, obtained with the Modal Analysis method presented in the following sections – have a large impact on the overall configuration and dynamic response of the tyre under consideration and determine the quality of the results.

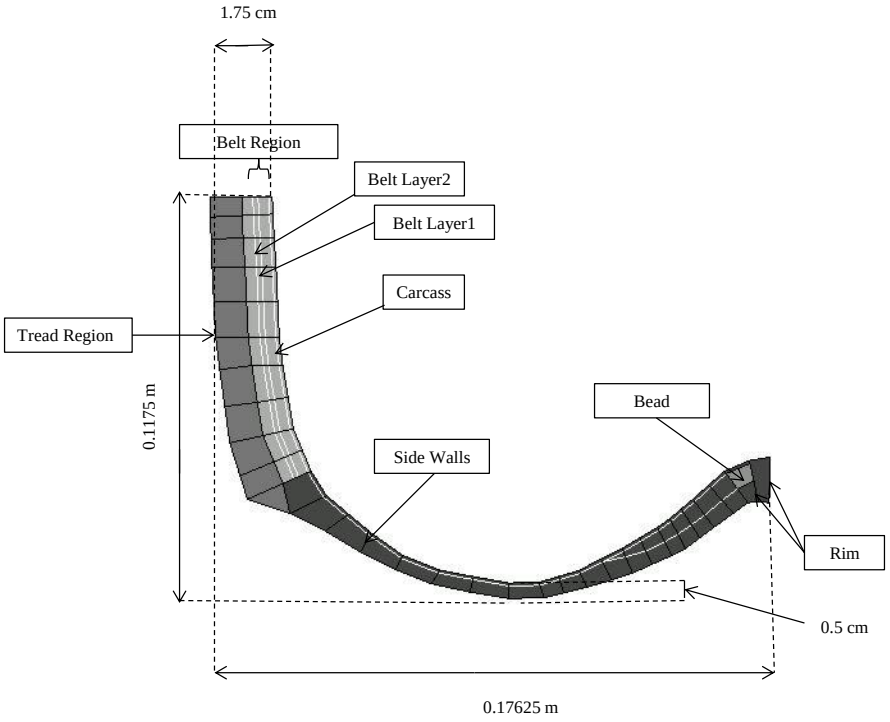

Figure 4.2.*Tyre half-cross section geometry.*

4.3. Material Model

The tread, the belt and the sidewall are modelled as hyperelastic materials with viscoelasticity, properties representative of rubber. The hyperelastic material is represented by the one-term polynomial strain energy potential, i.e. the Mooney–Rivlin model:

$$U = C_{10}(\bar{I}_1 - 3) + C_{01}(\bar{I}_2 - 3) + \frac{1}{D_1}(J^{el} - 1)^2 \quad (4.1)$$

where $C_{10}=10^6$Pa, $C_{01}=0$ and $D_1=5.085\cdot10^{-8}$Pa-1 and J^{el} is the elastic volume ratio. The material used for the rubber incorporates a time-domain viscoelastic component, defined using one-term Prony series parameters. The parameters used are $\overline{g_1}^p = 0.3, \overline{k_1}^p = 0, \tau_1 = 0.$. The belt and the carcass layers, which serve as reinforcement in the main body of the tyre and are discretised with surface finite elements (SMFGAX1) embedded into the latter, are modelled as linear elastic materials with properties $E_{belt}=1.722\cdot10^{11}$Pa, $E_{carcass}=9.87\cdot10^9$Pa and the Poisson ratio is equal to 0.3 for both materials. Also the densities are equal to 5900kg/m^3 and 1500kg/m^3 respectively. Finally, the density of the rubber material is equal to 1100kg/m^3.

The frequency analyses during the optimisation process were performed for a stationary and unloaded inflated tyre, a condition which implies that the strain rates at all cross sections of the tyre are zero, and therefore the tyre does not experience any specific strain rate (or small band of strain rates) during the calculation of its Mooney-Rivlin parameters. Consequently, the Mooney-Rivlin parameters are valid for zero strain rates. In addition, the instantaneous static elastic solutions were obtained for time-domain viscoelasticity; the analyses were not transient in the sense of the incorporation of time-dependent viscoelastic material behaviour in the static response. Since the expected eigenfrequencies (and stiffness) of the tyre are expected to be lower for a loaded tyre in rolling conditions, compared to a stationary unloaded tyre (see e.g. Dorfi et al. (2005)), the stiffness of the tyre model will be greater than the actual stiffness of the tyre under loading and rolling conditions, which is considered in this study. Furthermore, frequency analysis is a linear perturbation procedure about a base state of the model which has resulted from the last general nonlinear loading step. Apart from this, during the static analysis of the tyre for the inflation loading prior to eigenfrequency extraction, the instantaneous elastic solution is obtained for time-domain viscoelasticity and no transient static stress/displacement analysis with time-dependent material response was considered. This implies that, although viscoelasticity was defined for the rubber with one-term Prony series expansion of the shear and bulk relaxation moduli, rate-dependent effects, which are related to the strain rates present in the tyre model, were not taken into consideration. The only use of the viscoelastic parameters is to convert the hyperelastic material constants defining the long-term behavior into their corresponding instantaneous values, or vice-versa, which are then used for the calculation of the instantaneous static response.

4.4. Modal Analysis

Tyre vibration modes have been widely used over the years to represent dynamics in tyre models. The dynamic response of tyre models has been studied analytically, experimentally or semi-empirically, and numerically, however due to the limitations of the analytical and experimental studies, numerous researchers in the literature employ numerical – often finite element – models, which can simulate complex geometries as well as material, geometric and boundary nonlinearities. In this study,

the effect of the various parameters on the tyre response is incorporated into an optimisation procedure, which ultimately determines the optimum values of these parameters, in order to minimise the error between the numerical model and the available data. Relevant studies about tyre dynamics, as well as optimisation procedures are mentioned in the following section.

Experimental studies about the eigenmodes analysis of tyres have been performed by Bandel & Monguzzi (1983), Scavuzzo et al. (1993) and Matsuoka & Okuma (2002). More specifically, within the work conducted by Scavuzzo et al. (1993) the dynamic response of the vehicle in terms of accelerations was monitored at the wheel axis and the passenger compartment. The tyre vibration modes were identified from the peaks in the response. Bandel & Monguzzi (1983) developed a lumped parameter model to study the behaviour of a tyre running on a road surface with irregularities characterized by short wave-length spectrum components. However, the parameters of the lumped model are given by empirical relations, which have resulted from an experimental methodology. Matsuoka & Okuma (2002) presented an experimental modal parameter estimation method, in which the frequency response function (FRF) of a tyre is decomposed into the components of individual modes.

The analytical models developed for the estimation of the eigenproperties of a tyre, range from simple mass/spring systems to various forms of idealized, spring supported, and flexible rings. Representative studies are these conducted by Vinesse (1996) where a rotating and vibrating tyre coupled at its spindle to a secondary structure is simulated. A model of a membrane on an elastic foundation is used for the description of the vibration of a rolling tyre, as well as models for the calculation of the forces at the spindle of a tyre rolling over a small cleat. Following that, Molisani (2004), modelled the tyre as a shell structure in contact with the road surface. The contact patch is simulated as a prescribed deformation, and the coupled tyre-cavity governing equation of motion is solved analytically to obtain the tyre structural and acoustic responses.

With regards to the numerical studies on modal analysis, in work conducted by Wheeler et al. (2005) the vibration modes of radial tyres on a fixed spindle can be observed and the effect of the tyre components and their contribution to the mode shapes is investigated. The corresponding tyre model under rolling conditions was

considered by Dorfi et al.(2005) and it was shown that non-rolling tyre models are inferior to their rolling counterparts, as they do not take into account the proper kinematics. In a work directed by Chatterjee & Ranjan (2012), the finite element commercial software ANSYS was used to study the effects of the inflation pressure, the ply angle, the tread pattern and the thickness of the belt on the natural frequencies of the tyre. A basic assumption in this study was that the rubber was simulated as a linear elastic material. Another commercial finite element software (ABAQUS) was used by Bolarinwa & Olatunbosun (2015) whereby using various capabilities of ABAQUS, the footprint under purely vertical load was obtained for a vertically loaded tyre. Afterwards, the existing contact between the road and the nodes (node coordinates) was maintained by applying an equivalent distributed vertical load, while the centre of the wheel was unconstrained for every degree of freedom. Finally, a frequency analysis was performed on this condition of the model and it was found that the boundary conditions on the tyre model can have large impact on its eigenmode response.

Optimisation Model

A novel method for extracting the geometric and constitutive material properties of pneumatic tyres from available numerical or experimental data for the development of realistic and reliable tyre numerical models is proposed. This method involves an optimisation procedure, which incorporates a finite element model as a solver (ABAQUS) properly coupled with an optimiser function (MATLAB). An initial tyre model (P235/75R17) is developed, and then its properties are suitably adjusted via the optimisation process, in order for the former to best fit a target model available in the literature, with respect to eigenfrequency analysis results. After the termination of the algorithm, the "optimum" tyre model (i.e. the model which best conforms to the target model) is obtained, the response of which is further investigated to ensure its realistic behaviour, which warrants its use for various numerical simulations.

In general, the methods used to optimise a model – optimisation methods – range from relatively simple mathematical programming based – exact – methods to novel heuristic search techniques. The methods of the first category are very efficient for cases with a few design variables. More specifically these methods use the sequential quadratic programming procedure for nonlinear optimisation (which is also used in

this study), as well as others. More details regarding these methods are presented by Nocedal & Wright (2006). More robust optimisation techniques, which are capable of searching effectively the whole design variable domain and not being trapped into local optima, can be used for increased number of design variables, or non-differentiable functions. Recently developed heuristic methods, such as genetic algorithms, simulated annealing, threshold accepting, tabu search, ant colonies, particle swarm, provide more attractive alternatives.

By utilizing the capabilities of ABAQUS with regard to symmetric model generation (SMG), symmetric results transfer (SRT) and restart option, the full 3d numerical model of the tyre was developed, as shown in Fig. 4.3 and Fig. 4.4. Inflation pressure was imposed on the inner surface of the tyre as a distributed load. Regarding the boundary conditions, the rim was set to be fixed in all six degrees of freedom, and the tyre was constrained with the rim through a rigid body constraint (fixed-spindle).

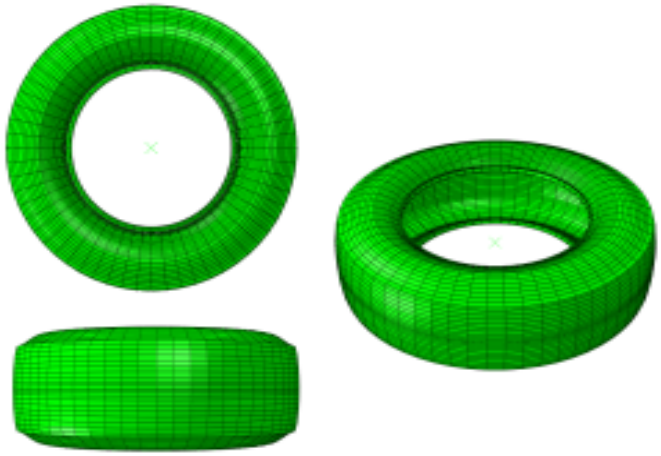

Figure 4.3.*Illustration of the tyre model.*

The geometric properties of the belts and carcass reinforcement, as well as the hyperelastic Mooney-Rivlin C_{10} constant, presented in Table. 4.1,were selected as design variables. The reinforcement layers were defined in ABAQUS as smeared layers with a thickness equal to the ratio of the area of each reinforcing bar to the reinforcing bar spacing. This calculated thickness was assumed to remain constant on the entire extent of the layer. This consideration has a significant effect on the selection of the design variables, since the stiffness of each reinforcement layer contributes to the eigenproperties of the tyre. Due to the fact that the rebar stiffness is given by a fraction of two separate input parameters, in the case of constant layer

stiffness they become dependent on each other. Therefore, it is objective that only one of the two parameters for each layer is selected as an independent design variable and the other remains fixed. The variable which is to remain fixed is the easiest to be measured, in terms of order of magnitude. It is also worth mentioning that, because the two belt layers have symmetric orientation with respect to the plane of the tyre, and the tyre is a centre symmetric structure, its eigenmodes are expected to be also symmetric; this means that the cross section areas of the two belt reinforcements have to be equal, and therefore the belt reinforcement cross sectional area has been considered as a single design variable. The design variables of the optimisation problem, as well as their upper and lower bounds are shown in Table 4.1.

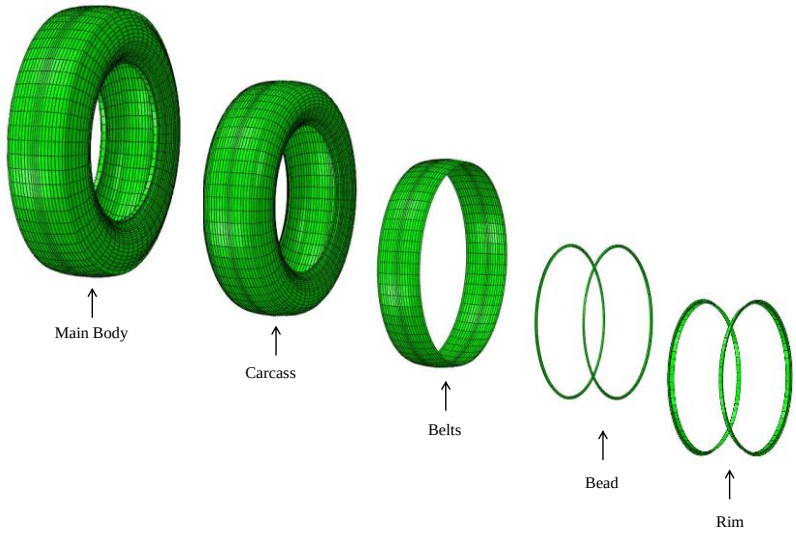

Figure 4.4.*Inner components of the detailed 3D FE tyre model.*

Design variable	Lower bound	Upper bound
A_{belt}	10^{-7}	10^{-5}
$A_{carcass}$	10^{-8}	10^{-5}
C_{10}	10^{5}	10^{7}

Table 4.1. *Design variables of the optimisation problem and their lower and upper bounds.*

The parameters of the optimisation problem were the design input data that remain fixed during the optimisation process. These include as already mentioned, the spacing of the rebar layers, which was set to be equal to 0.00116m for the belts and 0.001m for the carcass. Furthermore, the constants of the Mooney-Rivlin strain energy potential are C_{01}=0 and D_1=5.085*10-8Pa^{-1}. In addition, the cord angles were 70 and 110 degrees for the two belt layers, and 0 degrees for the carcass. The material

properties of the belts and the carcass were also held fixed during the optimisation process. The inflation pressure with which the tyre was inflated is 240 kPa.

No constraints were imposed to the model being optimised, apart from the upper and lower limits of the design variables. The latter require some experience to be specified, because large upper bounds or small lower bounds can lead to numerical instabilities in the solver, such as excessive element distortion, which result in the premature termination of the optimisation procedure. The objective function for the optimisation problem has to be of an appropriate form, so that it is reduced to the minimum if the numerically calculated eigenfrequencies coincide with the ones available from the literature, Eq.4.2. The first 16 eigenfrequencies of the tyre were considered in the objective function, which was given by the equation:

$$obj = \sqrt{\sum_{i=1}^{16}(f_{i,num} - f_{i,lit})^2} \tag{4.2}$$

where $f_{i,num}$ is the ith eigenfrequency calculated by the numerical model in every iteration of the algorithm and $f_{i,lit}$ is the corresponding ith eigenfrequency available in the literature [Wheelet et al. (2005)]. The correspondence between the various eigenfrequencies was made by taking into account the deformed configurations of the various eigenmodes.

Algorithm utilised

The optimisation algorithm used in this study was a sequential quadratic programming (SQP) method. In this method, a quadratic programming (QP) subproblem is solved at each iteration. For this purpose the MATLAB built in function fmincon was used. This function used an active set strategy and updates an estimate of the Hessian of the Lagrangian at each iteration using the BFGS formula. An active-set method initializes by making a guess of the optimal active set, and if this guess is incorrect, it repeatedly uses gradient and Lagrange multiplier information to proceed towards the optimum solution.

The fmincon optimiser (MATLAB) was properly coupled with the analysis solver (ABAQUS) in order to obtain the frequency analysis results. This was done inside the objective function in which ABAQUS was called to perform the necessary analyses. The necessary input (*.inp) files for the ABAQUS runs were created by suitable MATLAB functions. To read the results of the analyses from the corresponding

ABAQUS results (*.fil) files, special MATLAB functions were used. While the analysis solver was running the optimiser was halted and its execution was continued after the lock (*.lck) file had been deleted.

Optimisation Results

The results of the optimisation process as described in the previous paragraphs are shown in Table 4.2.

	Initial model	***Optimised model***	***Wheeler et al. (2005)***	***Deviation (%)***
Design Variables				
A_{belt} (m^2)	$2.11868*10^{-7}$	$3.64826*10^{-7}$	N/A	-
$A_{carcass}$ (m^2)	$4.20835*10^{-7}$	$8.01133*10^{-8}$	N/A	-
C_{10} (Pa)	10^6	10^6 +0.01489	N/A	-
Eigenfrequencies				
f_1 [0,0] (Hz)	36.85	30.86	31.7	2.66
f_2 [0,0] (Hz)	37.17	35.85	35	2.43
f_3 [1,1] (Hz)	43.85	36.92	37.8	2.33
f_4 [1,1] (Hz)	43.85	36.92	37.8	2.33
f_5 [1,0] (Hz)	65.07	58.75	58.5	0.43
f_6 [1,0] (Hz)	65.07	58.75	58.5	0.43
f_7 [2,1] (Hz)	76.33	68.41	66.1	3.49
f_8 [2,1] (Hz)	76.33	68.41	66.1	3.49
f_9 [2,0] (Hz)	86.65	78.67	79.5	1.04
f_{10} [2,0] (Hz)	86.65	78.67	79.5	1.04
f_{11} [3,0] (Hz)	104.36	96.42	97.6	1.21
f_{12} [3,0] (Hz)	104.36	96.42	97.6	1.21
f_{13} [3,1] (Hz)	117.07	107.9	102.7	5.06
f_{14} [3,1] (Hz)	117.07	107.9	102.7	5.06
f_{15} [4,0] (Hz)	122.65	114.9	115.9	0.83
f_{16} [4,0] (Hz)	122.65	114.9	115.9	0.83
Algorithm Details				
Min. value of obj. function	-	8.59	-	-
Number of obj. function evaluations	-	25	-	-

Table 4.2.*Results of the optimisation procedure of the tyre frequency analysis considered in this study.*

It is noted that each natural frequency corresponds to a pair of integers enclosed in brackets ([c,m]). The first integer denotes the number of sinusoidal waves in the circumferential direction of the wheel, whereas the second integer shows the number of waves in the meridional direction at a specific location, where the deformation of the eigenmode shape is maximum. In addition, only the first 16 eigenmodes were considered for the development of the realistic tyre model, in order to reduce the computational cost.

The first column of Table 4.2 shows the data of the initial model, used as the starting point of the optimisation process. It is evident that the eigenfrequencies of the initial model presented significant difference from the eigenfrequencies of the model published by Wheeler et al. (2005). In the second column, the parameters of the optimum model are shown, as well as the values of the design variables leading to it. Regarding the eigenfrequencies, it is observed that they are much closer than those of the initial model, leading thus to a numerical model that conforms more to the available numerical data, and therefore it is more realistic. The maximum deviation of the eigenfrequencies was noted to be roughly 5%. Moreover, the optimum model had a higher cross section of the reinforcement of the belts, and lower cross section area of the reinforcement of the carcass than the initial model. The hyperelastic constant C_{10} was only slightly increased after the optimisation. Furthermore, regarding the algorithm output, the minimum value of the objective function was equal to approximately 8.59Hz, and the algorithm converged after 25 objective function evaluations. The reason for the termination of the algorithm was that the magnitude of the search direction was less than the corresponding tolerance. Finally, the most important factor affecting the tyre modal behaviour during the optimisation procedure was proved to be the cross section area of the carcass ($A_{carcass}$). Due to the fact that the initial model had generally higher eigenfrequencies than those of the target model [Wheeler et al.(2005)], its stiffness had to be decreased, in order for the model to approach the latter. The decrease in stiffness was achieved with a relatively large decrease in the cross sectional area of the carcass, despite the increase of the cross section area of the belt reinforcement.

In Fig. 4.5 the various eigenmodes of the optimised tyre model are shown. The figure is divided into 9 subfigures, each of which shows a tyre eigenmode shape viewed from 4 different perspectives. The fundamental eigenmode is the axial or lateral

mode, and after this the torsional, pitch, diametric, and higher modes follow. There is total correspondence between the integer pairs which appear in the bottom of each subfigure, and the ones shown in the first column of Table 4.2.

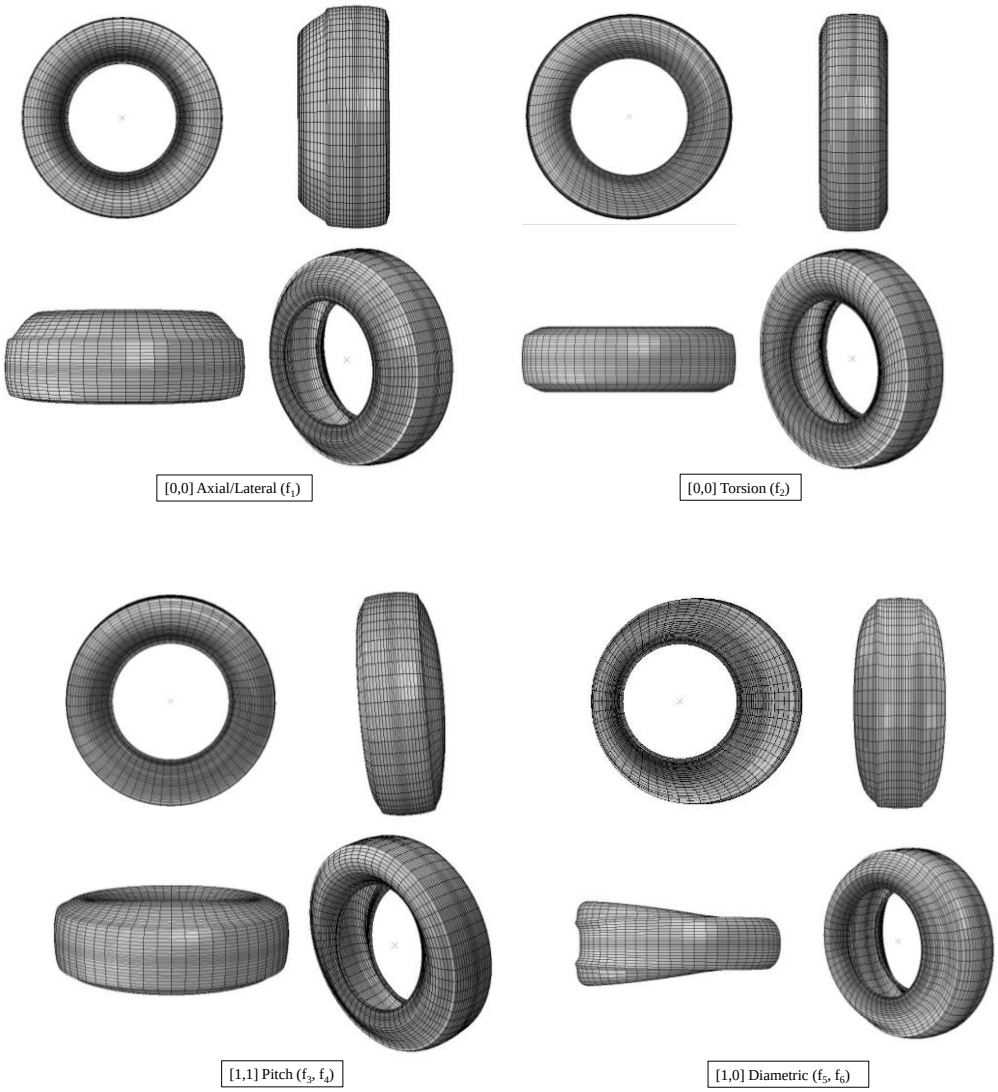

Figure 4.5. *Eigenmode shapes of the optimised tyre model (continued in the next page).*

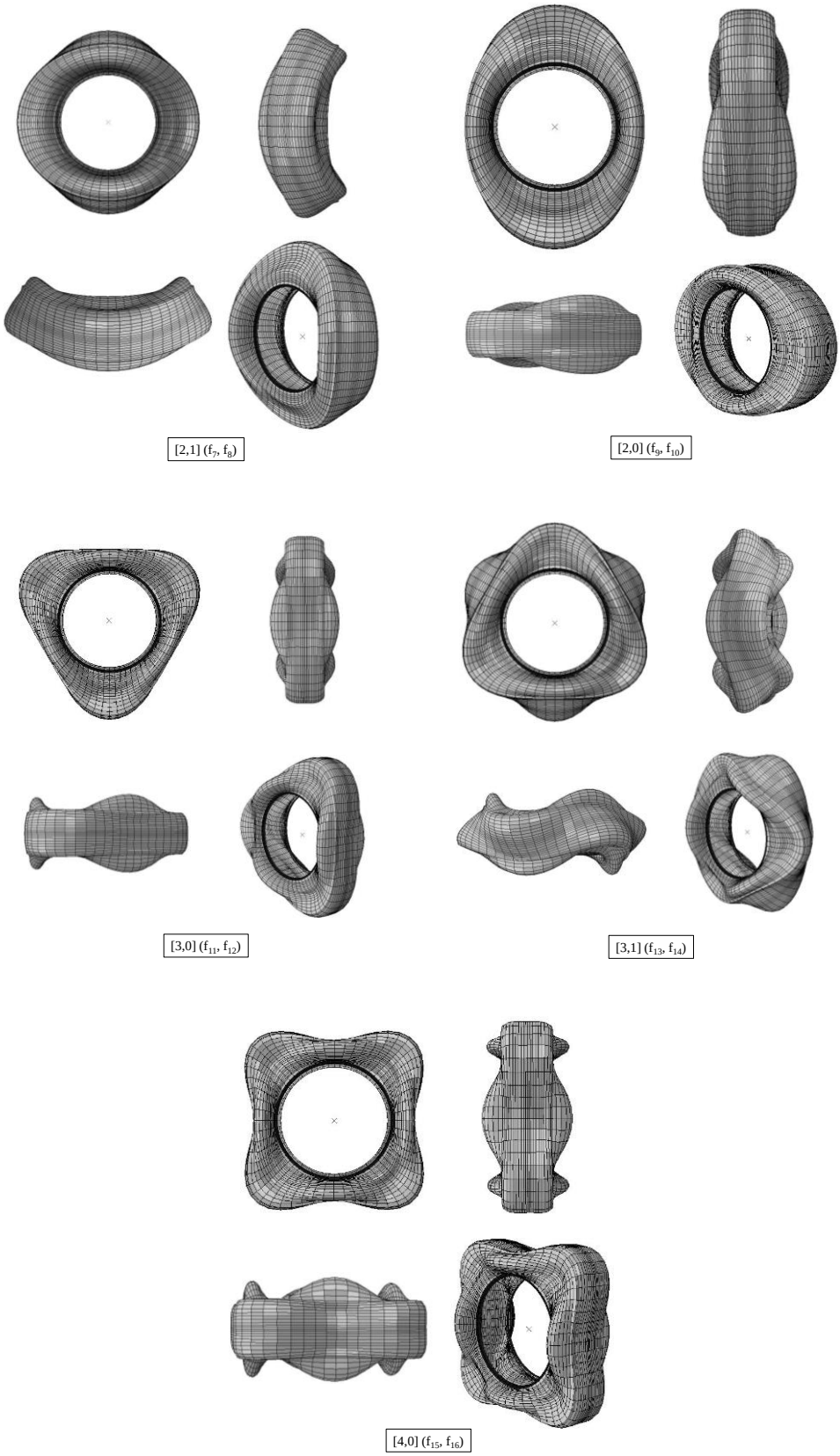

Figure 4.5. *Eigenmode shapes of the optimised tyre model (continued from previous page).*

The optimised model was the most realistic version of the selected tyre type (P235/75R17) with respect to its natural frequencies response. It was close to the

modal data available by Wheeler et al. (2005), and for this reason, it allowed its use for dynamic response analyses. In an attempt to further validate the optimised model, the variation of its eigenmodes and eigenfrequencies was studied for varying inflation pressure.

In Fig. 4.6 the effect of the inflation pressures on the eigenfrequencies of the tyre can be observed. As it can be expected, as the inflation pressure rises, the eigenfrequency of a specific eigenmode increases, as the increased inflation pressure makes the tyre stiffer. This is a trend widely observed in the literature and once again corroborates the realistic behaviour of the optimum tyre. Moreover, it is apparent that the increase of the eigenfrequency of each mode for increasing inflation pressure is nonlinear. Specifically, for lower values of the inflation pressure, the rate of increase in the eigenvalues becomes higher than that for higher values of the inflation pressure. Finally, for the higher order eigenmodes, the increase in the eigenfrequency for the same difference in the inflation pressure is larger than that for the lower eigenmodes, which is in agreement with relevant results published by Chatterjee & Ranjan (2012).

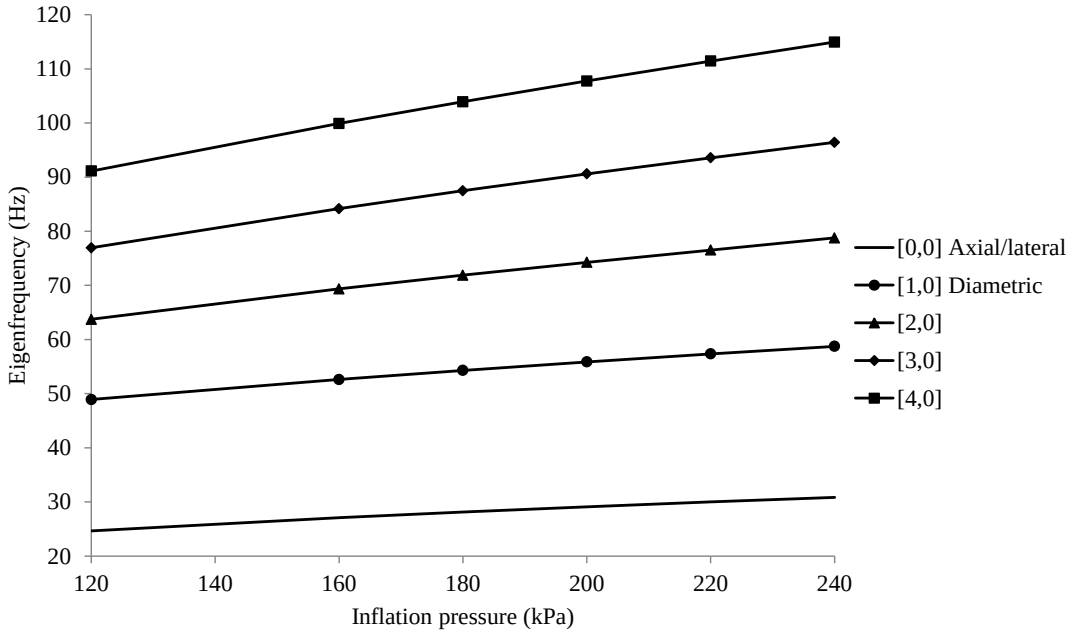

Figure 4.6. *Eigenfrequencies of various mode shapes of the optimised tyre model for various inflation pressures.*

The results produced from the developed algorithm show clearly the efficiency of the optimisation procedure proposed, as well as the realistic response of the tyre model developed. The next step towards the complete validation of the tyre model would be

the investigation of its dynamic interaction in contact with a rigid road for a variety of loads and inflation pressures.

4.5. Discussion

A novel technique has been developed which permits an accurate characterization of difficult to obtain geometrical characteristics of the tyre – such as the thickness of the belt – via a coupled optimisation algorithm. This technique initiates with an initial tyre configuration developed in ABAQUS, where the eigenfrequencies of the structure are calculated, and compared with available experimental results. Following that, if the difference between the numerical results and the experimental data is higher than a specified tolerance, the configuration of the tyre alters – according to the design variables – and the new eigenfrequencies are calculated for the new reference configuration of the tyre.

Three design variables were set in this optimisation, namely as: (i) the area of the carcass, (ii) the area of the belt, and (iii) a material parameter of the rubber according to the Mooney-Rivlin model, C_{10}. Finally, the natural frequency response of the reference tyre configuration was tested for various inflation pressures and its response was qualitatively matched with results from the literature.

Chapter 5

Tyre – Terrain Interaction: FE method

5.1. Introduction

The preceding chapters presented results of both finite element soil modelling and a detailed representation of a complex tyre structure. In this chapter, it will be shown how the two separately described components can be brought together. As each has been independently verified, it provides confidence that the joined result will be representative, provided the interface between tyre and soil is adequately captured.

The rolling response of a pneumatic tyre P235/75R17 interacting with rigid or deformable terrain was modelled numerically using the finite element code ABAQUS 6.13. Initially, a 2D half-axisymmetric tyre model, illustrated in Fig.4.2, was developed from which the final configuration of the inflated tyre was acquired. Using the symmetric model generation (SMG) and the symmetric results transfer (SRT) capabilities of ABAQUS, this 2D half-axisymmetric model was extended to a half 3D tyre model, where the footprint of the tyre was obtained either by imposing a displacement – displacement control – or by imposing a vertical load – load control – at a rigid analytical surface against the tyre, with its centre fixed (in the cases of steady state transport analysis of the tyre and of the latter rolling on a rigid surface with bump). The SMG and SRT were reused to extend the half 3D tyre model into a full 3D tyre configuration. From this point, modelling proceeded in two directions which will be referred from now on as (a) pneumatic tyre-rigid terrain interaction model and (b) pneumatic tyre-deformable terrain interaction model.

In the former, the analysis began from the results of the 3D model described above, and using the Steady State Transport (SST) utility of ABAQUS /Standard, the steady

state response of the tyre rolling on a rigid analytical surface was obtained. Details about the capabilities and characteristics of this type of analysis are presented in a subsequent section, section 5.1.1 and 5.1.2. The main result of the SST analysis was the free rolling condition of the tyre. The results related to this condition were imported into another model which contained a rigid analytical surface with a bump, also presented in greater detail a subsequent section, section 5.1.3. In this latter model a transient dynamic explicit analysis – using ABAQUS/Explicit – was conducted to investigate the dynamic response of the tyre travelling in a free rolling state due to the impact force imposed by the bump.

In the second part of the models considered in this study, the results of the 3D model analysis were imported into another model which contained the soft soil. A transient dynamic explicit analysis (with ABAQUS/Explicit) was performed to investigate the dynamic behaviour of the tyre rolling on this soft soil layer under various inflation pressures, linear and/or angular velocities and vertical loads. The modelling procedures involved in the present study are schematically illustrated in Fig. 5.1.

For both models, the rim of the tyre model was rigidly constrained to the motion of a reference point defined at its centre. Contact interaction was defined between the tyre and the underlying surface (be it an analytical rigid surface or the surface of a deformable part), in order to avoid interpenetration between the two surfaces and Coulomb friction was specified in the tangential direction of the tyre-terrain interface, with a friction coefficients of 1.0 for model (a) and 0.5 for model (b). The kinematic formulation was used in all the analyses, which, although computationally more intensive, provides increased accuracy in the results, especially when it was used in conjunction with adaptive meshing techniques (ABAQUS 6.13, 2013). Before imposing the vertical force load at the tyre centre or the road, initial contact was established to avoid spurious dynamic effects originating from the impact of the tyre on the rolling surface. Finally, in model (b), the deformable part representing the soil was considered to be homogeneous. For both models (a) and (b), lumped mass was added at the centre of the tyre, as well as rotary inertias in all degrees of freedom, in order to avoid numerical problems emerging from zero pivots during the explicit finite element analysis. The lumped mass assigned to the centre of the tyre was considered to be 10kg, whereas the rotary inertias assigned had a very small value, so

that their contribution in the rotary inertia of the whole tyre is negligible, with the latter resulting mainly from the density of the various components of the tyre as $1.94 kgm^2$.

It has to be noted here that in each increment of ABAQUS/Explicit, the acceleration is calculated by the multiplication of the inverse of the diagonal mass matrix with the difference between the imposed load and the internal forces,a fact which does not ensure perfect equilibrium conditions in each time step. Apart from this, the central-difference operator used in ABAQUS/Explicit is conditionally stable, and its stability limit depends on the highest eigenfrequency of the system. As a result, the acceleration calculated in this way may show spurious oscillations in certain cases, especially for impact loading conditions, an example of which will be presented in section 5.1.3, and which, become smoother and eventually disappear as the acceleration is integrated according to the explicit central-difference integration rule. For example, to reduce the spurious oscillations in the acceleration response, the time increment size had to be reduced significantly in the part of the analysis after the bump impact.

To avoid high element distortion and consequent numerical errors and/or instabilities the adaptive meshing (ALE) option offered in ABAQUS/Explicit was utilised in the simulation, similarly with section 3.1.3. One remeshing sweep every 10 increments was performed. It should be noted that these parameters affect the simulation time to a large extent. The simulation time of the models analyzed in this study [model (b)] ranges from 16 hours to 35 hours for an Intel core computer with 3.4GHz (i-5 3570 CPU) and 16GB of RAM. The ALE was again set only on the region of the model where the mesh was refined. A mesh sensitivity study was performed and the final mesh configuration was obtained. It should be highlighted that ALE works only with the contact pair formulation and not with general contact.

5.2. Pneumatic Tyre – Rigid Terrain

In model (a) the rigid terrain was represented by a rigid analytical surface of 3.5m in length with a bump which was a circular arc with its ends located at 0.5m and 0.7m respectively in front of the initial contact point of the tyre with the terrain. Following

conventions according to SAE (2008) the centre of the circular arc was located at 0.6m from the latter contact point along x axis, and at 0.1m below the level of the surface along *y* axis. It is noted that the position of the analytical surface depends on the deformed configuration of the tyre, which results due to the inflation pressure and the vertical load, since at the beginning of the SST and subsequent transient dynamic explicit analyses the deformed tyre must be in contact with the rolling surface.

Two different vertical loads were imposed at the tyre centre ($1.2\gamma gbd^2$ and $2\gamma gbd^2$) at the inflation pressure of 242 kPa (~35 psi) and the response of the rim after the impact on the bump was studied. For the vertical load of $2\gamma gbd^2$ three different cases of inflation pressures (160 kPa, 200 kPa, 242 kPa) were considered and the effect on the dynamic response of the tyre centre was observed. In all the above cases the linear velocity of the tyre centre in the *x* direction is prescribed to be equal to 10 km/h (~2.7778 m/s). Following this, for the tyre with vertical load of $2\gamma gbd^2$, inflation pressure of 200 kPa and two different linear velocities were considered (10 km/h and 20 km/h).

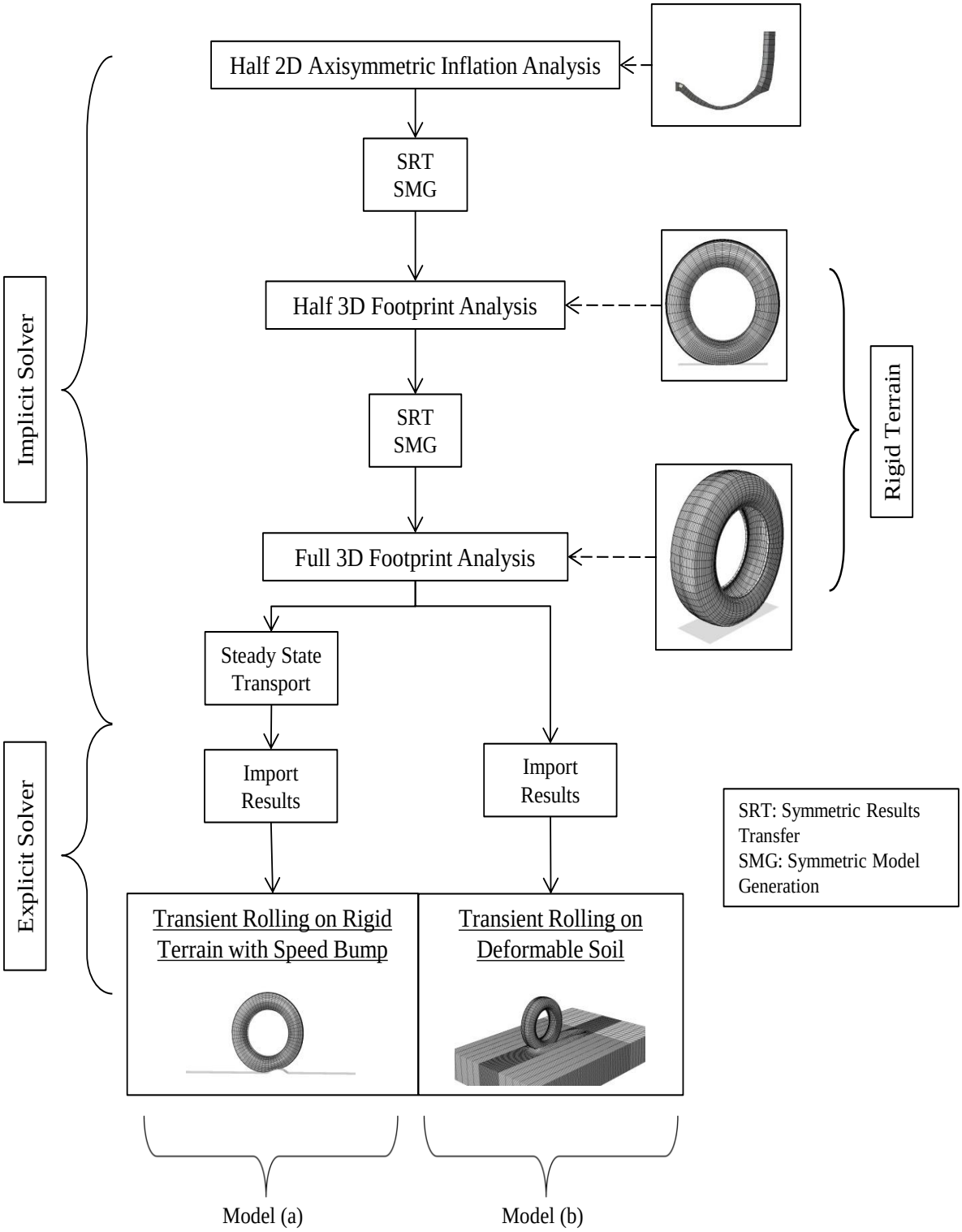

Figure 5.1.*Procedure of development and analysis of the various models used in this study.*

For all implicit analyses conducted in this model the rim was fixed and the rigid analytical surface was either displaced by a specified displacement control boundary condition or loaded by a concentrated force while being allowed to move only along the vertical global *z* axis. In the steady state transport analysis, the angular velocity is

considered to be the imposed loading, whereas the linear velocity is imposed as a boundary condition. The angular velocity ranges from 7.2 rad/s to 8.2 rad/s. These limits are calculated as follows: the radius of the undeformed tyre is equal to 0.381m, therefore for travelling speed equal to 2.78 m/s, the angular velocity is found to be $2.78/0.381 \approx 7.3$ rad/s$>$7.2 rad/s. For vertical load 5kN and inflation pressure 242 kPa, the radius of the deformed tyre is equal to 0.348m, which corresponds to angular velocity $2.78/0.348 \approx 8$ rad/s$<$8.2 rad/s.

5.2.1 Footprint Analysis

The mesh configuration which was used for the footprint analysis is shown in Fig. 5.2(a). This includes a refinement near the contact area and was used to extract the results shown in Fig. 5.3 and Fig. 5.4. In Fig. 5.3 the vertical deflection versus the vertical load is plotted for various values of the inflation pressure. It is evident that as the inflation pressure increases, the vertical deflection decreases, for all values of the vertical load considered. Moreover, as the vertical load increases, the vertical deflection increases. In Fig. 5.4, the contact area of the footprint is plotted versus the vertical load, for the same values of the inflation pressures as in Fig. 5.3. The contact area seems to have higher fluctuations as the vertical load changes. The results presented in Fig. 5.3 and Fig. 5.4 correspond to frictionless contact between the tyre and the analytical surface.

An investigation was made of the effect of the rebar orientation of the two belt layers on the deflection of the tyre. The rebar orientation was defined as the angle between the axis of the rebar with respect to the local 1-direction. In the three cases considered include belt layers with rebar orientation ±18, ±20 and ±22 degrees. The results are shown in Fig. 5.5, where the deflection of the tyre versus the vertical load is plotted for the three different rebar orientations. It can be noted that by increasing the rebar orientation angle there is a decrease in the stiffness of the tyre since the vertical deflection increases.

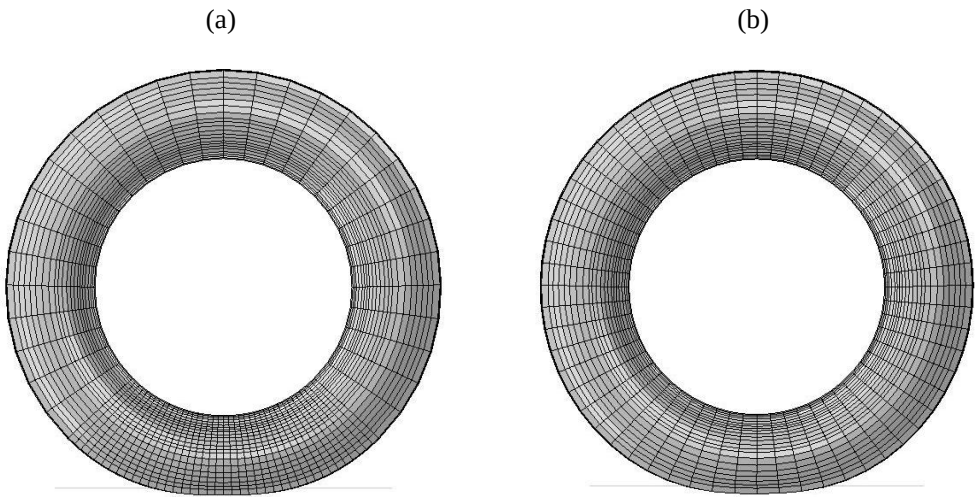

Figure 5.2. *Mesh configuration of the tyre used (a) for the steady state transport analysis and (b) for the transient dynamic analysis in this study.*

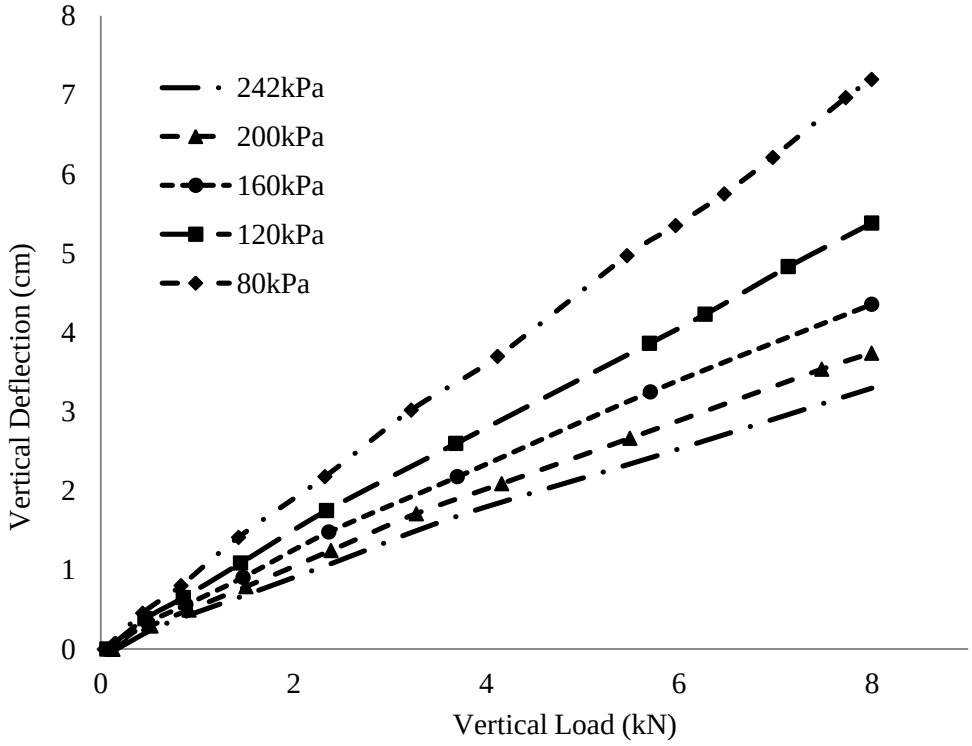

Figure 5.3*. Results of footprint analysis for model in Figure 5a: vertical deflection versus vertical load for various inflation pressures.*

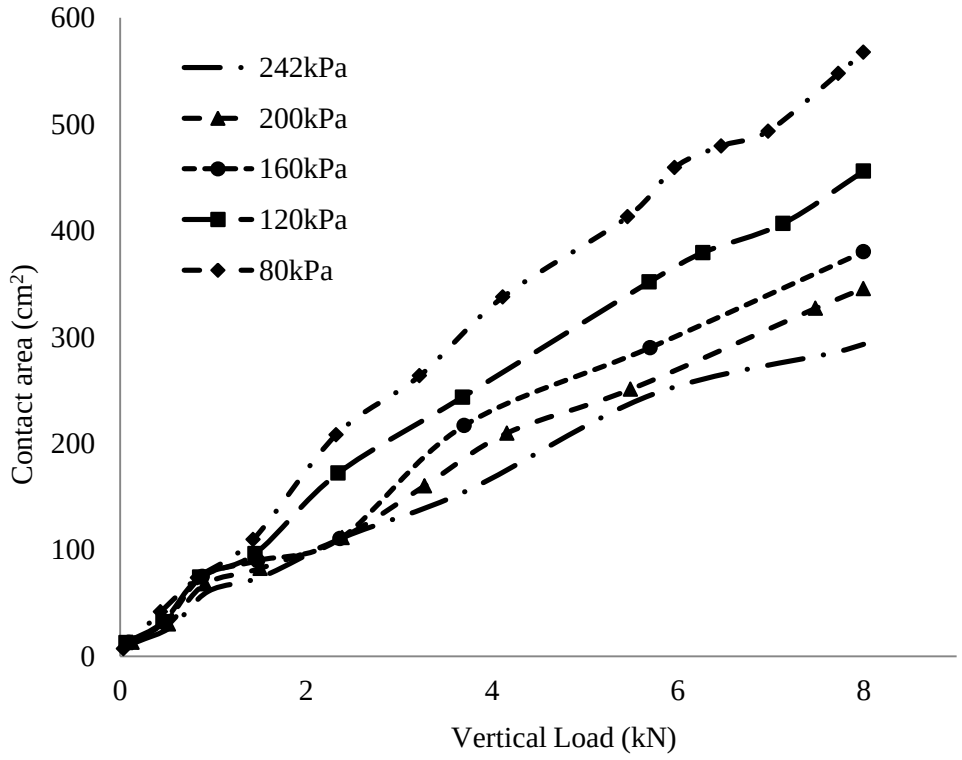

Figure 5.4*. Results of footprint analysis for model in Figure 5a: contact area versus vertical load for various inflation pressures.*

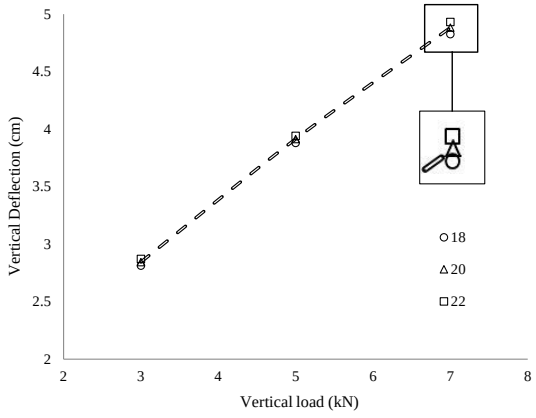

Deflection (cm)	**Vertical load (kN)**		
Orientation (deg)	**3**	**5**	**7**
18	2.81447	3.88069	4.8271
20	2.84556	3.91523	4.88356
22	2.87342	3.94343	4.93374

Figure 5.5.*Deflection versus vertical load for various orientations of the rebar of the belt layers.*

Figures 5.6 and 5.7 illustrate the deformed configuration of the tyre model used for the SST analysisunder a vertical load of 5kN and inflation pressures of 242kPa and 160kPa respectively. As expected, it is noted that by reducing the inflation pressure and for the same vertical load the vertical deformation of the tyre is increasing. More specifically, the case study with 242kPa results in a vertical displacement of $2.23 \cdot 10^{-}$

^{2}m, whereas the same tyre inflated with pressure 200kPa and loaded with the same vertical load exhibits a displacement of $2.91 \cdot 10^{-2}$m.

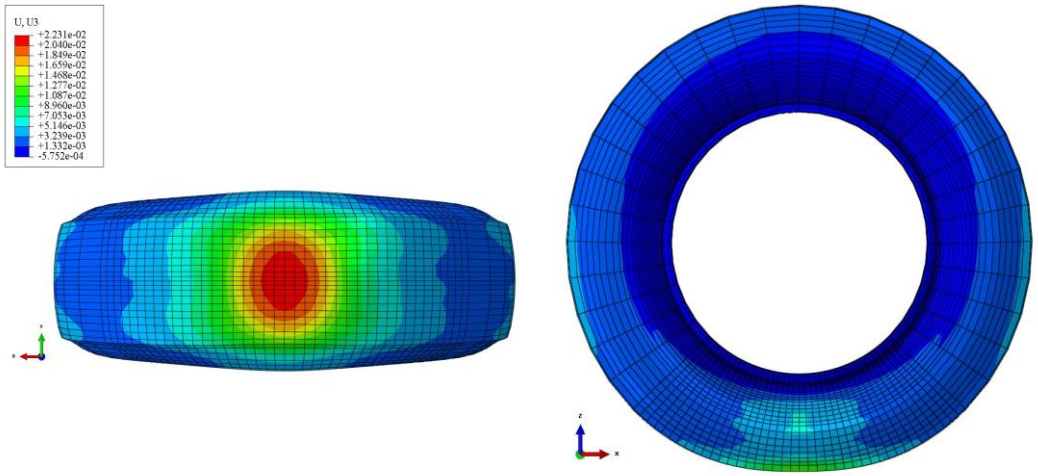

Figure 5.6.*Vertical deformation of tyre in the static footprint analysis, with 242kPa inflation pressure and 5kN vertical load.*

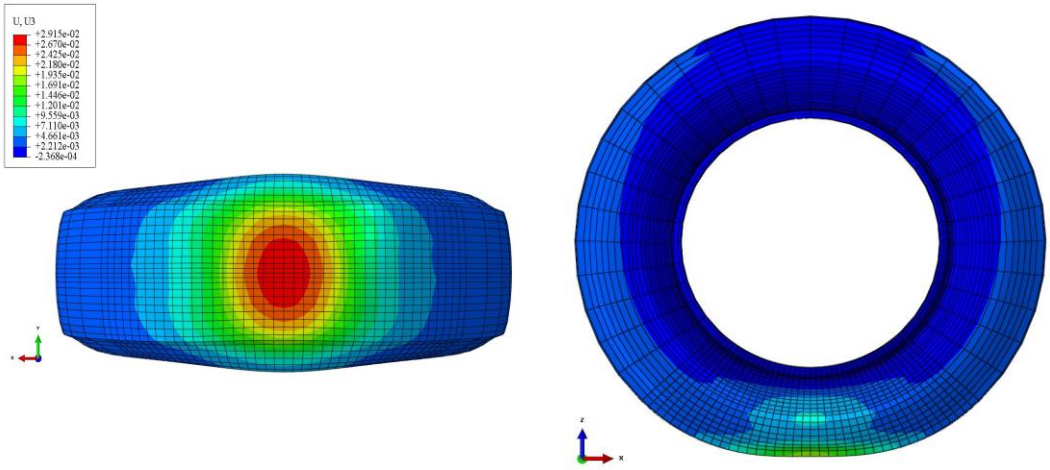

Figure 5.7.*Vertical deformation of tyre in the static footprint analysis, with 160kPa inflation pressure and 5kN vertical load.*

5.2.2 Steady State Transport (SST)

For a vertically loaded tyre rolling over a surface the combination of linear and angular velocity which results in free rolling conditions is not known in advance. The steady state transport capability implemented in Abaqus can be considered as a mixed Lagrangian-Eulerian method, where the rotation of the tyre is described in a spatial or Eulerian manner, and the tyre deformation is described in a material or Lagrangian manner. This description of the steady state rolling tyre with moving contact with the above formulation results in a spatially dependent simulation.

In Fig. 5.8 and Fig. 5.9, results of the SST analysis are presented for various values of the vertical load, in terms of resistance force and torque with respect to the axis of revolution of the tyre. At the left area of each graph, braking conditions prevail, which lead to resistance forces opposite to the direction of travel and negative torque. After the point in which each curve intersects the horizontal axis and in the right area of each graph, traction conditions are being imposed at the tyre, which lead to negative resistance force and positive torque. At the extreme left and right ends of each graph, the friction between the tyre and the surface is predominant. In this regime, the resistance forces tend asymptotically to the corresponding sliding friction forces, whereas the torques tend asymptotically to the product of the friction forces with the radius of the deformed tyre. As a matter of course, the two asymptotic values of each quantity corresponding to the left asymptote and the right end are opposite in sign. The conditions in which the resistance force and the torque become zero (free rolling conditions) are different for the various values of the vertical load, although this difference is subtle. As the vertical load increases, the angular velocity corresponding to the free rolling conditions increases, for constant linear velocity, which in Fig. 5.8 and 5.9 is assumed to be equal to 2.78 m/s.

In Fig. 5.10, the angular velocity is plotted against the linear velocity, for free rolling conditions of the tyre. The results presented in this figure are useful to identify the angular velocity which leads to free rolling conditions, for a given linear velocity, and they hold for the specific tyre considered in this study. It is obvious that there is a linear relation between the linear velocity and angular velocity in the graph of Fig. 5.10. This fact implies that there is a unique radius of the tyre which corresponds to free rolling conditions. In the subsequent transient analyses of the tyre rolling on an analytical rigid surface, combinations of linear and angular velocities were selected, which lie on the curve of Fig. 5.10.

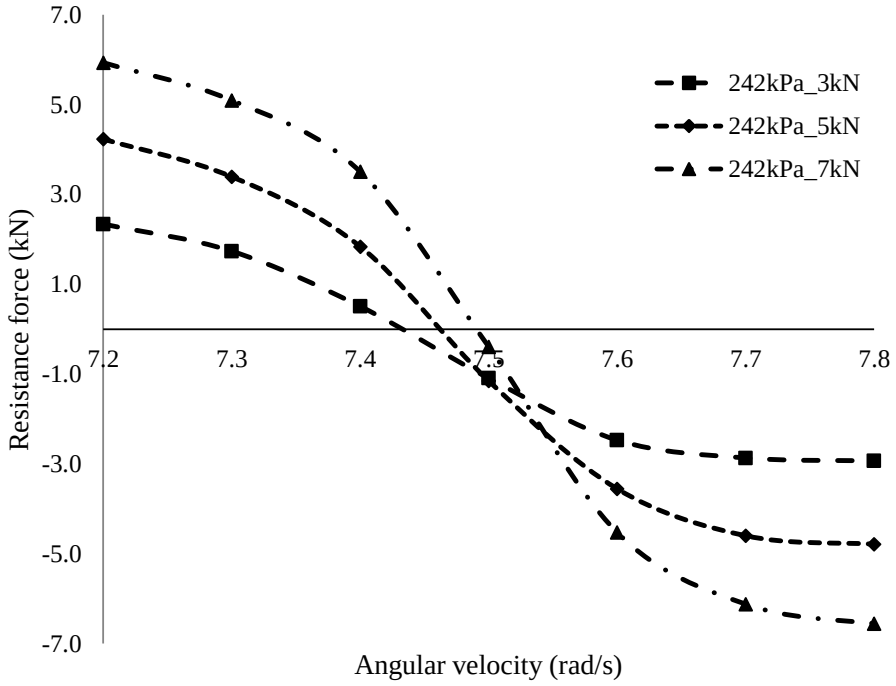

Figure 5.8. *Results of SST analysis for model in Figure 5.2(a): rolling resistance force versus angular velocity.*

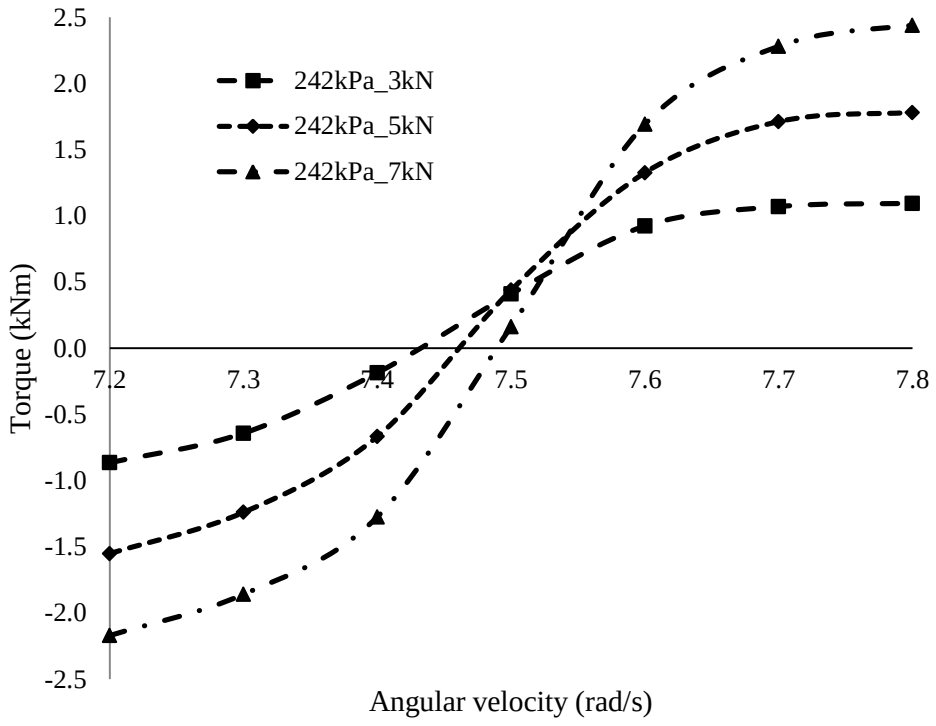

Figure 5.9. *Results of SST analysis for model in Figure 5.2(a): torque versus angular velocity for various vertical loads.*

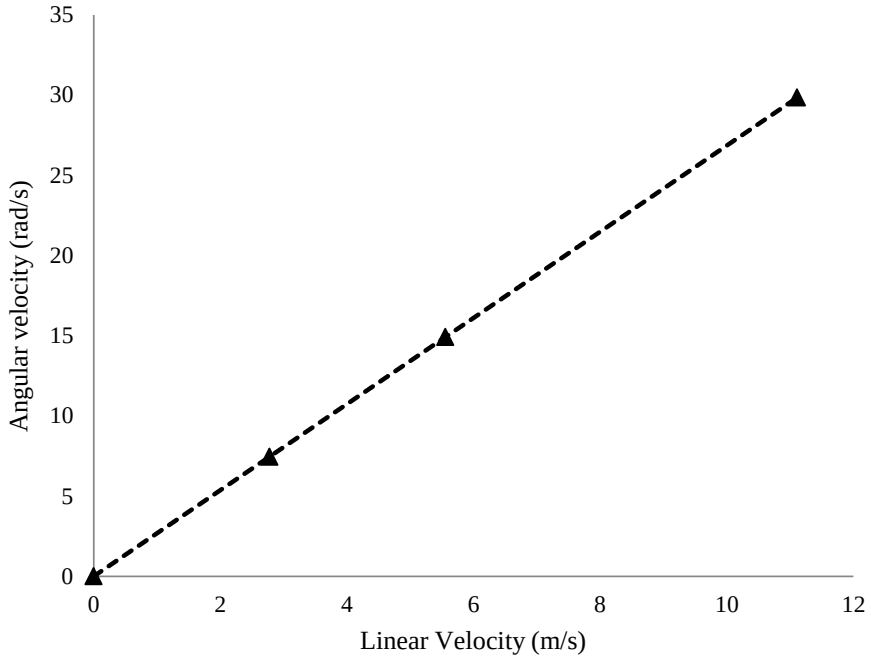

Figure 5.10. *Results of SST analysis for model in Figure 5.2(a): identification of free rolling conditions.*

5.2.3 Rigid Terrain with Speed Bump

In this study, various cases of vertical loads and rolling velocities were considered for a pneumatic tyre which, while rolling on a rigid surface free of irregularities in free rolling conditions, hits on a speed bump with specific configuration, as mentioned in section 5.1. This analysis is a dynamic transient and its results exhibit the effects of the dynamic response due to the load imposed by the bump (Fig. 5.11). The values of the parameters for the various cases considered in this section are shown in Table 5.1.

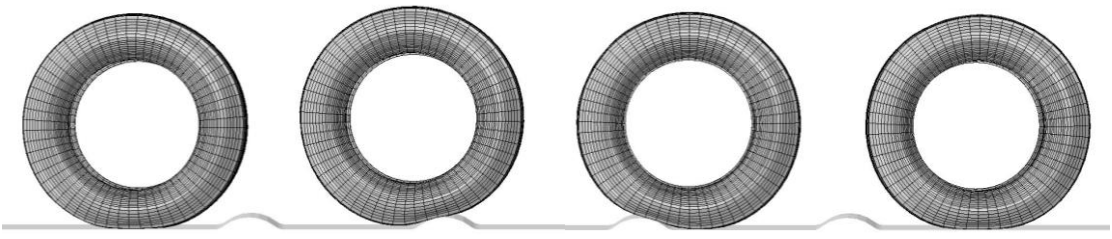

Figure 5.11.*Transient rolling process of a wheel impacting on a rigid bump.*

Figure	Inflation pressure (kPa)	Vertical load (kN)	Linear velocity (m/s)
5.12	160	5	2.78
	200		
	242		
5.13	242	3	2.78
		5	
5.14, 5.15	200	5	2.78
			5.56

Table 5.1. *Values of inflation pressure, vertical load and linear velocity considered for the cases analyzed in Fig.12-15 of the current study.*

In Fig. 5.12 and Fig. 5.13 results of the dynamic response of the tyre due to the impact on the rigid bump are presented, in terms of the vertical displacement at its centre. More specifically, Fig. 5.12 displays the effect of the inflation pressure on the vertical displacement for vertical load of 5kN and linear velocity equal to 2.78 m/s, whereas in Fig. 5.13 the effect of vertical load applied at the centre of the tyre is shown for inflation pressure 242 kPa and linear velocity 2.78 m/s. It is worth mentioning that the tyre configuration used for the tyre/bump impact analysis is shown in Fig. 5.2(b), since uniformity along the tyre perimeter is required. It was ensured that the mesh refinement used for the tyre is as low as possible in order to give consistent results with the refined version and at the same time keep the computational cost in the explicit analysis as low as possible. It is apparent that the increase of the inflation pressure in Fig. 5.12 reduces the oscillations, due to the change of the eigenvalues of the tyre. However it should be emphasized that the response of the tyre is highly dependent on the geometry of the bump; for instance a long and narrow bump will accelerate the tyre in the vertical direction to a different degree than a short bump. In loading cases such as the speed bump impact considered here, the free response of the system depends on the ratio between its eigenperiod and the duration of the bump impact; however, no monotonic dependence exists between this ratio and the maximum free dynamic response of the system, and this relation is rather complicated. It is apparent that in Fig. 5.12 damping increases with decreasing inflation pressure. This conclusion is drawn by noting that the decrease between the consecutive peaks of the response is largest for 160 kPa while for the highly inflated tyre (242 kPa) it is much lower. In addition, in Fig. 5.13 the effect of the vertical load on the dynamic

response denotes that for increasing vertical load, the tyre is experiencing larger compression ratios, which results in a more stable condition for the tyre and therefore reduced vibration amplitude of the spindle.

It has to be noted here that the ongoing oscillation of the tyre spindle after it passes the bump diminishes gradually due to the viscoelastic properties of the rubber, and eventually becomes zero, a condition which is not shown in Fig. 5.12 and Fig. 5.13 as it is not reached for the time span of the analyses performed in this study. However, the tyre can be considered underdamped since only viscoelasticity is defined in the material definition, neglecting other damping types, due to lack of relevant material constitutive properties. The amplitude of this oscillatory response is determined by the ratio of the time duration of the impact load to the eigenperiod of the most significant tyre eigenmode excited from the dynamic loading, in accordance to the basic theory of dynamics of single degree of freedom systems (Chopra, 2012) and results published by Li & Schindler (2014).

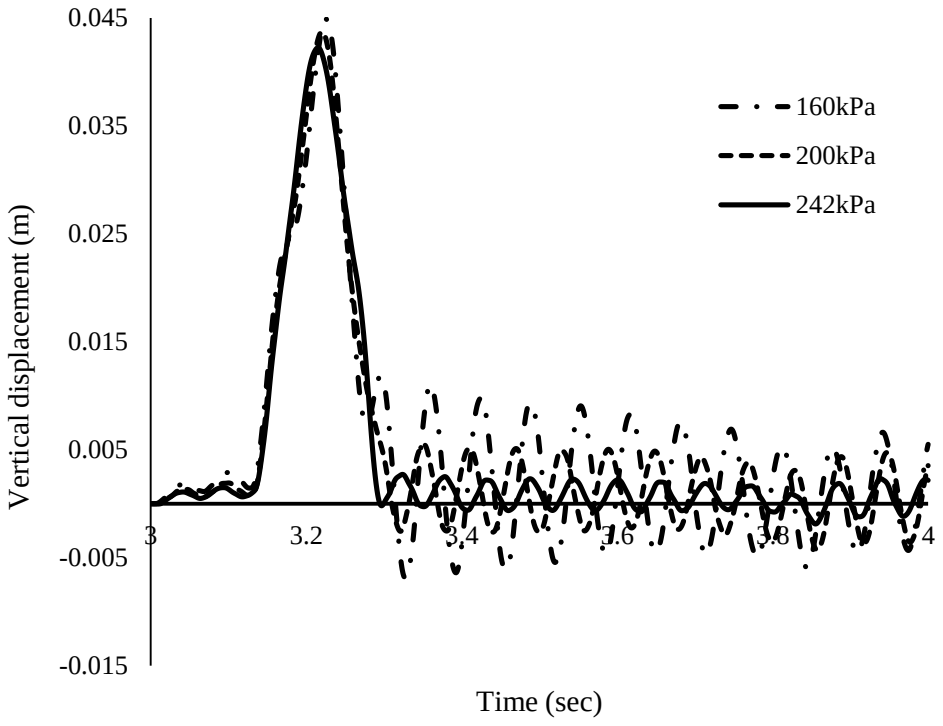

Figure 5.12.*Effect of inflation pressure on the vertical displacement of the centre of the tyre during and after its impact with the bump.*

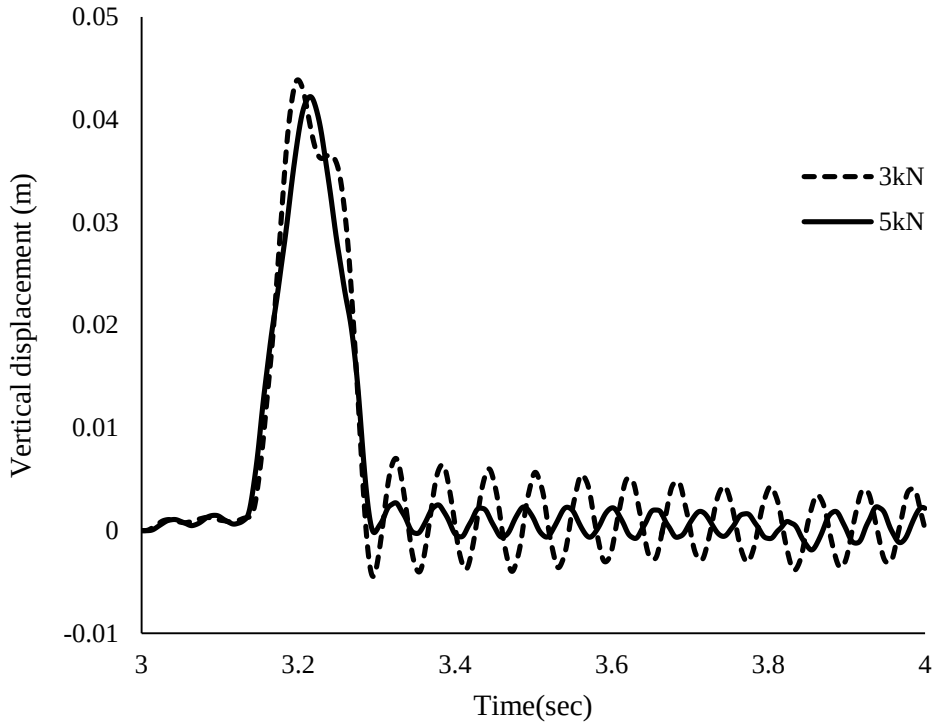

Figure 5.13.*Effect of vertical load on the vertical displacement of the centre of the tyre during and after its impact with the bump.*

In Fig. 5.14 and Fig. 5.15 the effect of the free rolling velocity on the vertical dynamic response of the tyre spindle is depicted, for a tyre with vertical load equal to 5kN and inflation pressure 200 kPa. In particular, Fig. 5.14 displays the time history of the displacement at the centre of the tyre, whereas in Fig. 5.15 the time history of the acceleration at the centre of the tyre for the same case studies is presented. It is noted that for increased velocity the time duration of the bump impact decreases, which alters the ratio of the duration time to the eigenperiod of the tyre, a substantial factor which determines the displacements, velocities and accelerations in the vertical direction during and after impact loading. It is a matter of course that due to the complexity of the impact phenomenon (which depends on many factors, such as the bump geometry for example), there is no universal trend regarding the aforementioned effects. In Fig. 5.15 the respective accelerations for the same cases are shown. It is obvious that the acceleration response in the case of the higher velocity is much more pronounced, reaching a maximum value of 300 m/s^2, whereas

the maximum value of the acceleration in the case of the lower velocity is roughly equal to 100 m/s^2.

It is observed in Fig. 5.15 that the time history of the vertical acceleration response is slightly corrupted with noise. The sources of this noise are primarily the nature of the explicit solver procedure, as outlined in the beginning of chapter 5, as well as the contact formulation at the tyre-rigid surface interface. Contact-induced noise can occur if a surface of a much denser body is weighted as a slave surface, as was done in the numerical procedure followed to obtain the presented results. The solution noise can be reduced in terms of reaching a more stable solution regarding vertical displacement and acceleration of the spindle after the impact with the specification of contact damping in ABAQUS/Explicit, use of the penalty contact formulation and/or reduction of the time increment of the analysis after the impact as suggested by Cho et al. (2005). However, contact damping is not available for hard kinematic contact which was nevertheless preferred here in terms of maintaining a consistency among models (a) and (b) and the time increment was not altered in order to maintain an affordable computational cost for the analyses performed herein, since the main objective of the current section was the dynamic response of the tyre due to inflation pressure, velocity and vertical load changes at the moment of impact.

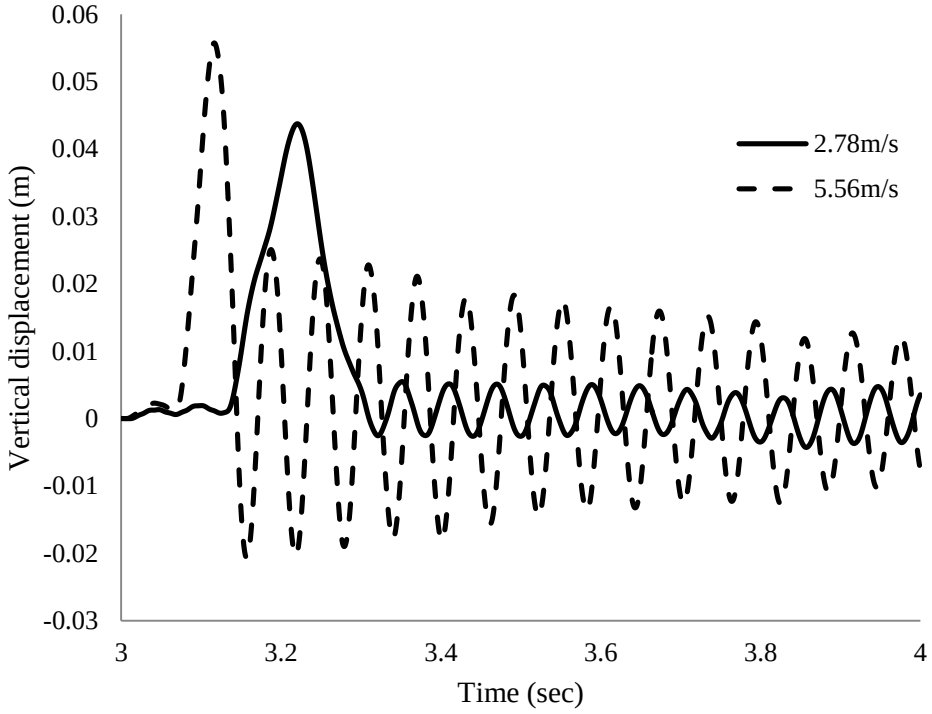

Figure 5.14. *Vertical response of the spindle due to rigid bump impact: effect of free rolling velocities on displacement.*

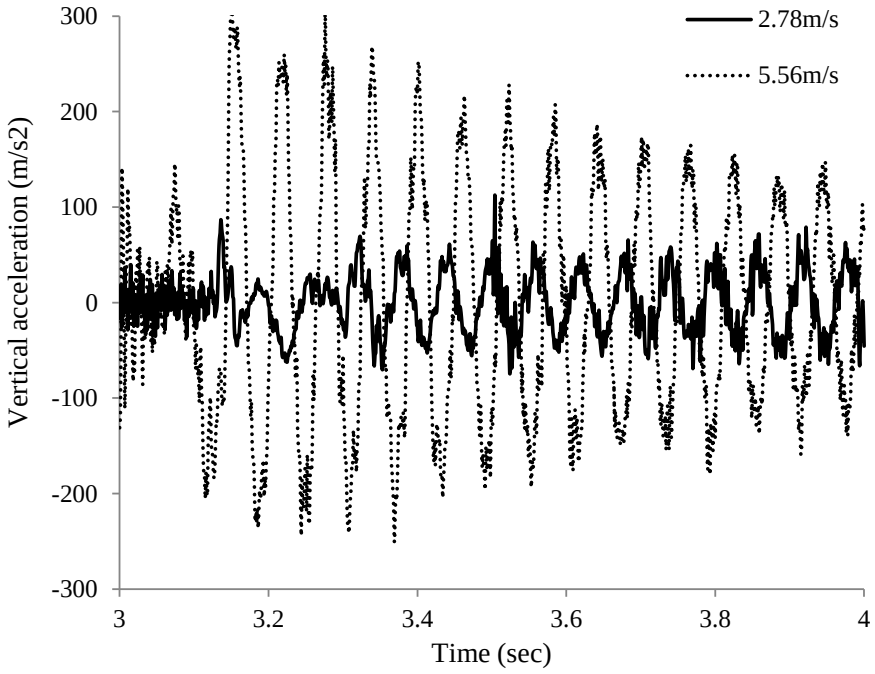

Figure 5.15. *Vertical response of the spindle due to rigid bump impact: effect of free rolling velocities on acceleration, for a tyre with vertical load 5kN and inflation pressure 200 kPa.*

The oscillations of the spindle during impact observed may be caused by (i) the assumption about zero strain rate for the calculation of the Mooney-Rivlin parameters during the optimisation process and/or (ii) induced numerical noise by the Abaqus/Explicit solver which was used for the dynamic analyses. It should be noted that this kind of oscillations (noise) is also observed in the literature (e.g. Palanivelu et al, 2015).

5.3. Pneumatic Tyre – Deformable Terrain

With regards to model (b), the soft soil was represented by a solid deformable part, with dimensions 2.9m in length, 2m in width and 0.4m in height. It was discretized with C3D8R elements and was partitioned appropriately, so that in the areas closer to the surface and to the rolling region the mesh was finer while the mesh was coarser in the regions far from the tyre. The configuration used for the analysis of this section is shown in Fig. 5.16 with the tyre configuration presented in Fig. 5.2(b) and a total number of elements for the road of 150,000 C3D8R. The values of the parameters for the various cases considered in this section are shown in Table 5.2.

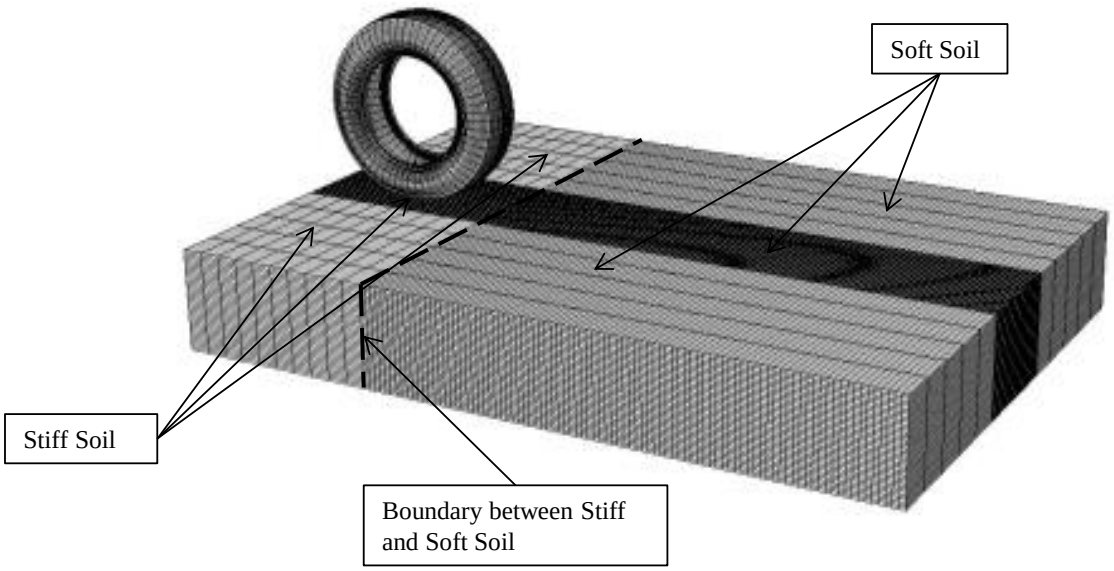

Figure 5.16.*Reference configuration of the model (b) of this study.*

Figure	Inflation pressure (kPa)	Vertical load (-)	Linear velocity (m/s)	Angular velocity (rad/s)	Cohesion (-)	Friction angle (^{o})
5.17	242	$1.2\gamma gbd^2$	1.39	-	$1.25\gamma gd$	0
			2.78			
5.18	242	$1.2\gamma gbd^2$	2.78	-		
		$2\gamma gbd^2$				
5.19	200	$1.2\gamma gbd^2$	1.39	-		
	242					
5.25	120	$1.2\gamma gbd^2$	-	7.46		
	160					
	200					
	242					
5.26	120	$1.2\gamma gbd^2$	-	7.46		
	242					
5.27	242	$0.8\gamma gbd^2$	-	7.46		
		$1.2\gamma gbd^2$				

Table 5.2. *Values of inflation pressure, vertical load, linear velocity, angular velocity, cohesion and friction angle considered for the cases analyzed in Figures 5.17-5.19 and 5.25-5.27 of the current study.*

The flow stress ratio in the DP model was set to unity which means that the yield stress in triaxial tension is equal to the yield stress in triaxial compression. Purely cohesive soil was considered for all analyses involving model (b)while a non-dilatant flow was assumed and the friction angle was set equal to a very small value to avoid numerical convergence problems. Furthermore, the cohesion is equal to $c/\gamma gd=1.25$ and the Young modulus is equal to $E/\gamma gd=10^3$. In addition, the deformable part used for model (b) was divided into two regions (Figure 5.16), i.e. a region containing stiff soil and a region containing soft soil. The region of stiff soil serves for equilibrium purposes so that the final results of the implicit solver where the footprint was obtained can then be used for the initialization of the transient explicit analysis. The soft soil region participates in the tyre-terrain dynamic interaction during the transient phase.

In model (b) two different driving conditions were assumed for the pneumatic tyre (towed and driven). For the towed wheel with inflation pressure 242 kPa and vertical load equal to $1.2\gamma gbd^2$, two different linear velocities were considered (5 km/h and 10 km/h). For a towed wheel with inflation pressure 242 kPa and linear velocity 10 km/h two different vertical loads were assumed ($1.2\gamma gbd^2$ and $2\gamma gbd^2$). For a towed wheel with linear velocity 5 km/h and vertical load of $1.2\gamma gbd^2$, two different inflation pressures were used (200 kPa and 242 kPa).

For the driven wheel with $1.2\gamma gbd^2$ vertical load, the corresponding angular velocity for the free rolling condition for linear velocity equal to 10 km/h (7.46 rad/s) was assumed for four different inflation pressures (120 kPa, 160 kPa, 200 kPa, 242 kPa). For the driven wheel with inflation pressure equal to 242 kPa and angular velocity 7.46 rad/s, two different vertical loads were specified ($0.8\gamma gbd^2$ and $1.2\gamma gbd^2$). For the driven wheel with inflation pressure 242 kPa and vertical load $1.2\gamma gbd^2$ two different angular velocities were used (3.73 rad/s and 7.46 rad/s).

For the implicit analyses of this model the analytical rigid surface was considered to be fixed and a vertical concentrated force was applied at the tyre centre, while the latter was allowed to move freely in the vertical direction. Following that, the rigid analytical surface was replaced with a deformable soil layer, on which the tyre is rolling during the transient stage of the analysis. The displacement along *y* axis and the rotations along the x and z axes of the model at the rim of the tyre were held fixed during this final stage. It is noted that the way the amplitude of the various loads is applied in the model significantly affects the quality of the results. In particular, it was found that by applying a smooth step amplitude instead of its simple definition, lead to the elimination of numerical noise associated with the assumptions mentioned in section 5.1. Ideally, the application of ramp amplitude for prolonged time duration would yield results of optimum accuracy; however this case involves a computationally heavier model (greater number of elements) in terms of maintaining an acceptable aspect ratio of the elements since the dimensions of the road would increase.

5.3.1 Towed Wheels

Towed wheels considered in this study were loaded only with horizontal linear velocity and vertical force, imposed on the centre of the rim. Their rotation occurred due to the friction between the tyre and the rolling surface. However, yielding of the soil material may cause the immobilization of the wheel, depending on the combination of the vertical load, the linear velocity and the inflation pressure. Based on these, a parametric study was conducted in which the effect of the aforementioned parameters was taken into account for the calculation of the dynamic interaction between towed wheels and the supporting soil.

In Fig. 5.17 and Fig. 5.18, results of the angular velocity of the towed wheel are shown, versus its horizontal displacement at the direction of travel. The inflation pressure of the tyre was considered to be equal to 242 kPa. In Fig. 5.17 the effect of linear velocity is demonstrated for wheel with vertical load equal to $1.2\gamma gbd^2$. Initially, the wheel rolls over the rigid domain of the rolling surface. After travelling a distance of 0.4m, it enters the deformable region of the soil, and the angular velocity gradually decreases. This happens due to the fact that as the soil yields due to the loading of the wheel, the stress distributions under the tyre become lower due to the soil strength limitations; therefore the friction force is reduced at the tyre-soil interface. As a result, due to the decreased friction force, the angular velocity decreases gradually, until it becomes zero at a certain point, meaning that the wheel exhibits pure translational motion without rotation. The angular velocity further decreases, becoming negative for a very small travelling distance, after which it becomes constantly zero. Comparing the two curves for different velocities and observing that for the higher velocity the peak negative angular velocity increases, this fact can be explained by taking into account that the accumulation of the soil in the front of the wheel leads to opposite friction forces, which cause the rotation of the wheel with negative angular velocity. This motion is further reversed due to the rotational inertia that has been developed by the wheel. The tyre with the higher velocity will exhibit exactly the same pattern of motion for a longer traveling distance, but this has not been plotted explicitly due to space reasons. In Fig. 5.18 the angular velocity versus the horizontal displacement of the wheel is illustrated for a wheel with the same inflation pressure and translational velocity but two different vertical loads applied at the spindle. It is observed that the wheel with vertical load $1.2\gamma gbd^2$ experiences a higher friction force, which develops due to the decreased yielding response of the underlying soil. In addition, the decreasing slope of the curve is lower than that of the curve corresponding to vertical load $2\gamma gbd^2$, till the wheel travels at a distance of 1m. After this point, as the increased vertical load incurs increased compaction of the underlying soil, the distance needed for the immobilization of the wheel with vertical load $2\gamma gbd^2$ is higher than that for vertical load $1.2\gamma gbd^2$. In order to avoid numerical noise associated with the assumptions mentioned in section 5.1, filtering (of the butterworth type) was performed during the post-processing of the results.

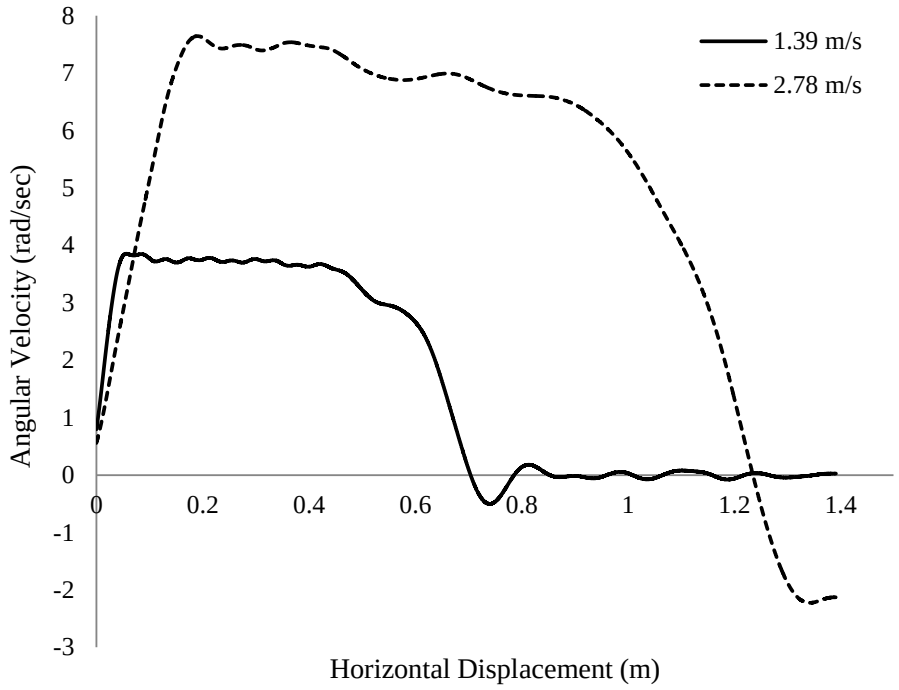

Figure 5.17. *Angular velocity of the towed wheel considered in this study rolling on soft soil (c=1.25γgd, φ=0, ψ=0): effect of linear velocity.*

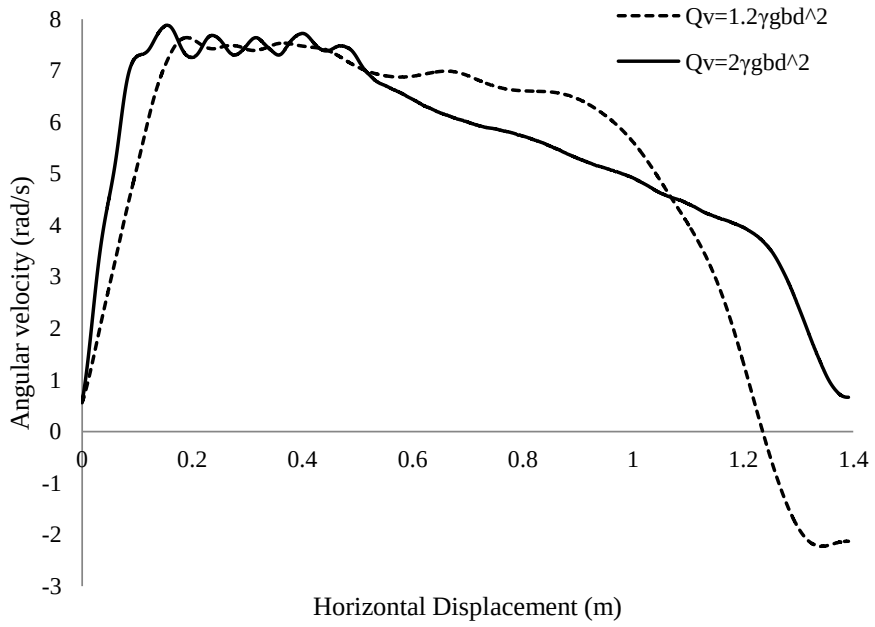

Figure 5.18. *Angular velocity of the towed wheel considered in this study rolling on soft soil (c=1.25γgd, φ=0, ψ=0):effect of vertical load.*

In Fig. 5.19, a wheel with a vertical load of $1.2\gamma gbd^2$ and translational velocity of 1.39 m/s for two different inflation pressures is investigated. The angular velocity is

plotted in Fig. 5.19, whereas in Fig. 5.20 the deformed configuration of the tyre and the soil is shown. A clear trend observed in Fig. 5.19 is the longer distance that is travelled by the wheel with decreased inflation pressure, since a decrease of 20% in the inflation pressure leads to an increase of 15% of the allowed distance prior to the immobilization of the wheel. This occurs due to the fact that for lower inflation pressures (considering the same amount of vertical load) the contact area at the tyre-soil interface increases, which results in lower pressures transmitted into the soil, which in turn leads to slower yielding response and consequently longer travelling distance. In Fig. 5.20 it is apparent that the mesh adaptivity technique has successfully captured the soil accumulation in the region surrounding the wheel footprint causing the bulldozing effect. Although the phenomenon of soil accumulation – observed both numerically and experimentally by Hambleton & Drescher (2008) and Wong & Reece (1967a, 1967b) respectively – does not validate any specific numerical results, Fig. 5.20 provides a clear indication of the realistic dynamic tyre-terrain response that has been observed in all models considered in the current thesis.

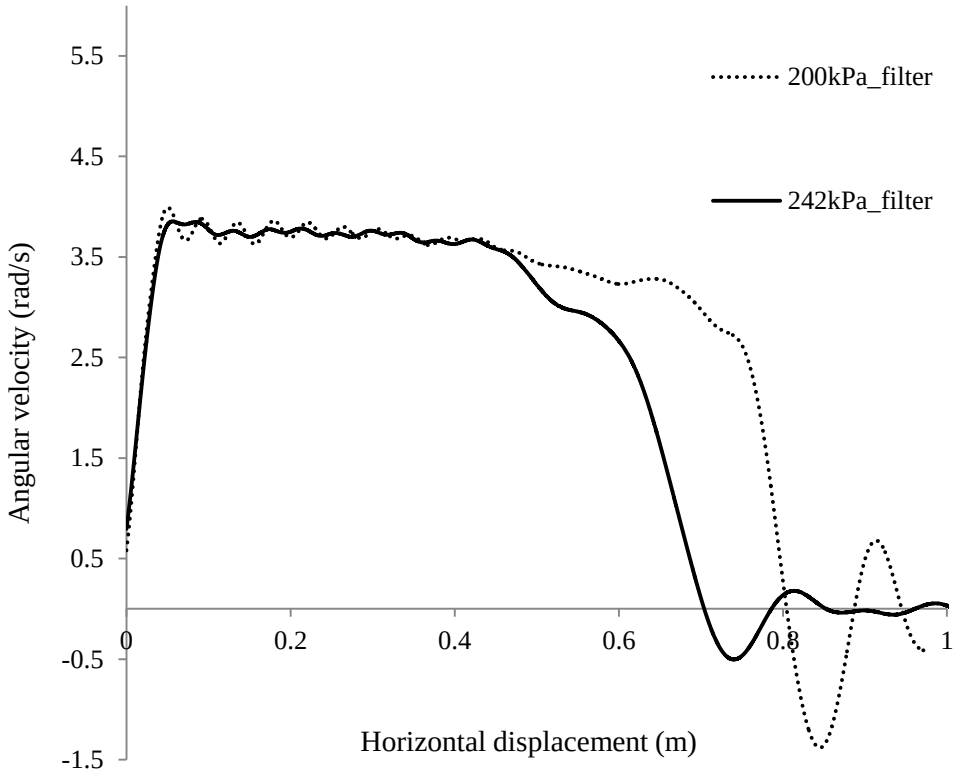

Figure 5.19. *Angular velocity of a towed wheel rolling on soft soil (c=1.25γgd, φ=0, ψ=0) versus horizontal travelling distance for various inflation pressures.*

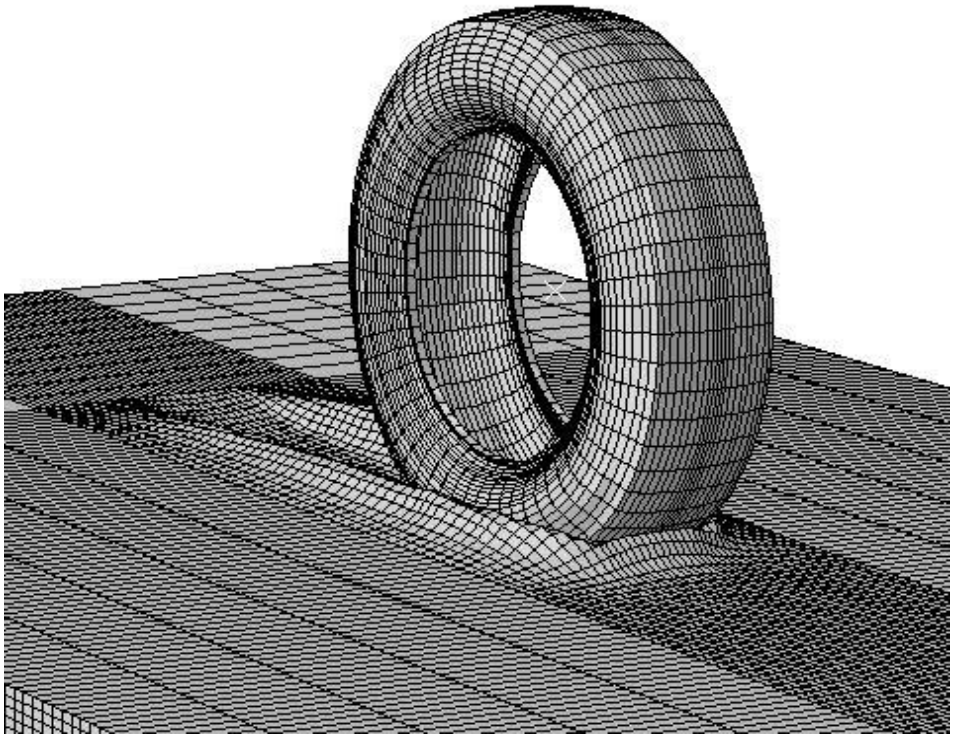

Figure 5.20.*Deformed geometry of the tyre-soil system.*

Due to the already increased computational cost of the analysis – each of the simulation lasted approximately 30 hours on an Intel computer of 3.4Ghz and 16Gb of RAM – a simplified FE tyre model representative of no realistic tyre was developed, shown in Fig. 5.21, and the significant effect of the inflation pressure on the overall driving response of the tyre was investigated to a greater extent. The latter model was considered in this study with an aspect ratio of 0.33 and a given diameter of 0.381m. The inflation pressure of the tyre was set equal to four distinct values ranging from 80 kPa to 242 kPa. The vertical force (parallel to the z axis) Q_v exerted at the centre of the tyre was set equal to four different values ranging from $1.25\gamma gbd^2$ to $2.4\gamma gbd^2$. The value of the translational velocity imposed at the tyre centre was defined so that the tyre travels along the distance available from the soil layer in 1.2sec. It was from the results of the analyses that after this time period the tyre responds in quasi-steady state conditions. The time required to attain this state depends highly on the tyre dimensions and the soil properties. Similarly with the detailed FE tyre model – model (a) – and in order to avoid numerical problems emerging from zero pivots during the explicit finite element analysis, lumped mass was again added at the centre of the tyre, as well as rotary inertias in all degrees of freedom. The hyperelastic and viscoelastic

material law used for the definition of the simplified FE model is identical with the one presented in section 3.2.2.

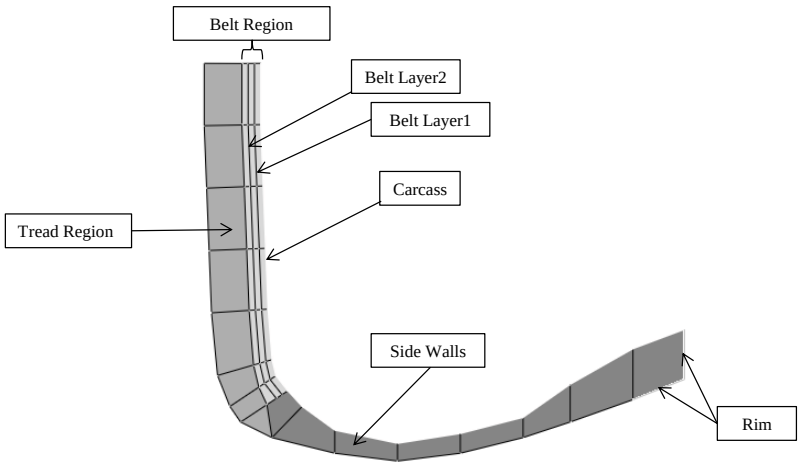

Figure 5.21.*Cross section of the simplified deformable tyre (half-axisymmetric model).*

The latter FE model was developed under the scope that the inner parts of the tyre with principal effect on the rolling behaviour – belts and carcass – will be included, and their respective number of elements will be reduced to the lowest level possible. Following that the effect of the inflation pressure was investigated via a large number of test cases. The dimensions of the tyre – aspect ratio and diameter – were chosen in terms of creating a relatively stiffer soil with $c/\rho gd=1.25$ which will not yield under the compression and shear tension of a towed wheel.

In Fig. 5.22 the average ratio of the resistance force to vertical load is plotted versus the inflation pressure for the simplified FE tyre model with aspect ratio of 0.33. The average value of the horizontal resistance force is taken for the time interval corresponding to the rolling of the tyre. It is seen that for small inflation pressures the non-dimensional resistance force decreases slightly as the inflation pressure increases. This trend results from the fact that as the inflation pressure increases, the contact area decreases, and therefore the soil accumulation in front of the tyre decreases. As the inflation pressure becomes higher (exceeding 220 kPa in this case), the tyre stiffness increases, which for the given soil conditions leads to a rigid tyre behaviour with higher dimensionless sinkage, higher soil accumulation, and therefore higher rolling resistance. These two different tendencies invoke a resistance force minimum (which occurs for inflation pressure somewhat lower than 220 kPa in the case shown in Fig.

5.22). In Fig. 5.23 the phenomenon of soil accumulation in front of the towed wheel is presented. It was ensured in the analyses performed in this study that the ALE adaptive mesh algorithm used captured this phenomenon in a satisfactory way.

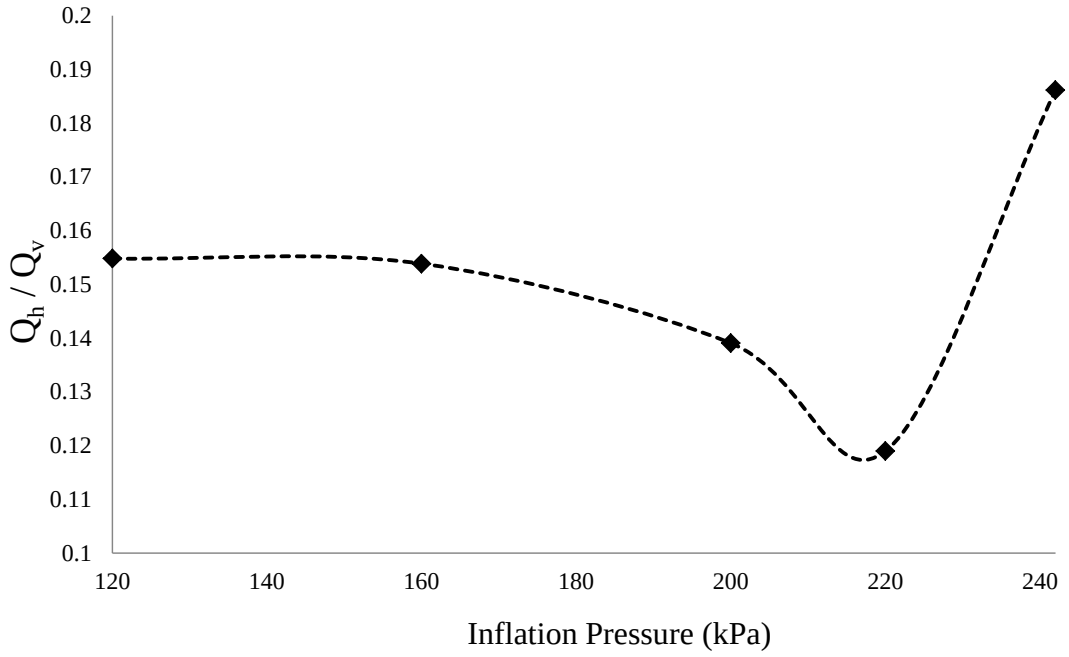

Figure 5.22. *Average ratio of resistance force to vertical load for various inflation pressure.*

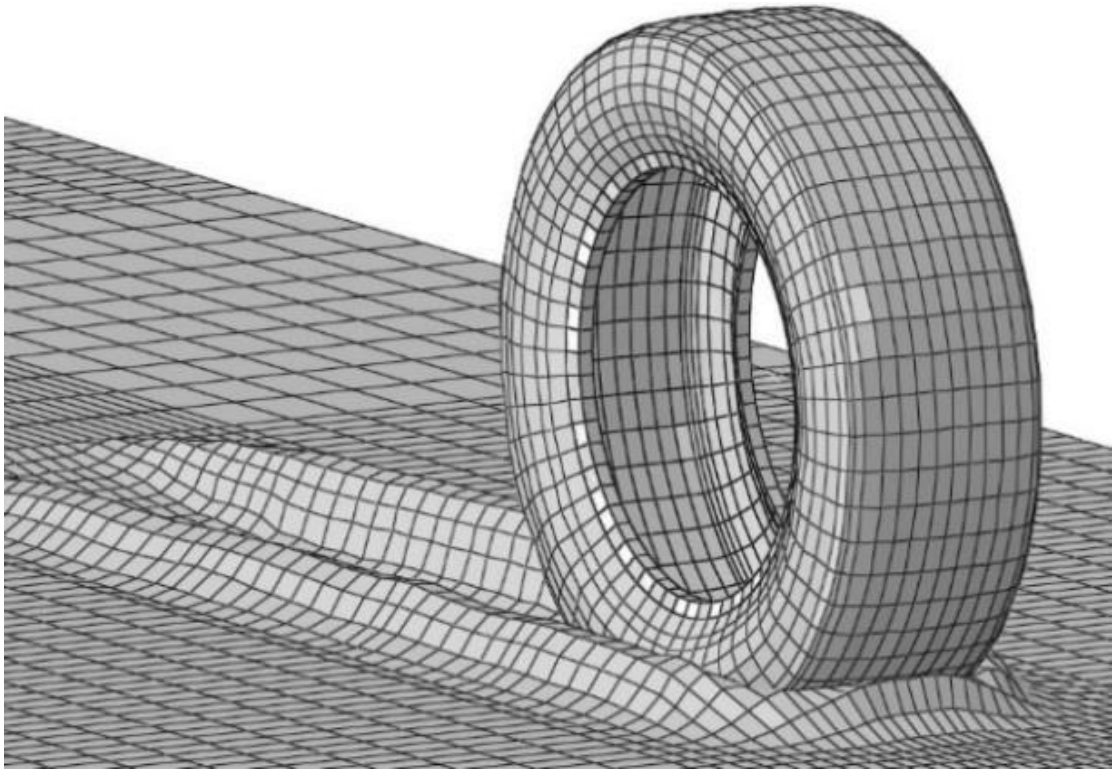

Figure 5.23.*Deformed configuration of the simplified FE tyre – soil model.*

In Fig.5.24 the average slip ratio of the simplified deformable towed tyre and vertical load of $1.5\gamma bd^2$ is plotted versus the inflation pressure. It is observed that by reducing the inflation pressure, the slip ratio is also reduced, with a different rate of decrease, depending on the pressure range and the soil conditions. For the given soil the biggest slip ratio decrease is observed for inflation pressure varying from 200 kPa to 160 kPa. In addition, a further decrease from 160 kPa to 120 kPa does not result in a significant variation in the slip ratio, whilst at the same time as shown in Fig. 5.22, the resistance force increases. Furthermore, the results presented in Fig. 5.22 and Fig. 5.24demonstrate a main trade-off between the slip ratio and the bulldozing force. While minimum slip ratio accompanied with minimum resistance force is desired in vehicle dynamics, mainly for safety and economical reasons respectively, there is only one optimum (case-dependent) value of the inflation pressure which will satisfy both of these requirements.

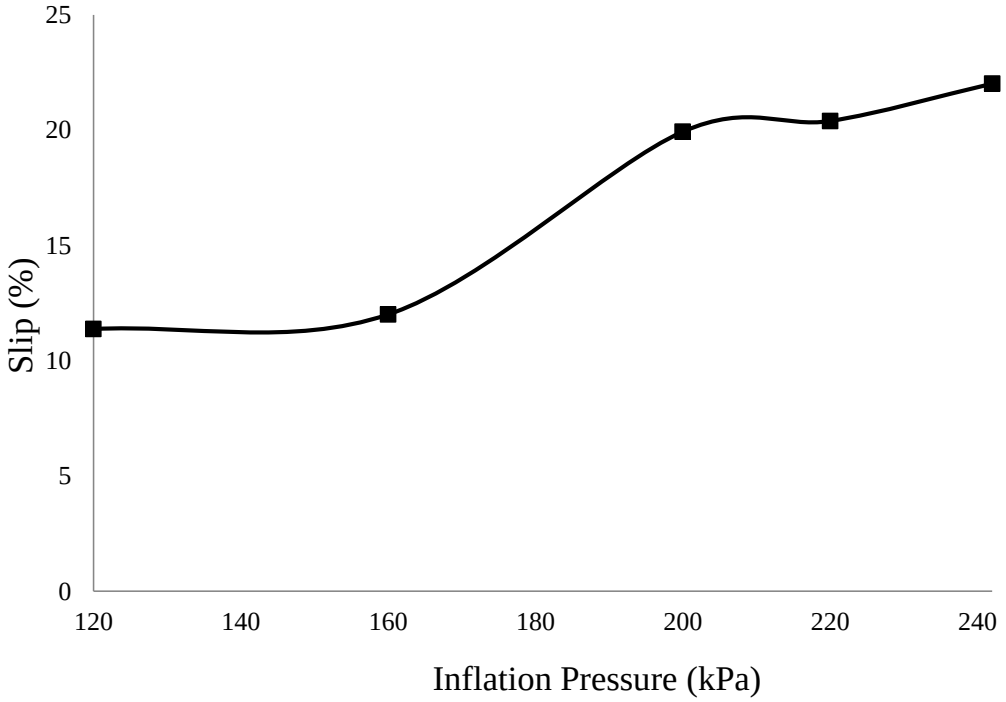

Figure 5.24. *Slip ratio of the tyre versus its inflation pressure, for b/d=0.33 and Qv=1.5γbd2.*

5.3.2 Driven Wheels

A more common representation of the wheels used for off road vehicles is the one of the driven wheel, where an angular velocity is imposed on the spindle of the wheel through the shaft axle and the wheel moves due to the friction that develops at the interface between the tyre and the rolling surface. Although the inflation pressure

should be relatively high for on-road vehicles in order to reduce various parameters such as the rolling resistance, in off-road vehicles a balance should maintained between the sinkage of the wheel into the soil and the resistive forces being developed by the tyre terrain interaction.

In Fig. 5.25 the dimensionless sinkage of the driven wheel – the detailed FE tyre model – with ω=7.46 rad/s and vertical load $1.2\gamma gbd^2$, for four distinct values of inflation pressure is plotted against travelling time. The sinkage (s) is non-dimensionalized by dividing it with the sinkage of the wheel resting on a rigid surface (s_0), which occurs purely due to the tyre deformation. The reasoning behind this is that the effect of the tyre deformability is isolated after the normalization of the sinkage, and therefore the variation of the normalized sinkage with time is affected only due to the soil compliance. The configuration of the various curves if the initially computed sinkage is plotted does not show a clear trend of the effect of the inflation pressure on the sinkage stemming from the soil deformation, which is now obvious after the normalization has been done. It appears that as the inflation pressure increases, the dimensionless sinkage increases also, and this trend is more pronounced after the wheel fully enters the soft soil. This is a direct consequence of the fact that by reducing the inflation pressure, the contact area of the tyre footprint increases, and therefore lower pressures are found at the tyre-soil interface. It is observed that the sinkage of the wheel into the soil increases until it reaches a peak value, which occurs approximately at 0.25sec (1.25sec at the horizontal axis). After this peak value, the sinkage decreases and oscillates around a constant value, which is called the quasi-steady-state sinkage. Quasi-steady-state response is presented for a simulation time of 0.5sec. More specifically and for the cases of 242kPa and 120kPa it is noted that a reduction of 50% on the inflation pressure results in approximately 15% reduction of the dimensionless sinkage. It has to be noted that the time period required for the wheel to attain its steady-state response is a function of its size, inflation pressure, vertical load and the soil properties. Furthermore, similar trends for wheels interacting with deformable terrains have been observed in the literature (Hambleton & Drescher, 2009). In that study, rigid wheels with various widths have been considered, whereas in the current study the variation of width is indirectly addressed through the variation of the inflation pressure; the effects of the two parameters are similar, since by decreasing the inflation pressure the contact area (and consequently the tyre width)

increases. Therefore, the qualitative similarity between the two different trends shows that the corresponding effects have been adequately captured in the models.

In Fig. 5.26 it seems that in steady state conditions the tyre with the higher inflation pressure travels with a lower velocity, which results from the higher dimensionless sinkage and narrower footprint area compared to the tyre with the lower inflation pressure, in which case a smaller dimensionless sinkage and wider footprint area occur. For driven wheels, the linear velocity is primarily determined by two main effects: the rolling radius and the vertical displacement of the wheel into the soil. Regarding the rolling radius, its value results from the combined effect of the inflation pressure and the vertical load. For instance, for a given inflation pressure and two different vertical loads, two different rolling radii will result. Regarding the sinkage of the wheel, it depends on the pressure distribution transmitted from the footprint to the soil; this distribution is a function of the combined effect of the inflation pressure, the vertical load and the soil properties. The outcome of this interdependence isthat there are two conflicting trends relating the inflation pressure and/or the vertical load, and the linear velocity.

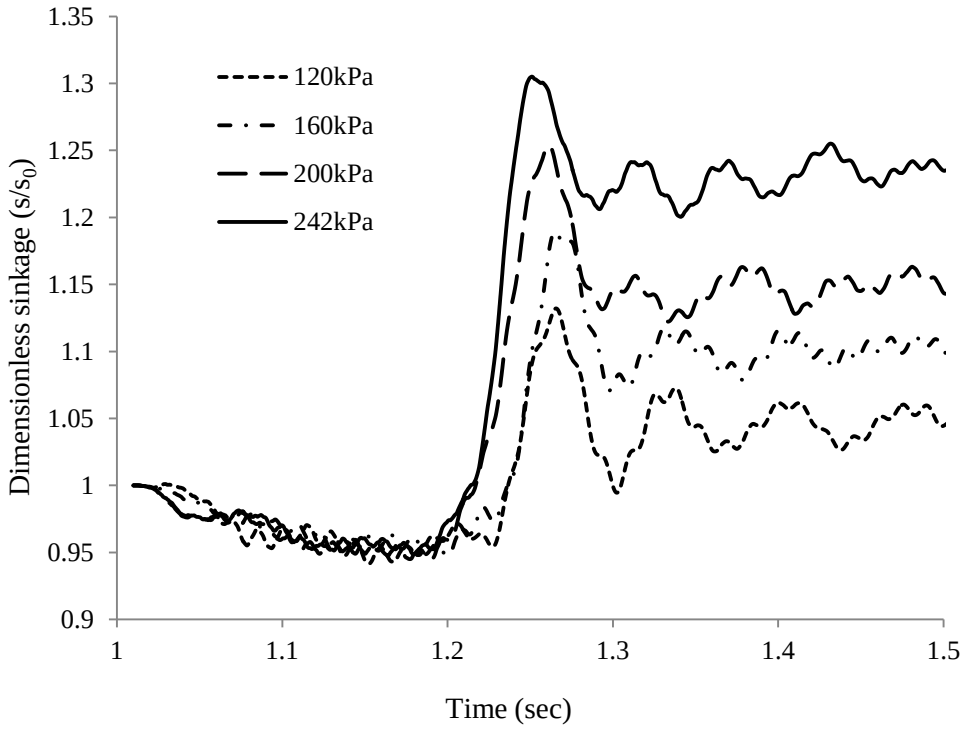

Figure 5.25. *Dimensionless sinkage on soft soil (c=1.25γgd, φ=0, ψ=0) with ω=7.46 rad/s and Qv=1.2γgbd2 for a wide range of inflation pressures.*

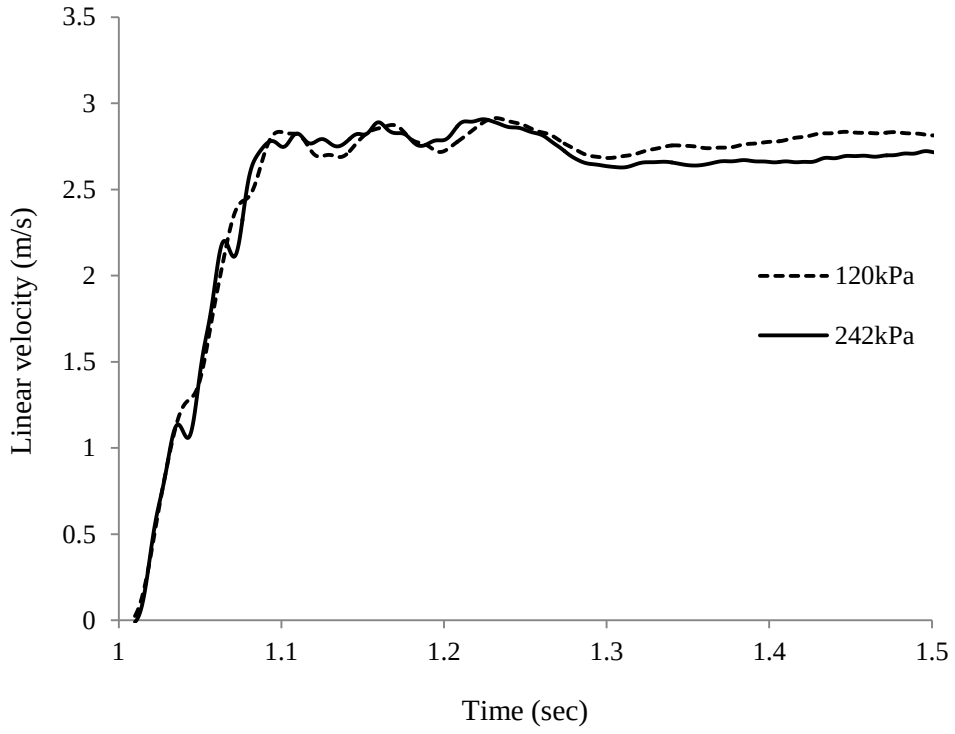

Figure 5.26. *Linear velocity of a wheel on soft soil (c=1.25γgd, φ=0, ψ=0) with ω=7.46 rad/s and Qv=1.2γgbd2 for two distinct inflation pressures.*

In Fig. 5.27, the dimensionless sinkage of the wheel with angular velocity equal to 7.46 rad/s and inflation pressure equal to 242 kPa is plotted versus time. For the time duration from 1sec to 1.2sec the wheel is rolling over the rigid surface, whereas for the remaining time duration of the analysis the wheel is rolling on soft soil. It is shown that by increasing the vertical load the dimensionless sinkage increases. Moreover, the undulations during the quasi-steady state response are more pronounced for increased vertical load. It is noted that the peak in the dimensionless sinkage which exists at the time instant of roughly 1.25sec (as noted at the axis) occurs due to the steep variation of the rolling surface as the wheel enters the soft soil from the rigid surface. Due to this discontinuity, an oscillation begins, which lasts all over the steady state response, eventually attained by the tyre-soil system. For larger values of vertical load, the quasi- steady state sinkage increases as expected. However, the applied vertical force cannot exceed certain limits, at which the underlying soil comes to a state of failure. These limits are determined by the bearing capacity of the soil.

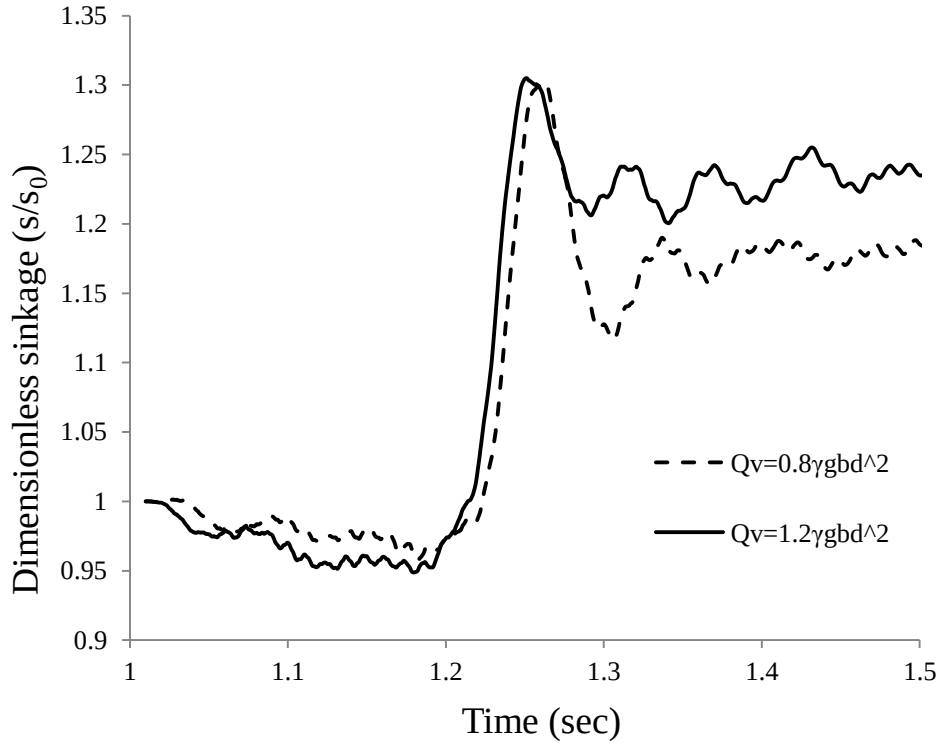

Figure 5.27. *Dimensionless sinkage of a wheel on soft soil (c=1.25γgd, φ=0, ψ=0) with ω=7.46 rad/s and inflation pressure 242 kPa for two values of the vertical load.*

5.4. Discussion

The final reference configuration of the tyre model, developed in Chapter 4, was designed to interact with a rigid road – model (a) – and a deformable terrain – model (b). With regards to the rigid road, a SST analysis was conducted and the free rolling conditions of the tyre were extracted. Based on the latter rolling conditions, the interaction between the tyre and a rigid road with bumps was modelled and the rolling responses of the tyre under various loading conditions were studied. Subsequently, the rigid road was replaced by a soft deformable terrain described by a linear constitutive material criterion, being either MC or DP, and the response for driven and towed wheel conditions under various loading effects was investigated.

In model (a), the vertical displacement of the rim and the contact area of the tyre with the road were measured, for a number of inflation pressures and loads, in order to confirm the validity of the tyre model. Then, the effect of the linear velocity, the inflation pressure and the vertical load acting on the tyre and their effect on its rolling

response were studied. It was found that by increasing the linear velocity there is an increase on the resulted oscillations at the spindle while by increasing the inflation pressure the same oscillations were reduced. Furthermore, it was observed that by increasing the vertical load the tyre was experiencing larger compression rates which resulted in reduced vibrations at the spindle.

In model (b), driven and towed wheels were designed and the effects of the inflation pressure, the angular velocity and the vertical load on the rolling response of the wheel were investigated. It was observed that by reducing the inflation pressure the vertical displacement of the wheel into the soil was reduced which resulted in an improved rolling response of the tyre, being either towed or driven. Furthermore, it was noted that an increase on the applied vertical load of a towed wheel resulted in an improved rolling response of the wheel which however was limited by the bearing capacity of the soil. Finally, it has been shown that the inflation pressure is one of the key parameters with principal effect on the driving response of the tyre and it should be maintained at intermediate-low levels (lower than 160 kPa), opposite to on road tyres where highly inflated tyre are desired in terms of reducing the rolling resistance.

Chapter 6

Tyre – Terrain Interaction: Analytical Method

6.1. Introduction

In this chapter, a novel semi-analytical formulation has been developed for the calculation of the static and dynamic response of an off-road tyre interacting with a deformable terrain, which utilizes soil parameters independent of the size of the contact patch (size-independent). The tyres involved in the solution presented, can be categorized in rigid and/or deformable, with or without tread pattern. A detailed presentation of the proposed semi-analytical solution is developed, along with its assumptions and limitations. A flowchart of the proposed solution is provided, showing the main steps of the numerical implementation. With regards to the pressure – sinkage response, Lyasko's (2010a) equation is used along with additional modifications, so that the geometry of the tyre can be accurately represented. Furthermore, Janosi-Hanamoto's (1961) equation is implemented for the shear stress response in conjunction with Wong & Reece (1967a) shear displacement mathematical formulation. After the development of the analytical solution, a parametric study is conducted, and the effect of the inflation pressure, the geometry of the tyre and the tread pattern, on the overall driving behaviour is illustrated. Various test cases have been examined, characterized in terms of vertical load, tyre dimensions, soil properties, deformability of the tyre, and tread pattern. It has been found that the proposed model can qualitatively capture the response of a rolling wheel on deformable terrain.

In order to apply the proposed analytical solution, the parameters related to the LSA model of the soil have to be specified, since the LSA model is part of the novel analytical solution. Due to lack of suitable experimental data, these parameters are calculated indirectly, through the use of the finite element models already developed

in the previous chapters. The steps followed toward this purpose are mentioned in the following.

Given that the bevameter tests in general involve large deformation of the soil, a transition is needed from the Lagrangian formulation of the soil to the Eulerian formulation, since the latter can accommodate much larger strains, and is less prone to premature termination of the finite element analysis. For this change between the two soil formulations it has to be ensured that these exhibit similar load-sinkage response. For the case of static indentation of a rigid wheel in a deformable soil, it was found that the two formulations yield results in good agreement with those of the literature (Hambleton & Drescher, 2008), as well as with each other, as shown in Figure 6.2.

After establishing that the Eulerian numerical model of the soil is reliable, the rigid wheel is replaced with a rigid plate, so that the whole numerical model reflects a virtual bevameter test. This model was analysed for various deformable terrains subject to increasing values of vertical load applied to the plate. In this way, the pressure-sinkage curves were obtained for various soils.

In order to obtain a pressure-sinkage curve for a specific soil by applying the LSA model, its constitutive parameters have to be specified first. It is considered that, if realistic values are assigned to these parameters, the LSA model will yield a dependable pressure-sinkage curve associated with the soil response. Apart from this, the inverse is assumed to be possible, i.e. to obtain the values of the unknown parameters from the pressure-sinkage curve. This is possible given the fact that the two models share similar soil parameters. This concept constitutes the basis of the development of an optimisation scheme, in each iteration of which directed values are set to the LSA soil parameters, aiming at minimizing the difference between the pressure-sinkage curve provided by Abaqus as above, and the pressure-sinkage curve provided by the LSA model. Eventually, this optimisation procedure will converge to the proper values of the unknown constitutive parameters of the soil, which can reproduce the pressure-sinkage curve obtained by the finite element models.

At this point, where reliable soil parameters of the LSA model have been calculated, they are inserted in the novel analytical solution, the results of which are validated by analogous numerical results, presented in chapter 3. It is shown that satisfactory agreement exists between the results.

Finally, the novel analytical solution is applied for various cases of treadless and treaded rigid and/or deformable wheels, and useful conclusions are drawn. Three analytical and/or semi-analytical models were developed as follows: (a) a rigid plate, (b) a rigid wheel and (c) a pneumatic tyre, all of them interacting with various deformable terrains. The qualitative response presented in the results is a clear indication that the proposed model can efficiently capture the basic characteristics of a rolling tire.

6.2. Soil formulation

In this section, the method utilised for the extraction of the unknown soil parameters required for the implementation of the LSA model is illustrated. Initially, the Coupled Eulerian Lagrangian technique for a rigid wheel indented into the soil is depicted and a virtual pressure-sinkage test, where a rigid plate is indented into the soil, is developed. Subsequently, the numerical pressure-sinkage response obtained is used in an optimisation scheme for the extraction of the soil parameters necessary for the application of the novel analytical solution developed in this study.

6.2.1 Transition from Lagrangian to Eulerian soil formulation

Initially, the ALE method – described in Chapters 3 and 5 – was used and was proven insufficient to control the excessive element distortions of the soil. Therefore, the development of a FE model capable to simulate the large deformation involved in the indentation of a rigid wheel and/or rigid plate into the soil necessitated the transition from a Lagrangian soil formulation to an equivalent Eulerian soil formulation. An advantage of the latter formulation is that, in the Eulerian parts, the mesh is stationary and the material is allowed to flow through it, allowing in this way the investigation and development of models where large deformation exists such as a highly nonlinear indentation of the plate and/or the wheel into the soil. This method is commonly referred as the Coupled Eulerian Lagrangian (CEL) method and it should be noted that with this method the computational cost increases substantially compared to purely Lagrangian techniques.

Figure 6.1 illustrates the CEL configuration of the rigid wheel – terrain interaction in three different states. In Fig. 6.1 (a) the undeformed configuration of the CEL model is presented. It can be noted that the elements of the wheel initially seem to penetrate

the mesh of the soil. Although there is an overlap of the wheel and soil meshes, no penetration issues exist, since the material of the soil is set to be located under the horizontal plane passing through the contact point of the wheel and the soil. The mesh above this plane is considered to be initially void. Figure 6.1 (b) and Figure 6.1 (c) depict the deformed configuration of the soil with and without the initial void mesh above the wheel contact patch, in order to illustrate the differences in the deformed configuration. The material assignments for the elements were modelled with the volume fraction tool where a discrete field is required, which is implemented at the initial step of the solver as a predefined material field. The same boundary conditions and constraints presented in section 3.2 were used for the CEL model. Since a Static step definition for eulerian models is not available in Abaqus, a Dynamic/Explicit step was specified with a velocity boundary condition so that the wheel moves vertically until it reaches the maximum dimensionless sinkage s/d=0.1. The process was modelled with displacement and/or velocity control where the dynamic effects are not taken into consideration.

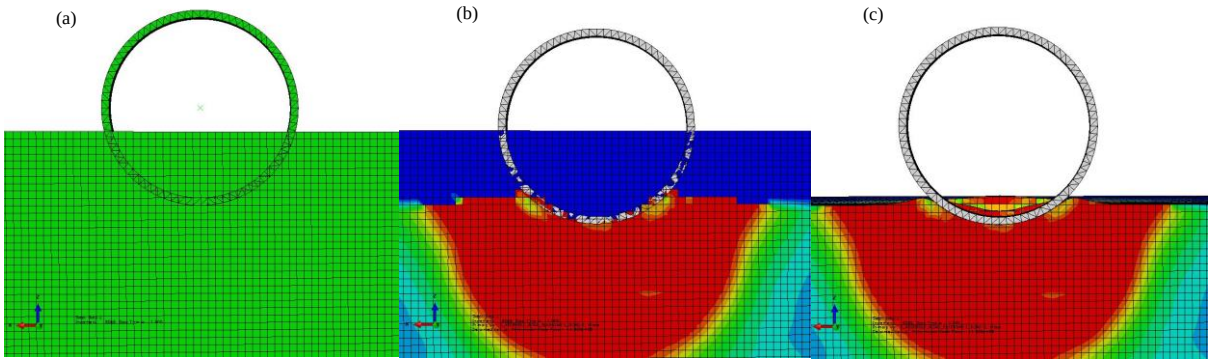

Figure 6.1. *Coupled Eulerian Lagrangian (CEL) model, average Von Mises stress for (a) un-deformed configuration, (b) deformed configuration with void elements and (c) without void elements, for a cohesive soil ($\varphi=0^o$, $\psi=0^o$ and $c/\gamma gd=1.25$).*

The numerical results obtained from the Lagrangian and the Eulerian techniques for a rigid wheel being indented into the deformable soil described by the linear MC and linear DP failure criteria in comparison with results from the literature are presented in Fig. 6.2. It is evident that the numerical results associated to the Lagrangian model fit closely results found in Hambleton & Drescher (2008), while the results obtained

from the CEL model and for the DP failure criterion tend to overestimate the behavior. At the same time, by using the MC constitutive model in the CEL model, the results obtained are in close agreement with the results from the literature and with the Lagrangian model. The Eulerian model with MC and the Lagrangian model with DP were found to yield the most accurate response compared to the results from the literature. From the above, it is concluded that the CEL model developed is reliable, and therefore, the research in this section was focused mainly on the CEL method.

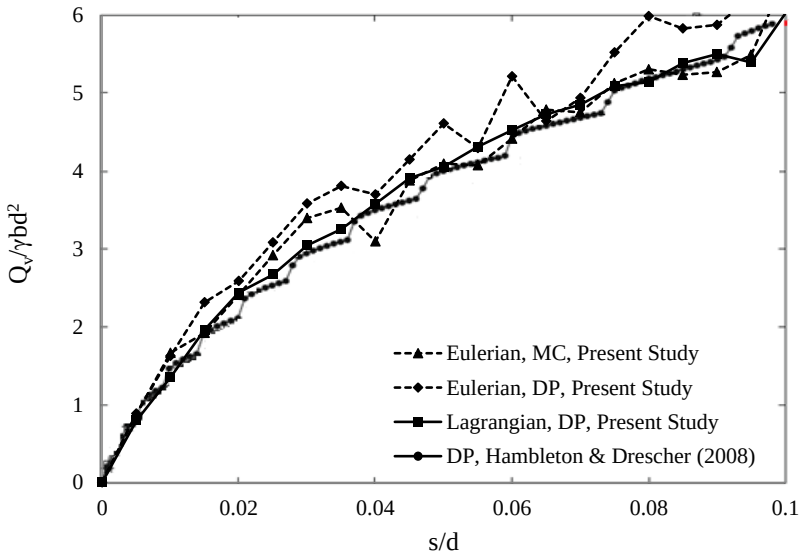

Figure 6.2.*Dimensionless vertical load versus dimensionless sinkage for wheel with b/d=0.3 and cohesive soil ($\varphi=0^o$, $\psi=0^o$ and $c/\gamma gd=1.25$).*

6.2.2 Virtual pressure-sinkage test in FE

Following the acquisition of a realistic soil model governed by the MC failure criterion as described in the previous section, the rigid wheel was replaced by a rigid rectangular plate and a model which simulates a virtual pressure-sinkage test was developed.

Figure 6.3 presents the deformed configuration of a cohesive soil described by the linear MC failure criterion into which a rigid rectangular plate is indented, using the same values for the cohesion and the friction angle as for the rigid wheel illustrated in Fig. 6.1. The virtual pressure-sinkage test was performed with a plate of 0.15m width

and 0.3048m length and for a number of different deformable terrains – cohesive and frictional soils – frequently used in the literature. The total duration of the penetration step was 1sec and the full amplitude of the pressure was reached at 0.5sec in an effort to extract a quasi-static response of the plate in terms of vertical displacement. In terms of maintaining consistency with the road part utilised in Chapter 3, 67,500 EC3D8R elements were used with a uniform discretization. The minimum size of the element was set to 20mm for the region of interest. As illustrated, in Figure 6.3 no passive wedge is formed under the plate after it is loaded. This is mainly due to the fact that the sinkage of the plate into the soil is relatively large compared to the dimensions of its contact area and larger than the sinkage of the wheel shown in Figure 6.1. This has invoked larger flux of the soil material through the finite element mesh in the case of the plate and, therefore this prevents the explicit formation of a passive wedge.

(a) (b)

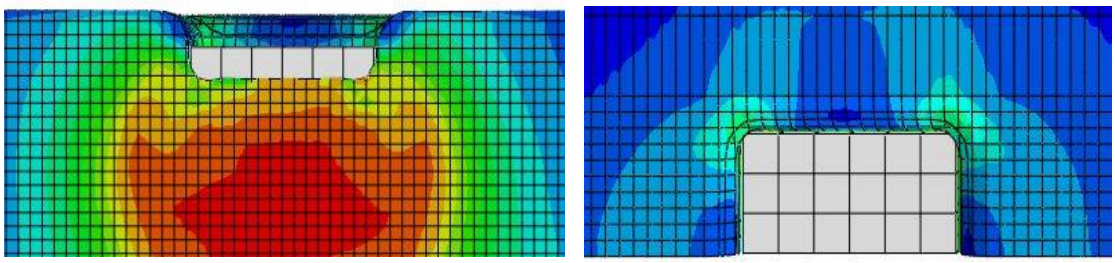

Figure 6.3. *Average Von Mises stress of the CEL model of a rigid rectangular plate with dimensions 0.15m by 0.3048m indented into a cohesive soil ($\varphi=0^o$, $\psi=0^o$ and $c/\gamma gd=1.25$), (a) Side view and (b) Top view of the reference configuration.*

Subsequently, the numerical pressure-sinkage response was extracted for a number of different soil samples and was used as input for an optimisation procedure. A least square method was utilised and the missing soil parameters – presented in Table 6.1 – were extracted so that the analytical pressure – sinkage behavior obtained from Lyasko's model, matches the numerical sinkage response of the rigid rectangular plate. Figure 6.4 illustrates the aforementioned fitting process for a frictional sandy soil. It is noted that the Mohr-Coulomb soil parameters (c, φ) are not necessarily equal between the Abaqus CEL model and the Lyasko's analytical solution. This happens because these parameters in Lyasko' s model are calibrated from experimental data from the surface layer of the soil, limited by the hardpan depth H, whereas in Abaqus the soil is considered homogeneous without variation in c and φ along its depth. Due

to this difference between these soil parameters, which are additionally affected by the hardpan depth itself, the hardpan depth H along with the cohesion c and friction angle φ of the soil were considered as the design variables during the optimisation procedure. Attention has to be paid in the specification of the upper and lower boundaries of the design variables, as this requires careful consideration of each case study as well as experience in soil mechanics. The objective function of the optimisation procedure to be minimized is set to be equal to the absolute value of the difference between the numerical and the LSA pressure-sinkage curves.

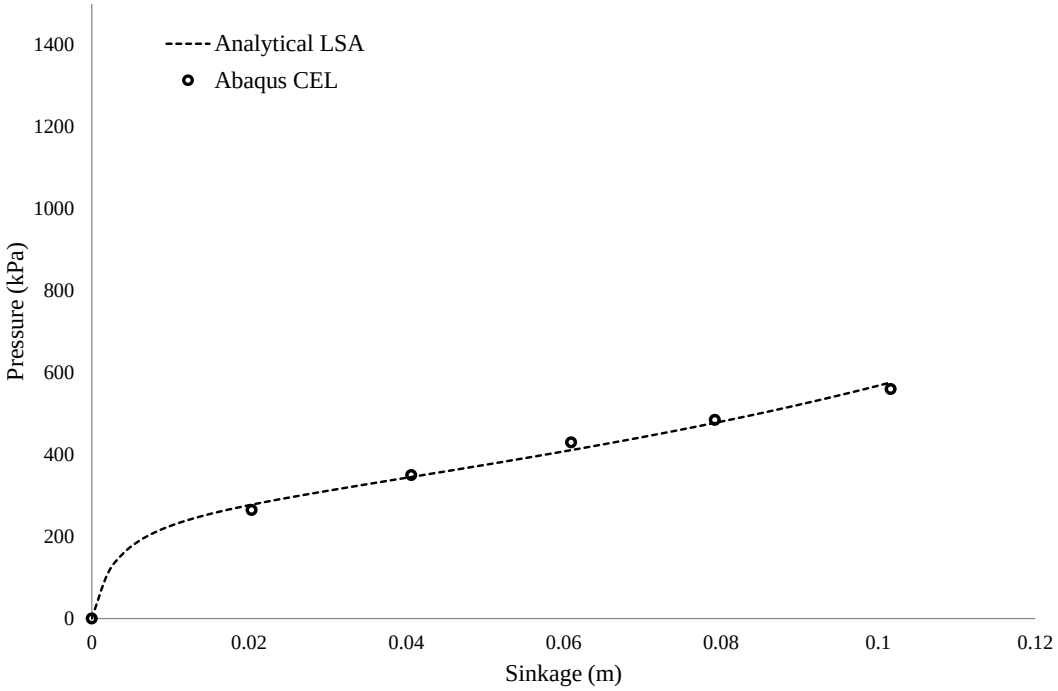

Figure 6.4.*Fitting of LSA model to numerical pressure-sinkage response for frictional sand.*

	c (kPa)	φ (deg)	K (mm)	mew (-)	H (m)	Soil Unit weight (kg/mm^3)	Moisture Content (%)
Sand 1	0.1	32.5	25	0.8	1.4	1442	2.3
Sand 2	0.25	33	10	0.8	0.95	1773	2.3
Sand 3	2.4	32	10	0.8	0.25	1773	2.3
Sand 4	0.7	30	10	0.8	1.22	2000	2.3
Loam	1.95	32.5	10	0.6	0.33	1330	11.4
Sandy Loam	1	32	10	0.7	0.52	1350	2
Wet Loam	20.5	28.5	10	0.55	0.35	1153	23.4
Wet Clay 1	13.05	1	6	0.5	0.58	2100	22
Wet Clay 2	7.58	6.5	6	0.5	0.71	1912	31
Wet Clay 3	10	1	6	0.5	0.51	2000	22

Table 6.1 Optimised Material properties (c, φ and H) utilised for the mathematical formulation of the soil. Parameters K, mew, Unit weight and Moisture were utilised as found in Wong (2001).

Figure 6.5 illustrates the pressure-sinkage response according to the analytical formulation of a rigid rectangular plate – described by equation 2.25 according to LSA model – being indented into various terrains, with material properties illustrated in Table 6.1, subject to an increasing vertical load. It is clear that initially the vertical displacement is increasing quite sharply, while after a certain value of normal load, the vertical displacement tends to reach a maximum sinkage notated as z_{max}. Thus, after a certain limit of normal pressure there is a clear indication that the soil compaction tends to create a relatively stiffer soil specimen with higher compaction resistance. Following that, it can be argued that the material parameters of the soil interacting with the front and the rear wheel of the vehicle will be completely different, since the latter wheel rolls over an already compacted region of terrain with different constitutive properties. The maximum allowed penetration of the plate was set as $z_{max}=0.8H$, where H is defined as the hardpan depth of the soil, which is virtually equal to the depth of the upper soil layer. The high dependency of the results on the hardpan depth should be highlighted since misuse of this parameter may be the source of large uncontrollable errors. It is noted that loam terrains yield the highest rate of pressure increase for the lowest sinkage, while at the same time on clayey types the highest rate of sinkage occurs for the lowest pressures. Sands are exhibiting an intermediate state where they can bear the same amount of pressure with the loamy terrains at a lower sinkage.

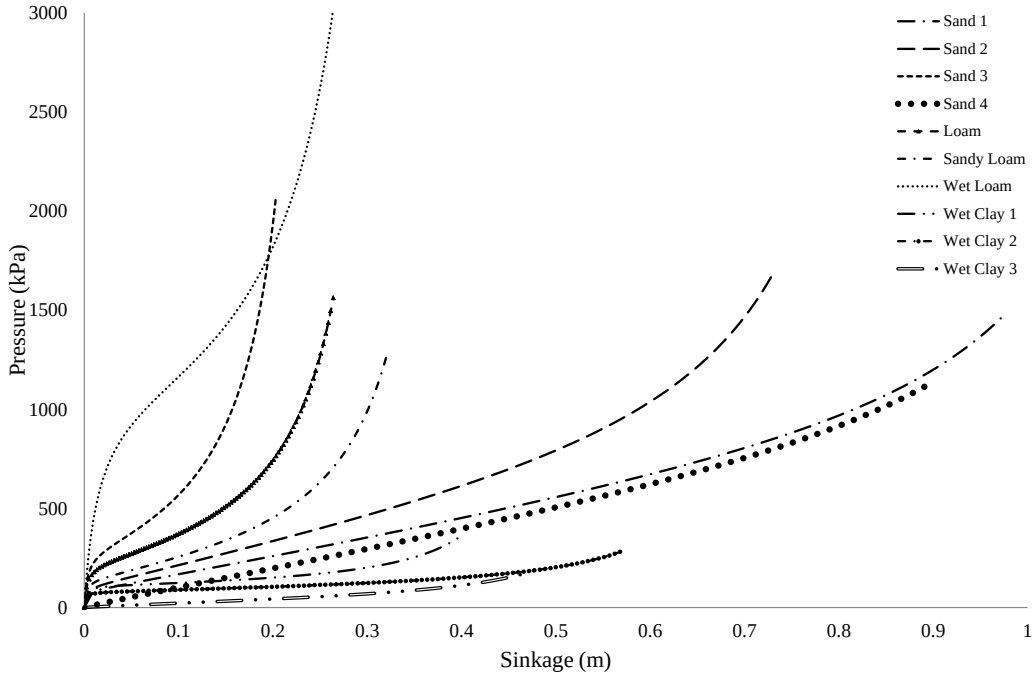

Figure 6.5.*Pressure-Sinkage response for various soils, using LSA model.*

Figure 6.6 presents the shear behavior of frictional sand under the effect of an increasing normal pressure. Each of these curves represents a shear stress response for an increasing vertical load. It is noted that by increasing the shear displacement the shear stress sharply increases up to a certain point of maximum shear stress, usually located on early stages of shear displacement, and this value cannot be exceeded with further increase in the shear displacement. Mohr-Coulomb failure criterion is used for the determination of the maximum local shear stress and Janosi-Hanamoto's (1961) equation for the local shear stress displacement.

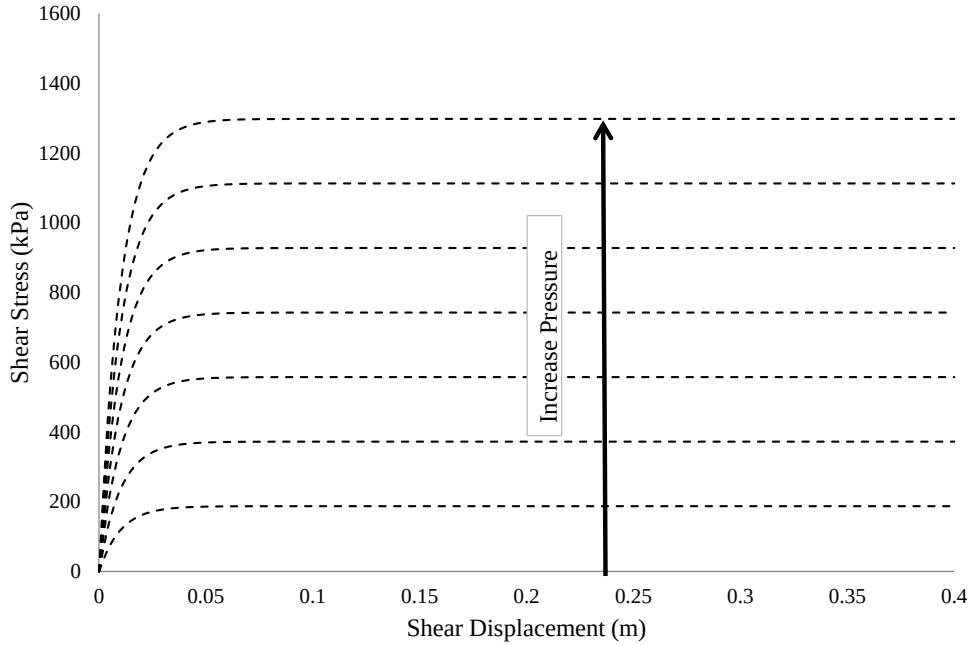

Figure 6.6.*Shear Stress response for frictional sand, as per Janosi-Hanamoto's model.*

Figure 6.7 illustrates the pressure-sinkage response of a rigid plate pressed into a frictional sandy soil and for various size dimensions of the plate. By increasing the length of the rectangular plate the state of maximum vertical penetration is reached at lower pressures. Similar trend with the one observed in the FE models where by increasing the width either of the rectangular plate or the rigid/deformable tyre – increase of the aspect ratio of the wheel – the dimensionless sinkage was decreasing for the same amount of vertical load. It should be highlighted that Lyasko's equation takes under consideration simultaneously, the length and the width of the plate, while Bekker's equation, deals only with the smaller dimension between these two. For instance use of Bekker's equation for a plate with a fixed and relatively small width and a variable length would not yield any difference on the pressure-sinkage results.

Following a thorough literature review on Bekker's model and the simplified examples illustrated in the above-mentioned figures of the analytical model with the use of a rectangular plate, the most fundamental limitations of Bekker's equation can be presented as: (a) It utilizes non-invariant soil parameters which are highly dependent on the dimensions of the plate used; hence, no universal trend can be extracted, (b) utilization of the smallest side of the plate and/or contact patch of the tyre, which translates to no deviation on the results if the biggest dimensions changes and (c) a constant pressure distribution is assumed along the width of the plate and

consequently along the width of the tyre. In our effort to overcome some of these limitations a new semi-analytical pressure sinkage expression was developed based on invariant soil parameters.

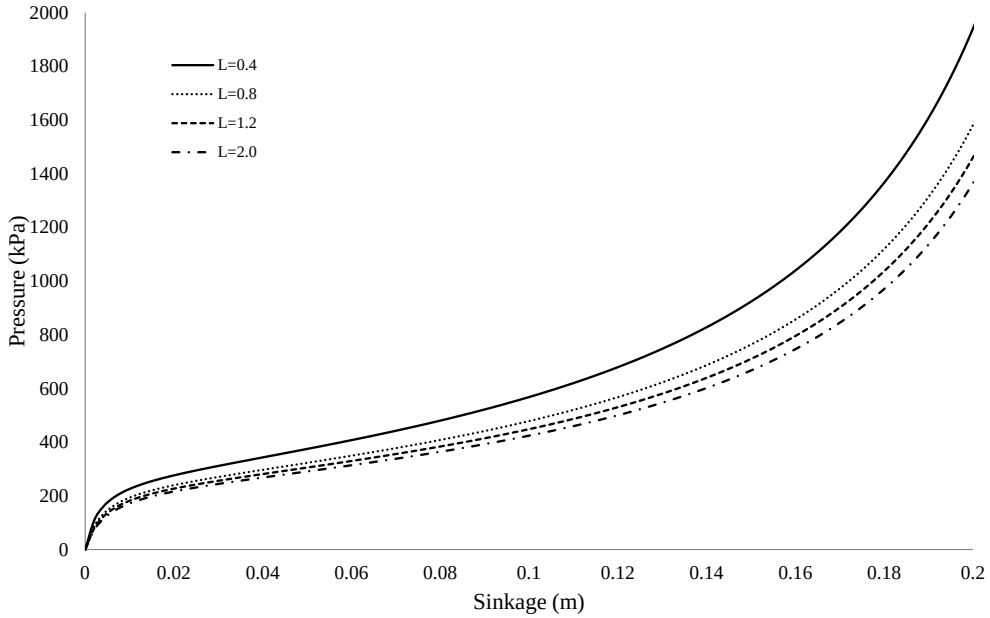

Figure 6.7.*Pressure vs sinkage for a rectangular plate of various sizes interacting with frictional sand, using LSA model.*

6.3. Rigid Wheel

Following the parameterisation of the soil for use with the analytical model, the formulation of the rigid wheel is presented first and some results are obtained for both treadless and treaded variations, before the derivation of the analytical deformable wheel model.

The tyre is assumed to interact with a homogeneous terrain, described by invariant soil parameters. It is considered that no stress concentrations are present, and the vertical load does not exceed the bearing capacity of the soil, as described by the Terzaghi theory. The tyre is assumed to move only in the longitudinal direction with no side forces affecting the overall traction. The pressures acting on the tyre are assumed to be in the radial direction and constant along the width of the tyre. Regarding the treaded wheels, interlocking action is assumed for the soil inside the region between the successive tread blocks; this means that the soil acts only in a shear mode. For the external surface of the tread blocks, the minimum force given by either the friction force (stemming from the vertical load and given by the Coulomb

friction law) or the maximum shear force (which develops due to the stresses in the soil and is given by the Mohr-Coulomb law) is selected, since the shear strength of the tyre-soil system is determined by the lower of the two above forces.

Static Sinkage

The configuration of the wheel model is shown in Fig. 6.8. The angle θ_s is the static entry angle and becomes zero at the point where the maximum pressure occurs. The pressure distribution is symmetric; only the part involving the positive angle θ is considered in the integration and then the result is doubled. The tyre footprint is discretized into a large number of segments (typically ≥ 1000), at each of which the soil pressures are calculated according to Eq. 6.1:

$$p = \frac{1}{\frac{D_1}{B_i} + \frac{D_2 \cdot \omega_1 \cdot \xi \cdot \left[\sin(\theta + d\theta) - \sin(\theta)\right]}{E \cdot \left[\cos(\theta) - \cos(\theta_s)\right]}} \tag{6.1}$$

where D_1, D_2 are given by the relations:

$$\begin{aligned} D_1 &= \frac{2}{\pi} \cdot \operatorname{atan}\left[\frac{\pi \cdot (H_0 - z)}{2 \cdot dL}\right] \\ D_2 &= \operatorname{atan}\left(\frac{H_0 - z}{A_0 \cdot dL}\right) \end{aligned} \tag{6.2}$$

and z, dL are given by the relations:

$$\begin{aligned} z &= R \cdot \left[\cos(\theta) - \cos(\theta_s)\right] \\ dL &= R \cdot \left[\sin(\theta + d\theta) - \sin(\theta)\right] \end{aligned} \tag{6.3}$$

respectively. It should be noted that in Eq. 2.25, B is the smaller dimension of the segment, in this case being its infinitesimal length, given that the width is unique for all segments. The soil pressures are considered to be constant along the width of each segment, and dependent on its local sinkage. The integration is performed by the summation of the forces (pressures multiplied by the infinitesimal area of each segment), and gives the total reaction force of the soil. If the soil reaction force, calculated as:

$$F_z = 2 \cdot R \cdot b \cdot \int_0^{\theta_s} p \cdot \cos(\theta) \cdot d\theta \tag{6.4}$$

is different from the applied vertical load, the value of the sinkage is updated according to the bisection method, in a way that leads to decrease of the difference,

until the last gets lower than a specified tolerance, a point at which the assumed value of sinkage is accepted as a solution. The angle θ_s is defined as:

$$\theta_s = \text{acos}\left(1 - \frac{z_{static}}{R}\right) \tag{6.5}$$

The number of infinitesimal segments considered for the integration was determined in this study using criteria related to the convergence of the desired results. Apart from this, given the relatively large approximation inherent in the numerical values of the produced results in practice (for example due to the inaccuracies in the determination of the soil parameters), usually there is no need for convergence within very small tolerances and consequently for large degree of discretization and therefore increased computational effort.

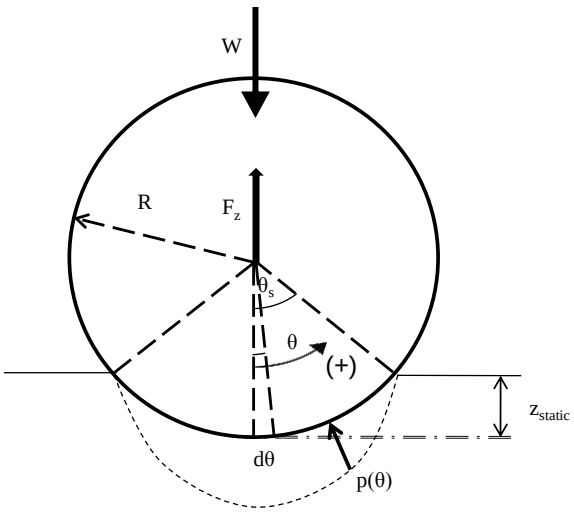

Figure 6.8.*Static indentation of a rigid wheel.*

Dynamic sinkage

After the calculation of the static sinkage, the dynamic sinkage (which in the current model includes the initial static sinkage and therefore is equal to the total sinkage z_{total},) is found from the relationship presented by Lyasko (2010d):

$$z_{dynamic} = \frac{1+i}{1-0.5 \cdot i} \cdot z_{static} \tag{6.6}$$

where$i>0$ is the slip ratio. Equation 6.6 has been verified by many tests – Lyasko (2010d) – on various vehicles (tracked, wheeled) and for numerous soil conditions. However, the latter equation remains an empirical equation developed through

experimental measurements. The effect of the slip ratio on the dynamic sinkage of a wheel is illustrated in Fig. 6.9. It is apparent that, as the slip ratio increases, the dynamic sinkage also increases, in accordance with Eq. 6.6.

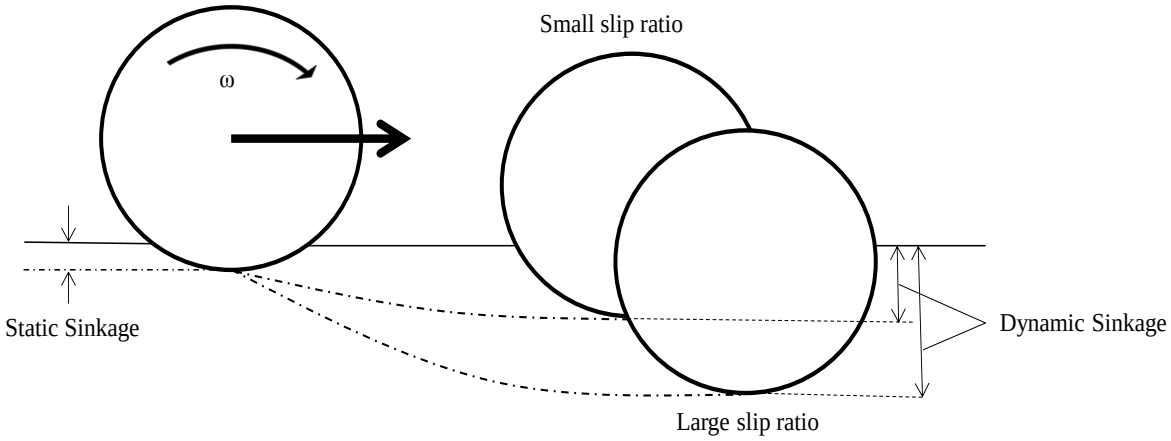

Figure 6.9.*Effect of slip ratio on the dynamic sinkage.*

In the reference configuration of a rigid wheel experiencing dynamic response, shown in Fig. 6.10, it is apparent that there is a rebound effect of the deformed soil after the wheel passes over its surface, i.e. the point C behind the point with the maximum sinkage (point A), is at a higher level than the latter. It should be noted that a similar rebound effect was noticed in the FEM models presented in the previous chapters. It is assumed that the footprint is divided into two regions, defined by the angle θ_M, in each of which different soil pressure relationships hold – angle θ_M represents the point where the maximum radial stress is acting. These are given in Eq. 6.7, which results from combination of Lyasko (2010a) and Wong (1967a).

$$p\left(\theta_{1,2}\right)=\begin{cases}\dfrac{1}{\dfrac{D_1}{B_i}+\dfrac{D_2\cdot\omega_1\cdot\xi\cdot\left[\sin\left(\theta_1+d\theta\right)-\sin\left(\theta_1\right)\right]}{E\cdot\left[\cos\left(\theta_1\right)-\cos\left(\theta_0-\theta_M\right)\right]}}, & \theta_M\le\theta_1<\theta_0 \\ \dfrac{1}{\dfrac{D_1}{B_i}+\dfrac{D_2\cdot\omega_1\cdot\xi\cdot\left[\sin\left(\theta_2+d\theta\right)-\sin\left(\theta_2\right)\right]}{E\cdot\left\{\cos\left[\theta_0-\left(\dfrac{\theta_2-\theta_r}{\theta_M-\theta_r}\right)\cdot\left(\theta_0-\theta_M\right)\right]-\cos\left(\theta_0\right)\right\}}}, & \theta_r\le\theta_2<\theta_M\end{cases} \tag{6.7}$$

The various angles appearing in Fig. 6.11 and Eq. 6.7 are given by the relations:

$$\theta_0 = \text{acos}\left(1 - \frac{z_{\text{dynamic}}}{R}\right)$$
$$\theta_M = (\alpha_0 + \alpha_1 \cdot i) \cdot \theta_0 \tag{6.8}$$
$$\theta_r = \text{acos}\left(1 - \frac{k_r z_{\text{dynamic}}}{R}\right)$$

where k_r, a_0 and a_1 are estimated as 0.2, 0.4 and 0.2 respectively. These parameters were estimated assuming that the realistic physical response of a rolling wheel on a cohesive soil will be maintained. Initially, parameter k_r was set to $k_r<1$, representative for soil where compaction occurs. Furthermore, k_r is directly related with the exit angle and is primarily responsible for the re-bouncing effect of the soil, namely the decrease of the total sinkage of the soil after the wheel passage. Values for a_0 and a_1 were estimated based on experimental results found in the literature (i.e Wong & Reece, 1967a, 1967b).

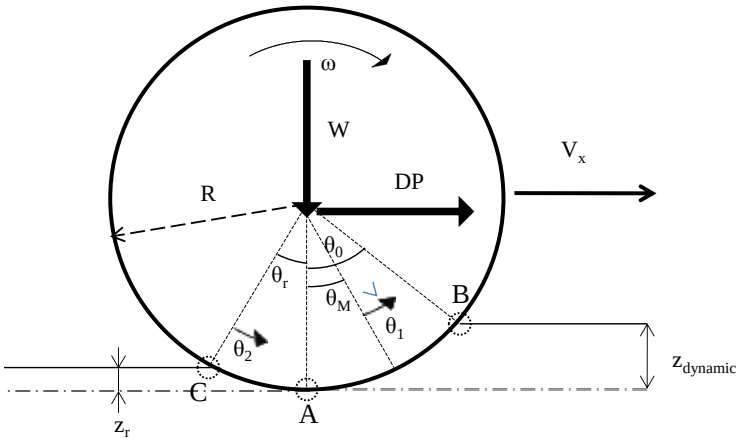

Figure 6.10.*Reference configuration for a driven wheel rolling on a soft soil.*

The shear stresses developed on the tyre - soilinterface, are given by suitable combination of Eqs. 2.18 and 2.30, for the two integration intervals. Finally, the so-called drawbar pull (DP) is calculated as:

$$\begin{aligned} DP &= \text{Soil thrust} - \text{Compaction Resistance} \\ &= R \cdot b \cdot \left[\int_{\theta_r}^{\theta_0} \tau \cdot \cos(\theta) d\theta - \int_{\theta_r}^{\theta_0} p \cdot \sin(\theta) d\theta \right] \end{aligned} \tag{6.9}$$

Semi-Analytical Procedure

In the flowchart presented in Fig. 6.11, an outline of the semi-analytical procedure followed in this study is presented.

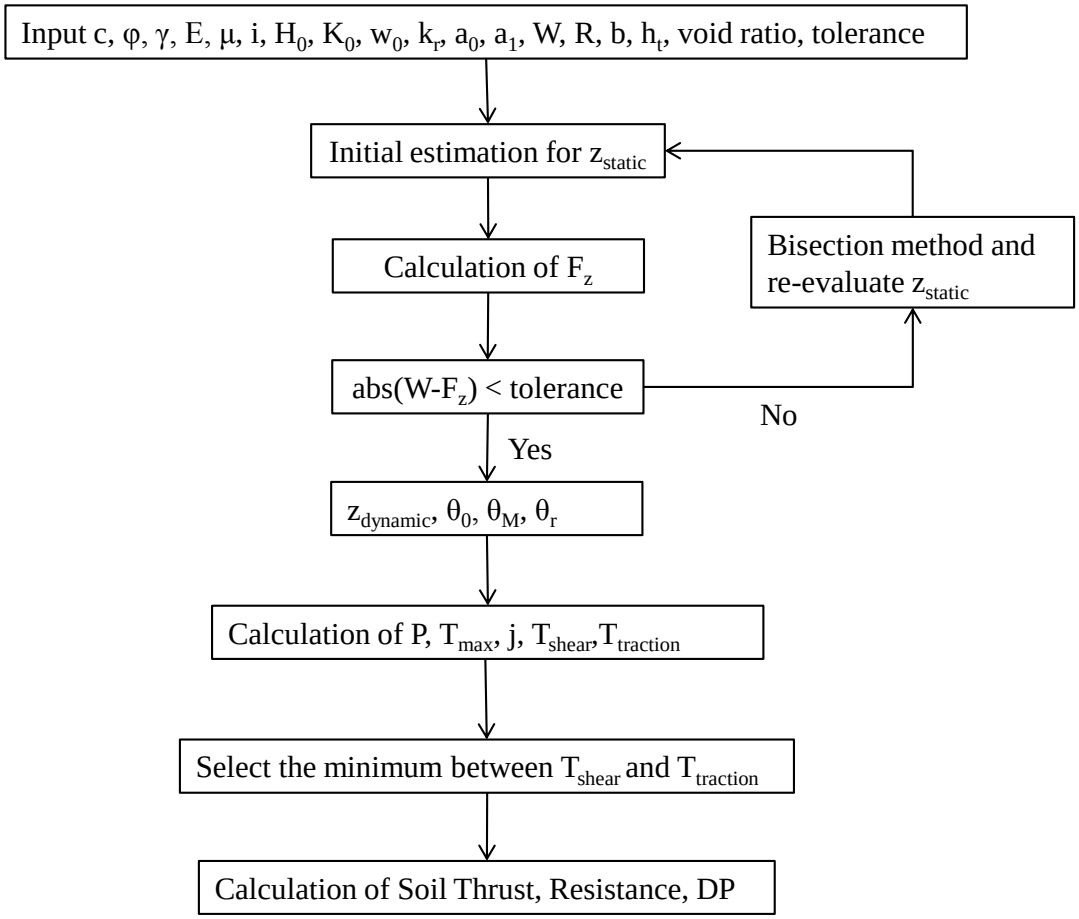

Figure 6.11.*Flowchart of the semi-analytical procedure for estimation of tyre-soil interaction forces.*

6.3.1 Validation of analytical solution

The analytical solution developed in this thesis is validated against corresponding numerical results – presented in Chapter 3 – to ensure that it is applicable for the estimation of the response of the wheel in various soil types. Three indicative cases were selected, as shown in Figures 6.12 – 6.14. The width of the wheel (b) was set to 0.16m and its diameter (d) to 0.53m for all cases considered.

The first case involves a purely cohesive soil described by the Mohr-Coulomb failure criterion, on which a rigid treadless analytical wheel is supported, subject to a vertical load simulating a static indentation response. The results are shown in Figure 6.12, where the dimensionless vertical load versus the dimensionless sinkage is plotted. Three curves are observed, one resulting from the analytical solution developed in this thesis, one resulting from the numerical simulations performed in this study and one taken from Hambleton & Drescher (2008) describing the same case. Good agreement

is observed between the three curves, which verifies the accuracy of the analytical solution.

In Figure 6.13 corresponding results are shown for static indentation of a rigid treadless wheel in purely frictional soil due to a vertical load. In this figure, the dimensionless vertical load versus the dimensionless sinkage are plotted. It is seen that the curve of the analytical solution slightly underpredicts the dimensionless wheel sinkage for a given vertical load, with respect to the numerical results of this study and of Hambleton & Drescher (2008). This can be explained by the fact that the effect of the dilation angle in the case of frictional soils becomes significant, in comparison with purely cohesive soils. The numerical results are associated with a very small dilation angle of the soil (nearly zero), whereas the result of the analytical solution is based on nonzero dilation angle. In the analytical solution the last is not explicitly considered as a soil parameter, but inherently affected by other soil parameters, which were adjusted during the optimisation procedure to describe a realistic soil. In addition, it has been shown in Figure 3.17 that the bearing capacity of the soil increases with an increase in the dilation angle which entails a decrease in the sinkage. Therefore, it is expected that the analytical solution will yield larger values of dimensionless vertical load than the numerical solution.

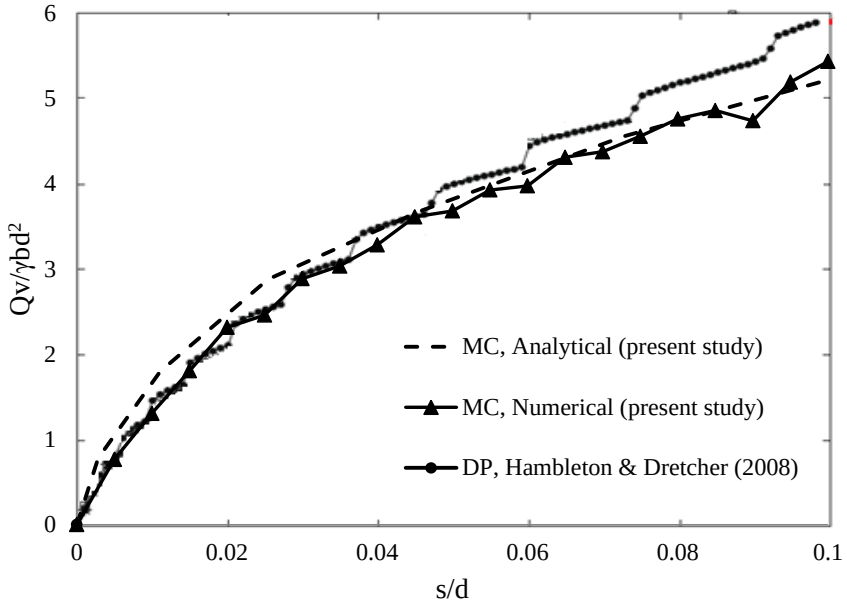

Figure 6.12*Dimensionless vertical load versus dimensionless sinkage for wheel with b/d=0.3 on cohesive soil.*

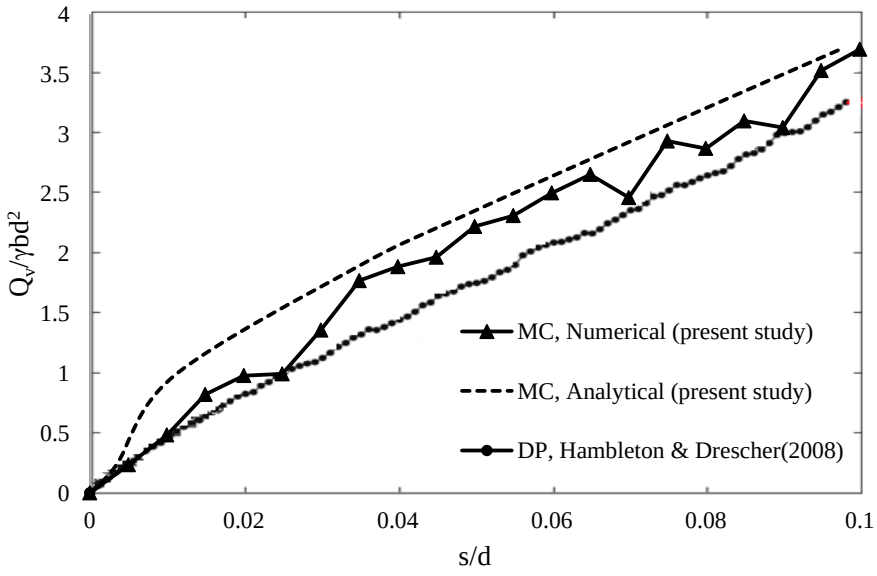

Figure 6.13*Dimensionless vertical load versus dimensionless sinkage for wheel with b/d=0.3 on frictional soil.*

The soil in which the best agreement was noted between the analytical and numerical solutions regarding its static response (purely cohesive soil) was selected for investigation of the dynamic rolling response of a rigid treadless wheel subject to a vertical load. In Figure 6.14 the same quantities with the two previous figures are plotted for the analytical and numerical solutions. It is noted that the analytical solution leads to a slight underestimation of the dimensionless sinkage resulting from a given vertical load, compared to the numerical results. However, this discrepancy can be explained by a variety of reasons. Firstly it is reminded that the equation utilised for the calculation of the dynamic sinkage remains an empirical equation calibrated throughout experimental tests, which treats the whole problem in a very simplistic way. In addition, empirical or experimentally measured parameters such as k_r, a_0 and a_1 are used for the determination of the exit angle and the angle where the normalized stress is maximized respectively. It is noted that the calculation of these angles is done using formulas determined empirically without any sound theoretical background. Finally, the shear deformation modulus, utilised for the calculation of the local shear stress developed at the tyre-terrain interface, has a principal effect on the dynamic rolling response of the wheel and, contrary to this study where average values found in the literature are used, should be determined experimentally for every type of terrain.

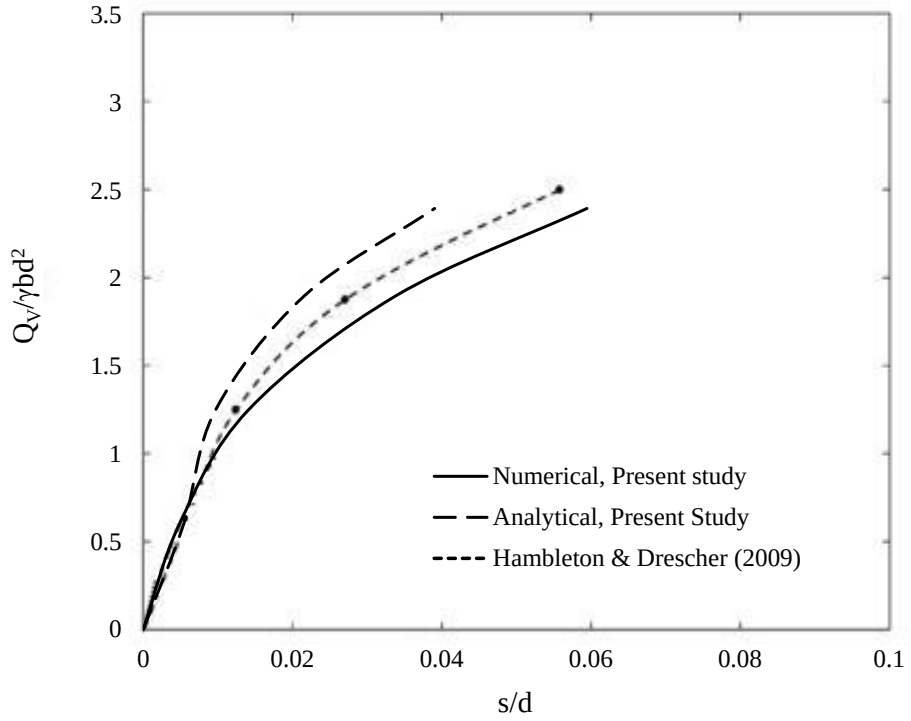

Figure 6.14*Dimensionless vertical load versus dimensionless steady state sinkage for wheel with b/d=0.3 rolling on cohesive soil.*

6.3.2 Rigid Treadless Wheel Response – Slick Tyre

The most basic model among those examined in this study is the tyre without any tread pattern, which behaves as a rigid wheel. This may occur due to many reasons, e.g. in case a deformable tyre is highly inflated, or a tyre with intermediate inflation pressure rolls on a very soft soil. In particular, the assumption of rigid wheel is very common in the field of Terramechanics, especially when the soil response is emphasized.

Drawbar Pull

In Fig. 6.15 the response of a rigid wheel rolling on wet clay is shown in terms of its drawbar pull versus its slip ratio. It is noted that as the vertical load increases, the curve becomes steeper and has higher maximum drawbar pull and lower minimum drawbar pull. In addition, it is observed that for positive values of slip ratio, the variation of the drawbar pull for various vertical loads is less pronounced than that for negative values of slip, since the resistance force is always opposite to the direction of

travel. Drawbar pull becomes positive at approximately 5% slip ratio, and stabilizes at its maximum value after 20% slip ratio.

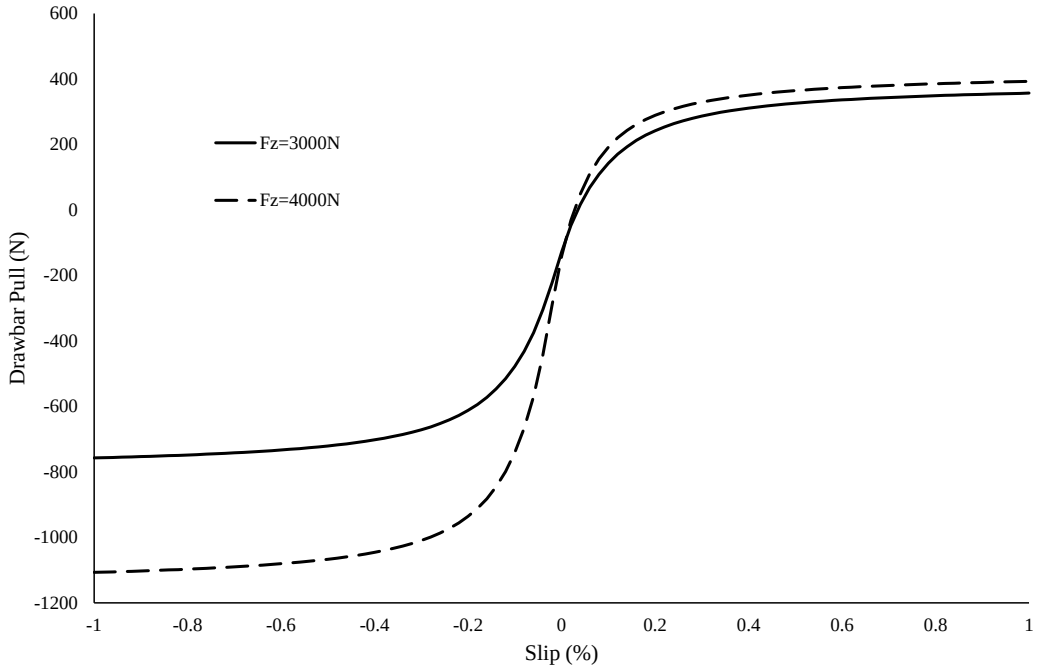

Figure 6.15. *Drawbar pull developed for a rigid wheel rolling on wet clay with various vertical loads, versus its slip ratio.*

In Fig. 6.16 the drawbar pull is plotted for two different wheels with equal diameters (0.8728m) and widths equal to 0.315m and 0.215m. It is observed that the wheel with the larger width develops a larger drawbar pull compared to the narrower wheel, which can be explained by taking into account that the wheel with larger width experiences a lower sinkage due to the larger footprint area. This leads in turn to lower compaction resistance. In addition the wider wheel due to its larger contact area develops a higher shear force. More specifically an increase of 45% on the width of the tyre results in an increase of 30% on the generated drawbar pull.

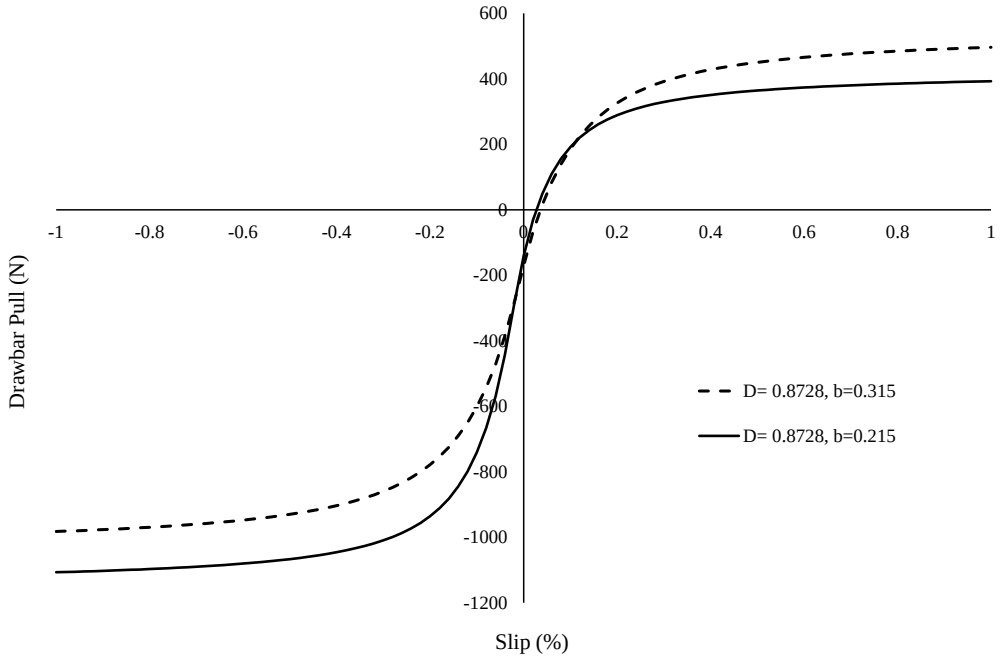

Figure 6.16. *Drawbar pull developed for two rigid wheels of different width, rolling on wet clay with vertical load equal to F_z=4kN, versus slip ratio.*

Three realistic commercially available tyres, with different geometries – namely as Wheel 1: b=0.315m and d=0.8728m, Wheel 2: b=0.317m, d=0.9347m, Wheel 3: b=0.267m, d=0.7798m – and inflation pressure set sufficiently high, so that they can be considered as rigid wheels, were compared in terms of traction response rolling on wet clay as illustrated in Fig. 6.17. It is again noted that the tyre with the smallest width – Wheel 3 – exhibits the lowest traction response compared to the other two wheels where a larger contact area between the wheel and the soil exists. Hence, it can be concluded that in terms of tyre geometry the optimum traction response appears in tyres with contact area of increased width. The latter can be achieved either by utilizing wider tyres or by reducing the inflation pressure of the tyre to appropriate levels where the compaction resistance being generated by the vertical displacement of the wheel into the soil is low. Further evidence for this is provided in a following section of this thesis, pertinent to the deformable pneumatic tyre.

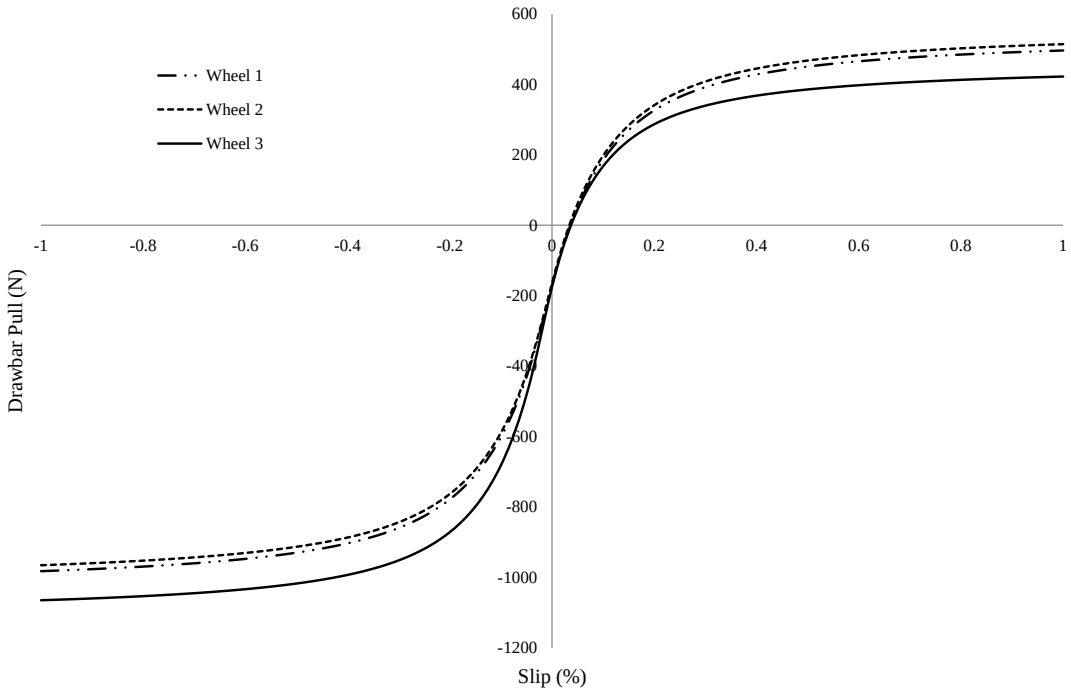

Figure 6.17. *Drawbar pull developed for three commercially available tyres rolling on wet clay with vertical load equal to F_z=4kN, versus slip ratio.*

The rolling response of Wheel 3 was investigated on three different types of soil, namely (a) loam, (b) clay and (c) sand for a vertical load of 2kN, Fig. 6.18. It can be observed that the wheel for the same amount of vertical load behaves completely different on the aforementioned soils. Furthermore, the amount of slip required for positive traction of the wheel is significantly lower on sand compared to clay and loam. However, there is no universal trend for any type of soil, since the optimum traction is determined primarily by the cohesion and friction angle of the deformable soil and not by the type of the soil itself. Finally, it should be noted that the amount of traction force developed on clay is lower compared to that measured on loam, which in return is smaller to that developed on sand. Therefore, it can be said that cohesive soils with small friction angles such as clay are incapable of generating the same amount of traction as the frictional soils.

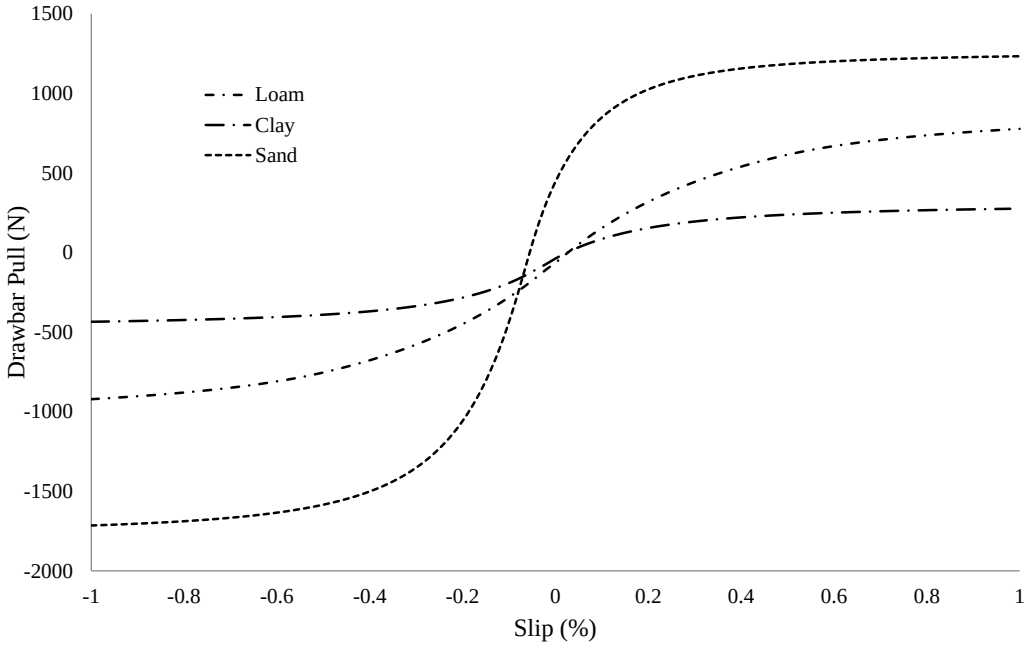

Figure 6.18. *Drawbar pull developed for Wheel 3 rolling on three deformable soils with vertical load equal to F_z=2kN, versus slip ratio.*

In Fig. 6.19 the total sinkage of a rigid wheel with width 0.215m, diameter 0.8728m, and vertical load equal to 4kN is plotted against the slip ratio, for two different types of underlying soil, namely moist loam and wet clay. It is observed that the dynamic sinkage increases with increasing slip ratio, a result which is well-documented in the literature – Steiner (1979), Lyasko (2010d), Senatore & Sandu (2011), Trease et al. (2011) – and can be explained by considering the digging action of any driven wheel with increasing slip. Generally, the sinkage seems to be larger for the wet clay than the moist loam, and does not increase linearly for increasing slip in both soil cases.

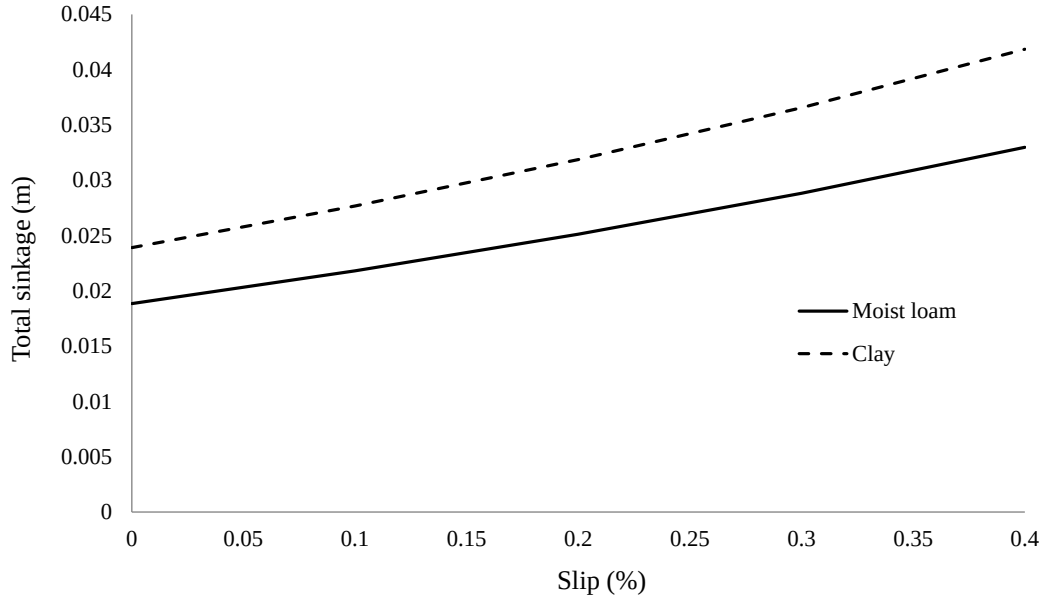

Figure 6.19. *Total sinkage versus slip ratio for a rigid wheel with dimensions b=0.215m, D=0.8728m and vertical load F_z=4kN, for two different types of soil.*

Lateral Force

The wheel which exhibited the minimum tractive response in Fig. 6.17 – Wheel 3 – was selected as the case study and its interaction with three different deformable soils was investigated in terms of lateral force versus slip angle. A similar approach with one presented by Yoshida & Ishigami (2004) and Liang et al. (2004), where the lateral force consists of two main components was followed. The first component is dealing with the lateral force caused by soil deformation (F_{ys}) and the second with the force caused due to the bulldozing effect (F_{yb}), as seen in Eq. 6.10. Based on these models, a similar approach will be adopted in the current study for the calculation of the generated lateral force.

$$F_y = F_{ys} + F_{yb} \tag{6.10}$$

For the component due to soil deformation F_{ys}, Eq. 6.11 will be used and will be integrated from the starting point of the entry angle until the last point of the exit angle. With regards to the lateral force caused by the bulldozing effect, the active or passive failure of the soil may be used. Generally for a running gear, soil causes a passive failure as in Eq. 6.12 (Wong, 2010), and assuming that no surcharge exists, F_{yb} is given by Eq. 6.16.

$$F_{ys} = rb\int_{\theta_2}^{\theta_1}\left\{\tau_y(\theta)\cos\theta\right\}d\theta \tag{6.11}$$

where

$$\tau_y(\theta) = \left(c + p(\theta)\cdot\tan\varphi\right)\left(1 - e^{-j_y/K_y}\right) \tag{6.12}$$

$$j_y = R\cdot(1-s)\cdot(\theta_0 - \theta)\cdot\tan a \tag{6.13}$$

$$\sigma_p = \gamma_s z N_\varphi + 2c\sqrt{N_\varphi} \tag{6.14}$$

$$F_{yb} = b\cdot\left[\left(\int_0^{h_b}\sigma_p dz\right)\cdot\sin a\right]\cdot\sin a = b\cdot\left\{\left[\int_0^{h_b}\left(\gamma_s z N_\varphi + 2c\sqrt{N_\varphi}\right)dz\right]\cdot\sin a\right\}\cdot\sin a \tag{6.15}$$

$$F_{yb} = b\cdot\left(\frac{1}{2}\gamma_s\cdot z^2\cdot N_\varphi + 2\cdot c\cdot z\cdot\sqrt{N_\varphi}\right)\cdot\sin^2 a \tag{6.16}$$

where,

$$N_\varphi = \tan^2\left(45 + \varphi/2\right) \tag{6.17}$$

It should be noted that F_{yb} given by Eq. 6.16 refers to the bulldozing force generated by the half region of the tyre interface. Thus, in order to calculate the total bulldozing force, the outcome from Eq. 6.16 needs to be multiplied with a coefficient of two. Furthermore, it is stated by Crolla & El-Razaz (1987) that the total shear displacement can be calculated as a magnitude of two vectors as in Eq. 6.18. Additionally to the previously mentioned researchers, the reader may refer to work conducted by Shwanghart (1968), El-Razaz (1988), Grecenko (1992) and Chan & Sandu (2008) for a more thorough approach and alternative approaches on the lateral force generation.

$$j = \sqrt{j_x^2 + j_y^2} \tag{6.18}$$

Following the above-stated mathematical approach, the lateral force developed between the wheel and three different deformable terrains is illustrated in Fig. 6.20 where the lateral force versus slip angle for a constant slip ratio of 0.2 and a predefined vertical load of 2kN is presented. Similar trends with the tractive response were found, where the wheel displayed the highest lateral force on sand and the minimum on clay, while on loam an intermediate response was observed.

Furthermore, it is noted that the lateral force does not exhibit a maximum value, since by increasing the slip angle the lateral force is continuously increasing – within the range of slip angle considered. In addition to this, the response of the same wheel in contact with clay was investigated, for various vertical loads and the results are presented in Fig. 6.21. It is observed that by increasing the vertical load there is an increase in the lateral force developed which can be explained by the monotonic increase of the bulldozing force caused by the increased sinkage due to the higher vertical load. However, again a maximum value is not observed and the lateral force is continuously increasing as the slip angle increases.

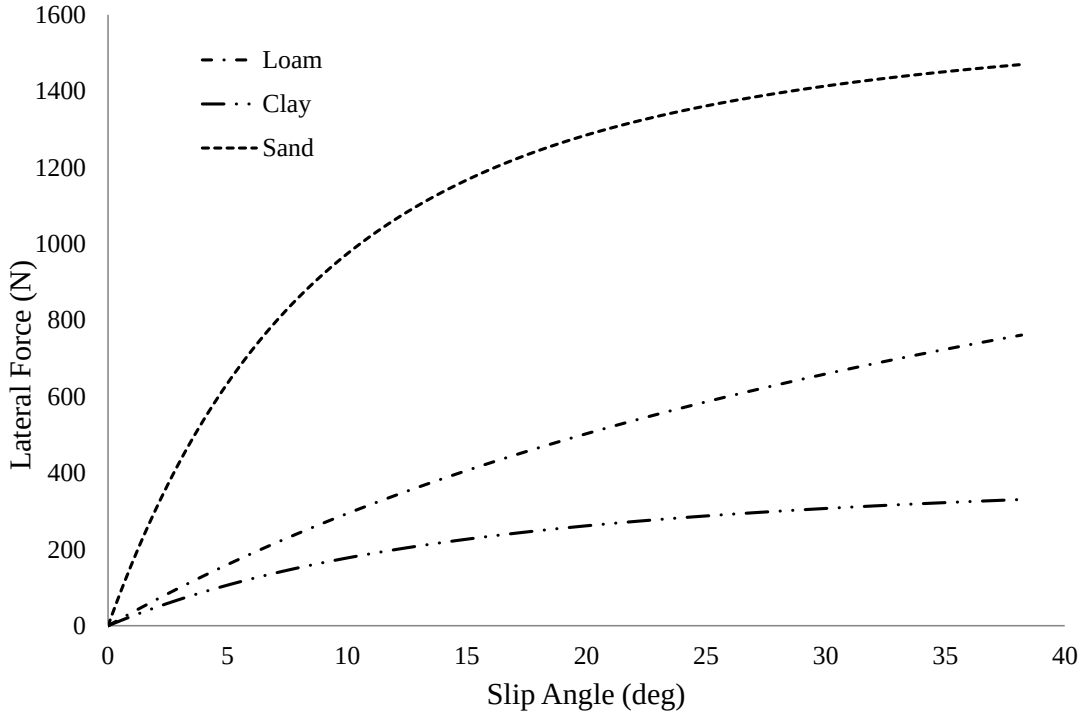

Figure 6.20. *Lateral Force developed for Wheel 3 rolling on three deformable soils with slip ratio equal to 0.2 and vertical load equal to F_z=2kN versus slip angle.*

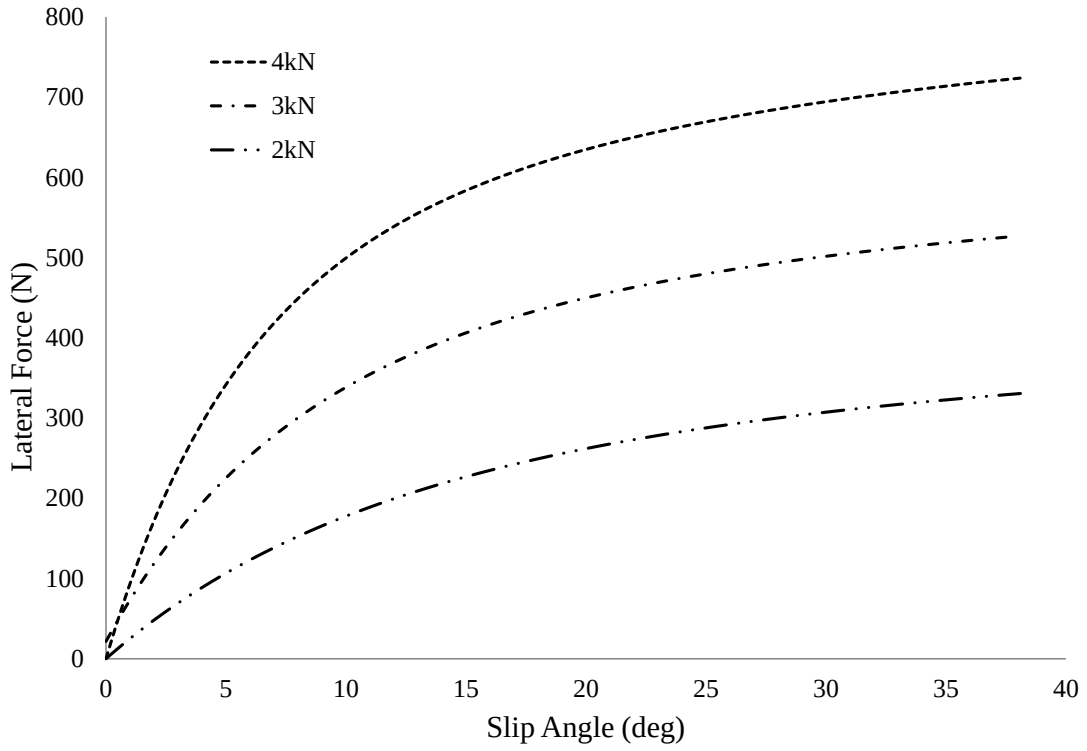

Figure 6.21. *Lateral Force versus slip angle developed for Wheel 3 rolling on clay, for slip equal to 0.2 and various vertical loads.*

6.3.3 Rigid Treaded Wheel Response

The effect of tread pattern is taken into account in the formulation of the models considered in this study. An approach similar to the one followed by Harnisch et al. (2005) has been adopted. The basic idea is that the response of a treaded tyre is considered as the sum of the responses of two treadless tyres with radii equal to the outer and the inner radius of the initial treaded tyre, weighted according to the void ratio (the fraction of the voids along the tyre perimeter to its total perimeter). Regarding the dynamic response, the dynamic sinkage is calculated by Eq. 6.6, for the tread blocks, whereas for the voids the sinkage is assumed to be equal to the dynamic sinkage of the treads minus the height of the tread blocks. A schematic representation of a simplified tread pattern is illustrated in Fig.6.22.

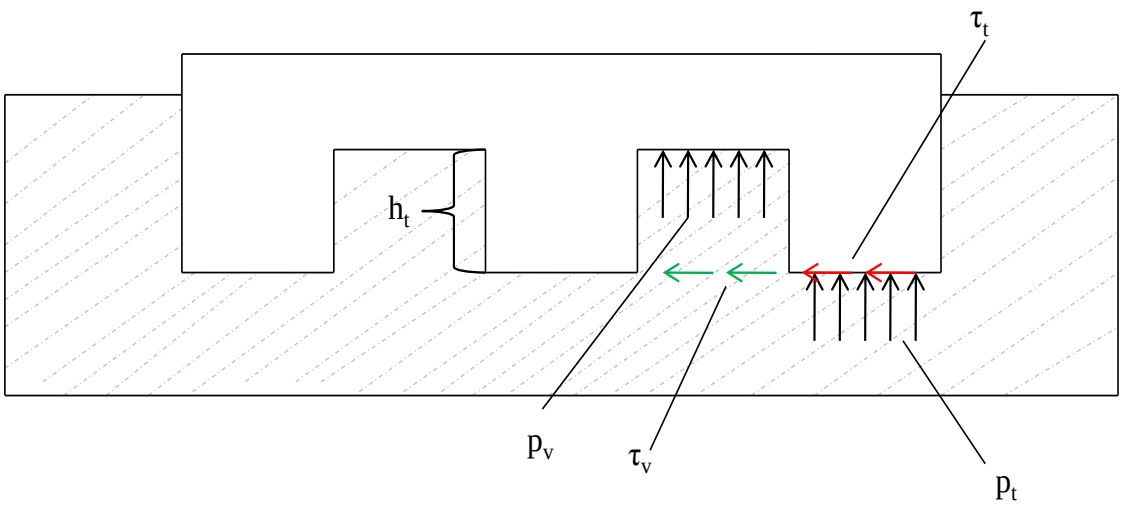

Figure 6.22.*Schematic representation of a tread block between a treaded tyre and the soil.*

The total sinkage of the treaded area is assumed to be equal to that of a treadless wheel with equal diameter and the sinkage of the voids is found by subtracting the tread height from the total sinkage. It should be noted that the vertical load should be sufficiently high in order to ensure that the voids are fully occupied by soil otherwise invalid results may occur. Consequently, two different pressure distributions are being calculated and weighted according to the void ratio of the tyre. It is evident from Fig.6.22 that the shear stress for the tread and the void is being calculated at the same depth of indentation and always the minimum value between the allowed shear force and friction force is chosen for the calculation of the developed drawbar pull. However, the shear stress in real tyre experiments is developed primarily due to the frictional strength of the soil (especially of its part being interlocked within the tread blocks) and not due to the friction between the rubber and the soil.

In Fig. 6.23, a treadless and a treaded wheel are compared. The two wheels have the same dimensions and the same vertical load. The treaded wheel has tread height 0.03m and void ratio 0.3. Comparison of the two curves shows that the treaded wheel shows larger drawbar pull for positive slip ratios and smaller drawbar pull for negative slip ratios, whereas its curve is steeper, compared to the treadless wheel. It should be noted that by increasing the void ratio, the contribution of the soil interlocked within the voids on the overall tractive response increases. However, the last should not exceed the value of 0.5, since this implies that the wheel under consideration would have a smaller radius. Subsequently, the effect of the void ratio on the overall rolling response of the wheel was studied, and the results are illustrated

in Fig.6.24. As expected, by increasing the void ratio there is an increase on the drawbar pull for slip conditions and a decrease for skid conditions. As a result, a treaded tyre would exhibit better rolling response compared to a slick tyre, where further increase on the tread height and on the percentage of void of the tyre would render the maximum shear stress of the soil as the dominant factor compared to the friction force at the tyre - soil interface.

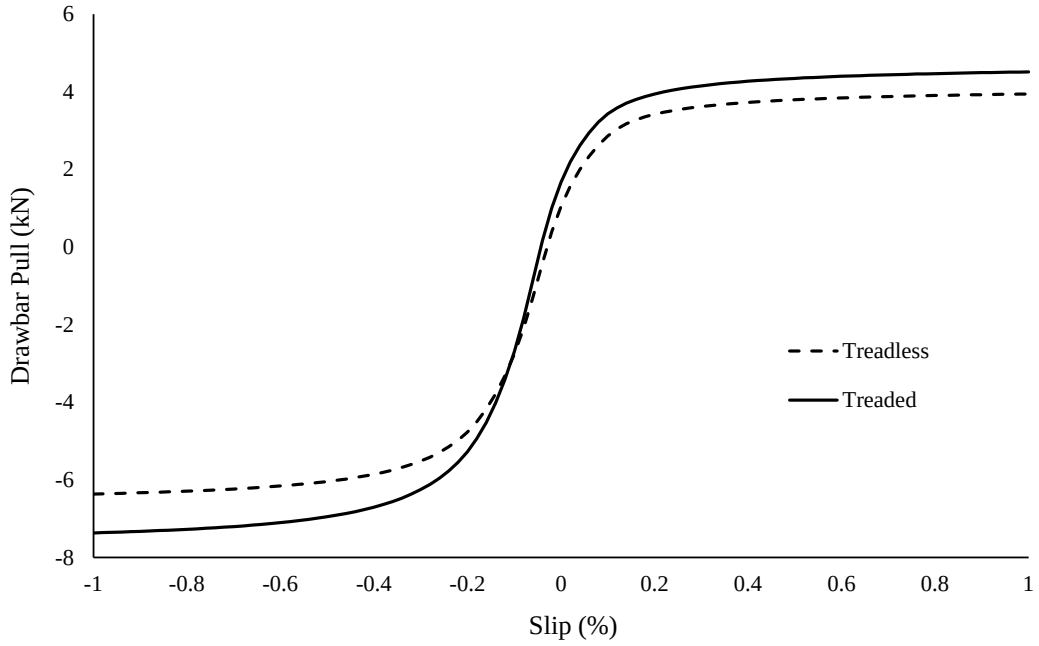

Figure 6.23. *Drawbar pull versus slip ratio developed for a treadless and a treaded rigid wheel, rolling on moist loam with vertical load equal to F_z=10kN.*

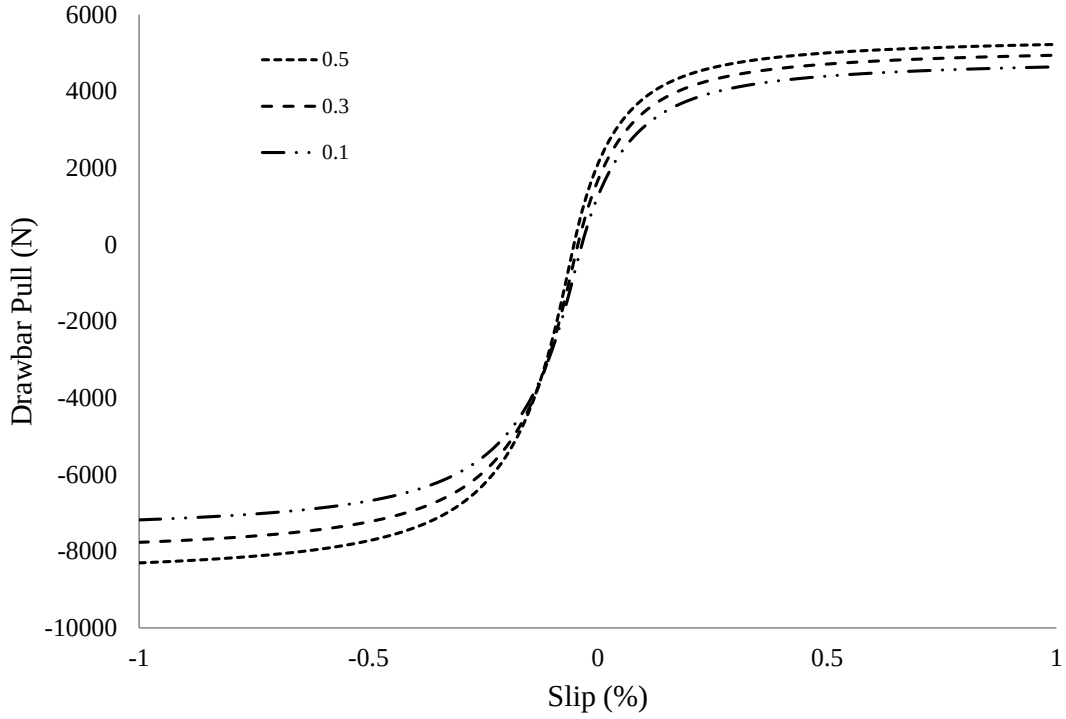

Figure 6.24. *Drawbar pull versus slip ratio developed for a rigid wheel with different void ratio, rolling on moist loam with vertical load equal to F_z=10kN.*

6.4. Deformable Wheel

The basic principle used in the present study to model a deformable tyre has been initially presented by Bekker (1956) and further developed by Harnisch et al. (2005), where the contact patch of the pneumatic tyre is assumed to be represented by the contact patch of a substitute circle considered as the perimeter of a rigid wheel with radius larger than that of the actual deformable tyre, given by:

$$R^* = R \cdot \left(\sqrt{1 + DF/z} + \sqrt{DF/z} \right)^2 \tag{6.19}$$

where

$$DF = \frac{W}{C_z} \tag{6.20}$$

Based on that concept such a substitute circle was developed which was analysed with the methodology outlined in the previous section to obtain its static and dynamic response. From this response, the static sinkage of the initial deformable wheel was calculated as follows. Firstly, the initial undeformed geometry of the deformable wheel is considered as a reference configuration with respect to which all values of

sinkage are calculated. This reference configuration is considered undeformable and is mapped to the geometry of the substitute circle at each equilibrium iteration. At the substitute circle, the difference between the total reaction force and the applied vertical load is calculated, and, if larger than a specified tolerance, the iterations proceed, by modifying appropriately the sinkage of the reference configuration (undeformed pneumatic tyre). Therefore, when static equilibrium is achieved, the resulting sinkage (denoted as $z_{maxstatic,ref}$) refers to the reference configuration, from which the sinkage of the deformable tyre has to be found (denoted as $z_{maxstatic,def}$). The relationship between the last two is:

$$z_{maxstatic,def} = z_{maxstatic,ref} - \left\{ R\left[1-\cos\left(\theta_s\right)\right] - R^*\left[1-\cos\left(\theta_s^*\right)\right] \right\} \tag{6.21}$$

It has to be noted that if the initial tyre is highly inflated, then R*=R and θ_s*=θ_s, meaning that $z_{maxstatic,def}$=$z_{maxstatic,ref}$, according to Eq. 6.21. The above procedure is illustrated in Fig. 6.25.

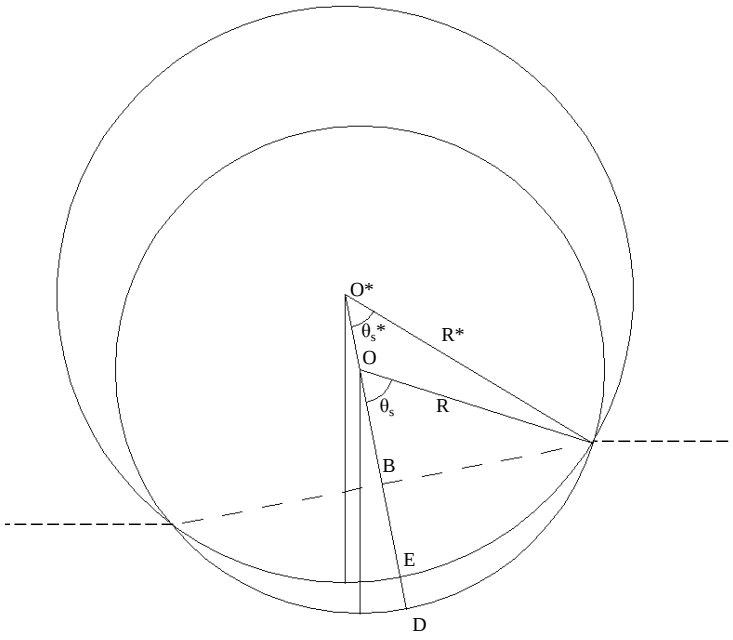

Figure 6.25.*Reference configuration of a pneumatic tyre, and the equivalent substitute circle.*

The main parameter controlling the deformability of the tyre is the stiffness C_z, which is a function of its properties. Herein, C_z will be used as a measure of the inflation pressure; high values of C_z (>10^7) imply a highly inflated tyre behaving as a rigid wheel and moderate values (10^5 - 5.10^5) imply inflation pressures ranging from 80kPa

to 250kPa. In Fig. 6.26 a highly inflated pneumatic tyre with a moderately inflated pneumatic tyre and a low inflated tyre are compared. It is obvious from the figure that the moderately inflated tyre exhibits larger drawbar pull compared to the highly inflated, whereas by further decreasing the inflation pressure – reaching the state of the tyre with reduced inflation – there is a further increase on the developed drawbar pull. This is caused mainly by the fact that larger footprint area is associated with a decrease on the inflation pressure representative for moderately and low inflated tyres, resulting in smaller sinkage of the tyre into the soil, and thus in smaller values of compaction resistance. Following this, it should be noted that, contrary to the on-road tyres, where high inflation pressure is recommended (reducing rolling resistance) the off-road tyres behave better for moderate or low values of inflation pressure. Thus, it is obvious that a medium width tyre – Wheel 3 – with low inflation pressure may present higher tractive force compared to a wider tyre with high inflation pressure.

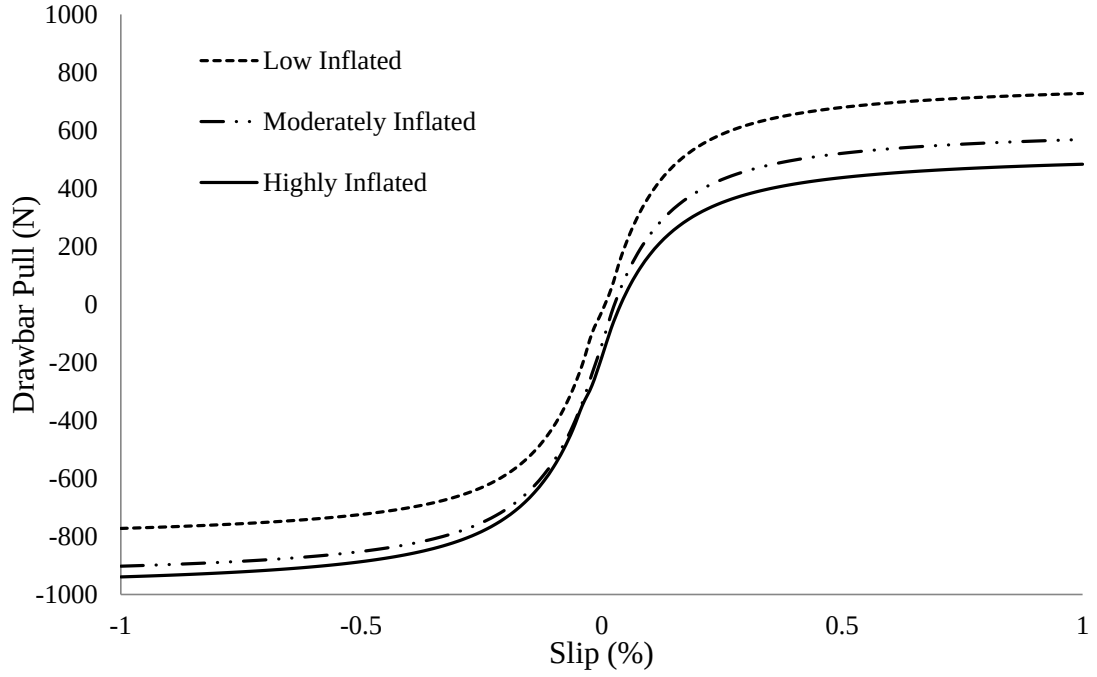

Figure 6.26. *Drawbar pull developed for a pneumatic tyre with different inflation pressures, rolling on moist loam with vertical load equal to F_z=4kN, versus slip ratio.*

Figure 6.27 illustrates the rolling response of two different wheels – namely Wheel 1 and Wheel 3 – rolling on the same deformable terrain under the same driving conditions and 4kN vertical load. In section 6.2.2, Fig. 6.17, a comparison between these two tyres, behaving as rigid wheels was illustrated and the effect of the width on the drawbar pull was presented. It was found that a wide tyre would respond better on

a deformable terrain compared to a narrow tyre. However, from Fig. 6.27 is apparent that a narrow tyre – Wheel 3 – would develop higher tractive forces for lower inflation pressures compared to a wide tyre with high inflation pressure. Therefore, the significant effect of the inflation pressure on the tyre behaviour is highlighted and it should be always considered as a recommendation to improve traction on soft soils. Under the same driving conditions of vertical load and slip ratio Wheel 3 developed almost double the drawbar pull compared to Wheel 1, for positive slip driving conditions.

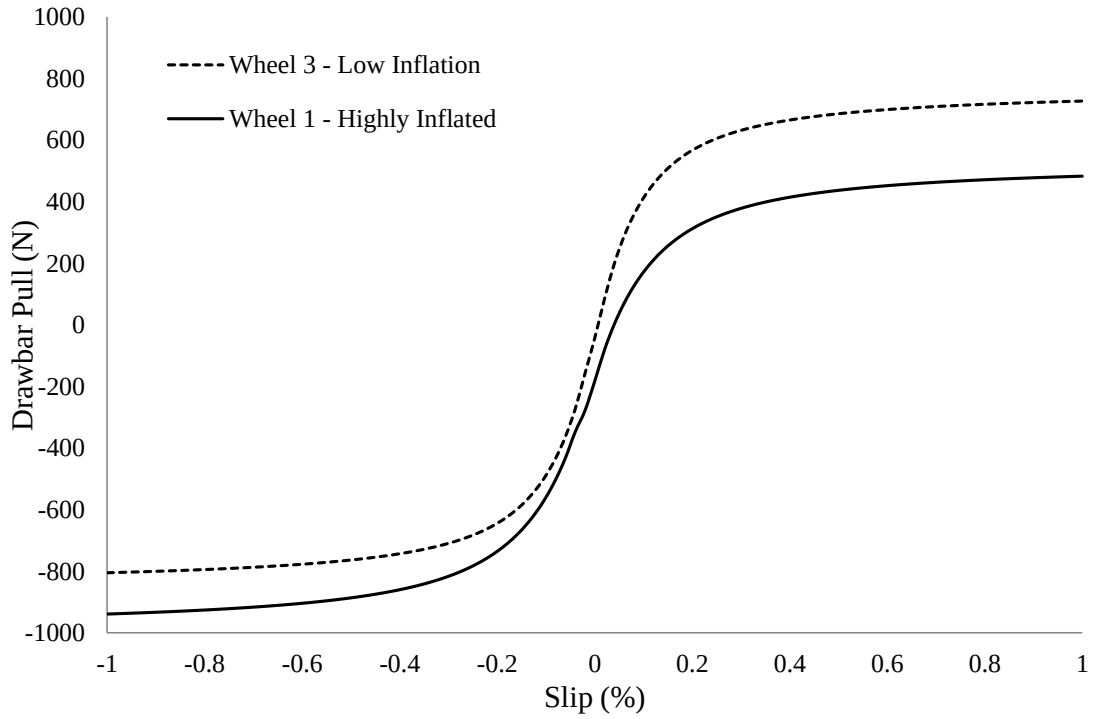

Figure 6.27. *Drawbar pull developed two pneumatic tyres, rolling on moist loam with vertical load equal to F_z=4kN, versus slip ratio.*

6.5. Multi-pass effect

The effect of a rear wheel rolling in and out of the rut path created by the front wheel of a moving vehicle is commonly referred to as the multi-pass effect. In this section, the assumption that the rear wheel is rolling over the exact same path created by the front wheel will be used. Initially, the deformable terrain is considered to be undistorted with known soil material properties. Following that, from the interaction of the front wheel with the terrain a new, completely different, soil condition is being created. Therefore, the new material properties of the already compacted rut path need

to be found in order to be used as initial soil parameters for the response of the rear wheel.

For instance, assuming that the front wheel rolls over soft snow; the rut path which will be created will consist of compacted snow with entirely different physical properties. Similarly for wet clay, the rolling response of the front wheel will generate compacted clay with higher values of cohesion than those in the undistorted condition, allowing the rear wheel to generate higher tractive force. In this model, the rear wheel will be assumed to follow the exact path of the front wheel and Eq. 6.13-6.19, which describe the material properties of the deformed region, will be used as in Lyasko (2010c). Lyasko's model includes the recalculation of every soil parameter in order to create a new set of data. Afterwards, identical equations for traction, rolling resistance and consequently drawbar pull used for the front wheel will be used for the rear wheel. After the passage of the front wheel the maximum dynamic sinkage has been calculated and can be used to measure the new hardpan depth as in Eq. 6.22. Following that the new soil unit weight must be computed along with the depth of soil deformation propagation H_p, Eq.6.23. Once the new material properties have been specified, the additional vertical displacement Z_{2_max} caused by the vertical load of the rear wheel can be measured. The total deformation of the soil would correspond to the summary of z_1 and z_2 and after the re-bouncing of the soil the final configuration of the soil will have a vertical deformation of Z_{total}. A schematic representation of the multi-pass effect is presented in Fig. 6.28.

$$H_1 = H_0 - z_0 \tag{6.22}$$

$$H_p = \min\left(H_0, 2.5 \cdot b\right) \tag{6.23}$$

$$\gamma_1 = \frac{\gamma_0 \cdot H_p}{H_p - z} \tag{6.24}$$

$$C_b = \left(\frac{C_0}{\left(1 + 0.37 \cdot MP\right)} \right)^{\left(\frac{1}{(0.81 + 0.0015 \cdot MP)} \right)} \tag{6.25}$$

$$C_{b,new} = C_b + a \cdot \gamma_1 \tag{6.26}$$

$$C_0 = \left(1 + 0.37\right) \cdot C_{b,new}^{(0.81 + 0.0015 \cdot MP)} \tag{6.27}$$

$$\varphi_1 = 45 \cdot \left(1 - e^{\left(\frac{(0.02 \cdot MP - 0.9)}{\left(C_{b,new}^{0.5} \right)} \right)} \right) \tag{6.28}$$

$$\varphi_2 = 20 \cdot C_{b,new}^{0.28 \cdot e^{(-0.03 \cdot MP)}} \tag{6.29}$$

$$\varphi = \min\left(45, \max\left(\varphi_1, \varphi_2\right)\right) \tag{6.30}$$

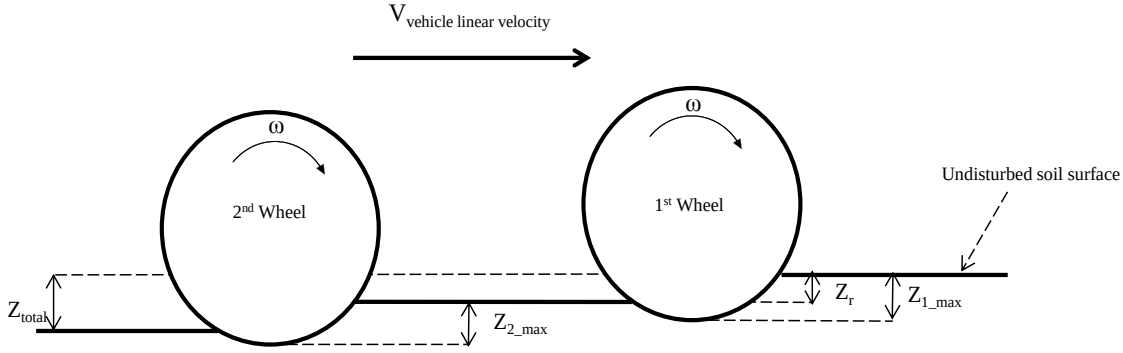

Figure 6.28.*Schematic representation of the multi-pass effect. The rear wheel rolls over the exact same rut path with the front wheel.*

A comparison between the drawbar pull developed for the front and the rear wheel of a vehicle rolling over the exact same rut path, for a vertical load of 4kN is illustrated in Fig. 6.29 for wet clay with 22% moisture content. It has to be noted that the soil properties and consequently the traction response of the wheel are significantly affected with variations in moisture content. It is noted that the rear wheel develops higher tractive forces compared to the front wheel for the same amount of slip. This effect is mainly caused due to the compaction of the terrain. For instance, the front wheel rolls over an undisturbed soil with well-known material properties, where the normal pressure acting on the soil tends to change its material properties. Following that, the rear wheel rolls over an already compacted soil – with higher values for cohesion, see Eq. 6.27 – which permits the development of higher tractive forces. It should be noted that the sinkage of the front wheel would be higher compared to the sinkage for the rear wheel (with respect to the conditions of the soil after the last of the preceding front wheels has passed). However, the significance of the disturbed terrain's material properties should be highlighted since the compaction resistance is lower on the rear wheel due to the smaller vertical displacement of the wheel into the

soil. Hence, in Fig.6.29 it is apparent that for positive slip the rear wheel develops almost double the tractive force compared to the front wheel.

However, apart from expected higher tractive forces for the rear wheel compared to the front wheel, no general trend exists with regards to the multi-pass effect and the respective tractive behavior of the rear wheel, since the rate of loading, the slip ratio and the degree of compaction of the deformable terrain vary significantly for purely cohesive as well as purely frictional soils. Thus, validation of the proposed model would be even more difficult for a soil with an intermediate value of cohesion and friction angle. The quantitative response of the proposed model and the respective trends can be validated with experimental and numerical results from the literature, e.g. Senatore & Sandu (2011). Finally, another basic assumption used in the aforementioned mathematical formulation of the multi-pass effect is the consistency of the soil moisture before and after the wheel passage.

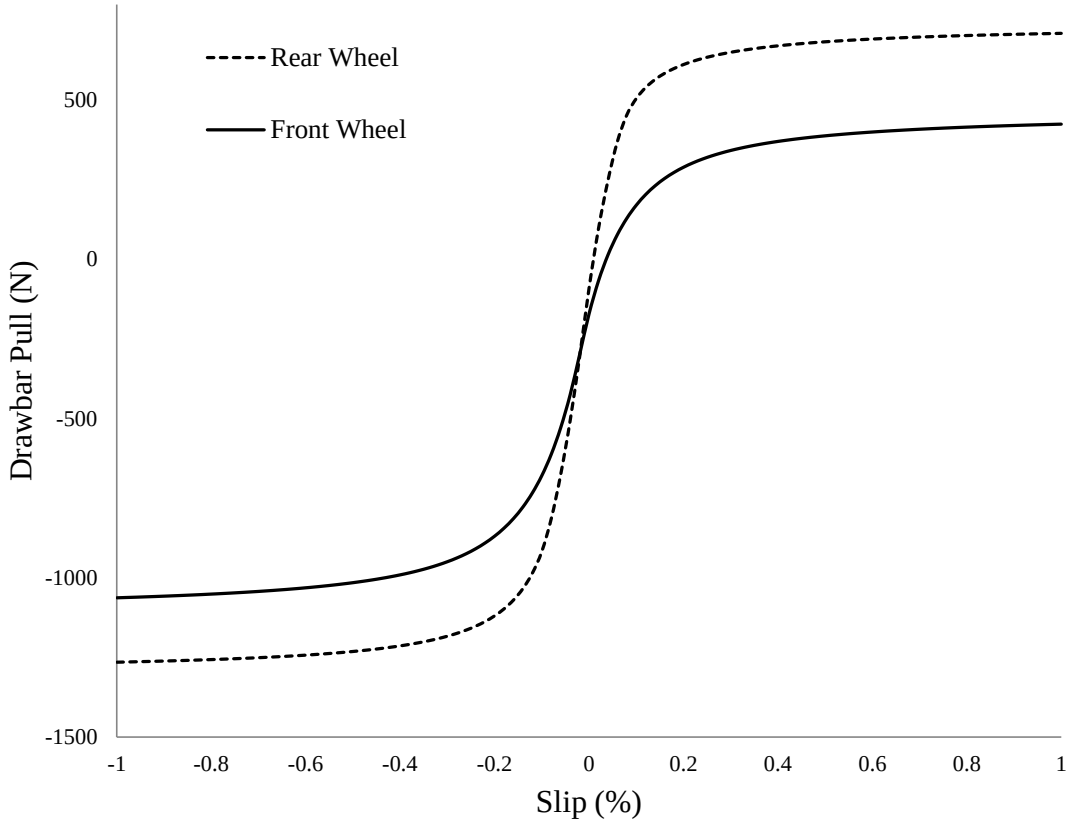

Figure 6.29.*Drawbar pull developed for a front and rear wheel under the assumption of rolling on the exact same rut path for a vertical load of 4kN and 0.2 slip, rolling on wet clay.*

6.6. Discussion

Although experimental data is available in the literature, this data is rarely provided together with a full account of soil invariant parameters. Thus, the initially developed Lagrangian models in this study (Chapter 3) were replaced after validation by analogous CEL models of a rigid wheel interacting with a deformable soil, and afterwards the rigid wheel in these CEL models was replaced by a rigid plate to simulate virtual pressure-sinkage tests.

The latter were used to obtain pressure-sinkage curves, based on which an optimisation routine was developed, in order to calculate the corresponding LSA soil model constitutive parameters. In order to extract the unknown soil parameters, the pressure sinkage curves obtained from the CEL model were fitted with corresponding curves obtained from Lyasko's (2010a) LSA model. In addition, a rigid plate with various sizes was modelled to interact with a number of different soils under the effect of various loading conditions and its response was investigated.

Based on the LSA soil model parameters obtained as described above, a novel semi-analytical equation was developed based on invariant soil parameters, capable of predicting the traction, the rolling resistance and the lateral forces developed under different slip angles. Furthermore, the tread pattern was modelled and the drawbar pull of a treaded wheel was compared with that obtained by a slick rigid wheel.

Finally, a deformable wheel was modelled in a similar manner with the methodology proposed by Bekker (1956) and the multi-pass effect of the rear wheel was investigated under the assumption that the latter wheel rolls over the exact same rut path created by the front wheel.

It was observed that by increasing the width of the wheel, the vertical displacement of the wheel into the soil reduces which results in higher tractive response. In terms of lateral force generation and under the same driving conditions it was found that a wheel rolling on frictional soils developed higher lateral forces compared to these obtained from cohesive soils. Furthermore, by modelling the tread pattern of a wheel it was found that the treaded wheel was developing higher tractive forces compared to a slick wheel under the assumption that the tread pattern was fully filled with soil. Subsequently, the effect of the void was studied and it noted that by increasing the

portion of void there is an increase in the tractive response of the wheel. In addition, it was observed that by reducing the inflation pressure of a deformable wheel, the tractive response was improving due to the increased contact area at the tyre-terrain interface which resulted in lower vertical displacement of the wheel into the soil. Finally, it was seen that the rear wheels exhibit a higher drawbar pull compared to the front wheels, since the former rolls over an already compacted soil with higher values of cohesion. The accuracy of the proposed analytical solution has been investigated both for cohesive and for frictional soils, and it was found that the developed solution can accurately predict the static and dynamic sinkage of the wheel into the soil.

It should be noted that the developed semi-analytical solution is governed by certain assumptions which limit its general applicability. These are the nature of the solution which is based on an empirical equation for the calculation of the dynamic sinkage calibrated through experimental tests and treats the problem in a simplistic way. Furthermore, some of the soil parameters utilized have been obtained from an optimisation routine where the pressure-sinkage behaviour as calculated by the analytical solution matches that of the Mohr-Coulomb soil model used in the finite element simulations introducing in this way an amount of approximation in the results. In addition, parameters which significantly affect the wheel rolling response, such as the exit angle, the angle where the normalized stress is maximised and the shear deformation modulus, have been calculated with the use of empirical relations, which highly influences the performance of the model. Therefore, the necessity for analytical, numerical and experimental studies which include both detailed invariant soil material properties and experimental tyre performance measurements should be highlighted.

Chapter 7

Conclusions & Future Work

7.1. Introduction

This chapter presents a summary of the results obtained and presented in the previous chapters, stemming from the outlined methodology and the developed models. Based on these findings, suggestions and recommendations for future work are proposed.

7.2. Conclusions and summary of findings

A concise review of the current state-of-the-art techniques with regards to off-road tyre modelling was conducted and the most fundamental limitations, such as the use of non-invariant soil parameters and the assumption of a constant pressure distribution along the width of the wheel, were identified. Utilization of non-invariant soil parameters necessitates continuous experimental testing, increasing in this way the overall economical cost. In addition, the numerical and the semi-analytical techniques were found to be the most prominent approaches in terms of tyre modelling. Subsequently, a Finite Element robust modelling technique was proposed which permits the minimisation of potential errors. This method included the development of two preliminary models namely (a) rigid wheel-deformable terrain and (b) pneumatic tyre-rigid road.

Model (a) permitted the validation of the deformable terrain solely as a soil engineering problem, where the indentation and the rolling process of wheel with infinite stiffness – rigid wheel – was modelled; the numerical results were validated with numerical and experimental results from the literature and close agreement was observed. The soils were separated into purely cohesive and purely frictional terrains in order to identify the effect of the cohesion and the friction angle on the rolling response of the wheel.

Linear and non-linear soil material responses were examined, and a novel relationship for the correlation of two different linear constitutive failure criteria, namely MC and DP, in triaxial tension and triaxial compression was developed. The results obtained using the proposed relationship were found to be in close agreement with results from the literature. The effects of the aspect ratio on the quasi-static steady state response of the rolling wheel were investigated and it was found that the wheel sinkage decreases as its width increases. More specifically it was found that, for a wheel with constant radius an increase of 60% in the aspect ratio may result to a decrease of more than 70% on the dimensionless steady state sinkage. Additionally the effect of the dilation angle was investigated and it was found that an increase of 10^{o} leads to an approximately 60% decrease of the dimensionless sinkage. Finally rigid wheels with purely longitudinal and purely lateral tread patterns were considered and their performance on the deformable terrain was examined. For the longitudinal tread pattern and for a cohesive terrain it was found that in some test cases where the tread depth was high the void of the wheel was not fully filled with soil, resulting in this way to smaller tractive forces compared to wheels with small values of tread depth. For the lateral treaded wheel it was found that by increasing the height of the tread there is a decrease in the produced slip ratio while no clear trend was observed when the tread contact area altered.

It has been shown that as the tyre rolls over soft terrains, the elements of the soil accumulate in front of the wheel. This accumulation affects the mesh of the road and the respective aspect ratio of the elements, leading in many cases to a premature termination of the solver. This bulldozing effect has been successfully reproduced during the previously stated model analyses with the help of a mesh adaptivity method, namely as the Arbitrary Lagrangian Eulerian – ALE.

Next, the realistic response of the tyre was obtained via model (b). In this model, a realistic tyre (P235/75R17) structure was developed via a coupled optimisation technique where the geometrical characteristics of the detailed tyre structure – carcass, belts, cords, bead – would change based on the natural frequency response. The outcomes of the frequency response were compared with experimental frequency response results and the geometry of the tyre was changed automatically within an optimisation scheme so that the response of the numerical model matches the experimental results. It has been shown that this optimisation method can yield

accurate tyre natural frequency response and thus generate a realistic finite element tyre without needing to know detailed knowledge of the material parameters of the tyre.

Once the correct frequency response was obtained, the tyre model was validated to a greater extent via examination of the vertical displacement and the contact areas under different inflation pressures and different vertical loads. Furthermore, the static footprint solution of the tyre loaded against a rigid analytical surface representing a stiff pavement verified that the tyre exhibits realistic behavior. The free rolling conditions were then obtained for the tyre rolling on a rigid surface using a steady state transport analysis and it was found that its results were reliable. Following this, the impact of the tyre in free rolling conditions on an obstacle (more specifically a bump) was simulated and it was shown that that the dynamic response is a function mainly of the bump geometry and the tyre eigenproperties which signifies that the overall problem can be reduced to a fundamental impulse excitation problem.

More explicitly it was found that for free rolling conditions, obtained from a steady state transport analysis which involves mixed Eulerian-Lagrangian descriptions, an increase in the inflation pressure of the tyre would reduce the oscillation of the tyre after the bump for a given vertical load. In addition, the effect of the vertical load for a constant inflation pressure was examined and it was found that for higher vertical loads the tyre is experiencing larger compression ratios which results in a more stable condition and therefore reduced vibration of the spindle. The results from this model were found in accordance with the basic theory for systems of a single degree of freedom where the amplitude of the oscillation is determined by the ratio of the time duration of the impact load to the eigenperiod of the most significant tyre eigenmode.

Following, the two preliminary models – model (a) and (b) – the final configuration of the pneumatic tyre – deformable terrain was developed with confidence. In addition, the tyre was considered to be rolling on a soft soil under towed conditions, and it was found that a reduction of 20% on the inflation pressure lead to an increase of 15% on the allowed distance of the wheel to travel in the deformable soil prior to its immobilization. In addition to that, the vertical load and linear velocity effects on the overall behavior of the wheel were examined. It was found that, by increasing the vertical load and the linear velocity, the towed wheel was traveling to a larger

distance compared to a wheel with less vertical load and smaller values of linear velocity. Moreover, the same tyre and soil as above were considered under driving conditions and it was found that contrary to the on-road tyres, reduction of the inflation pressure yields several benefits for the off-road tyres. More specifically, it was found that a decrease of 20% on the inflation pressure results in an increase of 15% on the allowed traveling distance into the soil prior to the immobilization of the wheel. This is mainly caused due to the fact that the contact area at the tyre-terrain interface is increasing which results in smaller vertical displacement of the wheel into the soil. Furthermore it should be noted that the behavior of the rolling wheel into the soil results from the combined effect of the rolling radius and its vertical displacement into the soil where both of the aforementioned factors are highly dependent on the inflation pressure and vertical load.

It should be highlighted that the development of the finite element models involves some inherent limitations such as the consideration of ideal constitutive soil models like purely cohesive and purely frictional homogeneous terrains governed by the linear (elastic-perfectly plastic) Mohr Coulomb or Drucker Prager models. Apart from this, the material properties of the tyre have been found by tuning its dynamic eigenresponse to be realistic, although these properties may be not representative of a realistic tyre in general. Far field boundary conditions have been considered for the soil model, which ensures that the results are not affected significantly. Finally, at the tyre-terrain interface the friction which develops is modeled by a Coulomb friction law with a constant coefficient throughout the analysis, which may be not realistic in most cases.

In conjunction with the FE models, a novel semi-analytical solution was developed. This model incorporated invariant soil parameters, compared to the literature where usually empirical or non-invariant soil parameters are used, in order to calculate the static and dynamic response of rigid and pneumatic tyres on deformable terrains. Lack of detailed soil material properties in conjunction with experimental data led this study to an alternative route. Thus, a CEL numerical model was initially developed where a rigid plate, modelled as a Lagrangian part, interacted with a deformable terrain, modelled as an Eulerian part, and the pressure sinkage response was extracted for a number of different terrains. The response of the CEL model was validated with results from the literature and close agreement was observed. Next, an optimisation

routine was developed in order to extract the unknown soil parameters, necessary for the utilization of the proposed semi-analytical model. Following that, rigid and deformable tyres, either treaded or treadless, were modelled and their interaction with a number of different deformable terrains was investigated. The qualitative response presented in the results is a clear indication that the proposed model can efficiently capture the basic characteristics of a rolling tire. Furthermore, the validity of the analytical equation was confirmed with the numerical results obtained from the FE models and the literaturefor cohesive and frictional terrains.

Based on the numerical predictions produced from the proposed semi-analytical model, it has been observed that for higher vertical loads, the drawbar pull – slip curve becomes steeper and has higher maximum drawbar pull and lower minimum drawbar pull. However, the difference at the maximum drawbar pull is not so intense, since the maximum drawbar pull is constrained by the soil strength. Furthermore, the tyres with larger width are experiencing lower vertical displacement, resulting in smaller compaction resistance and higher drawbar pull. Moreover, the soil interlocked in the void ratio has the effect of increasing the drawbar pull in the case of treaded tyres. In addition, the inflation pressure affects the overall rolling response of a pneumatic tyre, with the drawbar pull decreasing for increasing inflation pressure, a phenomenon caused by the higher values of vertical displacement. Furthermore, the multi-pass effect was sufficiently captured under the assumption that the rear wheels roll over the exact same rut path created by the front wheel and it was found that the rear wheel develops higher tractive forces compared to the front wheel. This effect is mainly caused due to the compaction of the terrain, whereas the front wheel rolls over an undisturbed soil, the rear wheel tends to roll over an already compacted soil with completely different constitutive material properties. Finally, the quantitative response of the proposed model and the respective trends were compared with experimental and numerical results from the literature, such as Senatore & Sandu (2011) and similar trends and physical behaviours were observed.

The developed semi-analytical solution constitutes a low fidelity modelling attempt to capture the principal characteristics of the tyre rolling response interacting with deformable terrain. This model involves a number of limitations due to the lack of analytical formulations with regards to parameters that have been calculated with the use of empirical methods. More specifically, the dynamic sinkage has been calculated

with the use of Lyasko's relationship (2010b) which, although validated through a number of experiments, still remains an empirical approach. In addition to that, following Wong's approach (2001) for the discretization of the tyre contact patch into front and rear regions separated by the angle in which the maximum radial pressure occurs, the two empirical relationships proposed by Wong (1967a, b) were utilized for the definition of θ_M and θ_r. Furthermore, an important limitation of the developed model is introduced with the use of values for the shear deformation modulus which are found in the literature and have not been calculated in an analytical manner.

7.3. Critical assessment & Research Contribution

Based on the summary of the findings mentioned in the previous section, the developed models were found to correlate well with the literature both qualitatively and in many cases quantitatively. Having established the capability of the models in terms of providing accurate predictions, the contribution of this work is mainly towards the development of robust and more importantly efficient simulation tools of tyre-soil interaction.

Considering the Finite Element approach, the relationship linking the linear Mohr-Coulomb with the linear Drucker-Prager failure criterion, can significantly reduce experimental test time for soil parameters obtainment. Typically Mohr Coulomb parameters are more readily available in the literature and therefore, utilisation of the developed relationship can easily transform the latter into the respective linear Drucker-Prager constitutive criterion.

Another area where data are sparse or expensive to obtain is that of material and/or construction parameters of realistic tyres. In this area, an optimisation approach has been proposed whereby unknown tyre parameters are identified by modal testing data. Since in most cases of tyre soil interaction, the soil is considered significantly more compliant than the tyre itself this level of structural description of the tyre seems to be adequate for tyre soil interaction studies.

In addition, direct measurements of the soil response can be costly and time consuming, especially for a vehicle manufacturer who is primarily interested in predicting the performance of a vehicle on soft soils. In this context, it is desirable to be able to obtain soil characteristic curves, such as the pressure-sinkage curve, from

nominal soils using a virtual pressure-sinkage test. This approach has been successfully implemented for the identification of the required soil parameters for the implementation of the analytical model.

In terms of computational efficiency the proposed semi-analytical tyre model is efficient enough to be used in full vehicle simulations while at the same time includes attributes like the utilization of invariant soil parameters. It is hoped that the methods described above will lead to a much wider adoption of soft soils tyre models in every day engineering practice in the automotive industry and Jaguar Land Rover in particular who have co-sponsored this project.

7.4. Recommended Future Work

A recommended next step towards the establishment of a universal methodology with regards to numerical FE off-road tyre modelling would be the development of a model where the tyre will be modelled as a Lagrangian part and the soil as an Eulerian part, also known as Coupled Eulerian Lagrangian method. This way, the solver will be able to handle the excessive material deformation of the soil without facing any premature termination; an error commonly occurred in the models developed in the current thesis. However, it should be highlighted that an Eulerian mesh increases the overall computational cost significantly, and therefore the ALE technique was chosen instead for the majority of the models used in this study.

In terms of soil modelling, additional complex non-linear constitutive material laws should be incorporated into the models in order to approach an even more realistic soil response, where the softening-hardening effect of the soil will be included. With regards to the tyre model, different hyperelastic material laws should be tested and their effect on the overall response of the tyre should be examined. Furthermore, although the above-stated tyre model was constructed based on a robust methodology, validation with real experimental data should definitely be performed to further increase its reliability. Different carcass and belt thicknesses should be checked in conjunction with their effect on the rolling response of the tyre. Next, suitable filtering methods should be developed in order to reduce the noise of the numerical results produced from the Explicit Solver – as explained in Chapter 4. In addition, the

multi-pass effect should be modelled and examined numerically and correlations and discrepancies with the trends from the analytical model should be investigated.

With regards to the analytical model, experimental soil testing should be performed where the necessary, for the model, soil parameters will be measured. Subsequently, the response of the analytical soil model should be validated with a pressure sinkage response obtained from a bevameter test for a rigid plate. Following that, the proposed semi-analytical tyre model should be incorporated and the results should be compared with experimental result measurements. However, it should be highlighted that the proposed model is based on invariant soil parameters; hence, once the necessary invariant material properties have been extracted no further soil measurements would be required. Furthermore, a common assumption used in the majority of the models is that of a constant pressure distribution along the width of the wheel; therefore, suitable expressions must be developed in order to overcome this deficiency. Finally once the model accuracy has been established, the next step should be the incorporation of the model into Multi Body Simulation (MBS) software, where further investigation on the dynamic behavior of an off-road vehicle rolling on various types of cohesive and frictional soils will be performed.

List of Publications

Journal

Bekakos, C.A., Papazafeiropoulos, G., O'Boy, D.J. and Prins, J. *"Finite Element Modeling of a Pneumatic Tire Interacting with Rigid Road and Deformable Terrain"*. International Journal of Vehicle Performance, 2016

Bekakos, C.A., Papazafeiropoulos, G., O'Boy, D.J., Prins, J. and Mavros, G. "*Off-Road Tire-Terrain interaction: An Analytical Solution*", SAE Int. J. Commer. Veh. 9(2):2016, doi:10.4271/2016-01-8029

Conference (International)

Bekakos, C.A., Papazafeiropoulos, G., O'Boy, D.J. and Prins, J. *"Pneumatic tyres interacting with deformable terrains"*.Journal of Physics: Conference Series 744: 012213, 2016

Bekakos, C.A., Papazafeiropoulos, G., O'Boy, D.J. and Prins, J. *"Development of accurate pneumatic tyre finite element models based on an optimisation procedure"*. ECCOMAS Congress, VII European Congress on Computational Methods in Applied Sciences and Engineering, Crete, Greece, June 5-10, 2016

Bekakos, C.A., Papazafeiropoulos, G., O'Boy, D.J. and Prins, J. "*Numerical modelling of pneumatic tires interacting with deformable terrains*". Tire Technology Expo, Hannover, Germany, February 16-18, 2016

Bekakos, C.A., Papazafeiropoulos, G., O'Boy, D.J. and Prins, J. *"Dynamic response of rigid wheels on deformable terrains",*Proc. 13th ISTVS European Conf., Rome, Italy, pp. 588-600, 2015

Bekakos, C.A., Mavros, G. and Prins, J. *"Analytical and finite-element study of the role of tread void ratio in terramechanics tyre behaviour"*. Proc. 4th International Tyre Colloquium, pp. 313–322, 2015

Reference List

ABAQUS 6.13.(2013). Documentations, Simulia Software, Inc.

AESCO, AS2TM - Matlab/Simulink Module AS2TM User's Guide, 1.12 ed., Hamburg: AESCO GbR, 2005.

Ageikin, J.S. (1987). Off the road mobility of automobile. New Delhi: Amerind Pub. Co. [translation from 1987 Russian book].

Aubel, T. (1993). FEM simulation of the interaction between elastic tire and soft soil. In Proceedings of 11th International Conference of the ISTVS, Lake Tahoe, Nevada.

Bandel, P., & Monguzzi, C. (1983).Simulation model of the dynamic behavior of a tire running over an obstacle. 2nd annual meeting of The Tire Society, The University of Akron, Akron, Ohio, March 23-24.

Bashford, L.L., & Kocher, M.F. (1999). Belts vs tires, belts vs belts, tires vs tires. Journal of Applied Engineering in Agricultural, 15(3), 175-181.

Bekker, M. G. (1957). Theory of Land Locomotion - The Mechanics of Vehicle Mobility. The University of Michigan Press, Ann Arbor.

Bekker, M. G. (1960). Off the Road Locomotion. The University of Michigan Press., Ann Arbor.

Bekker, M. G., & Semonin, E. V. (1975).Motion Resistance of Pneumatic Tires.Journal of Automotive Engineering, 6(2).

Bernstein, R. (1913). Probleme zur experimentellen Motorplugmechanik. Der Motorwagen 16:199-206.

Bhoopalam, A.K, Sandu, C., & Taheri, S. (2015a). Experimental investigation of pneumatic tire performance on ice: Part 1 – Indoor study. Journal of Terramechanics, v.60, 43-54.

Bhoopalam, A.K, Sandu, C., & Taheri, S. (2015b). Experimental investigation of pneumatic tire performance on ice: Part 2 – Outdoor study. Journal of Terramechanics, v.60, 55-62.

Bolarinwa, E., & Olatunbosun, O. (2015). On Finite Element Tyre Modal Analysis. SAE Technical Paper 2015-01-1518.

Brixius, W.W. (1987). Traction predicion equations for bias-ply tires. ASA paper,No 871622, St.Joseph (MI): ASAE.

Chan, B.J., & Sandu, C. (2008). Development of an off-road capalbe tire model for vehicle dynamic simulations. PhD thesis, Virginia Polytechnic Institute and State University, Blacksburg, VA.

Chatterjee, A., & Ranjan, V. (2012). Free vibration analysis of radial pneumatic tire using FEM. Int. J. Emerging Technology & Advanced Engineering, 2(8), 319-324.

Chiroux, R. C., Foster, W. A., Johnson, C. E., Shoop, S. A., & Raper, R. L. (2005). Three-dimensional finite element analysis of soil interaction with a rigid wheel. Applied Mathematics and Computation, 162(2), 707–722.

Cho, J.R., Kim, K.W., Jeon, D.H., & Yoo, W.S. (2005). Transient dynamic response analysis of 3-D patterned tire rolling over cleat. European Journal of Mechanics A/Solids, Vol. 24, 519–531.

Choi, J.H, Cho, J.R., Woo, J.S., & Kim, K.W. (2012). Numerical Investigation of snow traction characteristics of 3-D patterned tire. Journal of Terramechanics, 49, 81-93.

Chopra, A.K. (2012). Dynamics of Structures, theory and Applications to Earthquake Engineering, 4th Ed., Prentice Hall.

Crolla, D.A., & El-Razaz, A.S.A. (1987). A review of the combined lateral and Longitudinal Force Generation of Tyres on Deformable Surfaces. Journal of Terramechanics, 24(3), 199-225.

De Borst, R., & Vermeer, P.A., (1984). Possibilites and Limitations of Finite Elements for Limit Analysis Geotechnique, Vol. 34, No.2, 199-210.

Dhillon, R.S., Rustam, A., El-Gindy, M., Phillips, D., Oijer, F., & Johansson, I. (2013). Development of Truck Tire-Soil Interaction Model using FEA and SPH. SAE International.

Ding, L., Yoshida, K., Nagatani, K., Gao, H., & Deng, Z. (2009). Parameter identification for planetary soil based on a decoupled analytical wheel-soil interaction Terramechanics model. Proceedings of the International Conference on Intelligent Robots and Systems, October 11-15.

Ding, L., Gao, H., Deng, Z., Tao, J. (2010). Wheel slip-sinkage and its prediction model of lunar rover. Journal of Central South University of Technology, 17(1), 129-135.

Ding, L., Gao, H, Deng, Z., Li, Y., & Liu, G. (2014). New perspective on characterizing pressure-sinkage relationship of terrains for estimating interaction mechanics. Journal of Terramechanics, v.52, 57-76.

Ding, L., Deng, Z., Gao, H, Tao, J., Iagnemma, K., & Liu, G. (2015). Interaction mechanics model for rigid driving wheels of planetary rovers moving on sandy terrain with consideration of multiple physical effects. Journal of Field Robotics, 32(6), 827-859.

Dorfi, H.R., Wheeler & R.L., Keum, B.B. (2005). Vibration Modes of Radial Tires: Application to Non-rolling and Rolling Events. SAE 2005 Noise and Vibration Conference and Exhibition, Traverse City, Michigan.

Drucker, D.C.& Prager W. (1952). Soil Mechanics and Plastic Analysis or Limit Design. Quarterly of Applied Mathematics, Vol. 10, 157–165.

El-Gawwad, K. A. A., Crolla, D. A., Soliman, A. M. A., & El-Sayed, F. M. (1999a). Off road tyre modelling I : the multi-spoke tyre model modified to include the effect of straight lugs. Journal of Terramechanics, 36, 3–24.

El-Gawwad, K. A. A., Crolla, D. A., Soliman, A. M. A., & El-Sayed, F. M. (1999b). Off road tyre modelling II: effect of camber on tyre performance. Journal of Terramechanics, 36, 25–38.

El-Razaz, A.S.A. (1988). Lateral Tyre Forces on Off-Road Surfaces. PhD Thesis, University of Leeds.

Evans, I. (1964). The sinkage of tracked vehicles on soft ground. Journal of Terramechanics, 1(2), 33-43.

Fervers, C. (2004). Improved FEM simulation model for tire–soil interaction. Journal of Terramechanics, 41(2-3), 87–100.

Gan, J. K. M., Fredlund, D. G., & Rahardjo, H. (1988). Determination of the shear strenth parameters of an unsatured soil using the direct shear test.

Gazetas, G. (1983). Analysis of machine foundation vibrations: State of the art. International Journal of Soil Dyn. Earthq. Eng., 2(1), 2–42.

Gee-Clough, D. (1976). The Bekker theory of rolling resistance amended to take account of skid and deep sinkage. Journal of Terramechanics, 13(2), 87–105.

Ghoreishy, M.H.R. (2006). Steady state rolling analysis of a radial tyre: comparison with experimental results. Proc. IMechE, Vol. 220, Part D: J. Automobile Engineering, 713-721.

Gipser, M. (2003). The FTire tire model family. Esslingen, Germany: Esslingen University of Applied Sciences, 18.

Goriatchkin, B.P. (1936). Theory and Manufacturing of Agricultural Machines. Moscow: USSR Government.

Grecenko, A. (1992). The slip and drift model of a wheel with tyre compared to some other attempts in this field. Journal of Terramechanics, 29(6), 559-604.

Grisso, R.D., Perumpral, J.V, & Zoz, F.M. (2006). An emprical model for tractive performance of rubber-tracks in agricultural soils. Journal of Terramechanics, 43(2), 225-236.

Guskov, V.V. (1966). Optimum parameters of agricultural tractors. Moscow: Mashinostroenie. [in Russian]

Hambleton, J.P., & Drescher, A. (2008). Modeling wheel-induced in soils: Indentation. Journal of Terramechanics, 45(6), 201-211.

Hambleton, J.P., & Drescher, A. (2009). Modeling wheel-induced in soils: Rolling. Journal of Terramechanics, 46(2), 35-47.

Harnisch, C., Lach, B., Jakobs, R., Troulis, M., & Nehls, O. (2005). A new tyre–soil interaction model for vehicle simulation on deformable ground. Vehicle System Dynamics: International Journal of Vehicle Mechanics and Mobility, 43:sup1, 384–394.

Hetherington, J. G., & Littleton, I. (1978). The rolling resistance of towed, rigid wheels in sand. Journal of Terramechanics, 15(2), 95–105.

Ishigami, G. (2008). Terramechanics-based Analysis and Control for Lunar/Planetary Exploration Robots. PhD thesis, Tohoku University.

Iagnemma, K., Senatore, C., Trease, B., Arvidson, R., Bannett, K., Shaw, A., Zhou, F., Van Dyke, L., & Lindemann, R. (2011). Terramechanics modelling of mars surface exploration rovers for simulation and parameters estimation. ASME International Design Engineering Technical Conference & Computers and Information in Engineering Conference. Washington, DC, USA August 28-31.

Janosi, Z., &Hanamoto, B. (1961). The analytical determination of drawbar pull as a function of slip for tracked vehicles in deformable soils. Proceedings of the 1st International Conference on the Mechanics of Soil-Vehicle Systems, Torino, Italy, 707-727.

Jia, Z., Smith, W., & Peng, H. (2012). Terramechanics-based wheel-terrain interaction model and its applications to off-road wheeld mobile robots. Robotica, v.30, 491-503.

Kacigin, V.V., & Guskov, V.V. (1968). The basis of tractor performance theory. Journal of Terramechanics. 5(3).

Kamoulakos, A. & Kao, B. G. (1998).Transient Dynamics of a Tire Rolling over Small Obstacles – A Finite Element Approach with Pam-Shock. Tire Science and Technology, TSTCA, Vol. 26, No. 2, 84-108.

Kölsch, C. (2000). Vertical vehicle dynamics on soft ground-investigations with FEM. FISITA World Automotive Congress, 1–8.

Lee, J.H. (2009). A new indentation model for snow. Journal of Terramechanics, 46, 1-13.

Lee, J.H. (2011). Finite element modeling of interfacial forces and contact stresses of pneumatic tire on fresh snow for combined longitudinal and lateral slips. Journal of Terramechanics, 48, 171-197.

Li, H., & Schindler, C. (2012). Three-dimensional finite element and analytical modelling of tyre-soil interaction. Proceedings of the Institution of Mechanical Engineers, Part K: Journal of Multi-body Dynamics, 227(1), 42-60.

Li, H., & Schindler, C. (2013). Analysis of soil compaction and tire mobility with finite element method. Proceedings of the Institution of Mechanical Engineers, Part K: Journal of Multi-body Dynamics, 227(3), 275–291.

Li, H., & Schindler, C. (2014). Transient dynamics of an excavator tyre rolling over speed bump. Proceedings of the Institution of Mechanical Engineers, Part K: Journal of Multi-body Dynamics, 228(3), 229-240.

Li, H., & Schindler, C. (2014). Investigation of Tire-Soil interaction with analytical and finite element method. Mechanics Based Design of Structures and Machines: An International Journal, 41(3), 293-315.

Liang, C.Y., Allen, R.W., Rosenthal, T.J., Chrstos, J.P., & Nunez, P. (2004). Tire modeling for off-road vehicle simulation. SAE International.

Liu, C.H., & Wong, J.Y. (1996). Numerical Simulations of tyre-soil interaction based on critical state soil mechanics. Journal of Terramechanics, 33(5), 209-221.

Liu, C., Wong, J., & Mang, H. (2000). Large strain finite element analysis of sand: model, algorithm and application to numerical simulation of tire–sand interaction. Computers & Structures, 74, 253–265.

Lyasko, M., & Kurdenkov, A.G. (1989). Evaluation of reliability of standard methods of the assesment of the compaction action of wheeled vehicles of the soil. Tract Agricultural Machines, 19, 9-12.

Lyasko, M. (2010a). LSA model for sinkage predictions. Journal of Terramechanics, 47(1), 1–19.

Lyasko, M. (2010b). Slip sinkage effect in soil-vehicle mechanics. Journal of Terramechanics, 47(1), 21–31.

Lyasko, M. (2010c). Multi-pass effect on off-road vehicle performance. Journal of Terramechanics, 47(5), 275-294.

Lyasko, M. (2010d). How to calculate the effect of soil conditions on tractive performance. Journal of Terramechanics, 47(6), 423-445.

Matsuoka, H., & Okuma, M. (2002).A New Experimental Modal Parameter Estimation Method for Cylindrical Structures by Standing Wave Decomposition and Application to Tire Modelling. Proceedings of ISMA at The International Conference on Noise and Vibration Engineering, V1913 – 1919.

Meirion Griffith, G., & Spenko, M. (2010). A new pressure-sinkage model for small, rigid wheels on deformable terrains. Proceeding of the Joing 9th Asia-Pacific ISTVS Conferenceand Annual meeting of Japanese Society for Terramechanics. Sapporo, Japan, September 27-30.

Meirion Griffith, G., & Spenko, M. (2011a). A modified pressure–sinkage model for small, rigid wheels on deformable terrains. Journal of Terramechanics, 48(2), 149–155.

Meirion Griffith, G., & Spenko, M. (2011b). Toward establishing a comprehensive pressure-sinkage model for small diameter wheels on deformalbe terrains. Proceeding of the 17th International ISTVS Conference, Blacksburg, Virginia, USA, September 18-22.

Meirion Griffith, G., & Spenko, M. (2012). A comprehensive pressure-sinkage model for small-wheeled unmanned ground vehicles on dilative, deformable terrain. 2012 IEEE International Conference on Robotics and Automation, 4052–4057.

Meirion Griffith, G., & Spenko, M. (2013). A pressure-sinkage model for small-diameter wheels on compactive, deformable terrain. Journal of Terramechanics, 50(1), 37–44.

Meirion Griffith, G., & Spenko, M. (2014). Development and experimental validation of an improved pressure-sinkage model for small-wheeled vehicles on dilative, deformable terrain. Journal of Terramechanics, v.51, 19-29.

Meyerhof, G. G. (1951). The Ultimate bearing capacity of foundations. Geotechnique, 2, 301.

Molisani, L. (2004). A coupled tire structure-acoustic cavity model, PhD Thesis, Virginia Poly-technic Institute and State University, Blacksburg, Virginia, US.

Muro, T., & Raymond, N.Y. (1980). Rectangular plate loading test on snow. Journal of Japanese Society Snow and Ice, 42, 17. [in Japanese]

Muro, T., & Raymond, N.Y. (1980). Vane cone test on snow. Journal of Japanese Society Snow and Ice, 42, 25. [in Japanese]

Nakajima, Y. (2003). Analytical model of longitudinal tire traction in snow. Journal of Terramechanics, 40, 63-82.

Nakashima, H., & Oida, A. (2004). Algorithm and implementation of soil-tire contact analysis code based on dynamic FE-DE method. Journal of Terramechanics, 41, 127-137.

Nakashima, H., Fujii, H., Oida, A., Momozu, M., Kanamori, H., Aoki, S., Yokoyama, T., Shimizu, H., Miyasaka, J., & Ohdoi, K. (2010). Discrete element method analysis of a single wheel performance for a small lunar rover on sloped terrain. Journal of Terramechanics, 47, 307-321.

Nocedal, J., & Wright, S.J. (2006). Numerical Optimisation, 2nd Edition. Springer Series in Opera-tions Research, Springer Verlag.

Oida, A. (1979). Study on equation of shear stress displacement curves. Report No 5, Japan: Farm Power and Machinery Laboratory, Kyoto University.

Onafenko, O., & Reece, A. (1967). Soil stresses and deformation beneath rigid wheels. Journal of Terramechanics, 59(l), 59–80.

Palanivelu, S., Rao, & N.K.V Ramarathnam K.K. (2015).Determination of rolling tyre modal parameters using Finite Element techniques and Operational Modal Analysis.Mechanical Systems and Signal Processing, Vol. 64-65, 385-402.

Pi, W.S. (1988). Dynamic tire/soil contact surface interaction model for aircarft ground operations. Journal of Aircraft, 25(11), 1038-1044.

Pokrovsky, G.I. (1937). Investigations of soil physics. Moscow: Vodgeo, ONTI. [translation from Russian]

Priddy, J. D., & Willoughby, W.E. (2006). Clarification of vehicle cone index with reference to mean maximum pressure. Journal of Terramechanics, 43(2), 85–96.

Reece, A. (1965). Principles of soil-vehicle mechanics. Proceedings of the Institution of Mechanical Engineers: Automobile Division, 180(2), 45-66.

Reece, A. R., & Peca, J.O. (1981). An assessment of the value of the cone penetrometer in mobility prediction. Proceedings of the 7th International Conference of the International Society for Terrain-Vehicle Systems, III, A1-A33.

Scavuzzo, R.W., Richards, T.R., & Charek, L.T. (1993). Tire Vibration Modes and Effects on Vehicle Ride Quality. Tire Science and Technology, TSTCA, 21(1), 23-39.

Schwanghart, H. (1968). Lateral forces on steered tyres in loose soil. Journal of Terramechanics, 5(1), 9-29.

Senatore, C., & Sandu, C. (2011). Off-road tire modeling and the multi-pass effect for vehicle dynamics simulation. Journal of Terramechanics, 48(11), 265-276.

Seta, E., Kamegawa, T., & Nakajima, Y. (2003). Prediction of snow/tire interaction using explicit FEM and FVM. Tire Science and Technology, TSTCA, 31(3), 173–188.

Shoop, S. A., (2001). Finite Element Modeling of Tire-Terrain Interaction. University of Michigan, Report number: ERDC/CRREL TR-01-16.

Steiner, M. (1979). Analyse, Synthese und Berechnungsmethoden der Triebkraft-Schlupf-Kurve von Luftreifen auf nachgiebigem Boden, Dissertation, Technische Universität München.

Taheri, Sh., Sandu, C., Taheri, S., Pinto, E., & Gorsich, D. (2015). A technical survey on Terramechancis models for tire-terrain interaction used in modeling and simulation of wheeled vehicles. Journal of Terramechanics, v.57, pp. 1-22.

Terzaghi, K. (1944). Theoretical Soil Mechanics. N. Y. J. Wiley and Sons.

Trease, B., Arvidson, R., Lindemann, R., Bennett, K., et al. (2011). Dynamic modeling and soil mechanics for path planning of the mars exploration rovers.Proc. ASME 2011 Int. Des. Engrg Tech. Conf. and Computers and Information in Engrg Conf., 755-765.

Upadhyaya, S.K., Wulfsohn, D., & Jubbal, G. (1989). Traction prediction equations for radial ply tires. Journal of Terramechanics, 26(2), 149-175.

Upadhyaya, S. K., Wulfsohn, D. & Mehlschau, J.. (1993). An instrumented device to obtain traction related parameters. Journal of Terramechanics, 30(1), 1-20.

Upadhyaya, S.K., Rosa, U.A., Josiah, M.N., & Koller, M. (2001). Effect of belt width and grouser wear on the tractive charcteristics of rubber-tracked vehicles. Journal of Applied Engineering in Agricultural, 17(3), 267-271.

Vasil'ev, A.V., Dokychaeva E.N., & Utkin-Lubovtsov, O.L. (1969). Effect of tracked tractor design parameters on tractive performance.

Vehicle Dynamics Standards Committee (2008) "Vehicle Dynamics Terminology," SAE International (J670_200801).

Vinesse, E.P. (1996). Substructuring method and eigenfunction representation for a rolling tyre coupled to a secondary mechanical system. Proc Instn Mach Engrs, 210, 313-325.

Wei, C. & Olatunbosun, O.A. (2014).Transient dynamic behaviour of finite element tire traversing obstacles with different heights. Journal of Terramechanics, Vol.56, 1–16.

Wheeler, R.L., Dorfi, H.R., & Keum, B.B. (2005). Vibration modes of radial tires: measurement, prediction, and categorization under different boundary and operating conditions. SAE Noise and Vibration Conference and Exhibition, Traverse City, Michigan.

Wills, B.M.D. (1963). The measurement of soil shear strength and deformation moduli and a comparison of the actual and theoretical performance of a family of rigid tracks. Journal of Agricultural Engineering Research, No 2.

Wills, B.M.D., Barrett, F.M., & Shaw, G.J. (1965). An investigation into rolling resistance theories for towed rigid wheels. Journal of Terramechanics, 2(1).

Wismer, R.D, & Luth, H.J. (1973). Off-road traction prediction for wheeled vehicles. Journal of Terramechanics, 10(2), 49-61.

Wong, J.Y., & Reece, A. (1966). Soil failure beneath rigid wheels. Proceedings of the Second International Conference of the International Society for Terrain Vehicle Systems. Quebec, Canada.

Wong, J.Y., & Reece, A. (1967a). Prediction of rigid wheel performance based on analysis of soil-wheel stresses, part I: Performance of driven rigid wheels. Journal of Terramechanics, 4, 81-98.

Wong, J.Y., & Reece, A. (1967b). Prediction of rigid wheel performance based on analysis of soil-wheel stresses, part II: Performance of towed rigid wheels. Journal of Terramechanics, 4, 7-25.

Wong, J.Y. (1979). Review of Soil mechanics for off road vehicle engineering. Journal of Terramechanics, 16 (4), 191-194. Canadian Geotechnical Journal, 16(3), 13-41.

Wong, J. Y., & Preston-Thomas, J. (1983). On the characterization of the shear stress-displacement relationship of terrain. Journal of Terramechanics, 19(4), 107-127.

Wong, J.Y. (1983). Evaluation of soil strength measurements. NRCC Report No. 22881, National Research Council of Canada.

Wong, J. Y. (2001). Theory of Ground Vehicles. 3rd Edition. Ottawa, Canada, John Wiley & Sons, INC.

Wong, J.Y. (2010). Terramechanics and Off-Road Vehicles. Ottawa, Canada, Elsevier.

Xia, K. (2011). Finite element modeling of tire/terrain interaction: Application to predicting soil compaction and tire mobility. Journal of Terramechanics, 48, 113-123.

Yong, R.N., & Fattah, E.A. (1976). Prediction of wheel-soil interaction and performance using the finite element method. Journal of Terramechanics, 13(4).

Yong, R.N., Fattah, E.A., & Boonsinsuk, P. (1978). Analysis and prediction of tyre-soil interaction and performance using finite elements. Journal of terramechanics, 15(1), 43–63.

Yoshida, K., & Ishigami, G. (2004). Steering characteristics of a rigid wheel for exploration on loose soil. In Proceedings of the 2004 IEEE International Conference on Intelligent Robots and Systems (IROS 04'). Sendai, Japan.

Youssef, A.F., & Ali, G.A. (1982). Determination of soil parameters using plate test. Journal of Terramechanics,19(2),129–147.

Zoz, F.M. (1997). Belt and tire tractive performance. SAE technical paper series, 972731. Warrendale, PA: SAE.

Appendix

A. Additional Figures

In this section the corresponding figures concerning the results for MC soil model and mentioned in section 3.4 of this thesis are presented.

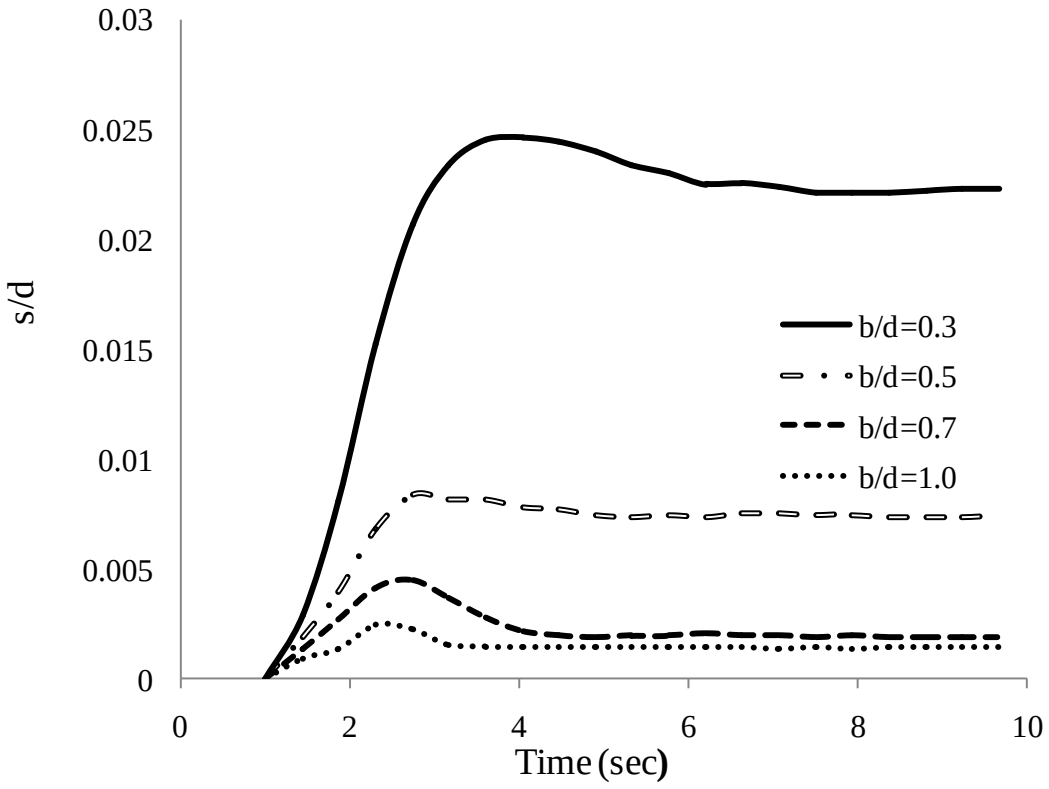

Figure A.1.*Dimensionless sinkage versus time for various aspect ratios of the wheel rolling on soil with* $\varphi=0^o$, $\psi=0^o$ *and* $c/\gamma gd=1.25$ *and* $Q_v/\gamma bd^2=1.9$.

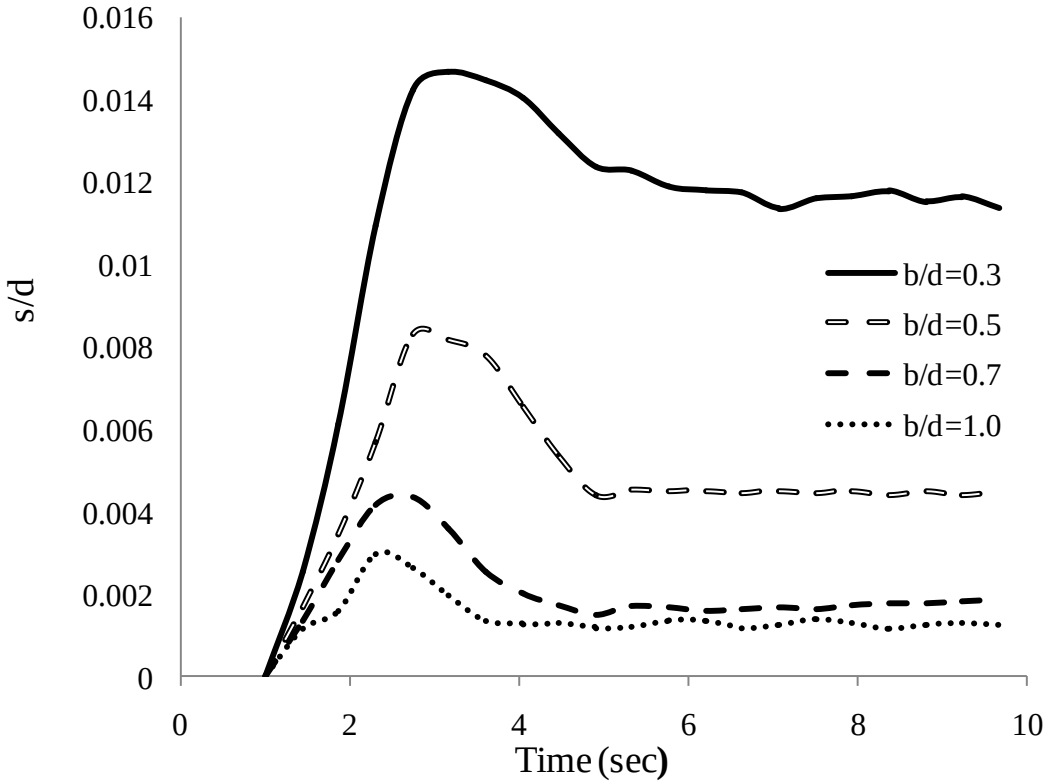

Figure A.2.*Dimensionless sinkage versus time for various aspect ratios of the wheel rolling on soil with $\varphi=30^o$, $\psi=0^o$ and $c/\gamma gd=0.25$ and $Q_v/\gamma bd^2=1.9$.*

B. Abaqus Input Deck

B1. Tyre model

An indicative input file that has been used by Abaqus for the numerical simulations of tyre models presented in this thesis (truncated for copyright reasons) is as follows:

```
*Heading
 *Preprint, echo=NO, model=NO, history=NO, contact=NO
 *RESTART,WRITE,FREQ=100
*Node
      1,  0.366495937,           0.
          .....
     11,   0.35505414, -0.0795796141
*Element, type=SFMGAX1
1, 2, 1
          .....
10, 10, 11
*Elset, elset=MEM_BELT1, generate
  1,  10,   1
*Surface Section, elset=MEM_BELT1
*Rebar Layer
 BELT1, 3.6482596525709419e-07 , 0.00116, ,BELT, 110., 1
*Node
    12,  0.367994398,           0.
         .....
```

```
     22,   0.35638693, -0.0801719651
*Element, type=SFMGAX1
11, 13, 12
         .....
20, 21, 22
*Nset, nset=MEM_BELT2, generate
 12,  22,   1
*Elset, elset=MEM_BELT2, generate
11, 20,  1
*Surface Section, elset=MEM_BELT2
*Rebar Layer
BELT2, 3.6482596525709419e-07 , 0.00116, ,BELT, 70., 1
*Node
     23,  0.363498986,           0.
         .....
     62,  0.262492061, -0.102351859
*Element, type=SFMGAX1
21, 24, 23
         .....
60, 44, 62
*Elset, elset=MEM_CARCASS, generate
 21,  60,   1
*Surface Section, elset=MEM_CARCASS
*Rebar Layer
CARCASS, 8.0113281250000171e-08 , 0.001, ,CARCASS, 0., 1
*NODE,NSET=RIM
 199, 0., 0., 0.
*Element, type=RAX2
61, 67, 66
         .....
109, 75, 72
*Elset, elset=RIM
61,107,108,109
*Nset, nset=RIMNODE
66, 70, 75, 72
*RIGID BODY, ELSET=RIM, REFNODE=199
*Node
     66,  0.221900001, -0.0869999975
         .....
    142,  0.362500012,           0.
*Element, type=CGAX4R
64, 70, 71, 67, 66
         .....
110, 52, 53, 54, 55
*Elset, elset=BELT, generate
 85, 103,   2
*Elset, elset=TREAD
 84, 86, 88, 90, 92, 94, 96, 98,100,102,105
*Elset, elset=SIDE
 64, 65, 66, 67, 68, 69, 70, 71, 72, 73, 74, 75, 76, 77, 78
         .....
*Elset, elset=CARCASS
SIDE,BELT
*Elset, elset=CARCASS_BEAD
110
*Elset, elset=Tread_1, generate
74,82,1
*Elset, elset=TREAD_CONTACT
TREAD, Tread_1
*Nset, nset=SYM, generate
140, 142,   1
*Surface, type=ELEMENT, name=TREAD_CONTACT
TREAD_CONTACT, S4
*Surface, type=ELEMENT, name=INSIDE
CARCASS, S2
*Nset, nset=NTIRE1, generate
1,60,1
*Nset, nset=NTIRE2
66,67
*Nset, nset=NTIRE3, generate
70,142
*Nset, nset=NTIRE
NTIRE1, NTIRE2, NTIRE3
*Section Controls, Name=ENH, Hourglass=Enhanced, Second Order Accuracy=Yes, Distortion
Control=No
*Solid Section, elset=TREAD, material=RUBBER, Controls=ENH
,
```

```
*Solid Section, elset=BELT, material=RUBBER, Controls=ENH
,
*Solid Section, elset=SIDE, material=RUBBER, Controls=ENH
,
*Solid Section, elset=CARCASS_BEAD, material=RUBBER, Controls=ENH
,
*Element, type=CGAX4R
106, 52, 53, 54, 55
*Elset, elset=BEAD
106,
*Solid Section, elset=BEAD, material=RIM
*System
*Embedded Element,HOST=BELT, roundoff tolerance=0.001
MEM_BELT1, MEM_BELT2
*Embedded Element, HOST=CARCASS, roundoff tolerance=0.001
MEM_CARCASS
*Embedded Element, HOST=CARCASS_BEAD, roundoff tolerance=0.001
BEAD
*Material, name=BELT
*Density
5900.,
*Elastic
 1.722e+11, 0.3
*Material, name=CARCASS
*Density
1500.,
*Elastic
 9.87e+09, 0.3
*Material, name=RIM
*Density
7800.,
*Elastic
 2.1e+11, 0.3
*Material, name=RUBBER
*Density
1100.,
*Hyperelastic, moduli=LONG TERM
         .....
*Viscoelastic, time=PRONY
         .....
*Step, name=Step-1, nlgeom=YES
1:INFLATION
*Static
0.25, 1.0
*Boundary
RIM, 1, 2
RIM, 5, 6
RIMNODE, 5
SYM, 2
SYM, 5
*DSLOAD
 INSIDE, P, 242.E3
*Restart, write, frequency=100
*Output, field, variable=PRESELECT
*Output, history, variable=PRESELECT
*End Step
```

B2. Terrain

An indicative input file that has been used by Abaqus for the numerical simulations of terrain presented in this thesis (truncated for copyright reasons) is as follows:

```
*HEADING
 IMPORT ROLLING TIRE: IMPACT WITH CURB
 UNITS KG,M
*PREPRINT,MODEL=YES,ECHO=YES,CONTACT=YES,HIST=YES
*IMPORT,STEP=1,STATE=YES,UPDATE=NO
TREAD, SIDE, BELT, MEM_CARCASS, MEM_BELT1,
 MEM_BELT2, RIM, CARCASS_BEAD, CARCASS, BEAD,
 TREAD_CONTACT
*NODE,NSET=ROAD
 99999,   0.0,   0.0,  0.0
*NODE
900001, -0.4,  -1.0, -0.39
```

```
...
1059681,  2.5,  1.0, -0.79
*NGEN, NSET=alphabeta
900001,900011,1
...
*NGEN, NSET=psiomega
1059591,1059681,1
*NFILL,NSET=edafos_up1_1
alphabeta,deltaepsilon,5,101
...
*NFILL
edafos_up1_1,edafos_down1_1,30,5151
edafos_up1_2,edafos_down1_2,30,5151
edafos_up2_1,edafos_down2_1,30,5151
edafos_up2_2,edafos_down2_2,30,5151
edafos_up3_1,edafos_down3_1,30,5151
edafos_up3_2,edafos_down3_2,30,5151
*ELEMENT,TYPE=C3D8R
900001,900002,900001,900102,900103,905153,905152,905253,905254
...
*ELEMENT,TYPE=C3D8R
1036501,904557,904556,904657,904658,909708,909707,909808,909809
*ELGEN,ELSET=ROADS1_1
900001,10,1,1,5,101,10,30,5151,50
...
*ELGEN,ELSET=ROADS3_2
1036501,90,1,1,5,101,90,30,5151,450
*SOLID SECTION,MATERIAL=edafos,ELSET=ROADS1_1
...
*SOLID SECTION,MATERIAL=edafos_malako,ELSET=ROADS2_2,controls=EC-1
*Section Controls, name=EC-1, hourglass=ENHANCED
*SOLID SECTION,MATERIAL=edafos_malako,ELSET=ROADS3_2
*MATERIAL,NAME=edafos
*ELASTIC
1e10,0.3
*DENSITY
5900
*Material, name=edafos_malako
*Density
2000,
*Drucker Prager
 0.01,   1., 0.01
*Drucker Prager Hardening, type=SHEAR
 37378.27401,0.
*Elastic
 14950440, 0.3
*ELSET,ELSET=ELCONTACT1, GENERATE
915001,915400,1
*ELSET,ELSET=ELCONTACT2, GENERATE
927001,930600,1
*ELSET,ELSET=EDAFOS_UP
ELCONTACT1,ELCONTACT2
*ELSET,ELSET=EDAFOS_ADAPTIVE
ROADS2_2
*NSET,NSET=NRBC, GENERATE
1054531,1059681,1
*Amplitude, name=Grav_Amp
            0.,              0.,            0.001,              1., 0.01, 1.
*AMPLITUDE,NAME=TFSTEP
0.0, 1.0,  1.0, 1.0
*ELEMENT,TYPE=MASS,ELSET=MRIM
200001,199
*ELEMENT,TYPE=ROTARYI,ELSET=IRIM
200002,199
*MASS,ELSET=MRIM
1.E1,
*ROTARY INERTIA,ELSET=IRIM
1.E-1,1.E-1,1.E-1,
EDAFOS_UP, S1
*Surface, type=ELEMENT, name=TREAD_CONTACT
TREAD_CONTACT, S6
*SURFACE,NAME=INSIDE,TYPE=ELEMENT
CARCASS, S4
*EMBEDDED ELEMENT,HOST=CARCASS,ROUNDOFF TOL=1.E-3
MEM_CARCASS,
*EMBEDDED ELEMENT,HOST=BELT,ROUNDOFF TOL=1.E-3
MEM_BELT1,MEM_BELT2
```

```
*Embedded Element, HOST=CARCASS_BEAD, ROUNDOFF TOL=1.E-3
BEAD
*Step, name=Step-1, nlgeom=YES
*Dynamic, Explicit
, 0.01
*Bulk Viscosity
0.06, 1.2
*Adaptive Mesh Controls, name=Ada-1, meshing predictor=PREVIOUS
1., 0., 0.
*Adaptive Mesh, elset=EDAFOS_ADAPTIVE, controls=Ada-1, op=NEW
*Dload, amplitude=Grav_Amp
EDAFOS_ADAPTIVE, GRAV, 9.81, 0., 0., -1.
*CONTACT PAIR,INTERACTION=SRIGID, MECHANICAL CONSTRAINT=PENALTY, WEIGHT=0.5
TREAD_CONTACT , SROAD
*SURFACE INTERACTION,NAME=SRIGID
*FRICTION
0.5,
*BOUNDARY,OP=NEW
NRBC,  1, 6
RIM, 1, 2
RIM, 4, 6
*DSLOAD
 INSIDE, P, 242.E3
*CLOAD
 RIM, 3, -5000.0
*Restart, write, number interval=1, time marks=NO
*End Step
*DYNAMIC,EXPLICIT
  , 0.5
*RESTART,NUMBER INTERVAL=10,WRITE
*MONITOR,DOF=3,NODE=199
*BULK VISCOSITY
0.06, 1.2
*BOUNDARY,OP=NEW,AMP=TFSTEP,TYPE=VELOCITY
 RIM, 1, , 2.7778
 RIM, 2
 RIM, 4
 RIM, 6
 NRBC, 1, 6
*OUTPUT,FIELD,OP=NEW,NUMBER INTERVAL=20
*ELEMENT OUTPUT
S,LE
*ELEMENT OUTPUT,REBAR
S,LE
*NODE OUTPUT
U,V,A
*CONTACT OUTPUT
CSTRESS,FSLIP,FSLIPR
*OUTPUT,HISTORY,OP=NEW,TIME INTERVAL=1.E-3
*NODE OUTPUT,NSET=RIM
U,V,RF,RM1,RM2,RM3,UR1,UR2,UR3,A3
*ENERGY OUTPUT,VAR=PRE
*END STEP
```